

THERMAL CHARACTERIZATION AND KINETICS OF DIESEL, METHANOL  
ROUTE BIODIESEL, CANOLA OIL AND DIESEL-BIODIESEL BLENDS AT  
DIFFERENT BLENDING RATES BY TGA AND DSC

A THESIS SUBMITTED TO  
THE GRADUATE SCHOOL OF NATURAL AND APPLIED SCIENCES  
OF  
MIDDLE EAST TECHNICAL UNIVERSITY

BY

ECE HATİCE TOPA

IN PARTIAL FULFILLMENT OF THE REQUIREMENTS  
FOR  
THE DEGREE MASTER OF SCIENCE  
IN  
PETROLEUM AND NATURAL GAS ENGINEERING

SEPTEMBER 2010

Approval of the thesis:

**THERMAL CHARACTERIZATION AND KINETICS OF DIESEL,  
METHANOL ROUTE BIODIESEL, CANOLA OIL AND DIESEL-BIODIESEL  
BLENDS AT DIFFERENT BLENDING RATES BY TGA AND DSC**

submitted by **ECE HATİCE TOPA** in partial fulfillment of the requirements for the degree of **Master of Science in Petroleum and Natural Gas Engineering Department, Middle East Technical University** by,

Prof. Dr. Canan Özgen \_\_\_\_\_  
Dean, Graduate School of **Natural and Applied Sciences**

Prof. Dr. Mahmut Parlaktuna \_\_\_\_\_  
Head of Department, **Petroleum and Natural Gas Engineering**

Prof. Dr. Mustafa Verşan Kök \_\_\_\_\_  
Supervisor, **Petroleum and Natural Gas Engineering Dept., METU**

**Examining Committee Members**

Prof. Dr. Mahmut Parlaktuna \_\_\_\_\_  
Petroleum and Natural Gas Engineering Dept., METU

Prof. Dr. Mustafa Verşan Kök \_\_\_\_\_  
Petroleum and Natural Gas Engineering Dept., METU

Prof. Dr. Nurkan Karahanoğlu \_\_\_\_\_  
Geological Engineering Dept., METU

Dr. A.Gürkan Işcan \_\_\_\_\_  
N. V. Turkse Perenco, ANKARA

Selçuk Erkeköl (M.Sc) \_\_\_\_\_  
TPAO, ANKARA

**Date:** 06/09/2010

**I hereby declare that all information in this document has been obtained and presented in accordance with academic rules and ethical conduct. I also declare that, as required by these rules and conduct, I have fully cited and referenced all material and results that are not original to this work.**

Name, Last name : Ece Hatice TOPA

Signature :

## **ABSTRACT**

### **THERMAL CHARACTERIZATION AND KINETICS OF DIESEL, METHANOL ROUTE BIODIESEL, CANOLA OIL AND DIESEL-BIODIESEL BLENDS AT DIFFERENT BLENDING RATES BY TGA AND DSC**

Topa, Ece Hatice

M.S., Department of Petroleum and Natural Gas Engineering

Supervisor: Prof. Dr. Mustafa Verşan Kök

September 2010, 163 pages

Application of thermogravimetric analysis to the renewable energy sources is a novel study and it has been becoming attractive by the researchers in recent years. In this thesis, thermal and kinetic properties of biodiesel as new energy source, diesel and canola oil have been analyzed by using very popular thermogravimetric analysis methods which are; Differential Scanning Calorimetry (DSC) and Thermogravimetry (TGA/DTG). The main aim of the study is to observe the combustion and pyrolysis behaviour of methanol route biodiesel and diesel blends at different blending rates. Additionally, combustion and pyrolysis behaviour of canola oil, the origin of biodiesel have been analysed to observe the transesterification reaction effect on biodiesel. Therefore, biodiesel, diesel, canola oil and blends of diesel and biodiesel at different percentages are exposed to isothermal heating under nitrogen and air atmosphere with a constant heating rate of 5, 10 and 15° C/min by using TGA/DTG and DSC to 600°C.

According to combustion thermograms of pure samples, it is observed that combustion temperatures of the samples taking place are in the order of canola oil>biodiesel>diesel, implying that the transesterification reactions are making the triglyceride molecules more ignitable. However, diesel molecules consisting of hydrocarbon chains still have lower ignition temperature than biodiesel. Also, it is found that as the heating rate of the reactions increase, peak temperatures of the reactions shift higher; implying that as the heating rate of the reactions increase reaction lose their sensitivity. According to the combustion thermograms of mixtures of the diesel-biodiesel mixtures, it is understood that B15 has better combustion properties combustion of B15 occurs at lower temperatures and has the highest exothermic enthalpy.

When the pyrolysis mechanisms of the pure samples are analyzed, it is noticed that the stability of the samples are in the order of canola oil>biodiesel>diesel, which means that transesterification reactions make the samples less stable. As the content of the biodiesel in the mixture of diesel-biodiesel increase, the stability of the samples increases.

By using some of the equations derived in literature, ignition temperatures and heat capacitances of the samples are calculated. Ignition temperatures of biodiesel, diesel and canola oil are 141.1, 108.7 and 209.5 °C, respectively and heat capacitances are in the order of; diesel>biodiesel>canola.

In addition to that several kinetic methods have been applied to determine the pyrolysis and combustion reaction parameters of the reactions. Activation energies of the samples are in the order of canola oil>biodiesel>diesel and for the different heating rates of reactions it is noticed that the activation energy is sensitive to the heating rate of the reactions and they are in the order of 5°C/min>10°C/min>15°C/min.

**Keywords:** thermogravimetry, differential scanning calorimetry, kinetic analysis, combustion, pyrolysis, diesel, biodiesel, canola oil.

## ÖZ

### **TGA VE DSC İLE DİZEL, METHANOL BİYODİZEL, KANOLA YAĞI VE DEĞİŞİK ORANLARDAKİ DİZEL-BİYODİZEL KARIŞIMLARININ TERMAL KARAKTERİZASYONU VE KİNETİĞİ**

Topa, Ece Hatice

Yüksek Lisans, Petrol ve Doğal Gaz Mühendisliği Bölümü

Tez Yöneticisi: Prof. Dr. Mustafa Verşan Kök

Eylül 2010, 163 sayfa

Termogravimetrik analiz metotlarının, yenilenebilir enerji kaynaklarının araştırılması için uygulanması, yeni bir konudur ve son yıllarda araştırmacılar tarafından önem kazanmaktadır. Bu çalışmada, biyodizel, dizel ve kanola yağının termal ve kinetik özellikleri, termogravimetrik analiz metotlarından iki yaygın ısıl analiz yöntemi olan, Diferansiyel Taramalı Kalorimetri (DSC) ve Termogravimetrik Analiz (TGA/DTG) cihazları kullanılarak analiz edilmiştir. Çalışmanın temel amacı, biyodizel, dizel, kanola yağı ve biyodizel-dizelin değişik oranlardaki karışımlarının yanma ve piroliz davranışlarının incelenmesidir. Kanola ve biyodizelin yanma ve piroliz davranışları incelenerek transesterifikasyon reaksiyonunun biyodizel üzerindeki etkileri analiz edilmiştir. Biyodizel, dizel, kanolanın ve dizel-biyodizelin değişik oranlardaki

karışımları TGA/DTG ve DSC ısı analiz cihazları ile 5, 10 ve 15° C/dk'lık sabit ısıtma hızları ile nitrojen ve hava ortamlarında 600 C'ye kadar ısıya tabi tutulmuştur.

Saf maddelerin yanma termogramlarına göre, maddelerin yanma reaksiyonları sıcaklıkları şu sıra ile gerçekleşmektedir; kanola>biyodizel>dizel. Bu sonuç transesterifikasyon reaksiyonlarının sayesinde trigliserit moleküllerinin tutuşmasının kolaylaştığını göstermektedir. Ancak, hidrokarbonlu bağlardan oluşan dizel molekülleri biyodizele göre daha kolay tutuşmaktadırlar. Öte yandan, reaksiyonların ısıtılma hızları arttıkça reaksiyonların tepe noktalarının daha üst sıcaklıkları kaydığı gözlemlenmiştir. Karışımlardan B15'in daha düşük sıcaklıklarda yanma profili göstermekte olması ve diğerlerine göre daha yüksek ekzotermik ısıya sahip olması nedeniyle, bu karışımının diğerlerine göre daha iyi yanma özelliğine sahip olduğu sonucuna varılmıştır.

Saf maddelerin piroliz mekanizmaları incelendiğinde bu maddelerin kararlılıklarının şu sıralamada olduğu sonucuna varılmıştır; kanola>biyodizel>dizel. Buna göre, transesterifikasyon reaksiyonları biyodizeli daha az kararlı bir yapıya ulaştırmaktadır. Dizel-biyodizel karışımında biyodizel miktarı arttıkça maddenin kararlılığı artmaktadır.

Literatür çalışmalarının sonucunda elde edilmiş, maddelerin tutuşma sıcaklıklarını ve ısı kapasitelerini hesaplamada kullanılan formüller ile saf maddelerin bazı ısı özellikleri hesaplanmıştır. Buna göre saf maddelerin tutuşma sıcaklıkları biyodizel, dizel ve kanola için sırası ile 141.1, 108.7 and 209.5 °C'dir. Isı kapasitelerinin ise şu sıralamada olduğu sonuca varılmıştır; dizel>biyodizel>kanola.

Buna ek olarak reaksiyon parametrelerinin hesaplanması için çeşitli kinetik metotlar kullanılmıştır. Aktivasyon enerjileri, kanola>biyodizel>dizel şeklinde sıralanmaktadır. Reaksiyonların değişik ısıtma hızları için aktivasyon enerjilerinin de değişim gösterdiği ve sıralamanın 5°C/dk>10°C/dk>15°C/dk olduğu gözlemlenmiştir.

**Anahtar Sözcükler:** termogravimetri, diferansiyel taramalı kalorimetri, kinetik analiz, yanma, piroliz, dizel, biyodizel, kanola yağı.

*to my family*

## **ACKNOWLEDGMENTS**

I wish to express my deepest gratitude to my supervisor Prof. Dr. Mustafa Verşan KÖK for his guidance, advice, criticism and encouragements throughout the research.

I would like to thank my whole family for their endless patience and moral support, to my workmates especially to Asli Gündoğar, Özge Demirel and Selçuk Güreşçi for their suggestions and technical support.

Besides, my great thanks to New Dizeline and Izmir Tupras Refinery for their sample delivery for my thesis study.

Finally, I would like to express my appreciation for the financial support of TUBITAK, The Scientific and Technological Research Council of Turkey, throughout my master education.

## TABLE OF CONTENTS

ABSTRACT .....	iv
ÖZ .....	vi
ACKNOWLEDGMENTS .....	ix
TABLE OF CONTENTS .....	x
LIST OF FIGURES .....	xiii
LIST OF TABLES .....	xx
NOMENCLATURE.....	xxii
CHAPTERS	
1.INTRODUCTION .....	1
2.LITERATURE REVIEW.....	5
3.STATEMENT OF THE PROBLEM .....	12
4.KINETIC ANALYSIS AND METHODS .....	13
4.1 Arrhenius Method .....	15
4.2 Coats-Redfern Method.....	15
4.3 Ingraham-Marrier Method .....	16
4.4 Differential Method.....	17
4.4 Horowitz Metzger .....	17
5.PYROLYSIS MECHANISMS OF HYDROCARBONS .....	19
5.1 Pyrolysis of Petroleum Products .....	20
5.2 Biodiesel Pyrolysis.....	23
6.EXPERIMENTAL METHOD AND MATERIALS .....	28
6.1 Thermal Analysis .....	28
6.1.1 Thermogravimetric Analyzer (TGA) .....	28

6.1.1.1	Calibrating the TGA.....	30
6.1.1.1.1	Temperature Calibration .....	30
6.1.1.1.2	Weight Calibration.....	31
6.1.1.2	Experimental Procedure of TGA Analysis .....	31
6.1.2	Differential Scanning Calorimeter (DSC).....	32
6.1.2.1	Calibrating DSC.....	35
6.1.2.1.1	T-Zero Calibration (Cell Calibration) .....	36
6.1.2.1.2	Enthalpy/Temperature Calibration (Cell Constant) .....	36
6.1.2.2	Experimental Procedure of DSC Analysis.....	37
6.2	Materials.....	38
6.2.1	Biodiesel.....	38
6.2.2	Canola Oil .....	42
6.2.3	Diesel .....	43
7.	RESULTS AND DISCUSSION .....	46
7.1	Combustion Experiments.....	46
7.1.1	TGA/DTG Experiments.....	46
7.1.2	DSC Experiments.....	51
7.2	Pyrolysis Experiments.....	56
7.2.1	TGA/DTG Pyrolysis .....	56
7.2.2	DSC Pyrolysis Experiments.....	60
7.3	Ignition Temperature and Heat Capacitance Derivation.....	64
7.4	Kinetic Analysis.....	71
7.4.1	TGA/DTG Kinetic Analysis for Combustion Experiments.....	74
7.4.2	TGA/DTG Kinetic Analysis for Pyrolysis Experiments.....	84
8.	CONCLUSION .....	92
	REFERENCES.....	97
	APPENDICES	
A.	PETROLEUM FRACTIONS BY GC ANALYSIS.....	104

B.TA INSTRUMENTS CHARACTERISTICS .....	105
C.HEAT CAPACITANCE CURVE DERIVATION OF SAPPHIRE .....	111
D.TGA/DTG AND DSC COMBUSTION RESULTS .....	114
E.TGA/DTG AND DSC PYROLYSIS RESULTS .....	121
F.PLOTS OF TGA/DTG KINETIC METHODS .....	128

## LIST OF FIGURES

<b>Figure 1.1:</b> Evolution from 1971 to 2007 of world total final consumption by fuel .....	1
<b>Figure 5.1:</b> HRGC-MS total ion chromatogram and constituents identified in volatile fraction up 150°C of petroleum sample .....	20
<b>Figure 5.2:</b> Normal paraffins, aromatics and naphthenes composition .....	21
<b>Figure 5.3:</b> Structure of a triglyceride oil, biodiesel and the pyrolysis product .....	24
<b>Figure 5.4:</b> GC/MS spectra of esters showing presence of different fatty acid components .....	26
<b>Figure 5.5:</b> Structure of the main components of methyl esters .....	26
<b>Figure 6.1:</b> Schematic diagram of TGA.....	29
<b>Figure 6.2:</b> Components of DSC; <b>a.</b> DSC Module <b>b.</b> Mass Flow controller .....	35
<b>Figure 6.3:</b> Overall transesterification reaction of biodiesel.....	38
<b>Figure 6.4:</b> Basic production scheme of biodiesel .....	40
<b>Figure 6.5:</b> <b>a.</b> Flower of canola <b>b.</b> Rapeseed of canola .....	43
<b>Figure 6.6:</b> Fractions of crude oil and the refinery processes .....	44
<b>Figure 7.1:</b> Biodiesel TGA/DTG combustion curve analysis at 5°C/min.....	48
<b>Figure 7.2:</b> Analysis of diesel DSC combustion curve at 5 C/min.....	53
<b>Figure 7.3:</b> Analysis of biodiesel TGA/DTG pyrolysis curve at 5 C/min.....	57
<b>Figure 7.4:</b> DSC pyrolysis curve analysis of diesel at 5°C/min heating rate .....	63
<b>Figure 7.5:</b> Ignition temperature calculation graph of oil shale samples .....	65
<b>Figure 7.6:</b> Calculation of ignition temperature of diesel .....	66
<b>Figure 7.7:</b> Calculation of ignition temperature of biodiesel .....	66
<b>Figure 7.8:</b> Calculation of ignition temperature of canola oil.....	67
<b>Figure 7.9:</b> Evaluation of specific heat capacity of lubricating oils with respect to temperature .....	69

<b>Figure 7.10:</b> Calorific heat capacities of pure samples; biodiesel, diesel and canola oil with respect to temperature .....	70
<b>Figure 7.11:</b> Biodiesel combustion reaction Arrhenius plots of different heating rates of 5°C/min, 10°C/min and 15°C/min .....	74
<b>Figure B.1:</b> <b>a.</b> TGA balance segment, <b>b.</b> TGA furnace segment .....	107
<b>Figure B.2:</b> TGA curie temperature determination by using nickel as sample .....	108
<b>Figure B.3:</b> DSC pan type with sealing equipment of hermetic seal .....	110
<b>Figure B.4:</b> Squeezing instrument of hermetic seal .....	110
<b>Figure C.1:</b> Cp of Sapphire with respect to temperature and equation derivation .....	113
<b>Figure D.1:</b> TGA/DTG Thermogram of biodiesel combustion at different heating rates; 5, 10, 15°C /min .....	115
<b>Figure D.2:</b> TGA/DTG Thermogram of diesel combustion at different heating rates; 5, 10, 15°C /min .....	116
<b>Figure D.3:</b> TGA/DTG Thermogram of canola oil combustion at different heating rates; 5, 10, 15°C /min .....	117
<b>Figure D.4:</b> TGA/DTG Thermogram of biodiesel-diesel mixtures combustion at a constant heating rate of 10°C /min .....	118
<b>Figure D.5:</b> DSC Thermogram of biodiesel combustion at different heating rates; 5, 10, 15°C /min .....	119
<b>Figure D.6:</b> DSC Thermogram of diesel combustion at different heating rates; 5, 10, 15°C /min .....	119
<b>Figure D.7:</b> DSC Thermogram of canola combustion at different heating rates; 5, 10, 15°C /min .....	120
<b>Figure D.8:</b> DSC Thermogram of biodiesel-diesel mixtures combustion at a constant heating rate of 10°C /min .....	120
<b>Figure E.1:</b> TGA/DTG Thermogram of biodiesel pyrolysis at different heating rates; 5, 10, 15°C /min .....	122
<b>Figure E.2:</b> TGA/DTG Thermogram of diesel pyrolysis at different heating rates; 5, 10, 15°C /min .....	123
<b>Figure E.3:</b> TGA/DTG Thermogram of canola oil pyrolysis at different heating rates; 5, 10, 15°C /min .....	124

<b>Figure E.4:</b> TGA/DTG Thermogram of B100, B20, B15, B10, B05, B00 mixtures pyrolysis at a constant heating rate of 10°C /min.....	125
<b>Figure E.5:</b> DSC Thermogram of biodiesel pyrolysis at different heating rates; 5, 10, 15°C /min .....	126
<b>Figure E.6:</b> DSC Thermogram of diesel pyrolysis at different heating rates; 5, 10, 15°C /min .....	126
<b>Figure E.7:</b> DSC Thermogram of canola oil pyrolysis at different heating rates; 5, 10, 15°C /min .....	127
<b>Figure E.8:</b> DSC Thermogram of B100, B20, B15, B10, B05, B00 mixtures pyrolysis at a constant heating rate of 10°C /min .....	127
<b>Figure F.1:</b> Biodiesel combustion reaction Coats-Redfern (P1) plots of different heating rates of 5°C/min, 10°C/min and 15°C/min .....	129
<b>Figure F.2:</b> Biodiesel combustion reaction Coats-Redfern (n=1) plots of different heating rates of 5°C/min, 10°C/min and 15°C/min .....	129
<b>Figure F.3:</b> Biodiesel combustion reaction Coats-Redfern (n=2) plots of different heating rates of 5°C/min, 10°C/min and 15°C/min .....	130
<b>Figure F.4:</b> Biodiesel combustion reaction Ingraham Marrier plots of different heating rates of 5°C/min, 10°C/min and 15°C/min .....	130
<b>Figure F.5:</b> Biodiesel combustion reaction Differential Method P(1) plots of different heating rates of 5°C/min, 10°C/min and 15°C/min .....	131
<b>Figure F.6:</b> Biodiesel combustion reaction Differential Method (n=1) plots of different heating rates of 5°C/min, 10°C/min and 15°C/min .....	131
<b>Figure F.7:</b> Biodiesel combustion reaction Differential Method (n=2) plots of different heating rates of 5°C/min, 10°C/min and 15°C/min .....	132
<b>Figure F.8:</b> Biodiesel combustion reaction Horowitz-Metzger plots of different heating rates of 5°C/min, 10°C/min and 15°C/min .....	132
<b>Figure F.9:</b> Diesel combustion reaction Arrhenius plots of different heating rates of 5°C/min, 10°C/min and 15°C/min .....	133
<b>Figure F.10:</b> Diesel combustion reaction Coats-Redfern (P1) plots of different heating rates of 5°C/min, 10°C/min and 15°C/min .....	133

<b>Figure F.11:</b> Diesel combustion reaction Coats-Redfern (n=1) plots of different heating rates of 5°C/min, 10°C/min and 15°C/min .....	134
<b>Figure F.12:</b> Diesel combustion reaction Coats-Redfern (n=2) plots of different heating rates of 5°C/min, 10°C/min and 15°C/min .....	134
<b>Figure F.13:</b> Diesel combustion reaction Ingraham Marrier plots of different heating rates of 5°C/min, 10°C/min and 15°C/min .....	135
<b>Figure F.14:</b> Diesel combustion reaction Differential Method P(1) plots of different heating rates of 5°C/min, 10°C/min and 15°C/min .....	135
<b>Figure F.15:</b> Diesel combustion reaction Differential Method (n=1) plots of different heating rates of 5°C/min, 10°C/min and 15°C/min .....	136
<b>Figure F.16:</b> Diesel combustion reaction Differential Method (n=2) plots of different heating rates of 5°C/min, 10°C/min and 15°C/min .....	136
<b>Figure F.17:</b> Diesel combustion reaction Horowitz Metzger plots of different heating rates of 5°C/min, 10°C/min and 15°C/min .....	137
<b>Figure F.18:</b> Canola oil combustion reaction Arrhenius plots of different heating rates of 5°C/min, 10°C/min and 15°C/min.....	137
<b>Figure F.19:</b> Canola oil combustion reaction Coats-Redfern (P1) plots of different heating rates of 5°C/min, 10°C/min and 15°C/min .....	138
<b>Figure F.20:</b> Canola oil combustion reaction Coats-Redfern (n=1) plots of different heating rates of 5°C/min, 10°C/min and 15°C/min .....	138
<b>Figure F.21:</b> Canola oil combustion reaction Coats-Redfern (n=2) plots of different heating rates of 5°C/min, 10°C/min and 15°C/min .....	139
<b>Figure F.22:</b> Canola oil combustion reaction Ingraham Marrier plots of different heating rates of 5°C/min, 10°C/min and 15°C/min .....	139
<b>Figure F.23:</b> Canola oil combustion reaction Differential (P1) plots of different heating rates of 5°C/min, 10°C/min and 15°C/min .....	140
<b>Figure F.24:</b> Canola oil combustion reaction Differential (n=1) plots of different heating rates of 5°C/min, 10°C/min and 15°C/min .....	140
<b>Figure F.25:</b> Canola oil combustion reaction Differential (n=2) plots of different heating rates of 5°C/min, 10°C/min and 15°C/min .....	141

<b>Figure F.26:</b> Canola oil combustion reaction Horowitz Metzger plots of different heating rates of 5°C/min, 10°C/min and 15°C/min .....	141
<b>Figure F.27:</b> Biodiesel-diesel mixtures combustion reactions Arrhenius plots .....	142
<b>Figure F.28:</b> Biodiesel-diesel mixtures combustion reactions Coats Redfern (P1) plots .....	142
<b>Figure F.29:</b> Biodiesel-diesel mixtures combustion reactions Coats Redfern (n=1) plots .....	143
<b>Figure F.30:</b> Biodiesel-diesel mixtures combustion reactions Coats Redfern (n=2) plots .....	143
<b>Figure F.31:</b> Biodiesel-diesel mixtures combustion reactions Ingraham Marrier plots .....	144
<b>Figure F.32:</b> Biodiesel-diesel mixtures combustion reactions Differential (P1) plots	144
<b>Figure F.33:</b> Biodiesel-diesel mixtures combustion reactions Differential (n=1) plots .....	145
<b>Figure F.34:</b> Biodiesel-diesel mixtures combustion reactions Differential (n=2) plots .....	145
<b>Figure F.35:</b> Biodiesel-diesel mixtures combustion reactions Horowitz Metzger plots .....	146
<b>Figure F.36:</b> Biodiesel pyrolysis reaction Coats Redfern (P1) plots of different heating rates of 5°C/min, 10°C/min and 15°C/min .....	146
<b>Figure F.37:</b> Biodiesel pyrolysis reaction Coats Redfern (n=1) plots of different heating rates of 5°C/min, 10°C/min and 15°C/min .....	147
<b>Figure F.38:</b> Biodiesel pyrolysis reaction Coats Redfern (n=2) plots of different heating rates of 5°C/min, 10°C/min and 15°C/min .....	147
<b>Figure F.39:</b> Biodiesel pyrolysis reaction Ingraham Marrier plots of different heating rates of 5°C/min, 10°C/min and 15°C/min .....	148
<b>Figure F.40:</b> Biodiesel pyrolysis reaction Differential (P1) plots of different heating rates of 5°C/min, 10°C/min and 15°C/min .....	148
<b>Figure F.41:</b> Biodiesel pyrolysis reaction Differential (n=1) plots of different heating rates of 5°C/min, 10°C/min and 15°C/min .....	149

<b>Figure F.42:</b> Biodiesel pyrolysis reaction Differential (n=2) plots of different heating rates of 5°C/min, 10°C/min and 15°C/min .....	149
<b>Figure F.43:</b> Biodiesel pyrolysis reaction Horowitz Metzger plots of different heating rates of 5°C/min, 10°C/min and 15°C/min .....	150
<b>Figure F.44:</b> Diesel pyrolysis reaction Arrhenius plots of different heating rates of 5°C/min, 10°C/min and 15°C/min .....	150
<b>Figure F.45:</b> Diesel pyrolysis reaction Coats Redfern (P1) plots of different heating rates of 5°C/min, 10°C/min and 15°C/min .....	151
<b>Figure F.46:</b> Diesel pyrolysis reaction Coats Redfern (n=1) plots of different heating rates of 5°C/min, 10°C/min and 15°C/min .....	151
<b>Figure F.47:</b> Diesel pyrolysis reaction Coats Redfern (n=2) plots of different heating rates of 5°C/min, 10°C/min and 15°C/min .....	152
<b>Figure F.48:</b> Diesel pyrolysis reaction Ingraham Marrier plots of different heating rates of 5°C/min, 10°C/min and 15°C/min.....	152
<b>Figure F.49:</b> Diesel pyrolysis reaction Differential (P1) plots of different heating rates of 5°C/min, 10°C/min and 15°C/min.....	153
<b>Figure F.50:</b> Diesel pyrolysis reaction Differential (n=1) plots of different heating rates of 5°C/min, 10°C/min and 15°C/min.....	153
<b>Figure F.51:</b> Diesel pyrolysis reaction Differential (n=2) plots of different heating rates of 5°C/min, 10°C/min and 15°C/min.....	154
<b>Figure F.52:</b> Diesel pyrolysis reaction Horowitz Metzger plots of different heating rates of 5°C/min, 10°C/min and 15°C/min .....	154
<b>Figure F.53:</b> Canola oil pyrolysis reaction Arrhenius plots of different heating rates of 5°C/min, 10°C/min and 15°C/min .....	155
<b>Figure F.54:</b> Canola oil pyrolysis reaction Coats Redfern (P1) plots of different heating rates of 5°C/min, 10°C/min and 15°C/min .....	155
<b>Figure F.55:</b> Canola oil pyrolysis reaction Coats Redfern (n=1) plots of different heating rates of 5°C/min, 10°C/min and 15°C/min .....	156
<b>Figure F.56:</b> Canola oil pyrolysis reaction Coats Redfern (n=2) plots of different heating rates of 5°C/min, 10°C/min and 15°C/min .....	156

<b>Figure F.57:</b> Canola oil pyrolysis reaction Ingraham Marrier plots of different heating rates of 5°C/min, 10°C/min and 15°C/min .....	157
<b>Figure F.58:</b> Canola oil pyrolysis reaction Differential (P1) plots of different heating rates of 5°C/min, 10°C/min and 15°C/min .....	157
<b>Figure F.59:</b> Canola oil pyrolysis reaction Differential (n=1) plots of different heating rates of 5°C/min, 10°C/min and 15°C/min .....	158
<b>Figure F.60:</b> Canola oil pyrolysis reaction Differential (n=2) plots of different heating rates of 5°C/min, 10°C/min and 15°C/min .....	158
<b>Figure F.61:</b> Canola oil pyrolysis reaction Horowitz Metzger plots of different heating rates of 5°C/min, 10°C/min and 15°C/min .....	159
<b>Figure F.62:</b> Biodiesel-diesel mixtures pyrolysis reactions Arrhenius plots .....	159
<b>Figure F.63:</b> Biodiesel-diesel mixtures pyrolysis reactions Coats Redfern (P1) plots	160
<b>Figure F.64:</b> Biodiesel-diesel mixtures pyrolysis reactions Coats Redfern (n=1) plots .....	160
<b>Figure F.65:</b> Biodiesel-diesel mixtures pyrolysis reactions Coats Redfern (n=2) plots .....	161
<b>Figure F.66:</b> Biodiesel-diesel mixtures pyrolysis reactions Ingraham Marrier plots ..	161
<b>Figure F.67:</b> Biodiesel-diesel mixtures pyrolysis reactions Differential (P1) plots ....	162
<b>Figure F.68:</b> Biodiesel-diesel mixtures pyrolysis reactions Differential (n=1) plots ..	162
<b>Figure F.69:</b> Biodiesel-diesel mixtures pyrolysis reactions Differential (n=2) plots ..	163
<b>Figure F.70:</b> Biodiesel-diesel mixtures pyrolysis reactions Horowitz Metzger plots	163

## LIST OF TABLES

<b>Table 1.1:</b> Comparisons of Diesel and Biodiesel Properties .....	3
<b>Table 4.1:</b> Algebraic expressions of functions of the reaction mechanisms .....	16
<b>Table 5.1:</b> Distillation curve of 19° API Brazilian crude oil fractions .....	22
<b>Table 5.2:</b> TGA/DTG analysis of petroleum fractions.....	22
<b>Table 5.3:</b> Composition of fatty acid in methanol babassu biodiesel .....	25
<b>Table 5.4:</b> Ester composition of castor oil biodiesel .....	26
<b>Table 6.1:</b> Properties of biodiesel obtained from different origins .....	41
<b>Table 6.2:</b> Properties of methanol route canola oil originated .....	41
<b>Table 6.3:</b> Test results of ester content of biodiesel.....	42
<b>Table 6.4:</b> Diesel Specifications supplied from Tüpraş İzmir Refinery.....	45
<b>Table 7.1:</b> TGA/DTG Combustion reaction intervals, peak temperatures, and weight losses of combustion of pure samples under different heating rates.....	49
<b>Table 7.2:</b> TGA/DTG Combustion reaction intervals, peak temperatures, and weight losses of biodiesel-diesel mixtures under constant heating rate of 10 °C/min.....	51
<b>Table 7.3:</b> DSC Combustion reaction intervals, peak temperatures, and heat flows of combustion of pure samples under different heating rates; 5, 10, 15 °C /min .....	54
<b>Table 7.4:</b> DSC Combustion reaction intervals, peak temperatures, and heat flows of biodiesel-diesel mixtures under constant heating rate of 10 °C/min.....	55
<b>Table 7.5:</b> TGA/DTG Pyrolysis reaction intervals, peak temperatures, and weight losses of pure samples under different heating rates .....	58
<b>Table 7.6:</b> TGA/DTG Pyrolysis reaction intervals, peak temperatures, and weight losses of biodiesel-diesel blend samples under constant heating rate of 10 °C/min.....	60
<b>Table 7.7:</b> DSC Pyrolysis reaction intervals, peak temperatures, and heat flow of pure samples under different heating rates of 5°C/min, 10°C/min, and 15°C/min.....	62
<b>Table 7.8:</b> DSC Pyrolysis reaction intervals, peak temperatures, and heat flow of B100, B20, B15, B10, B05, and B00 mixtures at a constant heating rate of 10°C /min .....	64

<b>Table 7.9:</b> Ignition temperature calculation data.....	67
<b>Table 7.10:</b> Parameters used for kinetic models .....	73
<b>Table 7.11:</b> TGA/DTG Reaction equations and $R^2$ values of pure samples combustion curves .....	75
<b>Table 7.12:</b> TGA/DTG Activation energies of the combustion reactions.....	76
<b>Table 7.13:</b> TGA/DTG Arrhenius constants of the combustion reactions.....	76
<b>Table 7.14:</b> Average activation energies of pure samples of the 1 <sup>st</sup> order reaction rate assumption models .....	78
<b>Table 7.15-a:</b> TGA/DTG Reaction equations and $R^2$ values of mixtures combustion curves .....	79
<b>Table 7.15-b:</b> TGA/DTG Reaction equations and $R^2$ values of combustion curves .....	80
<b>Table 7.16-a:</b> TGA/DTG Activation energies of the combustion reactions .....	81
<b>Table 7.16-b:</b> TGA/DTG Activation energies of the combustion reactions .....	81
<b>Table 7.17-a:</b> TGA/DTG Arrhenius constants of the combustion reactions .....	82
<b>Table 7.17-b:</b> TGA/DTG Arrhenius constants of the combustion reactions .....	82
<b>Table 7.18:</b> TGA/DTG Reaction equations and $R^2$ values of pure samples pyrolysis curves .....	85
<b>Table 7.19:</b> TGA/DTG Activation energies of the pure samples pyrolysis reactions....	86
<b>Table 7.20:</b> TGA/DTG Arrhenius constants of the pure samples pyrolysis reactions...	86
<b>Table 7.21:</b> Average activation energies of pure samples of the 1 <sup>st</sup> order reaction rate assumption models .....	88
<b>Table 7.22:</b> TGA/DTG Reaction equations and $R^2$ values of mixtures pyrolysis curves .....	89
<b>Table 7.23:</b> TGA/DTG Activation energies of pyrolysis reactions .....	90
<b>Table 7.24:</b> TGA/DTG Arrhenius constants of the pure samples pyrolysis reactions...	90
<b>Table A.1:</b> Volatile fractions of petroleum sample chemical composition.....	104
<b>Table B.1:</b> TGA Instrument Characteristics.....	106
<b>Table B.2:</b> DSC Instrument Characteristics .....	109
<b>Table C.1:</b> $C_p$ (J/g°C) data of sapphire with respect to temperature.....	112

## NOMENCLATURE

### Abbreviations

TGA/DTG	: Thermogravimetry/ Differential Thermogravimetry
DSC	: Differential Scanning Calorimetry
BXX	: Volume (in percent) of biodiesel fuel in diesel-biodiesel blend

### Latin Symbols

A	: Arrhenius constant (pre-exponential factor), 1/min
$C_r/C_p$	: Heat capacity of reference sensor/sample, J/gr <sup>o</sup> C
$E_A$	: Activation energy, kJ/mol
k	: Specific rate constant, 1/min
n	: Order of reaction
q	: Heat flux, W/m
R	: Universal gas constant, 8.314 J/mole K
$R^2$	: Correlation coefficient
T	: Temperature, <sup>o</sup> C or K
$T_i$	: Ignition temperature of the samples, <sup>o</sup> C
$T_p$	: Inflection temperature of the reactions, K
t	: Time, min
$R_r/R_s$	: Thermal resistance of thermoelectric disc/sample, <sup>o</sup> C m/W
S	: Thermal displacement of sample, W/g
w	: Mass of sample remaining at the temperature of interest, mg

### Greek Symbols

$\beta$	: Heating rate, <sup>o</sup> C/min
$\theta$	: Temperature variable (T- $T_p$ ), K

# CHAPTER 1

## INTRODUCTION

Energy is considered as the main source of life and it is a key performance indicator used to determine the improvement level of a country quantitatively. Energy demands of the countries are usually supplied by the conventional sources such as petroleum, natural gas and coal. According to the statistical study of International Energy Agency, world's energy consumption has been drastically increased recently (Figure 1.1), and future projections imply that energy demand will continue to increase in the coming decades [1].

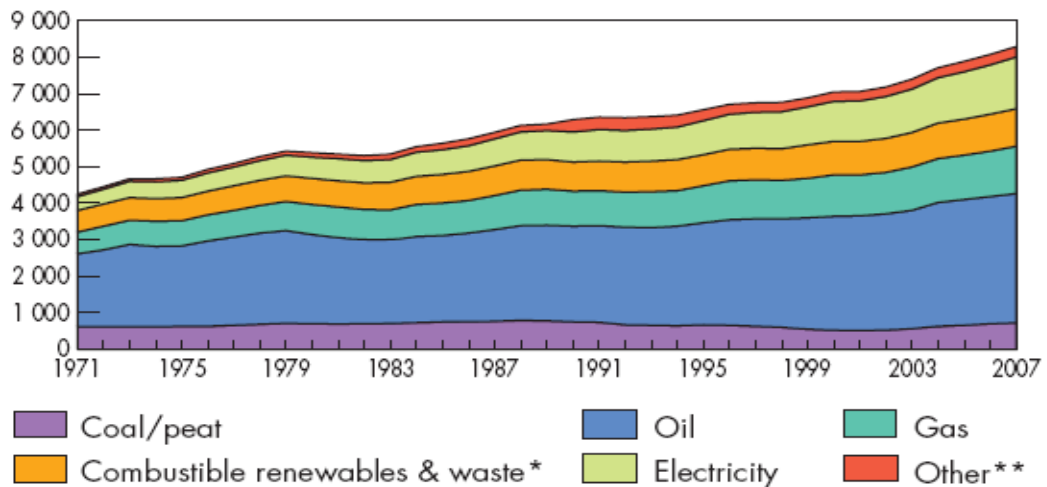


**Figure 1.1:** Evolution from 1971 to 2007 of world total final consumption by fuel (Mtoe) [1]

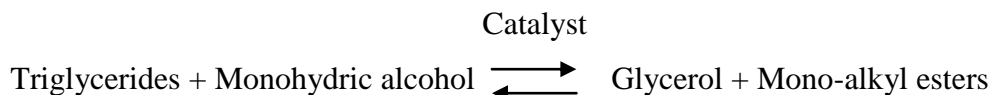
Increasing cost and the predicted reduction of conventional petroleum-derived fuels, appended to environmental pollution and global warming has encouraged searches investigating alternative fuels. Hence, biodiesel as a new energy source has been appealed to many researchers in the recent years and has been produced in several countries e.g. Germany, Italy, USA, France, Austria, and Czech Republic etc [2].

More than 100 years ago a brilliant inventor named Rudolf Christian Carl Diesel designed the original diesel engine to run on vegetable oil in 1900. Diesel was able to demonstrate that his engine ran perfectly well on vegetable oils. The idea behind that was to allow farmers to produce their own fuels to run their “diesel” engines. So, contrary to popular belief, the “diesel” engine was not developed to be fuelled exclusively with diesel fuel and was actually fed with vegetable oils for many years. This discovery was really important because diesel can be replaced by biodiesel only with small adjustment in engines, emission of almost zero sulfate and small contribution to CO<sub>2</sub> cycle [3].

Biodiesel is a cleaner-burning diesel replacement fuel, consisting of simple alkyl esters of fatty acids such as methyl and ethyl esters. It is a non-flammable, non-toxic, environmental friendly energy source [4]. Biodiesel is part of the family of biofuels and is produced from a biological source: vegetable oils and/or animal oils/fats [3]. When produced from vegetable oils, the terms vegi-diesel or vegi-fuel are also used, but to a lesser extent. Biodiesel can be used pure or blended with regular diesel fuel. ASTM International defines a biodiesel blend as: ‘ a blend of biodiesel fuel with petroleum-based diesel fuel.’ Biodiesel blends are often designated with the abbreviation of BXX, where XX represents the volume (in percent) of biodiesel fuel in the blend [5]. Thus, a blend of 80% diesel fuel and 20% biodiesel is designated as B20. A fuel consisting of pure biodiesel is designated as B100.

The process of converting vegetable oil into biodiesel fuel is called transesterification and is luckily less complex than it sounds. Chemically, transesterification is the process of using an alcohol (e.g. methanol, ethanol or butanol), in the presence of a catalyst,

such as sodium hydroxide or potassium hydroxide, to break the molecule of the raw renewable oil chemically into methyl or ethyl esters of the renewable oil, with glycerol as a by product [6]. If the reagent of the reaction is methanol then the biodiesel is called as “methanol route biodiesel”, if the alcohol agent is ethanol, the biodiesel is called as “ethanol route biodiesel”. The reaction mechanism is shown below.



A typical biodiesel molecule contains between 13 and 23 carbon atoms, approximately twice as many hydrogen atoms, and two oxygen atoms. Despite the fact that biodiesel is different from diesel regarding its chemical composition, it has many similar properties in terms of fuel characteristics. Therefore biodiesel becomes a strong candidate for replacing diesel [4,7]. The biodiesels are characterized and compared with diesel for their physical and fuel properties including density, viscosity, heating value, cetane number, cloud point, pour point and flash point [8]. In Table 1.1 some important characteristics of biodiesel and diesel and their generic values are given according to the researches done by some of the researchers.

**Table 1.1:** Comparisons of Diesel and Biodiesel Properties [3, 6, 9]

<b>Properties</b>	<b>Biodiesel</b>	<b>Diesel</b>
Density (g/ml)	0.87-0.89	0.84-0.86
Kinematic Viscosity (centi stoke)	3.7-5.8	1.9-3.8
Higher Heating Value (MJ/kg)	39.3-39.8	45.3-46.7
Cetane Number	46-70	47-55
Cloud Point (K)	262-289	256-265
Pour Point (K)	258-286	237-243
Flash Point(K)	408-423	325-350
Sulfur Content, ppm	0-0.1	10-125

Although higher heating value of biodiesel is 10% less than the diesel, cetane number of biodiesel is higher than diesel which shows that biodiesel burns more quickly than diesel. Cloud point and pour point of biodiesel is lower than diesel, so adding chemicals required to decrease these values. Also the flash point is higher than diesel, so that using blends of diesel and biodiesel is highly recommended [9]. Moreover biodiesel reduces the sulphate emission since it has less than 24 ppm sulphur in it which also shows that biodiesel is a more environmental friendly fuel.

In order to investigate the possibility of using biodiesel instead of diesel, a great deal of research has been in conduction by many researchers all around the world. Among the studies, thermal behaviour investigation of biodiesel and its blends with diesel is a new and search topic by using thermogravimetric methods. Although, thermogravimetry (TGA/DTG) and differential scanning calorimeter (DSC) in the petroleum derivatives have been widened among researchers, the application to biodiesel is quite new and promising technology [10].

In this study, thermogravimetric analysis of diesel, biodiesel, canola oil and biodiesel-diesel blends have been conducted by using TGA/DTG and DSC. Experiments are carried out under nitrogen and air atmosphere at different heating rates of 5, 10 and 15°C/min in order to search the fuels' pyrolysis and combustion properties. Experiment results have been analyzed by using the instruments software, *TA Universal Analysis*, in terms of the reaction regions, reaction peak temperatures, weight loss belonging to the reaction intervals, heat flows of the reaction and etc. Moreover, several kinetic methods, including differential and integral based approaches have been applied in order to calculate the kinetic parameters of the reactions. At the end of the analysis the kinetics of the reactions are presented and discussed in detail. Also, several thermal properties of the samples, namely ignition temperature and heat capacitance, have been calculated by using different approaches and equation derived by the researchers.

## **CHAPTER 2**

### **LITERATURE REVIEW**

Thermal analysis consists of a group of techniques in which a physical property of a substance is measured as a function of temperature, during the substance is subjected to a programmed temperature. There exist different types of thermal analysis; Differential Thermal Analysis (DTA), Differential Scanning Calorimetry (DSC), Thermogravimetry Analysis (TGA/DTG). Differential Thermal Analysis (DTA) is a technique in which the difference in temperature between the sample and reference pan is monitored against time and temperature while the temperature, in a specified atmosphere, is programmed. Differential Scanning Calorimetry (DSC) is a technique in which the difference in heat flow to a sample and reference pan is monitored against time or temperature, in specified atmosphere, is programmed. Thermogravimetry (TGA/DTG) measures the mass loss during the decomposition of the sample as it is being heated, or if the sample is held at a selected temperature. It is a technique in which the mass of a substance is measured as a function of temperature while the substance is subjected to a controlled temperature program.

In recent years the application of thermal analysis techniques to the investigation of the combustion behaviour and kinetics of oil has gained wide acceptance among research workers results indicated that oils can be categorized according to their oxidation characteristics. Bae [11] has searched the thermo-oxidative behaviour and fuel-forming properties of various crude oils using thermogravimetry (TGA/DTG). The results of the study have indicated that oils can be classified according to their oxidation

characteristics. No complete correlation could be established between viscosity, composition or density of the crude with the thermo-oxidative characteristics of the oil.

Vossoughi and El-Shoubary [12] applied differential scanning calorimetry (DSC) and thermogravimetry (TGA/DTG) to crude oil combustion in the presence of solid particles of various specific surface areas. According to the results of the study, the major transitions observed on the resulting curves have been classified into three groups, namely distillation, liquid hydrocarbon combustion and coke combustion.

Vossoughi and Bartlett [13] have developed a kinetic model of the in situ combustion process from data obtained from thermogravimetry (TGA/DTG) and differential scanning calorimetry (DSC). They used the kinetic model to predict fuel deposition and combustion rate in a combustion tube. Fuel deposition and combustion rate in a combustion tube are correlated well according to the predicted and observed experiment parameters.

Kamal and Verkocy [14] have used thermogravimetry (TGA/DTG) and differential scanning calorimetry (DSC) on two Lloydminster regions, heavy-oil cores, and extracted oils and mineral matter. TGA/DTG and DSC thermograms of two Lloydminster region cores and extracted oils obtained in inert gas of helium and air atmospheres have shown that at least three and usually 4 zones of chemical reactions are occurring in different temperature regimes. 1<sup>st</sup> zone is attributed to evaporation, distillation, thermolysis, and low-temperature oxidation (LTO), 2<sup>nd</sup> to distillation and thermal alteration of minerals, LTO, and combustion, 3<sup>rd</sup>/4<sup>th</sup> to pyrolysis, coking, polymerisation, mineral matter decomposition and combustion.

Kok [15] has characterized the pyrolysis and combustion properties of heavy crude oils by using two different types of crude oils. Results of the experiments have revealed that on combustion in air, three different reaction regions were determined, named as low-temperature oxidation, fuel deposition and high-temperature oxidation. Heat values and reaction parameters of crude oils have been determined by using the results of the DSC-

TGA/DTG curves. High-temperature oxidation region from the DSC and DTG curves have also been used to determine the kinetic data obtained from the. As the °API gravity of the crude oil decreases, higher activation energy values have been found.

Gonçalves et al. [16, 17] have used thermal analysis techniques (TGA-DTA/GC/MS) in order to investigate the thermal behaviour of asphaltenes from crude oil. Their approach is mainly based on kinetic studies of the thermal decomposition of asphaltenes under controlled temperature by thermogravimetry (TGA/DTG), determining the characteristics of volatile fractions by thermogravimetry and differential thermal analysis coupled with gas chromatography/mass spectrometry in the volatile recovered during the experiments. The coke formed has also been studied after being decomposed into smaller molecules using selective oxidation.

Kok and Karacan [18] presented the results of an experimental study on the determination of pyrolysis behaviour and kinetics of six crude oils by differential scanning calorimetry (DSC) and thermogravimetry (TGA/DTG). Crude oil pyrolysis indicated two main temperature ranges where loss of mass was observed. The first region between ambient and to 400°C was distillation. The second region between 400°C and 600°C was visbreaking and thermal breaking. It was observed that as crude oil gets heavier cracking activation energy increases. Activation energy of cracking also shows a general trend with asphaltene content.

Application of thermogravimetric analysis has also been common to vegetable oils, biomasses, biodiesel etc. in the recent years. Candeia et al. [19] evaluated thermal behaviour of B0, B5, B15, B25 and B100 biodiesel obtained from soybean oil by using TGA/DTA under air and nitrogen atmospheres. Under the nitrogen atmosphere, biodiesel exhibited similar behaviours as diesel with the advantage of emitting less harmful gases. On the other hand, under air atmosphere, during the main reaction zone evaporation/combustion of methyl esters of fatty acids of soybean oil take place as well as in diesel other components are evaporated/ combusted such as paraffins, naphthenes, olefins and aromatics.

Santos et al. [20] synthesized methanol route biodiesel from babassu biodiesel and analyzed its thermal behaviour by using TGA/DTG under air and nitrogen atmosphere at a heating rate of 10, 15, 20 °C/min. They observed that higher heating rates lead in shifted mass loss steps to higher temperatures. Babassu methanol biodiesel did not remarkably show different evaporation profile under different atmospheres. On the other hand under air atmosphere biodiesel exhibited more decompositions steps indicating more stable compound formation.

Souza et al. [21] also evaluated kinetic behaviour of cotton oil and methanol route biodiesel obtained from cotton oil similarly by using TGA/DTG. Whereas, under air atmosphere the samples displayed two or more reaction regions, under nitrogen atmosphere they displayed only one reaction region. Souza et al., also analyzed kinetic behaviour of cotton oil and biodiesel by using different methods such as Coast-Redfern, Madhusudanan, Van Krevelen and Horwitz-Metzger. Activation energy required for cotton oil to react is less than the biodiesel's activation energy under air. On the contrary, under nitrogen atmosphere cotton oil requires more activation energy compared to the biodiesel.

Pistachio shell biomass thermal characterization is investigated by Tonbul [22] by using TGA/DTG under nitrogen atmosphere with the heating rates of 5, 10, 15 °C/min. The pyrolysis behaviour of biomasses of different particle sizes (-0.600+0.250, -0.250+0.125,-0.125+0.71 particle size/mm) are characterized by using the kinetic methods Coast-Redfern and Flynn-Wall-Ozawa.

Commercial vegetable oils (olive, canola, corn, soybean, corn, sunflower) thermal decomposition under air atmosphere had also been investigated by simultaneous TGA/DTA with a constant heating rate of 10°C/min in order to explore the potentials of using them as fuel by Dweck et al. [23]. They concluded that as the lower is the thermal stability of oil, except corn oil (represented a very significant thermal behaviour), the higher is its heat of combustion.

Additionally, Garca et al. [24], has conducted a study in order to investigate the thermal decomposition of cerrado plant species. In that manner they studied the amburana, baru, pequi pulp and soybean oil under nitrogen and air atmosphere by using TGA/DTG. Thermal stability of the oils in nitrogen atmosphere showed similar behaviours due to their similar fatty acid compositions. However, pequi pulp oil showed the lowest thermal stability under air atmosphere most probably due to its larger amount of short chain fatty acids.

Conceicao et al. [25], have also investigated the kinetic behaviour of castor oil, ethanol route and methanol route biodiesel obtained from castor oil. TGA/DTG results were analyzed by using Coast-Redfern, Madhusudanan and Ozawa Methods. Methanol route biodiesel presented lower activation energy which can be expressed as methanol route biodiesel has better quality for combustion. On the other hand the thermal stability of the samples were in decreasing order of castor oil>ethanol biodiesel>methanol biodiesel.

Biodiesel's poor low temperature properties usually have been an obstacle against diesel. In order to investigate the cold properties of biodiesel, Dunn [26], made several experiments by using DSC under nitrogen atmosphere with a constant heating rate of 5°C/min from -60°C to +40°C. He used methyl soyate and methyl tallowate biodiesel and admixtures of it. According to the experiment results (melting, crystallization and freezing point temperatures), a regression model has been developed in order to estimate the cloud point (CP), pour point (PP), cold filter plugging point (CFPP) of biodiesel.

Hazra et al. [27] conducted several studies on linalyl acetate, clove oil and eucalyptus oil by using TGA/DSC in order to characterize their vapor pressure curves and calculate the k-value for Langmuir Equation. Moreover, activation energies and evaporation enthalpies of the samples were calculated and Clausius-Clayperon equation is derived for each of the samples tested.

Stenseng et.al [28], also applied TGA/DSC analysis to some of the biomass, coal and ash samples in order to investigate various aspects of combustion and gasification process such as: pyrolysis, char activity, ash melting behaviour and etc.

A different approach has been introduced by Han et al. [29] to thermal analysis research area, by calculating the ignition temperatures of the oil shale samples with the data gathered from TGA. The samples of 10 mg are heated in the nitrogen and pure oxygen mediums with different heating rates of 20, 40, 60 and 80°C/min.

Guo et al. [30] has investigated the delayed coking characteristics of petroleum residues and fraction by thermogravimetry. Five different petroleum samples obtained from different regions of China and their mixtures are exposed to TGA/DTG and kinetic properties of them have been calculated by using different methods. According to their research, the thermal cracking activity is in the order of saturates>aromatics>resins>asphaltenes as in the increasing order of carbon content of the samples.

Santos et al. [31] investigated thermal properties of mineral base lubricating oils by using DSC/TGA. According to TGA results, thermal stabilities of the lubricating oils have been determined. DSC enables them not only to predict the reaction mechanisms, but also to calculate the calorific heat capacities of the oils.

Gonçalves et al. [32] investigated the pyrolysis behaviour of different Brazilian petroleum fractions by using thermogravimetry by applying different heating rates. The activation energies for light and middle distillates within the range of 62-74 kJ/mole, and for heavy residues are within the range of 80-100 kJ/mole. They also claimed that the activation energies exhibit increasing tendency as the conversion level of the samples increase. Moreover, Gonçalves et al. [33] studied the thermal behaviour of five different atmospheric distillation residues (ATR) by applying TGA. Their study reveals that the heaviness of the crude oil has a great impact on carbonaceous residues formation during pyrolysis. The higher the crude oil, in other words, the lower the °API

of the crude oil the higher the amount of carbonaceous formation since the crude has higher amount of heavy aromatic hydrocarbon.

Kök et al. [34-37] used DSC in order to determine the combustion kinetics of oil shale by ASTM method. According to their study it is observed that higher heating rates result in higher reaction temperatures and higher heating rates of reactions. Furthermore, distinguishing peaks shift to higher temperatures as the heating rates are increased which is in consistent with the other studies done in this research area. They also applied TGA/DTG methods in order to investigate thermal characteristics and kinetic parameters of the oil shale samples. Activation energy values are found to be in the range of 131.8-185.3 kJ/mole by applying five different methods.

## CHAPTER 3

### STATEMENT OF THE PROBLEM

This study is conducted to determine the thermal characteristics and kinetics of biodiesel, diesel, canola oil and biodiesel-diesel mixtures at different blending rates in order to investigate the applicability of biodiesel as a new energy source instead of diesel by using thermogravimetric analysis methods.

Biodiesel, diesel, canola oil and blends of diesel and biodiesel at different percentages are exposed to isothermal heating under nitrogen and air atmosphere in order to analyze the pyrolysis and combustion behaviours respectively with a constant heating rate of 5°C/min, 10°C/min and 15°C/min by using TGA/DTG and DSC. Additionally, combustion and pyrolysis behaviour of canola oil, the origin of biodiesel are analysed to determine the transesterification reaction effect on biodiesel. Some of the experiments are performed at several times in order to test the reproducibility and reliability of the experiments.

Resulting curves of the experiments are analyzed by using *Universal Analysis* software in order to determine the reaction intervals, reaction interval, peak temperature, weight loss of the samples and heat flow of the reactions. In addition to that several kinetic methods are applied to determine the pyrolysis and combustion reaction parameters of the reactions such as  $E_A$ ,  $A$ . Moreover, by using the equations derived in literature, ignition temperature and heat capacitance of the samples are determined.

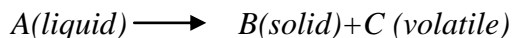
## CHAPTER 4

### KINETIC ANALYSIS AND METHODS

The kinetics of thermal decomposition reactions of carbonaceous materials is a complex as the process involves a large number of reactions in parallel and in series. Although TGA/DTG and DSC provides general information on the overall reaction kinetics, rather than individual reactions, it could be used as a tool for providing comparison of kinetic data of various reaction parameters such as temperature and heating rate. Other advantages include only a single sample, and few data are required for obtaining kinetics over an entire temperature range [38].

In this part kinetic models of the pyrolysis and combustion mechanisms of the TGA/DTG and DSC are reviewed.

The pyrolysis process may be represented by the following reaction scheme:



In order to determine the kinetic parameters, first order reaction kinetic is applied,

$$\frac{dx}{dt} = kf(x)^n \quad (4.1)$$

The rate of conversion,  $\frac{dx}{dt}$  for TGA experiment at constant rate of temperature change,

$$\beta = \frac{dT}{dt}, \text{ may be expressed by;}$$

$$\frac{dx}{dt} = \beta \frac{dx}{dT} = k(T)f(x) \quad (4.2)$$

Where x is the degree of advance defined by;

$$x = \frac{w_0 - w}{w_0 - w_f} \quad (4.3)$$

Where  $w$  is the weight of the sample at a given time  $t$ ,  $w_0$  and  $w_f$  refers to values at the beginning and the end of the weight event of interest.  $f(x)$  and  $k(T)$  are functions of conversion and temperature, respectively.  $k(T)$ , the temperature dependence of the rate of weight loss, is often modelled successfully by the Arrhenius equation [37, 39],

$$k(T) = A \exp\left(-\frac{E_A}{RT}\right) \quad (4.4)$$

Where  $E_A$ =Activation energy, kJ/mole,

$A$ =Pre-exponential factor or frequency factor,  $\text{min}^{-1}$

$R$ =Gas constant, 8.314 J/mole K

$T$ =Absolute temperature, K

$k$  is expressed as the specific reaction rate or rate constant. It is assumed to be only a function of temperature for liquid systems.

By combining Equations (4.1) and (4.3), reaction rate can be written in the form;

$$\beta \frac{dx}{dT} = A \exp\left(-\frac{E_A}{RT}\right) f(x) \quad (4.5)$$

**Energy of Activation ( $E_A$ ):** Is the barrier to energy transfer (from kinetic to the potential energy) between reacting molecules that must be overcome in order for a chemical reaction to occur (kJ/mole). If the reactants are free radicals that essentially react immediately on collision, there is not usually activation energy. However, for most of the atoms and molecules undergoing reaction there is activation energy.

**Arrhenius Constant ( $A$ ):** The frequency of collisions of molecules per second. (Pre-exponential factor, frequency factor,  $\text{min}^{-1}$ ) [39, 45].

In order to analyze the experimental data of TGA reaction kinetic methods are used commonly such as integral and differential methods by assuming  $f(x)$  based on different approaches.

The well-known methods; Arrhenius Method, Coats-Redfern Method, Ingraham-Marrier Method, Differential Method and Horowitz Metzger Method based on different assumption will be discussed in detail at the following section and the computer program will be developed for these methods.

#### 4.1 Arrhenius Method

This model assumes that [41] the rate of the total sample is dependent only on the rate constant, the mass of sample remaining ( $w$ ) and the temperature. The final form of the equation is as follows:

$$\log[dW/dt/w] = \log A - (E_A/2.303RT) \quad (4.6)$$

The plot of  $\log[dW/dt/w]$  versus  $1/T$  is plotted. The activation energy,  $E_A$  is obtained from the slope of the linear fit line which gives  $-E_A/2.303R$ . Also y-interception of the graph gives  $\log A$ , from which Arrhenius constant can be calculated.

#### 4.2 Coats-Redfern Method

Coats and Redfern [35] developed an integral method, which can be applied to TGA/DTG data, assuming the order of reactions. The correct order is presumed to lead to best linear plot, from which the activation energy is determined. The final form of the equation is [42]:

$$\ln(g(x)/T^2) = \ln(AR/\beta E_A) - E_A/(RT) \quad (4.7)$$

The plot of  $\ln(g(x)/T^2)$  versus  $1/T$  can be plotted by testing all the functions given in Table 4.1. The activation energy is obtained from the slope of the linear fit line which

gives  $-E_A / 2.303R$ . Also from the y- interception,  $\ln(AR / \beta E_A)$ , the Arrhenius constant can be obtained.

**Table 4.1:** Algebraic expressions of functions of the most common reaction mechanism [38, 46]

<b>Mechanism</b>	<b>f(x)</b>	<b>g(x)</b>
<b>Power Law</b>	$2 x^{1/2}$	$x^{1/2}$
<b>Power Law</b>	$3 x^{2/3}$	$x^{1/3}$
<b>Power Law</b>	$4 x^{3/4}$	$x^{1/4}$
<b>One dimensional diffusion model</b>	$1/2 x$	$x^2$
<b>Two-dimensional diffusion model</b>	$[-\ln(1-x)]^{-1}$	$[(1-x)\ln(1-x)]+x$
<b>Three-dimensional diffusion model</b>	$3(1-x)^{2/3}/[2(1-(1-x)^{1/3})]$	$1-(2x/3)-(1-x)^{2/3}$
<b>First-order reaction model</b>	$(1-x)$	$-\ln(1-x)$
<b>Second-order reaction model</b>	$(1-x)^2$	$(1-x)^{-1}-1$
<b>Third order reaction model</b>	$(1-x)^3$	$[(1-x)^{-2}-1]/2$

### 4.3 Ingraham-Marrier Method

Ingraham and Marrier [35] developed a simplified method for the determination of a heterogeneous reaction exhibiting linear kinetics. The rate constant,  $k$  may be expressed as  $dw/dt$ , where  $dw$  represents the loss in mass from unit area in the period of time  $dt$ .

$$\log(dw/dT) = -\log T - \log \beta + \log A - (E_A / 2.303 RT) \quad (4.8)$$

The plot of  $\log(dw/dT) + \log T + \log \beta$  versus  $1/T$  is plotted. The activation energy ( $E_A$ ) is obtained from the slope of the linear fit line which gives  $-E_A / 2.303R$ . According to this model, y-interception is  $\log A$ .

#### 4.4 Differential Method

One of the well known methods to identify kinetics of the samples is differential method. By using the Equations (4.1) and (4.4) to give [40,43];

$$dx/dt = Af(x) \exp(-E_A / RT) \quad (4.9)$$

The logarithmic form of the Equation 4.9 is taken to give;

$$\ln((dx/dt)/f(x)) = \ln A - E_A / RT \quad (4.10)$$

By using the experimental data from a single heating rate curve, a plot of  $\ln((dx/dt)/f(x))$  vs.  $1/T$  be obtained by testing the functions given in Table 4.1. The linear regression is calculated and then the activation energy and the Arrhenius constant can be calculated from the slope and intercept of the regression line.

#### 4.4 Horowitz Metzger

Horowitz and Metzger [44] derived the method by taking the integral of Equation 4.5 with the assumption of first order reaction approach. Therefore,  $\beta = dT/dt$  and first order reaction model,  $f(x) = (1-x)$  is assumed for  $n=1$ . After inserting these equations into Equation 4.5 and integrating both sides,

$$-\ln(1-x) = \int_0^T \frac{A}{\beta} \exp\left(-\frac{E_A}{RT}\right) dT \quad (4.11)$$

By defining a reference temperature,  $T_p$  at the point of inflexion of the reaction curve and changed the variable  $T$  to  $\theta$  using  $\theta = T - T_p$ . Hence the final form of their expression is,

$$\ln[-\ln(1-x)] = \left( \frac{E_A \theta}{RT_p^2} \right) \quad (4.12)$$

Thus, by plotting  $\ln[-\ln(1-x)]$  against  $\theta$ , the activation energy can be calculated from the slope,  $E_A/RT_p^2$ .

## CHAPTER 5

### PYROLYSIS MECHANISMS OF HYDROCARBONS

Pyrolysis is the breaking apart of chemical bonds by using thermal energy only. In other words, as energy is put into the larger molecules, the molecule breaks apart into the stable fragments. Analytical pyrolysis is the techniques of studying the molecules either by observing their behaviour during pyrolysis or by studying the resulting stable fragments. The analysis tells us the nature and the identity of the original larger molecule [47]. On the other hand, pyrolysis by thermogravimetric analysis is an analytical tool which helps us to determine the decomposition rate of reactions resulting from thermal effects and the kinetic parameters of these reactions [48].

Hydrocarbon pyrolysis has been an important research area in the industry since in the mid 1950s. It is one of the key processes of petrochemical industry, since it enlightens the investors as they are considering the economic feasibility of the projects. The historical development of pyrolysis is characterized by [49],

- a) continuously growing capacities of pyrolysis plants,
- b) increase of space-time yields in the overall process,
- c) an increase in ethylene severity,
- d) an improvement in energetic efficiency, especially by a better utilization of waste heat,
- e) the extension of running times,
- f) a wider range of feedstock flexibility
- g) expansion of feedstock basis toward high-boiling fractions.

## 5.1 Pyrolysis of Petroleum Products

In order to investigate the pyrolysis components of petroleum, Medeiros et al. [50] applied thermogravimetric analysis methods to ten different originated petroleum samples of 13.0-39.9°API range. MS/GC analyzer is used simultaneously with TGA analyzer and chromatography of the samples is used with the aim of obtaining paraffin-aromatic-naphthenic (PNA) content of the samples. Their main target was to proof that these methods can be used in substitution of distillation methods in petrochemical industry for petroleum fractions analysis in temperature range of 25°C to 150°C. As it is represented in Figure 5.1, GC/MS identifies the volatile fractions of petroleum and by using the ion chromatography PNA analysis is done (Figure 5.2). (For detailed GC/MS result see Appendix A, Table A.1)

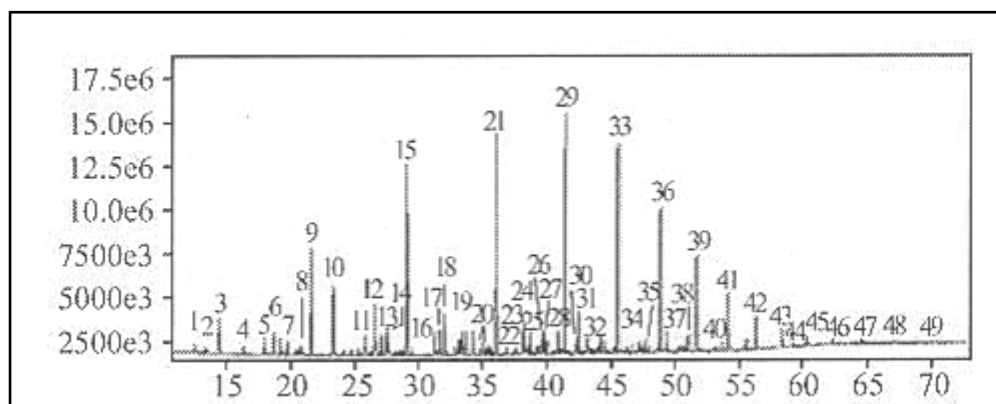


**Figure 5.1:** HRGC-MS total ion chromatogram and constituents identified in volatile fraction up 150°C of petroleum sample [50]

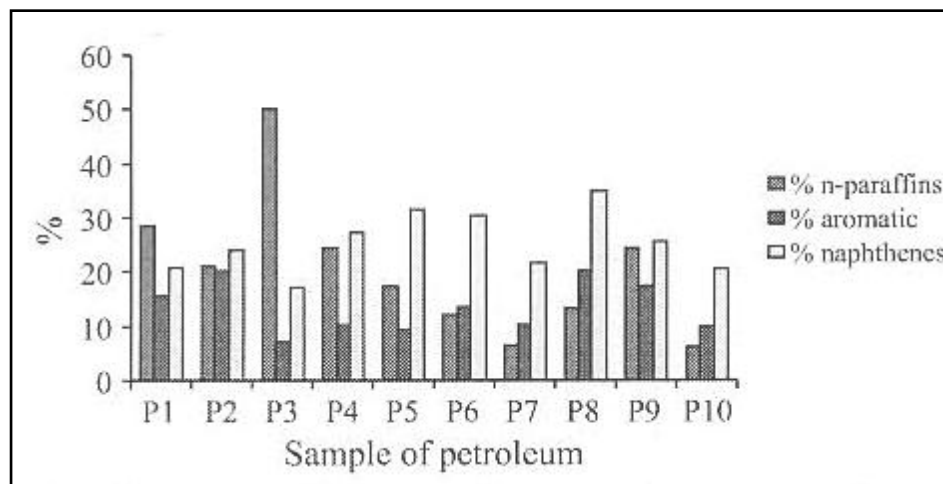


**Figure 5.2:** Normal paraffins, aromatics and naphthenes composition (%) at volatile fractions up 150 of different originated petroleum samples [50]

Gonçalves et al. [32] performed a thermogravimetric analysis in order to investigate the pyrolysis dynamics of petroleum fractions obtained from Brazilian crude of 19°API. Heavy residues from atmospheric (AR), vacuum residue (VR), heavy gas oil (HGO) which yields negligible amount of coke and light cycle oil (LCO) which is mainly contains C9 to C25 carbon mixture are exposed to different heating rates by using TGA/DTG analysis. On the other hand conventional distillation method ASTM D-2887 is applied in order to determine the boiling curves of the samples. (Table 5.1)

**Table 5.1:** Distillation curve of 19° API Brazilian crude oil fractions obtained by distillation standard methodology [32]

	LCO	HGO	AR	VR
Standard methodology	(a)	(b)	(b)	(b)
Distillation curve	<i>T/°C</i>			
Initial boiling point	200	239	242	386
2% (v/v)	242			
5% (v/v)	279	322	340	418
10% (v/v)	314	351	377	502
20% (v/v)	342			560
30% (v/v)	361	409	450	
40% (v/v)	379		513	
50% (v/v)	397	442	585	
90% (v/v)	495	524	660	
92% (v/v)	505			
95% (v/v)	526	543	684	
Final boiling point	595	591	715	569

In order to compare the conventional distillation curve results, the samples are heated from ambient temperature to 700°C under nitrogen atmosphere. TGA curves of the petroleum samples give the initial and final temperatures ( $T_{\text{onset}}$  and  $T_{\text{end}}$ ) and the lost mass and the volatile materials formed during the analysis. Besides, DTG peaks represent the maximum reaction rate temperature ( $T_{\text{max}}$ ). The results are shown in Table 5.2.

**Table 5.2:** TGA/DTG analysis of petroleum fractions [32]

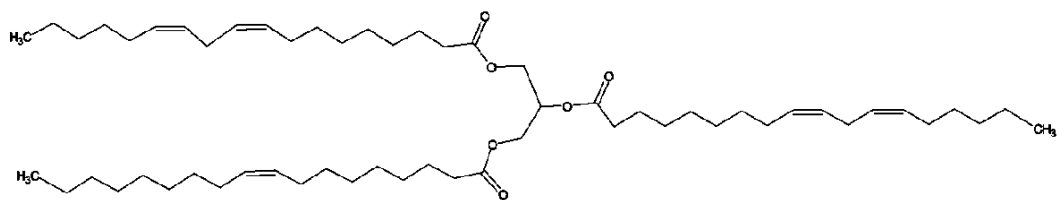
Sample	$T_{\text{onset}}/^{\circ}\text{C}$	$T_{\text{end}}/^{\circ}\text{C}$	Volatile material 35– 400°C % <sup>-1</sup>	Volatile material 35– 600°C % <sup>-1</sup>	Residue at 600°C % <sup>-1</sup>	DTG curve $T_{\text{max}}/^{\circ}\text{C}$
LCO	307	415	75	96	4	365
HGO	351	464	48	100	0	439
AR	420 (2 <sup>nd</sup> )	499	25	92	8	482
VR	452	513	3	84	16	488

Although the conventional distillation final points are in consistence with the TGA results ( $T_{end_{LCO}} < T_{end_{HGO}} < T_{end_{AR}} < T_{end_{VR}}$ ), VR exhibits different temperature profile. The reason is stated as carbon content of the material results in coke formation.

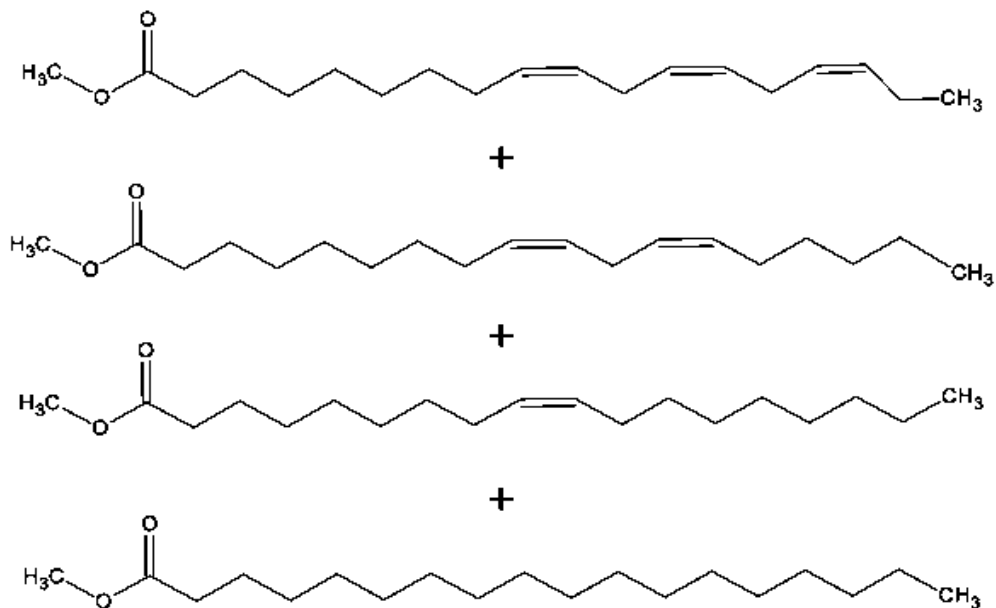
## **5.2 Biodiesel Pyrolysis**

Souza et. al [21] analyzed the quality of cotton oil and methanol route biodiesel obtained from the cotton oil by Gas Chromatography. The methyl ester composition in the cotton oil biodiesel is quite close to the original cotton oil composition and the overall amount of esters in biodiesel is 96.89%. According to the European standard EN1403 minimum methyl ester composition is determined as 96.50% which implies that the biodiesel has a better methyl ester composition.

Lima et al. [51] studied the pyrolysis mechanism of biodiesel obtained from edible soybean oil and soapstock by gas chromatography and mass spectrometry methods. Further characterization is made by using Fourier Transform infrared spectroscopy (FTIR). The molecular structure of the triglyceride, typical biodiesel and the pyrolysis molecules are given in Figure 5.3.



**Typical triacylglyceride**



**Traditional biodiesel**

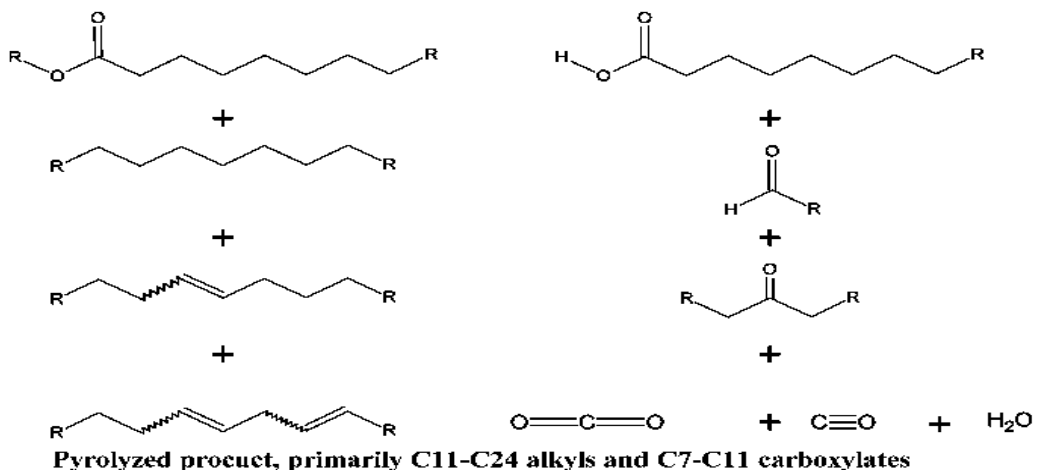


**Figure 5.3:** Structure of a triglyceride oil, biodiesel and the pyrolysis product [51]

Santos et al. [20] analyzed pyrolysis mechanism of babassu biodiesel obtained by methanol route by TGA/DTG and GC. The gas chromatography results indicate that the triglycerides are converted to methyl esters by 97.38%. Methyl laurate is the major constituent which is 25.81 wt%. The compositions of the acids are presented in Table 5.3.

**Table 5.3:** Composition of fatty acid in methanol babassu biodiesel [20]

<b>Numerical symbol</b>	<b>Systematic Name</b>	<b>Common Name</b>	<b>Fatty acid ester composition mass%</b>
C 6:0	hexanoic acid	caproic acid	0.37
C 8:0	octanoic acid	caprylic acid	3.81
C 10:0	decanoic acid	capric acid	5.63
C 12:0	dodenoic acid	lauric acid	25.81
C 14:0	tetradecanoic acid	myristic acid	17.27
C 16:0	hexadecanoic acid	palmitic acid	12.69
C 18:0	octadecanoic acid	stearic acid	19.36
C 18:2(9,12)	9,12-octadecadionic acid	linoleic acid	6.7
C 18:3(9,12,15)	9,12,15-octadecatrienoic acid	linolenic acid	0.15
		Others	5.78
<b>Total</b>			<b>97.38</b>

In addition to that, Conceição et al. [25] studied the GC of castor oil biodiesel which is obtained by both methanol and ethanol routes. Transesterification process resulted in 99.36% conversion of methyl esters and 99.60% of ethyl esters which is higher than the requested level 96.5% by the European standard EN 1403. (See Table 5.4)

**Table 5.4:** Ester composition of castor oil biodiesel  
(methanol and ethanol route) [25]

Ester	Methanol biodiesel,%	Ethanol biodiesel,%
Ricinolate	85.79	85.48
Stearate	4.88	1.17
Oleate	3.87	0.97
Palmitate	1.2	0.32
Linoleate	0.81	0.24
Linolenate	0.06	1.67
Others	2.75	9.75
<b>Total</b>	<b>99.36</b>	<b>99.6</b>

Dalai et al. [52] investigated the transesterification mechanism of canola biodiesel obtained by methanol and ethanol route using KOH as a catalyst. Using the GC/MS methods, they analyzed the ester composition of biodiesel and the spectra of the biodiesel are shown in Figure 5.4.

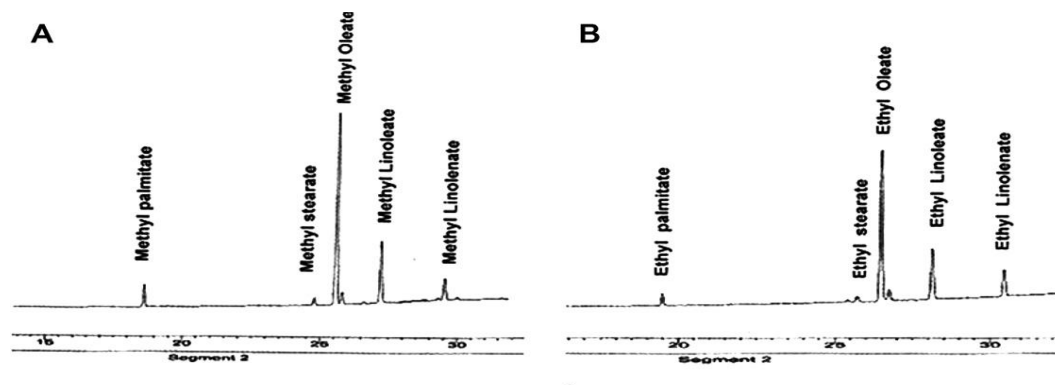


**Figure 5.4:** GC/MS spectra of esters showing presence of different fatty acid components, A: methyl esters, B: ethyl esters [52]

Herbinet et al. [53] investigated the rapeseed oil and soybean biodiesel obtained by methanol route transesterification mechanism. They have stated that, biodiesel is a complex mixtures mainly composed of five saturated and unsaturated methyl esters such as; methyl palmitate ( $C_{17}H_{34}O_2$ ), methyl stearate ( $C_{19}H_{36}O_2$ ), methyl oleate ( $C_{19}H_{34}O_2$ ), methyl linoleate ( $C_{19}H_{32}O_2$ ) and methyl linolenate ( $C_{19}H_{30}O_2$ ). The structures of these components are represented in Figure 5.5.

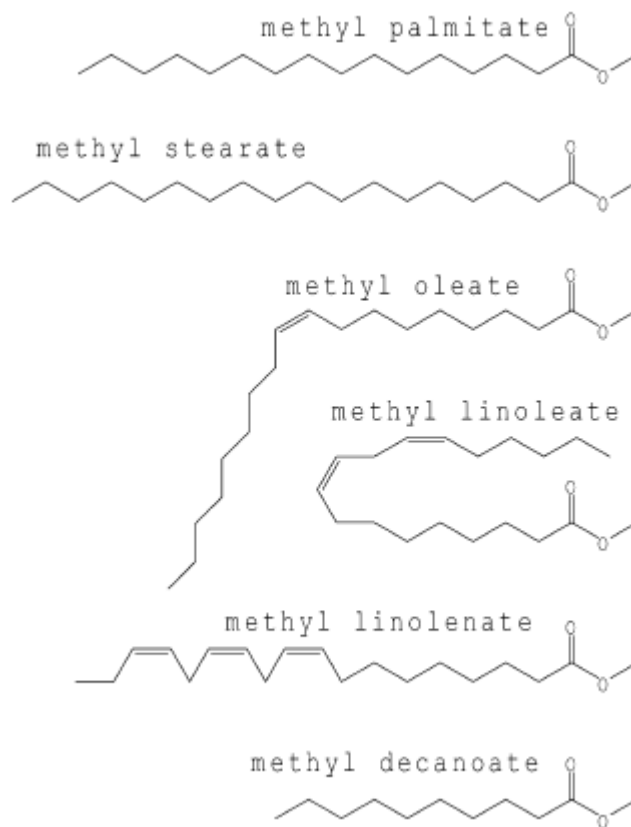


**Figure 5.5:** Structure of the main components of methyl esters

## **CHAPTER 6**

### **EXPERIMENTAL METHOD AND MATERIALS**

#### **6.1 Thermal Analysis**

##### **6.1.1 Thermogravimetric Analyzer (TGA)**

Thermogravimetric Analyzer (TGA) measures the amount and rate of weight change in a material, either as a function of increasing temperature, or isothermally as a function of time, in a controlled atmosphere (nitrogen, oxygen, argon, air etc.). It can be used to characterize any material that exhibits a weight change and to detect phase changes due to decomposition, oxidation, or dehydration. This information helps us identifying the percent weight change and correlate chemical structure, processing, and end-use performance. For the schematic view of TGA see Figure 6.1.

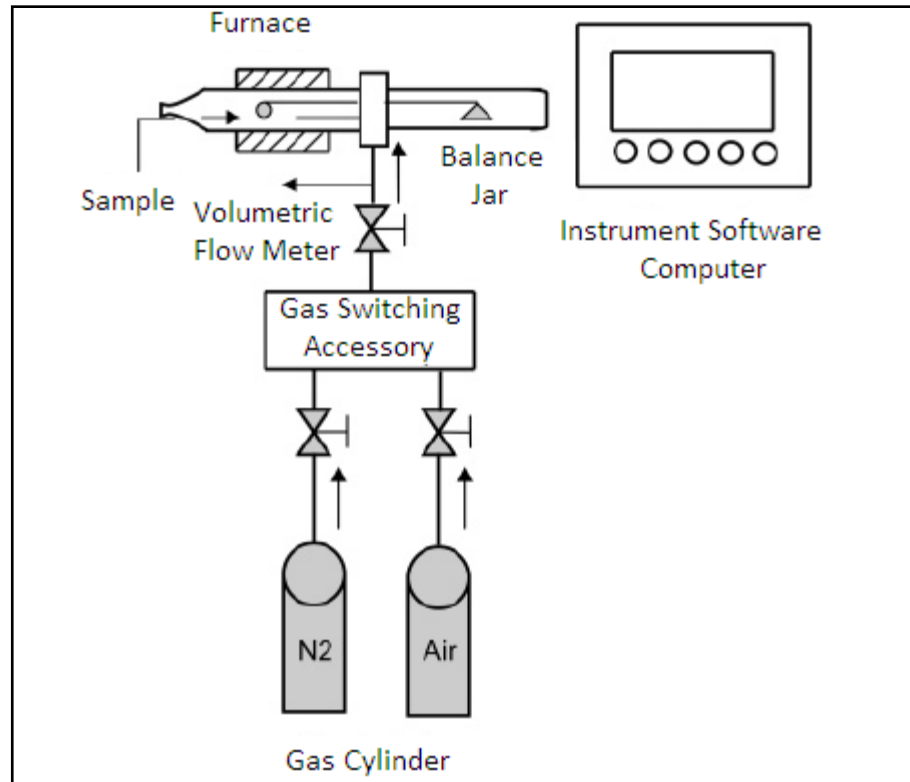


**Figure 6.1:** Schematic diagram of TGA

The TGA has six major components [54]:

- The balance, which provides precise measurement of sample weight. The balance is the key to the TGA system.
- The sample platform, which loads and unloads the sample to and from the balance.
- The furnace, which controls the sample atmosphere and temperature.
- The cabinet, where the system electronics and mechanics are housed.
- The heat exchanger, which dissipates heat from the furnace.
- TGA has two mass flow controllers, which control the purge gas to the balance and furnace.

Detailed characteristics of TGA Instrument are given in Table B.1 in Appendix B. (See Figure B.1 for detailed view of TGA)

### **6.1.1.1 Calibrating the TGA**

In order to obtain accurate experimental results TGA is calibrated depending on the type of experimental set-up applied. Two types of calibration are required for TGA: *temperature* and *weight* calibration [54, 55].

#### **6.1.1.1.1 Temperature Calibration**

Temperature calibration is useful for TGA experiments in which precise transition temperatures are essential. To calibrate the TGA in terms of temperature, it is needed to analyze a high-purity magnetic standard for its curie temperature, and then enter the observed and correct values in the temperature calibration table. The observed and correct temperatures correspond to the experimental and theoretical transition temperatures of the calibrant. Three different temperature calibration points (pairs of observed and correct temperature points) are entered in the calibration table. A multiple-point calibration is more accurate than a one-point calibration.

Steps of temperature calibration are;

- Determining curie temperature
- Analyzing data files for curie temperature
- Entering temperature calibration data

#### **i) Determining Curie Temperature**

According to ASTM Standards E1582-93, curie point of paramagnetic metals, is recommended for the TA Instruments TGA's. In this technique, a nickel Curie standard is heated in an alumina sample pan. A magnet is placed outside the TGA furnace so that it is just below the sample pan. As the nickel goes through its curie point, its attraction to the magnet changes, appearing as a weight loss. The onset of which is adjusted to agree with the material's known Curie point temperature.

## **ii) Analyzing Data Files for Curie Temperature**

The Curie temperature corresponds to the extrapolated endpoint on the “S” shaped thermal curve. This point is determined using the *Universal Analysis* software. A tangent line of downward sloping line and a tangent line to the baseline after the transition is occurred. The intersection of those lines corresponds to the curie temperature. (For the plot of temperature calibration curve of TGA see Figure B.2 of Appendix B.)

## **iii) Entering Temperature Calibration Data**

There is table named “temperature calibration table” in the menu of TGA. The data of “observed” and “theoretical” transition temperatures are stored in that table. Two temperature recordings are obtained and stored, nickel Curie temperature and room temperature.

Hence temperature calibration of TGA is completed.

### **6.1.1.1.2 Weight Calibration**

In order to perform the weight calibration of TGA, 1 mg, 100 mg and 200 mg of samples which are supplied by the kit of the TGA instrument are used. Before performing the calibration those samples are weighed by using other scale, the calibration parameters are stored internally in the instrument.

### **6.1.1.2 Experimental Procedure of TGA Analysis**

The steps of the procedure of a TGA experiment are described below.

- Before starting an experiment, appropriate pan type should be selected according to the temperature range and material type used in the experiment. Pan type is selected as platinum since it is easy to clean and does not react with most organics and polymers. Another reason of selecting this type is, platinum is durable up to 900°C temperature.
- Empty pan is tarred to ensure that the balance give us accurate readings.

- Approximately 20±2 mg of samples is placed in the sample pan, and pan is positioned on the sample platform.
- Experimental procedure is created using the instrument control software. The experiments are performed within the temperature range of 25-700°C, with a different heating rate of 5, 10 and 15°C/min.
- Attaching and setting up external accessories are required such as the purge and balance gas. Purge gas is selected as pure nitrogen and balance gas is selected according to the type of experiment performed. For the pyrolysis analysis, balance gas is selected as nitrogen and for combustion experiments air is used. Purge gas and balance gas flow rates are selected as, 80 ml/min and 120 ml/min accordingly.
- Other signals selected to be stored are as follows; temperature (°C), time (min), weight percent (%), balance and sample purge flow (ml/min), derivative weight amplitude (mg/min), activation energy (kJ/mole), Arrhenius pre-exponential factor (min<sup>-1</sup>).
- As the experiment starts, furnace closes down and the sample is started to be heated at a constant heating rate. Electronic signals are stored on instrument control software as the experiment is carried on.

### **6.1.2 Differential Scanning Calorimeter (DSC)**

Differential Scanning Calorimeter (DSC) measures heat flow associated with structure and changes in structure of materials as a function of time and temperature in a controlled atmosphere. These measurements provide quantitative and qualitative information about physical and chemical changes in a material.

In a "heat flux" DSC, the sample material, encapsulated in a pan, and an empty reference pan sit on a thermoelectric disk surrounded by a furnace. As the temperature of the furnace is changed (usually by heating at a linear rate), heat is transferred to the sample and reference through the thermoelectric disk. The differential heat flow to the sample and reference is measured by area thermocouples using the thermal equivalent of Ohm's Law [54]

$$q = \frac{\Delta T}{R_r} \quad (6.1)$$

Where,

$q$  = sample heat flow,

$\Delta T$  = temperature difference between sample and the reference,

$R$  = resistance of the thermoelectric disk

This simple relationship, however, does not take into account extraneous heat flow within the sensor or between the sensor and sample pan. The TA Instruments DSC's are specifically designed to account for those latter heat flows.

$$q = -\frac{\Delta T}{R} + \Delta T_0 \left( \frac{R_r - R_s}{R_r R_s} \right) + (C_r - C_p) \frac{dT_s}{dt} - C_p \frac{d\Delta T}{dt} \quad (6.2)$$

Where,

$\Delta T$  = measured sample temperature ( $T_s$ ) minus measured reference temperature ( $T_r$ )

$\Delta T_0$  = temperature difference between sample and the reference,

$T_0$  = temperature for control

$R_r$  = resistance of the thermoelectric disk

$R_s$  = sample sensor thermal resistance

$C_r$  = reference sensor heat capacity

$C_p$  = sample sensor heat capacity

The first term in Equation 6.2 is the equivalent of the conventional single-term DSC heat flow expression. The second and third terms account for differences between the sample and reference resistances and capacitances respectively. These terms have their largest impact during regions of the thermal curve where the heat capacity of the sample is the predominant contributor to heat flow. The fourth term accounts for the difference in heating rate between the sample and reference. This term has its largest impact during enthalpic events (e.g., melting).

DSC consists of mainly three components [54,56]:

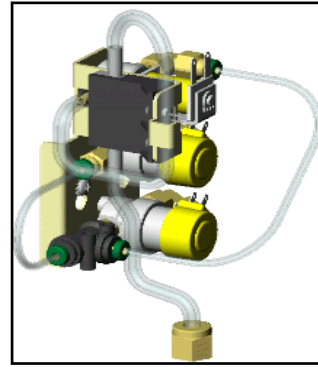
- *DSC Module (Base and cell)*: DSC cell uses a constantan (thermoelectric) sensor assembly as a primary heat flow element. A silver heating block, covered with a pair of vented silver lids, encloses the sensor assembly. The sample, contained in a sample pan, and an empty reference pan are placed on the sensor platforms. Heat is transferred from the furnace through the constantan sensor to both the sample and reference. Differential heat flow to the sample and reference is monitored by thermocouples, formed by welding discs to the underside of the constantan sensor platforms. These  $T_{zero}$  thermocouple measures the temperature of the base of the sensor. Sample temperature is determined by computing the  $\Delta T$  between the  $T_{zero}$  thermocouple and the sample thermocouple and adding that difference to the  $T_{zero}$  temperature. During experiments the cell is purged by a gas, which is preheated by circulation through the silver block before entry into the sample area. In addition, a base purge port circulates in the space below the cell to purge moisture from around the cell during cooling experiments with an air cool purge with the Finned Air Cooling System (FACS).

- *Mass Flow Controller*: Accurate and precise control of purge gas is important for obtaining good DSC results. A built-in Mass Flow Controller (MFC), with gas-switching capability is available for the DSC's. Flow rate is a selected parameter and the actual measured flow is automatically stored with each data point.

- *Cooling accessory*: The Finned Air Cooling System (shown to the left), also called the finned cooler, allows operation from ambient to 725°C, using flowing air as the coolant. An optional quench cool accessory can be used with the FACS for faster return to ambient. (See Figure 6.2 for the components of DSC).



a



b



c

**Figure 6.2:** Components of DSC; **a.** DSC Module **b.** Mass Flow controller, **c.** Cooling accessory (FACS) [56]

Detailed characteristics of TGA Instrument are given in Table B.2 in Appendix B.

### 6.1.2.1 Calibrating DSC

Calibration of DSC consists of two separate parts. T-Zero Calibration and Enthalpy/Temperature Calibration [54,56]:

#### **6.1.2.1.1 T-Zero Calibration (Cell Calibration)**

The DSC Tzero calibration requires two experiments. The first experiment is done without samples or pans (baseline); the second is performed with large (95 mg) sapphire disks (without pans) on both the sample and reference positions. Both experiments use the same method beginning with a cell preheat followed by an equilibration at an initial temperature, holding isothermal for 5 minutes, and heating at constant rate to a final temperature and holding isothermal for 5 minutes. The range of temperatures should be at least as broad as the desired experimental range. Tzero calibration is one at a heating rate of 20°C/min.

#### **6.1.2.1.2 Enthalpy/Temperature Calibration (Cell Constant)**

This calibration is based on a run in which a standard metal (*e.g.*, indium) is heated through its melting transition. The calculated heat of fusion is compared to the theoretical value. The cell constant is the ratio between these two values. The onset slope, or thermal resistance, is a measure of the suppression of temperature rise that occurs in a melting sample in relation to the thermocouple. Theoretically, a standard sample should melt at a constant heating rate. As it melts and draws more heat, a temperature difference develops between the sample and the sample thermocouple. The thermal resistance between these two points is calculated as the onset slope of the heat flow versus temperature curve on the front of the melting peak. The onset value is used for kinetic and purity calculations to correct for this thermal resistance. Temperature calibration is based on a run in which a temperature standard (*e.g.*, indium) is heated through its melting transition using the same conditions to be used in subsequent measures (*e.g.*, heating rate and purge gas). The recorded melting point of this standard is compared to the known melting point and the difference is calculated for temperature calibration. Up to five standards may be used for temperature calibration. A single-point calibration shifts the sample temperature by a constant amount. A two- or more-point calibration shifts the temperature by a constant amount below the first point, uses a

smooth curve through the calibration points and shifts by a constant amount after the last point.

### 6.1.2.2 Experimental Procedure of DSC Analysis

Steps of experimental procedure of DSC analysis are described below;

- *Selecting the most appropriate pan type:*

In order to perform reliable experiment with DSC, an appropriate pan type should be selected. The *Tzero low-mass aluminum pan* is selected since intended for small size samples that may benefit from the lower mass of the pan. The performance of the Tzero low mass pan is exceptional due to the precise flatness of the pan bottom and the contact of the lid to the upper and appropriate for the applications whenever volatiles generated by the sample during the experiment interfere with the transitions of interest. Hence Tzero Low-Mass Aluminium Pan is selected as the most appropriate one since the samples are liquid and volatile. (See Figure B.3 in Appendix B for the picture of the selected pan type and hermetic seal.)

In order not to damage the DSC cell during the experiments Tzero low mass pan and aluminium lid are pressed. Hence it is ensured that the sample to pan and sample to lid contact can be maximized and sealing mechanism is achieved. The maximum volume of the Tzero low-Mass Pan is 10  $\mu\text{L}$ . The maximum height of the sample is 0.51 mm (0.020 inches) and the average mass of the pan and lid is about 28.4 mg with a typical variability of 0.60%. The Tzero pans and lids are made of high purity aluminium and do not contain any intentional alloying elements. (See Figure B.4 of Appendix B for the squeezing equipment of DSC)

- *Loading the sample into the pan and loading that pan into the cell:*

$4\pm 1$  mg of sample is loaded into the pan selected and sealed with the lid. Sample pans are carefully placed on the right front raised platform and the reference pan on the left

rear platform. Centering the pans on platforms ensure that the sample will absorb equally distributed heat below.

- *Starting the experiment:*

In order to run experiments on DSC Analyzer, it is needed to specify a test procedure. During running the experiments, 25-600°C temperature range with a constant heating rate of 5, 10 and 15°C/min are selected depending on the experiment type. Also for pyrolysis experiments, nitrogen is selected as the purge gas, and for combustion experiments air is selected. Moreover, some signals are needed to be stored in order to analyze the experiment after it finishes. The signals selected are as follows; time (min), temperature (C), heating flow (W/mg), sample purge gas and flow rates (ml/min).

## 6.2 Materials

### 6.2.1 Biodiesel

Biodiesel can be obtained by transesterification process resulted by the reaction between an ester lipid and an alcohol in the presence of a catalyst (acid, basic or enzymatic) producing an ester (biodiesel) and a glycerine as a by-product. The goal of transesterification mechanism is to lower the viscosity of oil, as the physical characteristics of fatty acid methyl esters are close to those of diesel properties. Overall reaction mechanism is given in Figure 6.3 [57].

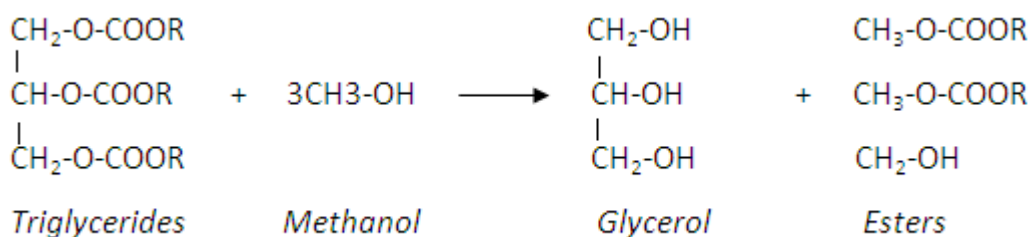
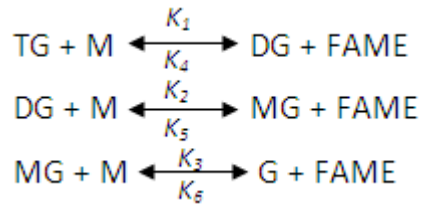


**Figure 6.3:** Overall transesterification reaction of biodiesel

Transesterification reaction mechanism consists of a sequence of three consecutive reversible reactions where triglycerides are converted to diglycerides; diglycerides are converted to monoglycerides followed by the conversion of monoglycerides to glycerol as shown the reaction steps below. In each step an ester is produced and thus three ester molecules are produced from one triglyceride molecule [57].



Where, TG, triglycerides; DG, diglycerides; MG, monoglycerides; M, methanol; FAME, fatty acid methyl esters. The values of rate constants for forward reactions; K1, K2 and K3 are reported to be as 5.00, 4.93 and 29.67 dm<sup>3</sup>/mole; for backward reactions K4, K5 and K6 are found to be 3.54, 2.99 and 0.79 dm<sup>3</sup>/mole.

In order to prepare biodiesel, conventional method is dissolving 1% catalyst (KOH) in alcohol (methanol or ethanol) with 1:6 oil:alcohol molar ratio. The reaction is stirred at room temperature for 30 min. After decantation process, the glycerine is removed and biodiesel is purified by wash water, biodiesel is dried and characterized. (See Figure 6.4)

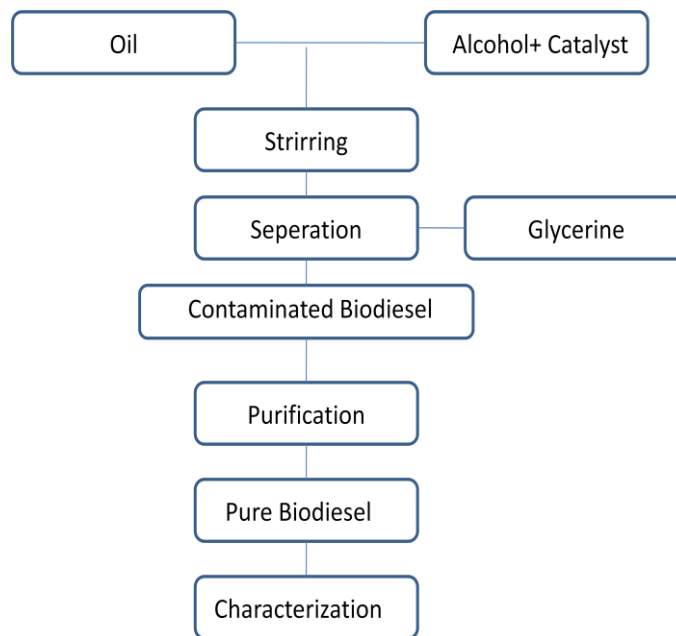


**Figure 6.4:** Basic production scheme of biodiesel [25, 58, 59]

Various feedstocks have been used in different countries as raw material. Soybean oil has been used in US and canola oil has been used in many European Countries whereas coconut oil and palm oils are used in Malaysia for biodiesel production. Type of the feedstock, molar ratio, catalyst type, stirring rate determine the yield of transesterification of biodiesel [57].

Some of the properties of biodiesel produced from different kind of feedstocks are presented in Table 6.1.

**Table 6.1:** Properties of biodiesel obtained from different origins [60, 61, 62, 63]

Source	Viscosity cSt at 40°C	Density g/ml at 25°C	Cetane number
Sunflower [60]	4.6	0.88	49
Soybean [61]	4.1	0.884	46
Palm [60]	5.7	0.88	62
Peanut [62]	4.9	0.876	54
Babassu [62]	3.6	-	63
Tallow [63]	3.6	-	58

Pure biodiesel and its blends with diesel; B5, B10, B15, B20 are analyzed by using thermogravimerty. Biodiesel, which is synthesized from canola oil by methanol route transesterification mechanism, is supplied by a biodiesel production firm named NewDizeline. Specifications of biodiesel used in the experiments are given in Table 6.2 which are supplied by the firm.

**Table 6.2:** Properties of methanol route canola oil originated biodiesel used in the experiments

Specifications	Unit	Guarantee Value DIN E 51, 606:1997
Molecular Weight	kg/kmole	295
Lower Heating Value	Mj/kg	37.1
Density (25°C)	Kg/m3	879
Kinematic Viscosity (40°C)	cSt	4.3
Cetane Number	-	>50
Sulphur	ppm	<10
Ignition Temperature	°C	148
Water Content	ppm	<300

In addition to that, biodiesel sample is subjected to transesterification analysis in order to measure the percent of ester in the biodiesel sample by Vitsan laboratory which is accredited by Turkish Accreditation Agency. The result of the test is presented in Table 6.3.

**Table 6.3:** Test results of ester content of biodiesel

<b>Test Name</b>	<b>Method</b>	<b>Unit</b>	<b>Result</b>
Ester Content	TS EN 14103	%	<b>97.60</b>

As it is stated in Chapter 5, according to European Standard EN1403, minimum ester content of biodiesel is 96.50%. Hence the biodiesel samples used during the experiments meet the requirements.

### **6.2.2 Canola Oil**

Canola, also known as rape, rapeseed is a bright yellow flowering member of the family plants called cruciferes (see Figure 6.5). It was developed in the 1970's by Canadian plant scientists who selected rapeseed populations looking for a crop that would produce a healthy, edible product. Rapeseed is not an edible product and canola is the name given to edible rapeseed. The word "canola" was derived from "**Canadian oil, low acid**" in 1978 [64]. The production of canola has been increased over the years, it comprises 12% of world oil seed production in 2006 [65].



**Figure 6.5: a.** Flower of canola **b.** Rapeseed of canola [66]

Canola oil has been widely used for the transesterification of biodiesel. Similarly, the biodiesel used as the sample for the experiments is produced from canola oil. Biodiesel's feedstock canola oil has also been supplied from the production firm, NewDizeline. Canola oil thermal investigation has been conducted by using thermogravimetric analysis methods (DSC/TGA).

### **6.2.3 Diesel**

Crude oil is a mixture of hydrocarbons with between 100,000 to 1,000,000 different molecules contributing to a boiling range of 20-538°C. (See Figure 6.6, for the fractions of crude oil)

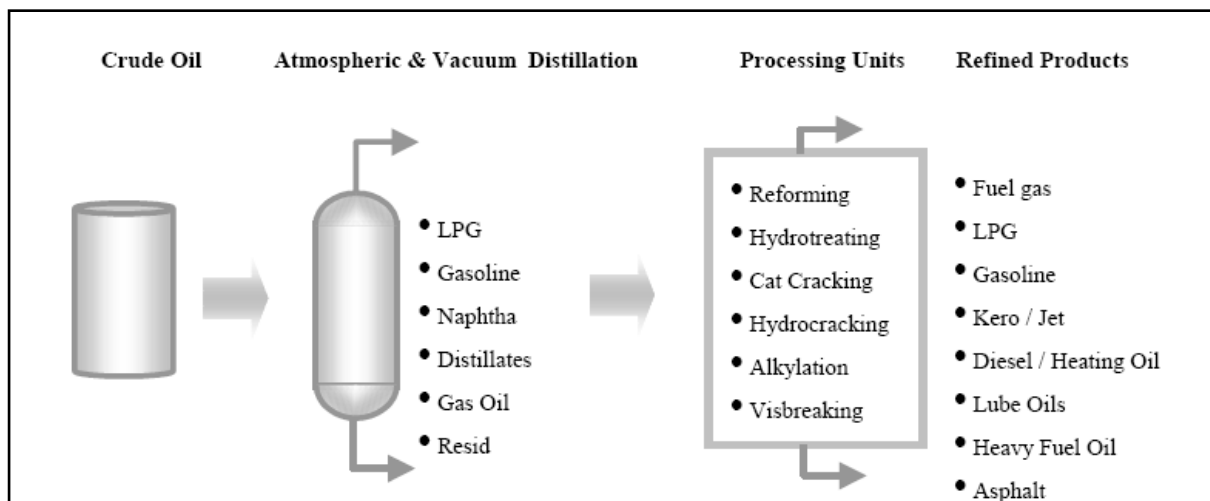


**Figure 6.6:** Fractions of crude oil and the refinery processes [67]

Diesel is termed as the middle distillate (has an ASTM boiling point range of of 176-371°C) which is obtained by both hydrocracking of gasoil and hydrotreating of distillate obtained from atmospheric and vacuum distillation processes. Diesel has been utilized for highway engine (75%), off-highway engine fuel, marine engines and railroad engines for several decades. The most important specifications of diesel fuels are cetane number, sulphur, and pour or cloud point. Cetane number is related to the burning quality of the fuel in an engine. The permissible sulphur content of diesel is being lowered (10 ppm) worldwide due to the environmental pollution concerns resulting from combustion of this fuel. Pour point or cloud point of diesel is related to the storage and handling properties of diesel and depends on the climatic conditions in which the fuel is being used [67, 68].

Diesel used in the experiments is supplied by Turkish Petroleum Refineries Corporation İzmir Refinery with the product specifications given in Table 6.4.

**Table 6.4:** Diesel Specifications supplied from Tüpraş İzmir Refinery

<b>Specifications</b>	<b>Unit</b>	<b>Guarantee Value</b>	<b>Test Method</b>
Density (15 °C)	kg/m <sup>3</sup>	820 - 845	EN ISO 3675
Flash Point (min)	°C	55	EN 2719
Polycyclic Aromatic Hydrocarbons (max)	wt%	11	EN 12916
Cold Filter Plugging Point (CFPP) (max)	°C	-15	EN 116
Sulphur (max)	ppm	10	EN ISO 20846
Viscosity (40 °C)	Cst	2.0 - 4.5	EN ISO 3104
Cetane Number (min)	-	51	EN ISO 5165
Water (max)	ppm	200	EN ISO 12937

# CHAPTER 7

## RESULTS AND DISCUSSION

In this chapter experiments performed by TGA/DSC under nitrogen and air atmosphere at different heating rates are presented and their results are discussed. Additionally, samples thermal properties namely ignition temperature and calorific heat capacitances are calculated by using the TGA and DSC results respectively. Moreover, experiment results are analyzed by kinetic methods defined in Chapter 4.

### 7.1 Combustion Experiments

Combustion experiments are performed under air atmosphere to biodiesel, diesel, canola oil and blends of diesel-biodiesel at different heating rates by using TGA/DTG and DSC. Experiment set consists of two main different parts; different heating rate application on pure samples and constant heating rate (10°C/min) application on different blending rate of biodiesel and diesel. The main purpose of 1<sup>st</sup> setup is to observe the effect of different heating rate on combustion and 2<sup>nd</sup> setup is to analyze the effect of blending biodiesel on combustion of diesel. Within the content of this part experiment results are given and results are discussed.

#### 7.1.1 TGA/DTG Experiments

TGA/DTG combustion mechanisms of hydrocarbon samples are complicated since too many different complex parallel and serial reactions take place as hydrocarbon chains have different number of carbons and different type of bonding. On the other hand,

combustion mechanisms of vegetable oils and bio-fuels are still under investigation as vegetable oils ingredients are varying according to their origins and reaction severities and conversion amounts of triglycerides to monoglycerides result in different combustion behaviours. According to literature [69], crude oil samples generally exhibit two combustion reaction regions such as LTO (low temperature oxidation) and HTO (high temperature oxidation) steps. During LTO step the mass loss of free moisture and volatile hydrocarbons such as alcohols, aldehydes, ketones, acids, and peracids take place [70, 71]. In HTO steps hydrocarbons molecules are fully oxidized by air. Bigger molecules are converted to smaller fractions and smaller molecules take the combustion reaction easily. This reaction step constitutes most of the exothermic heat of reaction when the crude oil is heated in an oxidizing environment [72]. However diesel combustion mechanism which will be discussed in detail does not exhibit two reaction intervals only one step which shows that as the crude oil is being refined, it loses its small volatile components and petroleum fractions are more homogenous fuels.

Within the scope of this study, TGA/DTG thermograms of samples are analyzed by using TA Universal Analysis® software in order to determine the reaction interval, peak temperatures and weight losses of the samples when they are exposed to different heating rates. In Figure 7.1 biodiesel combustion TGA/DTG curve analysis is presented. Similarly other experiment results have been analyzed and the results are tabulated in Table 7.1.

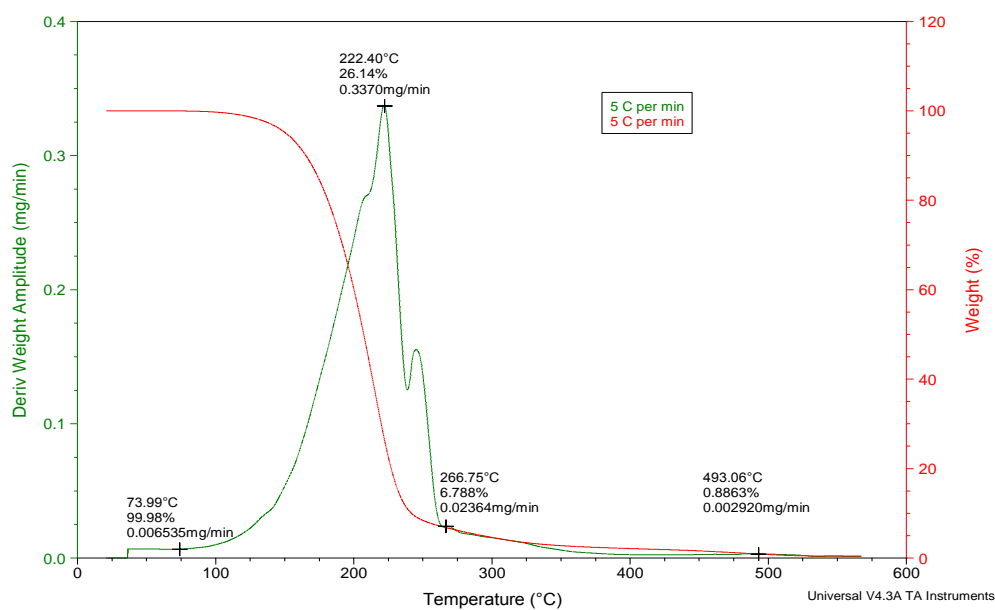


**Figure 7.1:** Biodiesel TGA/DTG combustion curve analysis at 5°C/min

Biodiesel combustion reaction takes place between 74-268°C with a mass loss of 99.11%, peak temperature is around 222°C under the heating rate of 5°C/min (Figure D.1, Appendix D). It is well known that as the sensitivity of the reactions decrease peak temperatures of the reaction increases with the scope of literature studies [76, 77]. Biodiesel combustion reactions also exhibit that, as the sensitivity of reactions decrease, i.e. the heating rate of the reaction increase, reaction intervals and the peak temperatures shift upper temperatures. Reaction intervals of 10°C/min and 15°C/min of biodiesel samples are 103-328°C and 110-301°C respectively, whereas peak temperatures are 254°C and 260°C. Also, recorded mass loss of the samples decrease as the heating rate of the experiments increase. Biodiesel samples loose their stability as the heating rate of the experiments increase. (Table 7.1)

**Table 7.1:** TGA/DTG Combustion reaction intervals, peak temperatures, and weight losses of combustion of pure samples under different heating rates

	$\beta$ , °C/min	Reaction Region, °C	Peak Temperature, °C	Weight Loss, %
Biodiesel	5	73.9 - 267.7	222.4	99.1
	10	103.4 - 328.1	253.7	98.92
	15	110.4 - 301.4	260.7	98.84
Diesel	5	42.7 - 241.7	161.5	99.90
	10	59.2 - 282.1	196.8	99.84
	15	79.7 - 313.8	220.9	97.62
Canola Oil	5	166.7 - 392.4	357.7	61.08
		392.4 - 565.3	414.7	34.77
	10	226.6 - 674.8	404.8	94.45
	15	260.9 - 516.9	408.9	93.84

Additionally, according to literature, methanol route biodiesel is mainly consists of ricinolic acid (around 85%), and boiling point of ricinolate is around 185-212°C [25]. TGA/DTG combustion reaction occurring with peak temperature of 222-254°C implies that dominant reaction taking place is the boiling of ricinolic acid firstly, after that one oxidative degradation of other esters takes place [2].

TGA/DTG thermogram of diesel combustion reaction occur between 43- 242°C having peak temperature of 162°C with mass loss of 99.9% under heating rate of 5°C/min. (See Figure D.2, Appendix D) Similarly, as the reaction rates increase reaction intervals shift upper (Table 7.1). Under the heating rate of 10°C/min and 15°C/min reaction peak temperatures are 196°C and 220°C with the mass loss of 99.84% and 97.63% respectively. This implies that under lower heating rate diesel burns better and leaves fewer constituents i.e. soot not burned out. Diesel is mainly consists of C5 to C12 with a boiling range of 176-371°C. As the diesel combustion reactions start around 50°C, diesel does not volatile up, it starts to burn and dissipate more energy to environment.

TGA/DTG curve of canola oil under air exhibits two distinct reaction regions at heating rate of 5°C/min. However, at other heating rates of 10°C/min and 15°C/min only one reaction region can be observed. As the reaction intervals are very close to each other, the sensitivity of the experiments are decreasing (heating rate is increasing) reaction regions are combining and only one reaction interval occurs. (See Figure D.3) Combustion reactions of canola oil occur at 10 and 15°C/min heating rate between 166-674°C attributed to the volatilization and combustion of triglycerides with mass loss of 94.45% and 93.84% respectively. On the other hand, under heating rate of 5°C/min, canola oil is less stable and combustion starts at 166°C. 1<sup>st</sup> reaction region ends at 392°C which is mostly volatilization of triglycerides and 2<sup>nd</sup> reaction region occurs between temperatures of 392-565°C, with a total mass loss of 96.85%. As the reaction intervals are analysed it is clearly seen that the peak temperatures of the reactions are increasing as the sensitivity of the reactions are decreasing (Table 7.1). In addition to that, it can be concluded that from Table 7.1 biodiesel represents lower combustion reaction region when compared to canola oil indicating that the transesterification reactions make biodiesel more ignitable.

In order to investigate the combustion behaviour of diesel and biodiesel mixture at different heating rates, B00, B05, B10, B15, B20 and B100 samples are exposed to heat under air with constant heating rate of 10°C/min. As the combustion thermograms of mixtures are presented in Figure D.4, mixtures combustion thermograms are very close to diesel since the volume percentage of diesel is higher than the biodiesel. In Table 7.2, combustion reaction parameters of biodiesel-diesel mixtures are given and the results show that the reaction intervals are very close to each other and weight losses are lower than the pure biodiesel. Among the blends of biodiesel and diesel, B05 and B10 show two different reaction regions. For B05 1<sup>st</sup> reaction interval takes place at 68-228°C and 2<sup>nd</sup> one takes at 228-287°C. Also for B10 1<sup>st</sup> reaction interval takes place between 64-207°C and 2<sup>nd</sup> one takes between 207-292°C. On the other hand, B15 and B20 only show one reaction region 67 -321°C and 68 -322°C respectively. This implies that B05 and B10 blends are not mixed at 100%, combustion reactions of diesel and biodiesel components take place separately. The peak temperatures of the separate reactions are

close to the pure samples peak temperature, which supports that 1<sup>st</sup> reaction interval combustion of diesel takes place and 2<sup>nd</sup> reaction interval biodiesel combustion occurs. On the other hand, B15 and B20 mixtures exhibit only one reaction interval, implying that the blends are mixed better. The reason of taking the combustion reaction together is that the biodiesel and diesel molecules perform a homogeneous mixture at 15 and 20% mixture of biodiesel. Hence it can be stated that for blending biodiesel in diesel, 15 and 20% is better than 5% or 10%. When the two combustion thermograms of B15 and B20 are compared, it can be stated that the weight loss of B20 is 95.84% and B15 is 99.32% implying that the B15 takes the combustion reaction better and the reaction starts earlier than the B20. This results in easier combustion in diesel engines.

**Table 7.2:** TGA/DTG Combustion reaction intervals, peak temperatures, and weight losses of biodiesel-diesel mixtures under constant heating rate of 10 °C/min

	$\beta, ^\circ\text{C}/\text{min}$	Reaction Region, $^\circ\text{C}$	Peak Temperature, $^\circ\text{C}$	Weight Loss, %
B00	10	59.2 - 282.1	196.8	99.84
B05	10	67.7 - 227.5	199.65	92.21
	10	227.5 - 287.2	242.3	3.62
B10	10	63.8 - 206.8	195.1	81.75
	10	206.8 - 291.8	239.4	15.25
B15	10	66.8 - 320.9	242.1	99.32
B20	10	68.3 - 321.9	244.0	95.84
B100	10	103.4 - 328.1	253.7	98.92

### 7.1.2 DSC Experiments

DSC combustion curves of hydrocarbon samples under oxidizing environment generally exhibit exothermic reaction configuration since the combustion takes place. As Aslı [73] mentions crude oil samples exhibit two reaction zones 1<sup>st</sup> one belongs to LTO region

and 2<sup>nd</sup> one stands for HTO combustion reaction. Additionally, crude oil samples demonstrate evaporation zone which is an endothermic process. In this study pure sample of biodiesel, diesel and canola oil demonstrate only one reaction interval zone implying that the components of the samples are homogenous and taking the reaction within the same temperature interval. The details of the DSC combustion experiments are discussed in detail at this part of the study.

In order to analyze the combustion behaviour of samples two sets of experiments have been conducted, at 1<sup>st</sup> one, pure samples are exposed to different heating rates of 5°C/min, 10°C/min and 15°C/min and in the 2<sup>nd</sup> part biodiesel and diesel mixtures are exposed to constant heating rate of 10°C/min. With the help of *Universal Analysis* software DSC curves are analyzed in terms of reaction interval, peak temperature, heat flow of the reactions. DSC curve analysis of biodiesel combustion at 5°C/min is given in Figure 7.2. On this plot area under the DSC curve gives the enthalpy change  $\Delta H$  (heat value) of the reaction. The calculation of the area under the curve is given in Equation 7.1;

$$\Delta H(J / g) = HeatFlow(W / g) \times Time(sec) \quad (7.1)$$

Sample: diesel  
Size: 5.0000 mg  
Method: Ramp  
Comment: diesel

DSC

File: C:\...\Ece-DSC\Yanma\Diesel\5 C per min  
Operator: Ece  
Run Date: 13-Nov-2009 12:20  
Instrument: DSC Q200 V23.5 Build 72

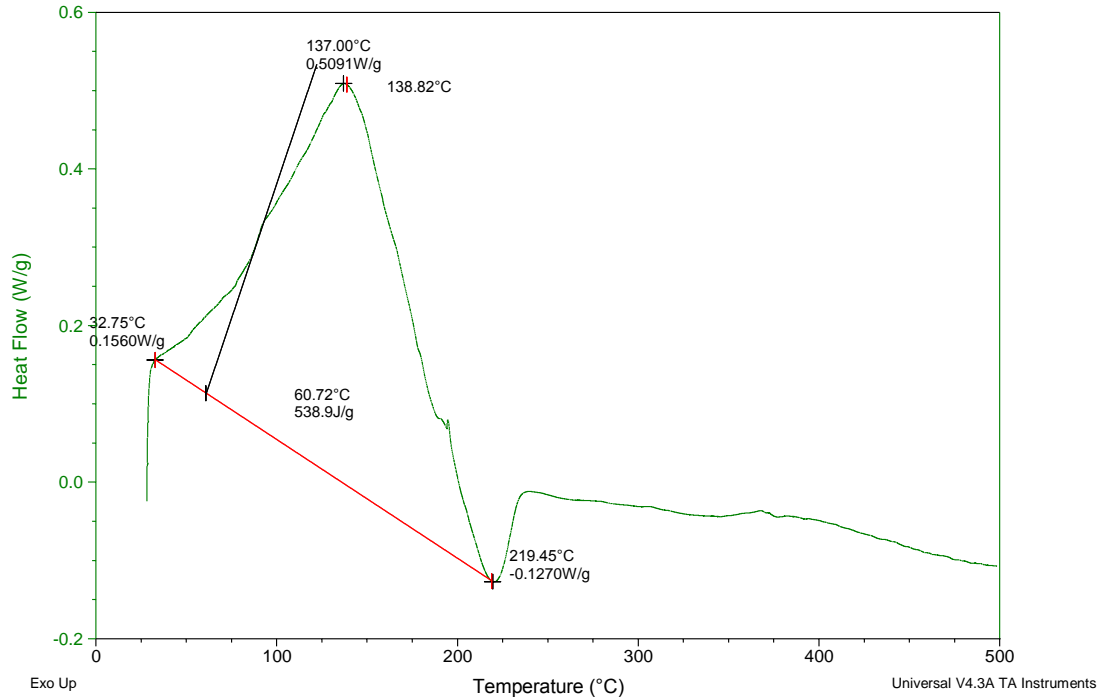


**Figure 7.2:** Analysis of diesel DSC combustion curve at 5 C/min

Similarly, other reaction curves are analyzed by using the software and the results are tabulated in Table 7.3. (DSC combustion curves of pure samples are represented in Appendix D in Figure D5-D7.)

**Table 7.3:** DSC Combustion reaction intervals, peak temperatures, and heat flows of combustion of pure samples under different heating rates; 5, 10, 15 °C /min

	$\beta$ , °C/min	Reaction Region, °C	Peak Temperature, °C	Heat Flow, J/gr
Biodiesel	5	27.9-240.0	199.9	457.0
	10	46.0-243.1	201.0	550.0
	15	46.9-250.3	202.4	569.7
Diesel	5	32.72-219.5	138.8	538.9
	10	32.8-227.9	147.2	592.3
	15	29.4-248.4	160.2	634.5
Canola Oil	5	307.7-468.6	358.9	501.3
	10	280.4-416.3	327.3	535.0
	15	318.5-461.6	361.8	718.6

As it can be seen from the Table 7.3, all of the reactions of pure samples are exothermic reactions dissipating heat to the surrounding. In addition to that, reactions of biodiesel occur at higher temperatures when compared to the diesel reaction intervals, which shows that the biodiesel is oxidized hardly when compared to diesel. This is a disadvantage of biodiesel since it results in hard burning in the engine of motors. In a particular motor engine higher cetane number fuels will have short delay times than lower cetane number fuels. Within the scope of DSC and TGA analysis it can be mentioned that cetane number of the biodiesel is lower than diesel and biodiesel has a time delay of burning leading to insufficient motor performance.

On the other hand, canola oil exhibits higher combustion enthalpies, but the reactions occur at very high temperatures which show that the cetane number of the canola oil is not sufficient to obtain the efficient combustion on engine motors. Moreover, the effect of heating rate can be clearly determined from the experiment results as the heating rate of the experiments increase, the peak temperatures of the reaction intervals shift to

upper levels. This phenomenon is being supported by the literature studies as well, as mentioned before.

Additionally, combustion kinetics of the mixtures of diesel and biodiesel at different volume percentages are analyzed by DSC analysis at constant heating rate of 10°C/min. Figures are represented in Figure D.8 of Appendix D and DSC curves reaction parameters are tabulated in Table 7.4.

**Table 7.4:** DSC Combustion reaction intervals, peak temperatures, and heat flows of biodiesel-diesel mixtures under constant heating rate of 10 °C/min

	$\beta, ^\circ\text{C}/\text{min}$	Reaction Region, $^\circ\text{C}$	Peak Temperature, $^\circ\text{C}$	Heat Flow, J/gr
B00	10	32.8-227.9	147.2	592.3
B05	10	28.0-228.9	136.5	476.7
B10	10	27.6-240.3	142.2	501.5
B15	10	35.5-235.2	155.3	585.7
B20	10	35.2-240.3	148.0	412.1
B100	10	46.0-243.1	201.0	550.0

Similarly, diesel-biodiesel combustion thermograms exhibit only one reaction region implying that the mixtures take the combustion reaction in one interval. Although TGA/DTG results of biodiesel-diesel mixtures of B05 and B10 exhibit two reaction regions as stated earlier, DSC results are implying that during the combustion of mixtures there is a continuous heat flow to surrounding (exothermic reaction flow) regardless of the weight losses of the samples. In addition to that as it can be concluded from Table 7.4, as the biodiesel is blended to diesel the heat dissipated by the exothermic reactions is decreasing except the B15 blending grade. B15 exhibits exothermic reaction of 585.7 J/gr of heat flow to surrounding which is relatively less than the pure diesel (which is 592.3 J/gr) but higher than the pure biodiesel and other blending grades. This result is consistent with the TGA/DTG results since B15 grade

exhibits higher combustion performance compared to the other grades according to TGA/DTG results as stated earlier. In addition to that, reaction interval of B15 grade is lower than the other grades implying that the cetane number of the grade is adequate to have efficient combustion performance on diesel engines.

## **7.2 Pyrolysis Experiments**

Pyrolysis mechanism of the fuels and samples play an important role since by using the experiment results the thermal stability of the samples can be characterized. Pyrolysis experiments are performed under nitrogen atmosphere to biodiesel, diesel, canola oil and blends of diesel-biodiesel at different heating rates by using TGA/DTG and DSC. Experiment set consists of two main different parts; different heating rates on pure samples and constant heating rate (10°C/min) on different blending rate of biodiesel and diesel. As in the case of combustion experiment set-up, the main purpose of 1<sup>st</sup> setup is to observe the effect of different heating rate on pyrolysis mechanism and 2<sup>nd</sup> setup is to analyze the effect of blending biodiesel on pyrolysis of diesel. Within the content of this part experiment results are given and results are discussed.

### **7.2.1 TGA/DTG Pyrolysis**

By using TGA pure samples and blends are analyzed and the results are given in this chapter and discussed.

Biodiesel TGA/DTG pyrolysis thermogram of 5°C/min heating rate is given in Figure 7.3, on which the reaction parameters can be determined as well. Biodiesel pyrolysis thermograms of different heating rates are represented in Figure E.1 in Appendix E at different heating rates of 5°C/min, 10°C/min and 15°C/min. The reaction parameters of the other pure samples TGA/DTG curves are analyzed and tabulated in Table 7.5.

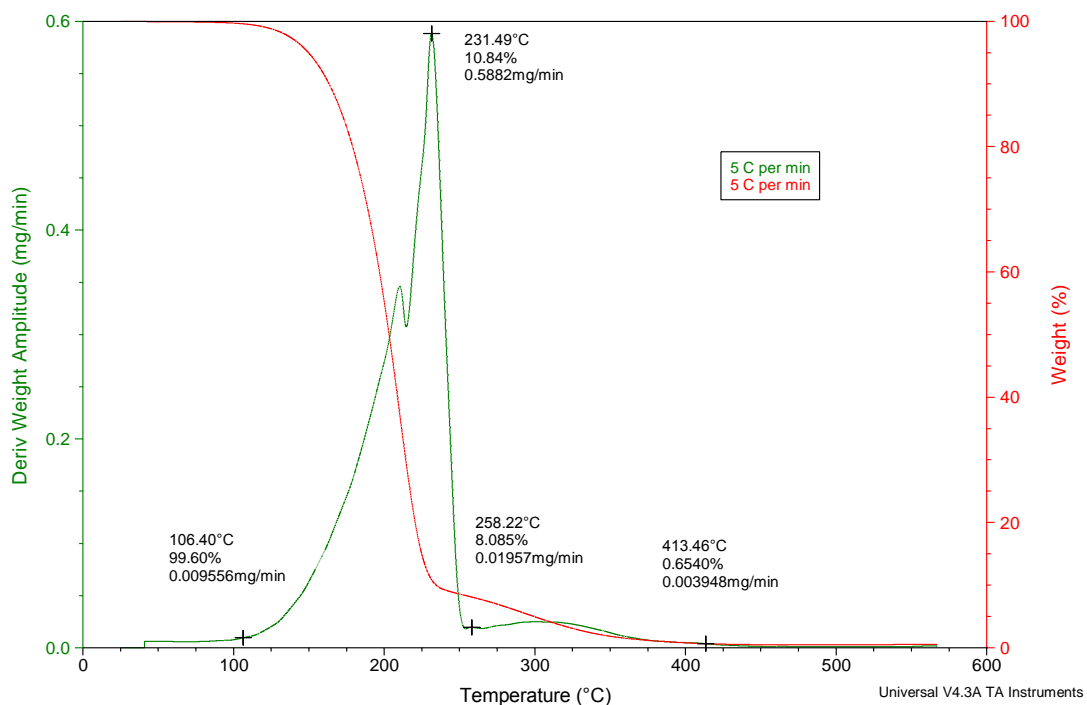


**Figure 7.3:** Analysis of biodiesel TGA/DTG pyrolysis curve at 5°C/min

As it can be seen from Table 7.5, biodiesel starts to decompose under nitrogen atmosphere with heating rate of 5°C/min around 106°C and pyrolysis reaction ends at 231°C with a peak temperature of 231°C. As the heating rate increases sensitivity of the reactions taking place decrease and reaction intervals shift up with the mass loss amount decreases. Biodiesel pyrolysis reactions showing only one mass loss step are endothermic reactions of which decomposition of methyl esters occurs. Firstly oxygen bonds are broken and C11-C24 alkyls are formed and remaining molecules form C7-C11 carboxylates also water vapour forms as by product [19].

**Table 7.5:** TGA/DTG Pyrolysis reaction intervals, peak temperatures, and weight losses of pure samples under different heating rates

	$\beta$ , °C/min	Reaction	Peak	Weight
		Region, °C	Temperature, °C	Loss, %
Biodiesel	5	106.4 - 258.2	231.5	99.35
	10	112.3 - 305.4	252.6	99.22
	15	151.7 - 364.9	277.8	98.56
Diesel	5	41.6 - 230.4	158.2	99.94
	10	62.0 - 280.9	201.4	98.82
	15	88.03 - 317.8	207.1	98.62
Canola	5	269.6 - 494.2	409.5	99.59
Oil	10	294.0 - 522.6	437.4	99.17
	15	320.2 - 529.5	458.4	98.56

As it can be seen from Figure E.2 diesel samples pyrolysis reactions takes similarly only at one step and reaction interval at 5°C/min heating rate occurs between 42°C and 230°C, with peak temperature of 158°C. As the sensitivity of reactions decrease reactions occur at higher temperature intervals (Table 7.5).

When diesel is exposed to constant heating under nitrogen atmosphere, it decomposes around 42°C which is relatively earlier when compared to the biodiesel. Similarly peak temperatures are lower than the biodiesel and weight losses are more than the diesel samples. This implies that biodiesel is more stable than diesel, the methyl ester molecules cannot be decomposed easily when compared to saturated hydrocarbon molecules of diesel.

When canola oil is exposed to constant heating rate under nitrogen atmosphere, it exhibits one reaction step between 270-494°C with a peak temperature of 410°C. (Figure E.3) When compared to biodiesel, canola oil is more stable than biodiesel since it is not decomposed until 270°C. (Table 7.5) Hence it can be inferred that

monoglyceride molecules make the sample less stable, transesterification reaction mechanism makes the substance less stable. Decomposition step of the canola oil can be attributed to decomposing triglyceride molecules and small molecules. Similarly, as the sensitivity of the reaction mechanisms decrease (as the reactions get faster) reaction intervals shift to upper temperatures. Also reaction intervals becomes more significant and derivative of weight loss at the peak temperature gets higher compared to the more sensitive reaction interval's.

Biodiesel and diesel mixtures are analyzed at a constant heating rate of 10°C/min under nitrogen atmosphere and the pyrolysis thermograms are presented in Figure E.4. As it can be seen from the thermograms, pure samples show only one reaction region and biodiesel exhibits a higher derivative of weight loss compared to diesel at its peak temperature. On the other hand, blends of biodiesel and diesel represents two reaction regions showing the non-homogenous mixture effect on pyrolysis mechanisms. At 1<sup>st</sup> reaction region diesel is decomposed and at 2<sup>nd</sup> reaction region biodiesel pyrolysis takes place.

The pyrolysis reaction mechanisms of TGA/DTG results analyzed and results are given in Table 7.6. It can be inferred that as the mixing content of biodiesel increases the reaction intervals shifts to lower temperatures. Moreover as the biodiesel content of mixtures increase mass loss of the 1<sup>st</sup> reaction region weight loss percentage increase when compared to the 2<sup>nd</sup> region, i.e. 2<sup>nd</sup> reaction interval becomes more dominant. As a result of that analysis, it can be concluded that the biodiesel mixing to diesel make the fuel more stable against heat.

**Table 7.6:** TGA/DTG Pyrolysis reaction intervals, peak temperatures, and weight losses of biodiesel-diesel blend samples under constant heating rate of 10 °C/min

	$\beta$ , °C/min	Reaction Region, °C	Peak Temperature, °C	Weight Loss, %
B00	10	62.0 - 280.9	201.4	98.82
B05	10	65.5 - 223.5	195.1	96.42
	10	223.5 - 279.3	238.3	2.17
B10	10	64.4 9- 206.5	195.1	86.25
	10	206.5 - 286.1	238.2	13.24
B15	10	63.5- 204.7	194.5	81.68
		204.7 - 283.8	238.3	16.83
B20	10	62.46 - 204.8	189.4	66.67
		204.8 - 286.7	237.8	32.29
B100	10	112.3 - 305.4	252.6	99.22

As it is stated earlier, for the combustion experiments B15 mixture makes the fuel ignitable better compared to the other grade mixtures. When the pyrolysis reaction results are examined it is realized that the B15 mass loss is around 94.92% whereas B20 mass loss is around 98.96%. This mass loss difference implies that B20 decomposes further than B15. So that it can be inferred that B20 is less stable than B15 which is consistent with the reaction intervals shifting lower temperature deduction as stated above. On the other hand mass loss of B10 is 99.49% which means that almost the entire sample decomposes under heating. Similarly B05 mass loss is around 98.59% close to B10. However B15 mass loss is around 94.92%, so that this grade blend is more stable than the others as a fuel.

### 7.2.2 DSC Pyrolysis Experiments

In order to analyze pyrolysis mechanisms, pure samples and mixtures of biodiesel and diesel are exposed to constant heating under nitrogen atmosphere. Under air atmosphere

samples exhibit exothermic reactions, which mean that the samples are oxidized. On the other hand under nitrogen atmosphere samples exhibit endothermic reactions, in other words samples take heat from surrounding in order the molecules to be cracked.

DSC thermograms of crude oil samples usually exhibit a slow reaction interval implying that the distillation of small molecules take place and a relatively dominant reaction interval of main cracking reactions [73]. On the other hand, biodiesel and diesel usually do not exhibit any distillation region only cracking reaction occurs [2].

DSC curves of pyrolysis of biodiesel are shown in Figure E.5 for different heating rates. The curves exhibit similar trends and the molecules start to crack at around 70-80°C. The first reaction interval is endothermic showing that the monoglyceride molecules absorb heat from the surrounding in order to be cracked. As it is stated before, biodiesel does not require any heat in order for the small fractions to volatile since biodiesel is also homogenous organic fuel type. Second reaction region states for an exothermic reaction interval which implies that the cracked molecules are some heat is dissipated to surrounding after the cracking of molecules. During the endothermic reaction region oxygen bonds are broken and C11-C24 alkyls are formed and remaining molecules form C7-C11 carboxylates [19]. See Figure 5.3 for the sequence of reactions taking place [51].

Reaction intervals are analyzed by taking the integrals of the area under the reaction curves so that the reaction enthalpies are calculated as J/gr and the results are given in Table 7.7. First reaction step requires around 160-200 J/gr in order for the oxygen bonds to be cracked. During the second reaction interval water vapor molecules form and enthalpy of the reaction is around 80-100 J/gr.

**Table 7.7:** DSC Pyrolysis reaction intervals, peak temperatures, and heat flow of pure samples under different heating rates of 5°C/min, 10°C/min, and 15°C/min

	$\beta$ , °C/min	Reaction	Peak	Heat
		Region, °C	Temperature, °C	Flow, J/gr
Biodiesel	5	81.9 - 277.6	226.7	159.69
		277.6 - 549.4	445.8	80.2
	10	70.6 - 297.5	224.5	197.9
		297.5 - 554.5	469.7	102.9
	15	92.2 - 275.9	237.0	206.1
		275.9 - 563.6	491.4	103.5
Diesel	5	33.2 - 220.7	155.7	291.1
	10	33.6 - 251.9	182.0	309.7
	15	58.1 - 262.2	194.0	398.9
Canola Oil	5	333.2 - 393.5	380.8	29.59
		393.5 - 539.7	474.1	860.6
	10	386.1 - 434.2	406.5	192.5
		434.2 - 551.6	488.8	1130
	15	395.8 - 432.7	413.0	81.9
		432.7 - 560.2	493.0	854.8

DSC pyrolysis reaction thermogram of diesel at 5°C/min is represented in Figure 7.4 with the reaction parameters calculated on the curve. Moreover, remaining DSC pyrolysis curves are given in Figure E.6. Thermograms indicate that there are not any small fractions of diesel volatilising, only one step endothermic cracking reaction occurs. This endothermic cracking reaction can also be declared as the distillation of the diesel which takes place around 34-260°C. Required heat for that reactions to take place is around 290-390 J/gr (Table 7.7). As it can be stated from the Table 7.7 as the heating rate of experiments increases the sensitivity of the reactions loose and the required heat for the reactions calculated as higher than the lower heating rate experiments.

Sample: Diesel  
Size: 20.0000 mg  
Method: Ramp  
Comment: Diesel Piroлиз (5 C/min)

DSC

File: C:\...\Ece-DSC\Piroлиз\Diesel\5 C per min  
Operator: Ece  
Run Date: 09-Nov-2009 12:17  
Instrument: DSC Q200 V23.5 Build 72

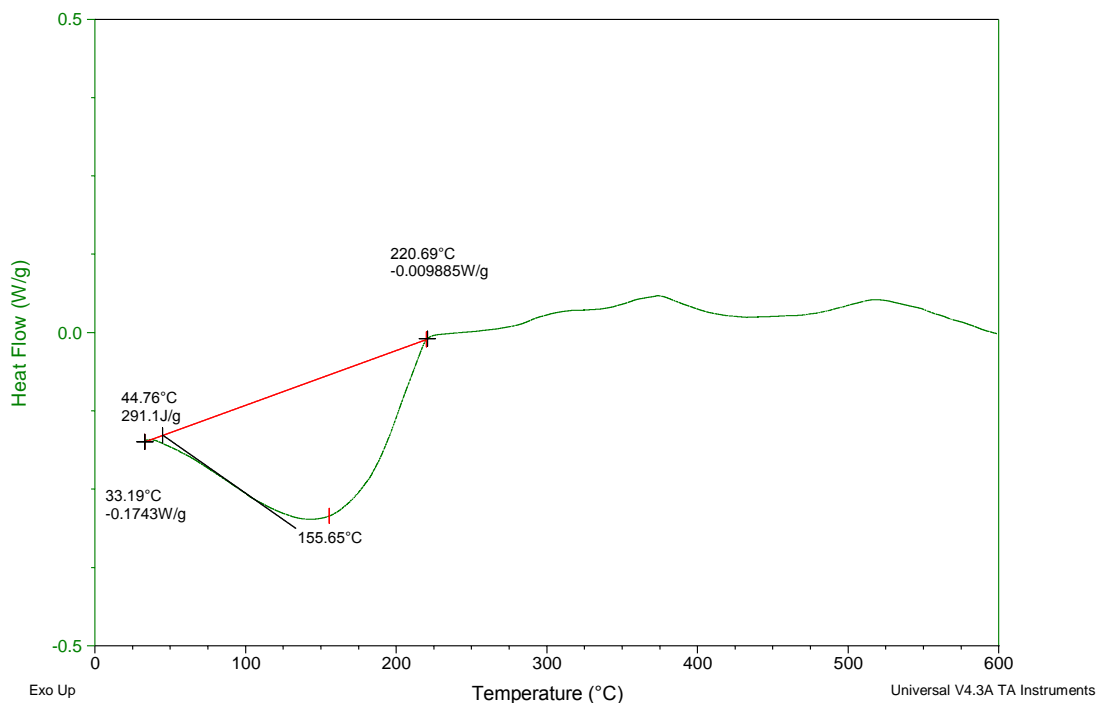


**Figure 7.4:** DSC pyrolysis curve analysis of diesel at 5°C/min heating rate

DSC pyrolysis thermograms of canola oil are given in Figure E.7 at different heating rates of 5°C/min, 10°C/min and 15°C/min. As it can be seen from the trends, canola oil exhibits slightly endothermic reaction up to 380°C which can be contributed to the volatilization of small molecules since canola oil is not refined and composed of organic molecules. Similar analysis done for biodiesel and diesel are done for the canola oil, reaction enthalpies are calculated and tabulated in Table 7.7. At around 400°C cracking of the canola molecules starts and requires around 1000 J/gr of heat in order to be cracked totally.

In the 2<sup>nd</sup> set for the experiments of pyrolysis biodiesel and diesel mixtures are exposed to constant heating rate of 10°C/min under nitrogen atmosphere and the thermograms are given in Figure E.8.

As it can be seen from the Figure E.8, diesel and biodiesel mixtures exhibit very similar pyrolysis trend as diesel does. There is only one step of reaction which is endothermic and this step implies that the cracking of the molecules mainly occur within that region.

**Table 7.8:** DSC Pyrolysis reaction intervals, peak temperatures, and heat flow of B100, B20, B15, B10, B05, and B00 mixtures at a constant heating rate of 10°C /min

	$\beta$ , °C/min	Reaction Region, °C	Peak Temperature, °C	Heat Flow, J/gr
B00	10	33.6 - 251.9	182.0	309.7
B05	10	34.7-248.5	182.5	350.2
B10	10	37.0-253.6	180.2	499.6
B15	10	23.2 - 233.8	156.4	502.9
B20	10	40.44-269.2	132.6	542.5
B100	10	70.6 - 297.5	224.5	497.9

As it can be concluded from Table 7.8 as the mixing rate of biodiesel increase heat required in order for cracking the molecules increase implying that the biodiesel is making the diesel more stable against heat. In addition to that, it has been determined in Section 7.2.1, as the biodiesel mixing rate increases, the mixture becomes less stable and pyrolysis reactions take place earlier which has been deduced from the TGA/DTG results. Therefore within the scope of all those deductions, it can be stated that as the mixing rate of biodiesel in diesel increases, cracking reactions occur at higher temperatures and more heat is required to crack the molecules, i.e. biodiesel mixing to diesel makes the fuel more stable.

### 7.3 Ignition Temperature and Heat Capacitance Derivation

Thermal properties of the fuels are determinant in order for them to be used as fuel. At this part of the study, ignition temperatures and calorific values of the pure samples are calculated by using one of the equations derived researchers.

Ignition temperature describes the point where a sample spontaneously ignites in a normal atmosphere without an external source of ignition such as flame or spark. Han et al. [29] derived the Equation 7.2 by in order to estimate the ignition temperature of samples,

$$T_i = \frac{T_{TG} + T_{DTG}}{2} \quad (7.2)$$

Where,  $T_{TG}$  is the temperature corresponding to the demarcation point between combustion TG curve and pyrolysis TG curve of the sample;  $T_{DTG}$  describes the temperature corresponding to the demarcation point between combustion DTG curve and pyrolysis DTG curve of the sample;  $T_i$  is the ignition temperature. (See Figure 7.5 in order to assign the temperatures described.) They also have realized that the ignition temperature of the samples have been decreased as the volatile content of the samples decreases.

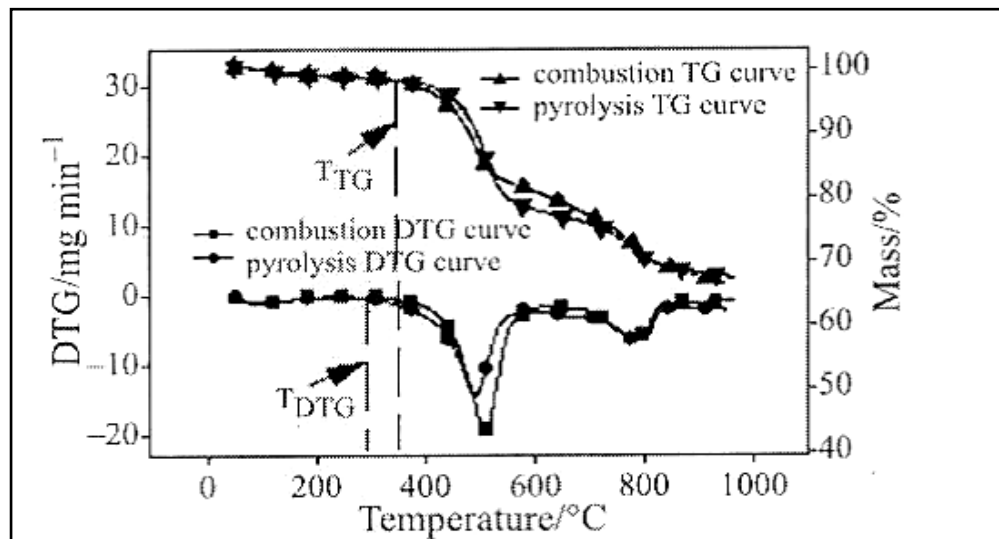


**Figure 7.5:** Ignition temperature calculation graph of oil shale samples [29]

Similarly ignition temperatures of diesel, biodiesel and canola oil are calculated by using the equation given above and the points derived from the pyrolysis and combustion graphs given in Figure 7.6-7.8.

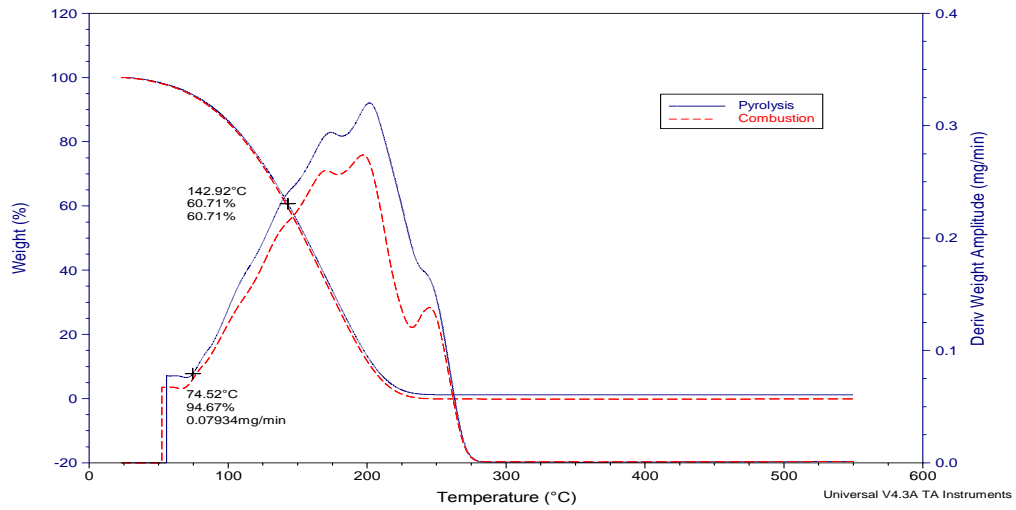


**Figure 7.6:** Calculation of ignition temperature of diesel (TGA/DTG curves of diesel pyrolysis and combustion of 5°C /min heating rate)

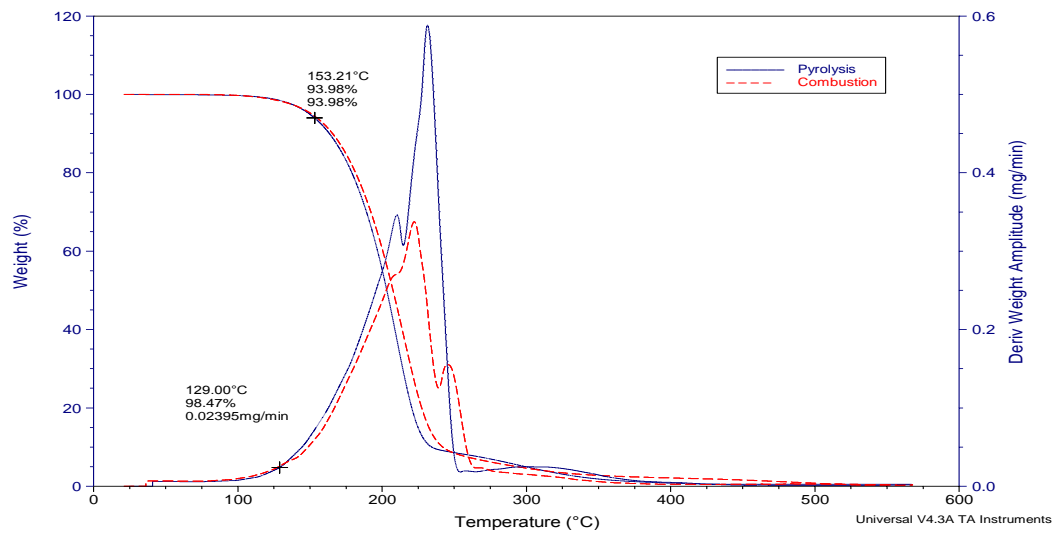


**Figure 7.7:** Calculation of ignition temperature of biodiesel (TGA/DTG curves of biodiesel pyrolysis and combustion of 5°C /min heating rate)

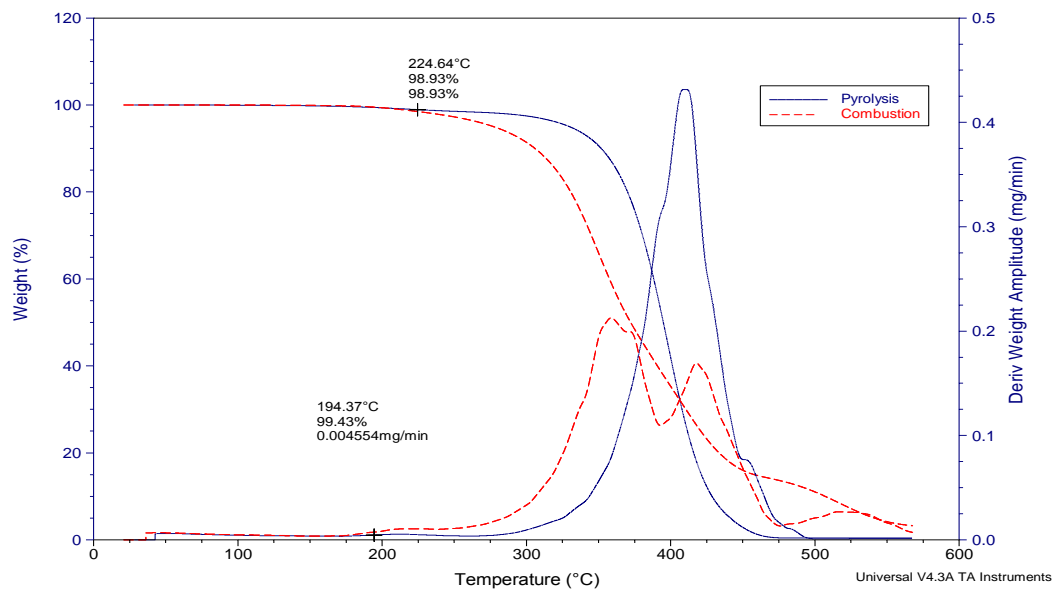


**Figure 7.8:** Calculation of ignition temperature of canola oil (TGA/DTG curves of canola oil pyrolysis and combustion of 5°C /min heating rate)

Demarcation points of the DTG and TGA curves and calculated ignition temperatures of the samples are given in Table 7.9.

**Table 7.9:** Ignition temperature calculation data

	$T_{TG}, ^\circ C$	$T_{DTG}, ^\circ C$	$T_i, ^\circ C$
Biodiesel	129.0	153.1	141.1
Diesel	74.5	142.9	108.7
Canola Oil	194.4	224.6	209.5

As it can be seen from Table 7.9, ignition temperature of biodiesel is higher than diesel and canola oil has the highest ignition temperature. In a particular motor engine, cetane number of the fuel is in relation with the ignition temperature of the fuel. As the cetane number increase, delay for the combustion decrease which means fuels ignite at low temperatures. So that it can be inferred that the ignition temperature of the biodiesel being lower than the diesel, makes the fuel less ignitable.

As it is stated in Chapter.1, biodiesel mixing to diesel increases the fuel's flash point, namely ignition temperature, so that the fuel becomes more stable under storing conditions [9, 29]. In addition to that, it is stated that as the volatility of the sample increases, ignition temperature decreases so that activation energy decreases in order to ignite the sample [29]. With the scope this phenomenon, it can be stated that biodiesel makes the fuel less volatile and more stable.

Moreover, Santos et al. [31] derived an equation (Equation 7.3) for the calculation of calorific heat capacities of the lubricant oils by using the DSC pyrolysis results.

$$C_p = \frac{w_0 c_0}{w} \frac{S_3 - S_1}{S_2 - S_1} \quad (7.3)$$

Where,  $c_0$  and  $C_p$  are the specific heats of the reference material and of the base oil respectively;  $w_0$  and  $w$  refer to the masses of the reference material and the sample respectively; and  $S_1$ ,  $S_2$ ,  $S_3$  are the thermal displacements of the DSC in relation to the blank, reference and sample respectively. However, heat capacitance are calculated for the regions where the reactions are not taking in place, since it is hard to estimate the amount of heat absorbed by the samples when reaction is also occurring. Heat capacitances of the samples with respect to temperature are presented in Figure 7.9.

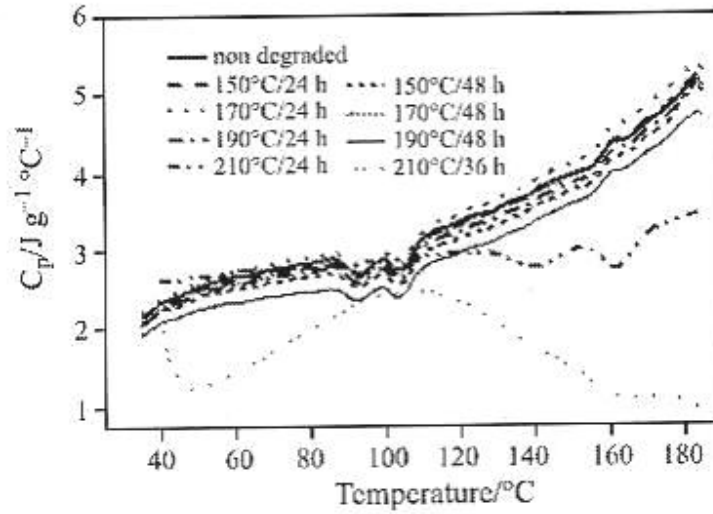


**Figure 7.9:** Evaluation of specific heat capacity of lubricating oils with respect to temperature [31]

Here the reference sample used is sapphire. Ditmars et al. [74] mention that heat capacitance of sapphire is dependent on temperature. In that manner the heat capacitance equation of sapphire has been derived by using the data resulted from Ditmars et al. [74] studies for  $C_p$  measurement of sapphire. (See Appendix C for the data of  $C_p$  with respect to temperature and  $C_p$  heat capacitance equation derivation.) Sapphire's heat capacitance with respect to temperature is dependent according to the following equation (7.4);

$$C_p = 4 \times 10^{-6} \times T^2 + 0.0023 \times T + 0.7192 \quad \text{when } 0^\circ \text{C} \leq T \leq 150^\circ \text{C} \quad (7.4)$$

Hence inserting the heat capacitance equation of sapphire into the Equation 7.3, and by using the experiment results of DSC pyrolysis, heat capacities of the pure samples are calculated with respect to temperature and results are represented in Figure 7.10.

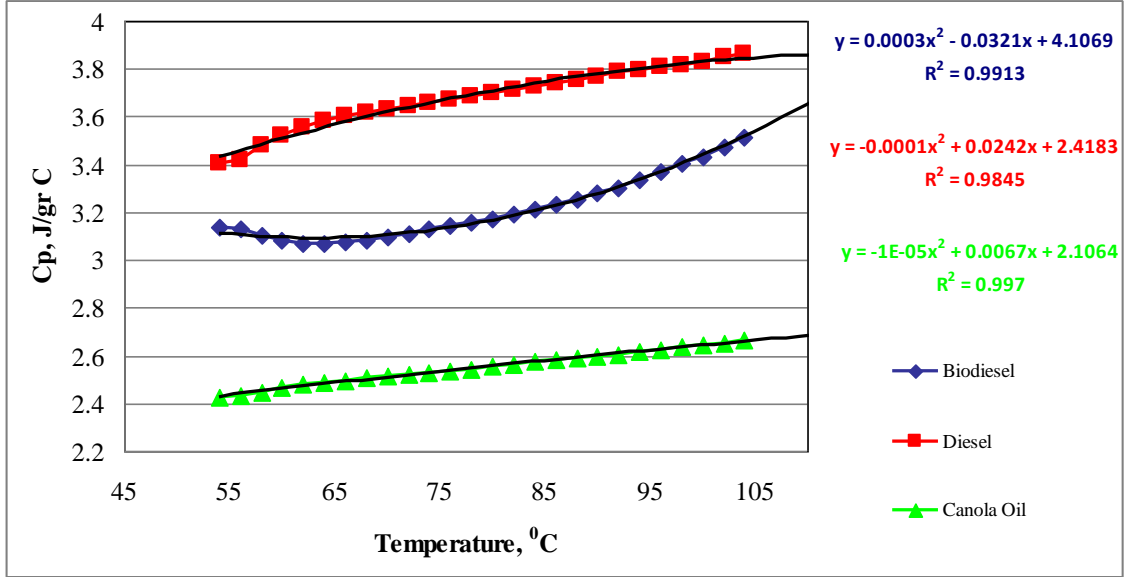


**Figure 7.10:** Calorific heat capacities of pure samples; biodiesel, diesel and canola oil with respect to temperature

As it can be seen from the Figure 7.10, heat capacities of the samples are increasing with respect to temperature and the equations derived for the samples are for biodiesel, diesel and canola oil respectively;

$$C_p = 3 \times 10^{-4} \times T^2 + 0.0321 \times T + 4.1069; \text{ for } 55^\circ C \leq T \leq 105^\circ C \quad (7.5)$$

$$C_p = -1 \times 10^{-4} \times T^2 + 0.0242 \times T + 2.4183; \text{ for } 55^\circ C \leq T \leq 105^\circ C \quad (7.6)$$

$$C_p = -1 \times 10^{-5} \times T^2 + 0.0067 \times T + 2.1064; \text{ for } 55^\circ C \leq T \leq 105^\circ C \quad (7.7)$$

Additionally it can be stated that, heat capacities of the samples are in decreasing order of; diesel > biodiesel > canola oil for the same temperature. This means that as the triglyceride molecules are cracked in to monoglycerides molecules the heat capacities of the samples are increasing but diesel can sink the heat better than the biodiesel molecules.

## 7.4 Kinetic Analysis

Thermogravimetric methods are efficient tools for the investigation of thermal and kinetic properties of the fuel types. Pyrolysis and combustion mechanisms of the hydrocarbons and fuels are complicated. Hence kinetic models have been developed by the researchers recently. Kinetic methods use the thermogravimetric data gathered during complex reactions occur and by the assumptions of numerous approaches mathematical models have been derived.

Within the scope of this study pure samples and mixtures' pyrolysis and combustion mechanisms of TGA/DTG results are analyzed by using five different models namely; Arrhenius, Coats-Redfern, Ingraham Marrier, Differential Method, Horowitz Metzger based on different assumptions and reaction parameters of the samples such as  $E$ ,  $A$  and  $n$  are determined. The parameters used for TGA/DTG analysis are given in Table 7.10. The details of the methods are given in the following sections. As it can be seen from Table 7.10, for Coats Redfern and Differential Method there are functions of  $x$  ( $f(x)$  and  $g(x)$ ). These functions are described in Table 4.1 based on different approaches. In the course of this study, since the samples are in liquid form and the reaction occurring are heterogenous reactions in both liquid and gaseous states, first and second order reactions fit best to the reaction mechanisms [25]. According to Murugan et.al., during the reactions taking place by thermogravimetric analysis, sample used is small (5-10 mg) and during the reaction taking place there is an excess of purge gas (nitrogen) which accelerates the reactions, non-isothermal pyrolysis and combustion reaction assumed to be first order ( $n=1$ ) [75]. Moreover Souza et.al [21] analyzed the thermogravimetric properties of cotton oil and biodiesel (both for methanol and ethanol route) and found out that the reaction order best fits when the order of the reaction is first order [2].

Within the scope of this study the reaction order of the reactions are assumed to be unity all of the methods being used. Moreover for Coats-Redfern and Differential Methods, 2<sup>nd</sup> order reaction and power law assumptions have been appraised and the calculations

have been performed accordingly. (Functions of the approaches are represented in Table 4.1.)

**Table 7.10:** Parameters used for kinetic models

	<b>Arrhenius</b>	<b>Coats-Redfern</b>	<b>Ingraham Marrier</b>	<b>Differential</b>	<b>Horowitz Metzger</b>
<b>y-axis</b>	$\log[dW/dt/w]$	$\ln[g(x)/T^2]^*$	$\log(dw/dT) + \log T - \log \beta$	$\ln[(dx/dt)/f(x)]^*$	$\ln[-\ln(1-x)]$
<b>x-axis</b>	$1/T$	$1/T$	$1/T$	$1/T$	$T-T_p^{**}$

\*Equations represent the governing of the equations, base on different approaches final version of the equations change

\*\*  $T_p$  is the point of inflexion of the reaction curve

### 7.4.1 TGA/DTG Kinetic Analysis for Combustion Experiments

Within the scope of this study, TGA/DTG combustion experiments results are analyzed by using the kinetic models as explained in detail in Chapter 3. Required parameters given in Table 7.11 are calculated and the graphs of the models have been plotted. The most linear regions for the curves are determined for the reaction region and slope of this region and interception y-axis are recorded. For instance for biodiesel at different heating rates, the graphs of Arrhenius model is shown in Figure 7.11.

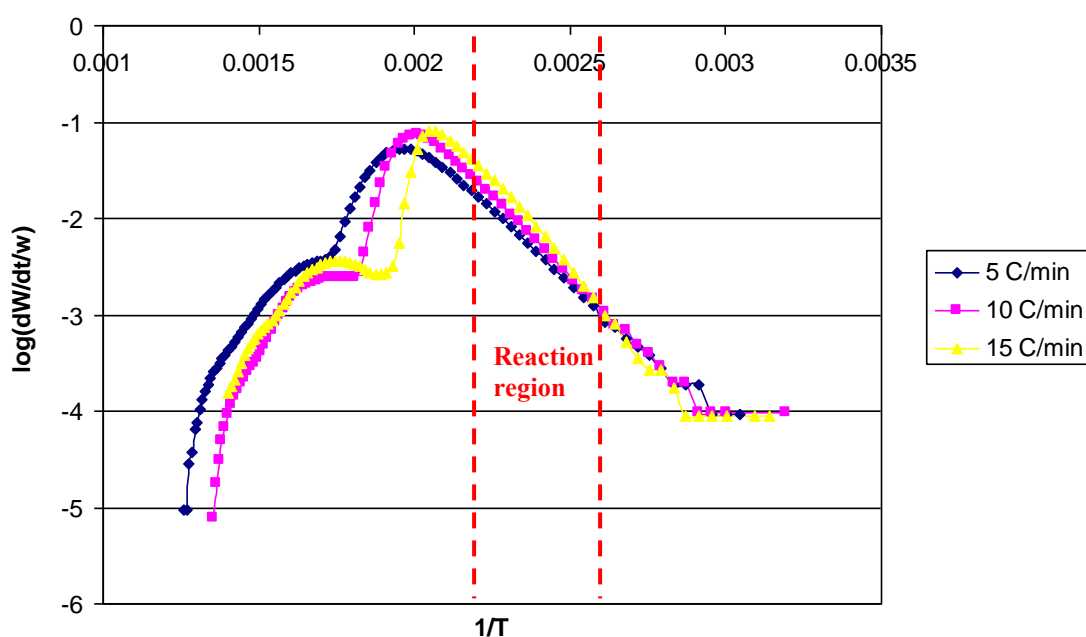


**Figure 7.11:** Biodiesel combustion reaction Arrhenius plots of different heating rates of 5°C/min, 10°C/min and 15°C/min

Graphs of the kinetic models with different approaches are given in Appendix F. Linear equations of the plots are given in Table 7.11. Corresponding reaction parameters,  $E_A$  and  $A$ , are calculated by using the equations of linear curves and given in Table 7.12 and Table 7.13, respectively.

**Table 7.11:** TGA/DTG Reaction equations and R<sup>2</sup> values of pure samples combustion curves

	$\beta, ^\circ\text{C}/\text{min}$	Arrhenius	Coast-Redfern P(1)	Coast-Redfern n=1	Coast-Redfern n=2	Ingraham-Marrier	Differential P(1)	Differential n=1	Differential n=2	Horowitz Metzger
Biodiesel	5	y = -2959x + 4.7113 R2 = 0.9945	y = -2534.2x - 7.5368 R2 = 0.9313	y = -8445.7x + 0.3294 R2 = 0.9443	y = -6345.7x + 2.0208 R2 = 0.924	y = -3860.2x + 12.237 R2 = 0.9948	y = -4467.9x + 4.0342 R2 = 0.9983	y = -4963.4x + 8.3184 R2 = 0.9943	y = -4302x + 6.6292 R2 = 0.9971	y = 0.0321x + 1.1726 R2 = 0.9217
	10	y = -3278.7x + 5.605 R2 = 0.9987	y = -3075x - 6.4091 R2 = 0.9992	y = -8283.7x + 2.4316 R2 = 0.997	y = -7409.6x + 4.7432 R2 = 0.9789	y = -3419.9x + 11.044 R2 = 0.9992	y = -3963.6x + 2.6883 R2 = 0.9992	y = -4230.5x + 6.4026 R2 = 0.9933	y = -3901.7x + 5.5107 R2 = 0.9991	y = 0.0262x + 0.8794 R2 = 0.9714
	15	y = -3990x + 4.7113 y = -3990.5x + 7.4543	y = -3194.6x - 9.4579 R2 = 0.9682	y = -7061.4x + 0.2424 R2 = 0.9969	y = -6563x + 1.5751 R2 = 0.9885	y = -3076.3x + 10.112 R2 = 0.9952	y = -3760.7x + 2.1291 R2 = 0.9993	y = -3835.3x + 5.3184 R2 = 0.9972	y = -3624.2x + 4.7647 R2 = 0.9988	y = 0.0336x + 0.4423 R2 = 0.9499
Diesel	5	y = -1077.3x + 1.2811 R2 = 0.9848	y = -1639.9x - 8.185 R2 = 0.9701	y = -3199.3x - 0.0355 R2 = 0.9623	y = -4872.1x + 1.0055 R2 = 0.9733	y = -3590.3x + 7.2027 R2 = 0.9832	y = -1728x - 1.1606 R2 = 0.9919	y = -3115.9x + 5.8247 R2 = 0.9961	y = -1999.3x + 2.4674 R2 = 0.9913	y = 0.0304x - 0.849 R2 = 0.9891
	10	y = -1159.2x + 1.901 R2 = 0.9904	y = -1319x - 9.3323 R2 = 0.963	y = -4523.7.1x - 2.6603 R2 = 0.996	y = -4119.1x - 1.4156 R2 = 0.9983	y = -3399.5x + 10.991 R2 = 0.9984	y = -3395.8x + 0.379 R2 = 0.9943	y = -2931.1x + 4.9687 R2 = 0.9987	y = -2313.6x + 3.099 R2 = 0.9942	y = 0.0224x + 0.9695 R2 = 0.974
	15	y = -1188.1x + 1.3447 R2 = 0.9856	y = -1778.7x - 7.2617 R2 = 0.9978	y = -5126.4x - 3.9617 R2 = 0.9977	y = -3695.5x - 0.1123 R2 = 0.9714	y = -3192.4x + 6.4163 R2 = 0.9679	y = -2001.7x - 0.766 R2 = 0.9932	y = -2840.5x + 4.6177 R2 = 0.9968	y = -2085.8x + 2.3898 R2 = 0.9924	y = 0.0336x - 1.439 R2 = 0.9994
Canola Oil	5	y = -4755.7x + 2.7573 R2 = 0.9652	y = -2662.7x - 9.1174 R2 = 0.9949	y = -8797.14x - 2.6726 R2 = 0.9934	y = -8816.4x - 3.8147 R2 = 0.9933	y = -4160.8x + 8.815 R2 = 0.9687	y = -5753.9x + 0.4414 R2 = 0.9965	y = -6727.3x + 3.3474 R2 = 0.9948	y = -5569.5x + 2.9816 R2 = 0.9963	y = 0.0165x - 0.5516 R2 = 0.9929
	10	y = -4842.2x + 1.852 R2 = 0.961	y = -3446x - 11.301 R2 = 0.9577	y = -9412.8x - 3.3288 R2 = 0.9798	y = -8419x - 9.3447 R2 = 0.9809	y = -4212.2x + 7.9022 R2 = 0.9319	y = -5180x - 2.5564 R2 = 0.9913	y = -6215.3x + 3.4707 R2 = 0.9824	y = -5120.7x + 2.2285 R2 = 0.9907	y = 0.0215x - 1.0707 R2 = 0.9818
	15	y = -4874.9x + 2.6589 R2 = 0.9908	y = -3836.9x - 7.3832 R2 = 0.9966	y = -9945.2x + 1.0858 R2 = 0.9953	y = -9314.8x + 2.3654 R2 = 0.9910	y = -4767.7x + 10.515 R2 = 0.9914	y = -5025.5x + 2.3883 R2 = 0.9966	y = -6079.5x + 5.4765 R2 = 0.9936	y = -4806.9x + 4.9076 R2 = 0.9954	y = 0.0269x - 1.44 R2 = 0.9761

**Table 7.12:** TGA/DTG Activation energies of the combustion reactions,  $E_A$ , kJ/mole

	$\beta$ , °C/min	Arrhenius	Coast-Redfern P(1)	Coast-Redfern n=1	Coast-Redfern n=2	Ingraham-Marrier	Differential P(1)	Differential n=1	Differential n=2	Horowitz Metzger
Biodiesel	5	56.63	48.50	161.56	121.45	73.88	37.15	41.27	35.77	65.68
	10	62.75	58.85	158.54	141.81	65.45	32.95	35.17	32.44	66.14
	15	76.37	61.14	135.15	125.61	58.88	31.27	31.89	30.13	72.25
Diesel	5	20.62	31.39	61.23	93.25	68.71	14.37	25.91	16.62	39.07
	10	22.19	25.24	86.58	78.83	65.06	19.92	24.37	19.24	42.58
	15	22.74	34.04	98.11	70.73	61.10	16.64	23.62	17.34	43.18
Canola Oil	5	91.02	50.96	168.37	168.74	79.63	47.84	55.93	46.30	53.27
	10	92.67	65.95	180.15	161.13	80.62	43.07	51.67	42.57	69.41
	15	93.30	73.43	190.34	178.27	91.25	41.78	50.54	39.96	86.85

76

**Table 7.13:** TGA/DTG Arrhenius constants of the combustion reactions,  $A^{-1}$ , min<sup>-1</sup>

	$\beta$ , °C/min	Arrhenius	Coast-Redfern P(1)	Coast-Redfern n=1	Coast-Redfern n=2	Ingraham-Marrier	Differential P(1)	Differential n=1	Differential n=2
Biodiesel	5	2.85E+07	3.05E+09	4.08E+07	5.65E+06	1.73E+12	1.08E+04	2.08E+08	4.26E+06
	10	4.04E+05	1.22E+09	6.20E+08	5.50E+07	1.11E+11	4.88E+02	2.53E+06	3.24E+05
	15	5.15E+04	2.72E+10	2.26E+07	5.55E+06	1.30E+10	1.35E+02	2.08E+05	5.82E+04
Diesel	5	1.91E+01	3.77E+09	5.60E+06	3.23E+06	1.60E+07	1.45E+01	6.68E+05	2.93E+02
	10	7.98E+01	9.72E+09	1.22E+07	3.84E+07	9.82E+10	2.40E+00	9.31E+04	1.26E+03
	15	2.21E+01	1.68E+09	3.81E+06	1.29E+08	2.61E+06	5.85E+00	4.15E+04	2.45E+02
Canola Oil	5	5.72E+02	1.55E+10	2.56E+08	8.18E+07	6.55E+08	2.76E+00	2.23E+03	9.59E+02
	10	7.13E+01	1.82E+11	1.74E+08	6.18E+10	7.99E+07	3.60E+02	2.96E+03	1.69E+02
	15	4.56E+02	4.10E+09	7.03E+07	1.83E+07	3.28E+10	2.45E+02	3.00E+05	8.09E+04

According to Table 7.12 activation energies of the samples are consistent within the group of kinetic models used. For the same kinetic models, similar activation energies are obtained but the activation energies are deviating according to the different kinetic models. Deviation of activation energies with respect to different kinetic models can be attributed to the models based on different parameters and different assumptions used to derive the equations of the models. As the average activation energies of the pure samples are assessed, it is realized that the activation energies are in the order of canola oil>biodiesel>diesel. This means that in order for the combustion reactions to take place the pure samples need to overcome the step of energy in that order. Hence diesel can be oxidized more easily compared to biodiesel and biodiesel is better than canola. This result is indeed consistent with the TGA/DTG results, in which the combustion of diesel was occurring at lower temperatures and there was not delay when compared to biodiesel. Canola on the other hand, was not a sufficient fuel to have efficient combustion on diesel engine motor.

Additionally, when the heating rate effect on samples are analyzed, it can be inferred that activation energy is really sensitive to the heating rate of the experiment i.e. as the heating rate of the experiment increases, activation energy required, to have the combustion process, has increasing trend, apart from the power law and second order reaction approaches of Coats-Redfern and Differential kinetic models. However as the Arrhenius constants of the reaction given in Table 7.13 imply there is not any correlation for the Arrhenius constants and heating rate, they are independent. Within the scope of this analysis it can be inferred that the first order assumption fits better to the liquid gas heterogeneous reactions of diesel, biodiesel and canola oil. Other assumptions are not appropriate as it is expected. Excluding the approaches apart from first order assumptions, the averages of the activation energies for the pure samples combustion are tabulated in Table 7.14.

**Table 7.14:** Average activation energies of pure samples of the 1<sup>st</sup> order reaction rate assumption models

	$\beta$ , °C/min	$E_A$ , kJ/mole
Biodiesel	5	79.8
	10	77.61
	15	74.91
Diesel	5	43.11
	10	48.15
	15	49.75
Canola Oil	5	89.64
	10	94.61
	15	102.46

As it can be seen from the Table 7.14, the averages of the activation energies (for the 1<sup>st</sup> order reaction rate assumption) of the pure samples are in the order of canola oil> biodiesel>diesel and for the different heating rates in the order of 5°C/min>10°C/min>15°C/min. The reason of increasing activation energy for the increasing heating rate is that, as the heating rate of the samples are increasing the effect of the heating process on sample diminishes. In other word heat supplied to the sample before reaction is taking place cannot be absorbed by the sample with the same sensitive response. Hence the activation energy required gets higher.

In consequence of all TGA/DTG analysis of combustion reactions, it can be inferred that the combustion efficiency of diesel is still better than biodiesel and canola oil cannot be used as fuel on diesel engines. Biodiesel has still needed to be improved to have the same combustion quality with diesel.

In addition to the pure samples kinetic method analysis, different grade blending of diesel and biodiesel are also analyzed by using the kinetic models given. Similarly, the reaction equations and results of the calculation of parameters of activation energy and Arrhenius constant are given in Table 7.15-a/b, 7.16-a/b and 7.17-a/b respectively.

**Table 7.15-a:** TGA/DTG Reaction equations and R<sup>2</sup> values of mixtures combustion curves

$\beta, ^\circ\text{C}/\text{min}$	Coast-Redfern P(1)	Coast-Redfern n=1	Coast-Redfern n=2	Differential P(1)	Differential n=1	Differential n=2	Horowitz Metzger
B00	10 $y = -1319x - 9.3323$ R2 = 0.963	$y = -4523.71x - 2.6603$ R2 = 0.996	$y = -4119.1x - 1.4156$ R2 = 0.9983	$y = -3395.8x + 0.379$ R2 = 0.9943	$y = -2931.1x + 4.9687$ R2 = 0.9987	$y = -2313.6x + 3.099$ R2 = 0.9942	$y = 0.0224x + 0.9695$ R2 = 0.974
B05	10 $y = -2531.7x - 6.7235$ R2 = 0.9823	$y = -5364.7x + 2.0138$ R2 = 0.9953	$y = -6694.4x + 2.9563$ R2 = 0.9975	$y = -3227.4x + 1.852$ R2 = 0.9849	$y = -3374.1x + 8.0996$ R2 = 0.9838	$y = -3107.5x + 4.5238$ R2 = 0.9868	$y = 0.0232x - 2.2708$ R2 = 0.9966
B10	10 $y = -1407.8x - 9.1864$ R2 = 0.9871	$y = -5215.6x - 2.7426$ R2 = 0.9884	$y = -4647.4x - 1.438$ R2 = 0.9951	$y = -2239.8x - 0.2198$ R2 = 0.9905	$y = -3226.1x + 5.0766$ R2 = 0.9935	$y = -2198.4x + 2.6123$ R2 = 0.9914	$y = 0.0239x - 1.456$ R2 = 0.9902
B15	10 $y = -2778.7x - 7.2617$ R2 = 0.9978	$y = -5181.9x - 3.2469$ R2 = 0.9872	$y = -4846.3x - 1.3046$ R2 = 0.9897	$y = -2572x + 0.514$ R2 = 0.9904	$y = -2918.3x + 4.2617$ R2 = 0.9993	$y = -2127.9x + 2.2302$ R2 = 0.9864	$y = 0.0238x - 1.8477$ R2 = 0.9987
B20	10 $y = -1999.9x - 7.7413$ R2 = 0.9792	$y = -5962.8x - 3.6468$ R2 = 0.9949	$y = -4530.9x - 1.9936$ R2 = 0.9954	$y = -2239.1x - 0.3946$ R2 = 0.9755	$y = -3421.8x + 6.0341$ R2 = 0.9618	$y = -2133.8x + 2.2875$ R2 = 0.9826	$y = 0.0293x - 1.7236$ R2 = 0.999
B100	10 $y = -3075x - 6.4091$ R2 = 0.9992	$y = -8283.7x + 2.4316$ R2 = 0.997	$y = -7409.6x + 4.7432$ R2 = 0.9789	$y = -3963.6x + 2.6883$ R2 = 0.9992	$y = -4230.5x + 6.4026$ R2 = 0.9933	$y = -3901.7x + 5.5107$ R2 = 0.9991	$y = 0.0262x + 0.8794$ R2 = 0.9714

**Table 7.15-b:** TGA/DTG Reaction equations and R<sup>2</sup> values of mixtures combustion curves

	$\beta, ^\circ\text{C}/\text{min}$	Arrhenius	Ingraham-Marrier
B00	10	$y = -1159.2x + 1.901$ R2 = 0.9904	$y = -3399.5x + 10.991$ R2 = 0.9984
B05	10	$y = -1270.6x + 1.4792$ R2 = 0.9721	$y = -1701x + 7.7682$ R2 = 0.9933
	10	$y = -1630.8x + 2.4863$ R2 = 0.9922	$y = -2102.8x + 3.9933$ R2 = 0.8339
B10	10	$y = -1556.9x + 2.0018$ R2 = 0.9882	$y = -1555.4x + 7.2736$ R2 = 0.9884
	10	$y = -2036.4x - 1.1499$ R2 = 0.8954	$y = -2610x + 5.2032$ R2 = 0.9587
B15	10	$y = -1351.7x + 1.3382$ R2 = 0.9753	$y = -2817.5x + 7.9434$ R2 = 0.9871
B20	10	$y = -2420.5x + 4.383$ R2 = 0.9845	$y = -3596.6x + 9.8308$ R2 = 0.9888
B100	10	$y = -3278.7x + 5.605$ R2 = 0.9987	$y = -3419.9x + 11.044$ R2 = 0.9992

**Table 7.16-a:** TGA/DTG Activation energies of the combustion reactions,  $E_A$ , kJ/mole

	$\beta, ^\circ\text{C}/\text{min}$	Coast-Redfern P(1)	Coast-Redfern n=1	Coast-Redfern n=2	Differential P(1)	Differential n=1	n=2	Horowitz Metzger
B00	10	25.24	86.58	78.83	19.92	24.37	19.24	42.58
B05	10	48.45	102.67	141.81	26.83	28.05	25.84	59.02
B10	10	26.94	99.82	125.61	18.62	27.65	18.28	52.32
B15	10	53.18	99.18	93.25	21.38	24.26	17.69	48.12
B20	10	38.28	114.12	78.83	18.62	28.45	17.74	55.69
B100	10	58.85	158.54	141.81	32.95	35.17	32.44	66.14

**Table 7.16-b:** TGA/DTG Activation energies of the combustion reactions,  $E_A$ , kJ/mole

	$\beta, ^\circ\text{C}/\text{min}$	Arrhenius	Ingraham-Marrier
B00	10	22.19	65.06
B05	10 1st Region	24.32	32.56
	10 2nd Region	31.21	40.25
B10	10 1st Region	29.80	29.77
	10 2nd Region	38.97	49.95
B15	10	25.87	53.92
B20	10	46.33	68.83
B100	10	56.63	73.88

**Table 7.17-a:** TGA/DTG Arrhenius constants of the combustion reactions,  $A^{-1}$ ,  $\text{min}^{-1}$ 

	$\beta$ , °C/min	Coast-Redfern P(1)	Coast-Redfern n=1	Coast-Redfern n=2	Differential P(1)	Differential n=1	Differential n=2
B00	10	9.72E+09	3.84E+07	5.75E+06	2.40E+00	9.31E+04	1.26E+03
B05	10	1.37E+09	2.62E+07	5.50E+07	7.13E+01	1.26E+08	3.34E+04
B10	10	8.96E+09	5.28E+07	5.45E+06	1.66E+00	1.19E+05	4.10E+02
B15	10	2.58E+09	8.69E+07	3.29E+06	3.27E+00	1.83E+04	1.70E+02
B20	10	3.00E+09	1.49E+08	3.84E+07	2.48E+00	1.08E+06	1.94E+02
B100	10	1.22E+09	6.09E+07	1.27E+08	4.88E+02	2.53E+06	3.24E+05

**Table 7.17-b:** TGA/DTG Arrhenius constants of the combustion reactions,  $A^{-1}$ ,  $\text{min}^{-1}$ 

	$\beta$ , °C/min	Arrhenius	Ingraham-Marrier
B00	10	7.98E+01	9.82E+10
B05	10 1st Region	3.01E+01	5.87E+07
	10 2nd Region	3.06E+02	9.85E+03
B10	10 1st Region	1.00E+02	1.88E+07
	10 2nd Region	1.41E+01	1.60E+05
B15	10	2.18E+01	8.78E+07
B20	10	2.42E+04	6.77E+09
B100	10	4.04E+05	1.11E+11

During the analysis of TGA/DTG results it is stated earlier that, among the biodiesel and diesel blends at different grades, B05 and B10 show two reaction regions during the combustion. Therefore, for the calculation of the reaction parameters by using kinetic methods for some of the kinetic models two reaction regions are obtained having linear slope and related parameters are calculated, accordingly. As it can be inferred from the Table 7.15-a/b, Arrhenius and Ingraham Marrier kinetic methods exhibit two reaction regions for B05 and B10 blends. Apart from them, remaining reaction models show only one reaction interval of linear slope. This result is in a way in conflict with the results of TGA/DTG analysis however as it is mentioned earlier the kinetic methods are derived to obtain the reaction parameters of overall reaction process, they are not sensitive to obtain the individual steps of the reactions. As it can be seen from the calculated activation energies, as the blending rate of the biodiesel increases activation energy of the reactions are getting higher. This means that as the biodiesel content of the fuel increases, more energy is required to have the combustion process. Moreover in the lower grades of biodiesel, for the 1<sup>st</sup> reaction steps required heat is related with the diesel content, 2<sup>nd</sup> step is attributed to the biodiesel combustion of the fuel since the combustion temperature of biodiesel is higher than the diesel (stated in Chapter 7.1.1). Therefore 1<sup>st</sup> step activation energy should be less than the 2<sup>nd</sup> step activation energy despite to the fact that diesel has lower activation energy requirement as given earlier. As the activation energies of the reactions steps are considered in Table 7.16-b, except Ingraham Marrier result of 2<sup>nd</sup> reaction interval for B10 grade, the results are consistent to what is expected.

#### **7.4.2 TGA/DTG Kinetic Analysis for Pyrolysis Experiments**

Additionally, TGA/DTG pyrolysis experiment results are analyzed by using the same kinetic models. Similarly, required parameters are calculated and the graphs of the models have been plotted. The most linear regions for the curves are determined for the reaction region and slope of this region and interception y-axis are recorded.

Graphs of the kinetic models with different approaches are given in Appendix F. Linear equations of the plots are given in Table 7.18. Corresponding reaction parameters,  $E_A$  and  $A$ , are calculated by using the equations of linear curves and given in Table 7.19 and Table 7.20, respectively.

**Table 7.18: TGA/DTG Reaction equations and R<sup>2</sup> values of pure samples pyrolysis curves**

	$\beta, ^\circ\text{C}/\text{min}$	Arrhenius	Coast-Redfern P(1)	Coast-Redfern n=1	Coast-Redfern n=2	Ingraham-Marrier	Differential P(1)	Differential n=1	Differential n=2	Horowitz Metzger
Biodiesel	5	y = -3639.1x + 6.5427 R2 = 0.9912	y = -1210.7x - 9.3552 R2 = 0.9808	y = -3774.1x - 3.0339 R2 = 0.9986	y = -3616.9x - 9.6302 R2 = 0.9924	y = -3891.3x + 12.308 R2 = 0.9955	y = -2381.1x - 2.5158 R2 = 0.9976	y = -3649.6x + 7.2334 R2 = 0.9886	y = -2174.3x - 0.0455 R2 = 0.9964	y = 0.035x - 2.1206 R2 = 0.9913
	10	y = -3106.8x + 5.1718 R2 = 0.9949	y = -1717.3x - 8.1711 R2 = 0.9935	y = -4262.1x - 2.1904 R2 = 0.9973	y = -2439x - 12.362 R2 = 0.9816	y = -3373.3x + 10.932 R2 = 0.9985	y = -1811.1x - 3.7649 R2 = 0.9921	y = -3304.4x + 6.0392 R2 = 0.9835	y = -1756.3x - 0.9806 R2 = 0.992	y = 0.0355x - 2.5194 R2 = 0.9926
	15	y = -2866.7x + 4.5076 R2 = 0.9956	y = -1678.7x - 7.2617 R2 = 0.9978	y = -3861.5x - 3.5669 R2 = 0.9891	y = -2243x - 13.036 R2 = 0.9894	y = -3085.1x + 10.154 R2 = 0.9973	y = -2101.8x - 3.2939 R2 = 0.9817	y = -3248.8x + 5.6589 R2 = 0.9899	y = -2054.8x - 0.4855 R2 = 0.9923	y = 0.0309x - 2.5944 R2 = 0.9902
Diesel	5	y = -1179.7x + 1.5617 R2 = 0.9887	y = -1349.8x - 11.964 R2 = 0.9908	y = -3576.3x - 9.7321 R2 = 0.9915	y = -4485.2x - 0.9353 R2 = 0.9989	y = -1390.3x + 7.2027 R2 = 0.9832	y = -1737x - 1.1518 R2 = 0.9898	y = -2356.4x + 0.351 R2 = 0.9977	y = -2207.2x + 3.0121 R2 = 0.9853	y = 0.028x - 0.8192 R2 = 0.9989
	10	y = -1418.1x + 2.0753 R2 = 0.994	y = -998.32x - 12.7 R2 = 0.9813	y = -2434.8x - 12.374 R2 = 0.9817	y = -4480.8x - 1.5175 R2 = 0.9987	y = -1481.5x + 7.2716 R2 = 0.9866	y = -1886.1x - 0.9784 R2 = 0.9919	y = -1774.9x - 0.9302 R2 = 0.9915	y = -2112.2x + 2.5029 R2 = 0.9859	y = 0.0256x - 1.2844 R2 = 0.9988
	15	y = -1259.8x + 1.5497 R2 = 0.99	y = -747.5x - 13.487 R2 = 0.9676	y = -2351.2x - 12.749 R2 = 0.9866	y = -4562.7x - 1.5301 R2 = 0.9933	y = -1291.3x + 6.6915 R2 = 0.9849	y = -1703.5x - 1.5195 R2 = 0.9881	y = -2042.7x - 0.5008 R2 = 0.9961	y = -1845.5x + 1.7771 R2 = 0.9971	y = 0.0234x - 1.4366 R2 = 0.9993
Canola Oil	5	y = -3992.27x + 7.0654 R2 = 0.9913	y = -3494.2x - 5.24 R2 = 0.9954	y = -7919.5x + 3.8871 R2 = 0.9928	y = -8073.5x + 4.2999 R2 = 0.9916	y = -6545.2x + 13.973 R2 = 0.9944	y = -4130.1x + 3.2535 R2 = 0.9923	y = -5148.8x + 8.7563 R2 = 0.9964	y = -4129.5x + 6.2251 R2 = 0.9946	y = 0.0493x - 4.4955 R2 = 0.9958
	10	y = -4383.9x + 7.9725 R2 = 0.9921	y = -3007x - 6.5641 R2 = 0.9971	y = -7076.8x + 1.6316 R2 = 0.9954	y = -7490.5x + 2.7722 R2 = 0.9872	y = -6690.7x + 14.015 R2 = 0.992	y = -3835.5x + 2.3985 R2 = 0.9972	y = -3991.5x + 5.8037 R2 = 0.9945	y = -3787.4x + 5.2534 R2 = 0.9977	y = 0.0431x - 4.6108 R2 = 0.9975
	15	y = -3911.94x + 6.6683 R2 = 0.9925	y = -1029.9x - 9.8575 R2 = 0.9846	y = -4177x - 1.985 R2 = 0.9939	y = -5113.3x + 0.7497 R2 = 0.9852	y = -7309.8x + 14.874 R2 = 0.9958	y = -3482.7x + 1.4889 R2 = 0.989	y = -3791.3x + 5.2815 R2 = 0.9906	y = -3518.1x + 4.5289 R2 = 0.9976	y = 0.0396x - 4.6944 R2 = 0.9965

**Table 7.19:** TGA/DTG Activation energies of the pure samples pyrolysis reactions,  $E_A$ , kJ/mole

	$\beta$ , °C/min	Arrhenius	Coast-Redfern P(1)	Coast-Redfern n=1	Coast-Redfern n=2	Ingraham-Marrier	P(1)	n=1	n=2	Horowitz Metzger
Biodiesel	5	69.65	23.17	72.23	69.22	74.47	19.80	30.34	18.08	44.98
	10	59.46	32.87	81.57	46.68	64.56	15.06	27.47	14.60	45.62
	15	54.87	32.13	73.90	42.93	59.05	17.47	27.01	17.08	39.71
Diesel	5	22.58	25.83	68.45	85.84	26.61	14.44	19.59	18.35	35.98
	10	27.14	19.11	46.60	85.76	28.35	15.68	14.76	17.56	32.90
	15	24.11	14.31	45.00	87.32	24.71	14.16	16.98	15.34	30.07
Canola Oil	5	76.41	66.87	151.57	154.52	125.27	34.34	42.81	34.33	63.35
	10	83.90	57.55	135.44	143.36	128.05	31.89	33.19	31.49	55.39
	15	74.87	56.07	79.94	97.86	139.90	28.96	31.52	29.25	50.89

**Table 7.20:** TGA/DTG Arrhenius constants of the pure samples pyrolysis reactions,  $A^{-1}$ ,  $\text{min}^{-1}$ 

	$\beta$ , °C/min	Arrhenius	Coast-Redfern P(1)	Coast-Redfern n=1	Coast-Redfern n=2	Ingraham-Marrier	Differential P(1)	Differential n=1	Differential n=2
Biodiesel	5	2.85E+07	3.05E+09	3.35E+07	5.65E+06	1.73E+12	1.08E+04	2.08E+08	4.26E+06
	10	4.04E+05	1.22E+09	6.20E+08	5.50E+07	1.11E+11	4.88E+02	2.53E+06	3.24E+05
	15	5.15E+04	2.72E+10	2.26E+07	5.55E+06	1.30E+10	1.35E+02	2.08E+05	5.82E+04
Diesel	5	1.91E+01	3.77E+09	9.10E+06	3.23E+06	1.60E+07	1.45E+01	6.68E+05	2.93E+02
	10	7.98E+01	9.72E+09	1.22E+07	3.84E+07	9.82E+10	2.40E+00	9.31E+04	1.26E+03
	15	2.21E+01	1.68E+09	3.81E+06	1.29E+08	2.61E+06	5.85E+00	4.15E+04	2.45E+02
Canola Oil	5	5.72E+02	1.55E+10	2.41E+08	8.18E+07	6.55E+08	2.76E+00	2.23E+03	9.59E+02
	10	7.13E+01	1.82E+11	1.37E+08	6.18E+10	7.99E+07	3.60E+02	2.96E+03	1.69E+02
	15	4.56E+02	4.10E+09	7.03E+07	1.83E+07	3.28E+10	2.45E+02	3.00E+05	8.09E+04

According to Table 7.20 activation energies are consistent within the same group of kinetic models as in the case of combustion TGA/DTG analysis. Deviation of the activation energies are occurring due to the different approaches of the models and equations being dependent on different parameters. As the averages of the activation energies of the pure samples are analyzed, it can be stated that the activation energies are in the order of canola oil>biodiesel>diesel. From the literature it is known that as the activation energies of the samples decrease, stability of the samples get worse, i.e. the samples can more easily be decomposed [21]. Hence it can be stated that biodiesel has better stability than diesel, which result is consistent with DSC results stated earlier, as well. The result is also indicate that by the aid of transesterification reaction mechanism monoglyceride molecules approaches to petrochemical fuels since biodiesel cracking mechanism is more similar to diesel mechanism. Hence it can be inferred that the fuel characteristics of biodiesel is improved. In addition to that when the heating rate effect on activation energy is analyzed, it can be stated that activation energy of the reactions are sensitive to the heating rate. Because as the heating rate of the samples are increased, activation energy required becomes higher. This means that as the heating rate of the reactions increase, the heat supplied to the sample by surrounding cannot be absorbed by the sample in same response severity. This result is also being supported by the literature studies done before by using many different kind of samples by using thermogravimetric methods [74] .

On the other hand as the different approaches of the models are compared, it can be seen from the Table 7.19, second order reaction assumption and power law assumptions do not fit to the experiment results as the first order reaction approaches do (See the Appendix F, pyrolysis plots). Hence excluding them, the averages of the remaining approaches are taken and tabulated in Table 7.21.

**Table 7.21:** Average activation energies of pure samples of the 1<sup>st</sup> order reaction rate assumption models

	$\beta$ , °C/min	$E_A$ , kJ/mole
Biodiesel	5	58.34
	10	55.74
	15	50.91
Diesel	5	34.64
	10	29.95
	15	28.18
Canola Oil	5	91.88
	10	87.19
	15	75.42

As it can be seen from the Table 7.21, the averages of the activation energies (for the 1<sup>st</sup> order reaction rate assumption) of the pure samples are in the order of canola oil > biodiesel > diesel and for the different heating rates in the order of 5°C/min > 10°C/min > 15°C/min. Hence as it has been stated earlier, as the heating rate of the reaction increases, samples cannot give the same severe response on absorbing the heat supplied. In other words, as the heating rate of the reactions increases the heat required to decompose the molecules gets higher.

In addition to the pure samples kinetic method analysis, different grade blending of diesel and biodiesel pyrolysis mechanisms are also analyzed by using the kinetic models given. Similarly, the reaction equations and results of the calculation of parameters of activation energy and Arrhenius constant are given in Table 7.22, 7.23 and 7.24 respectively.

**Table 7.22: TGA/DTG Reaction equations and R<sup>2</sup> values of mixtures pyrolysis curves**

	$\beta, ^\circ\text{C}/\text{min}$	Arrhenius	Coast-Redfern P(1)	Coast-Redfern n=1	Coast-Redfern n=2	Ingraham-Marrier	Differential P(1)	Differential n=1	Differential n=2	Horowitz Metzger
Biodiesel	5	y = -3639.1x + 6.5427 R2 = 0.9912	y = -1210.7x - 9.3552 R2 = 0.9808	y = -3774.1x - 3.0339 R2 = 0.9986	y = -3616.9x - 9.6302 R2 = 0.9924	y = -3891.3x + 12.308 R2 = 0.9955	y = -2381.1x - 2.5158 R2 = 0.9976	y = -3649.6x + 7.2334 R2 = 0.9886	y = -2174.3x - 0.0455 R2 = 0.9964	y = 0.035x - 2.1206 R2 = 0.9913
	10	y = -3106.8x + 5.1718 R2 = 0.9949	y = -1717.3x - 8.1711 R2 = 0.9935	y = -4262.1x - 2.1904 R2 = 0.9973	y = -2439x - 12.362 R2 = 0.9816	y = -3373.3x + 10.932 R2 = 0.9985	y = -1811.1x - 3.7649 R2 = 0.9921	y = -3304.4x + 6.0392 R2 = 0.9835	y = -1756.3x - 0.9806 R2 = 0.992	y = 0.0355x - 2.5194 R2 = 0.9926
	15	y = -2866.7x + 4.5076 R2 = 0.9956	y = -1678.7x - 7.2617 R2 = 0.9978	y = -3861.5x - 3.5669 R2 = 0.9891	y = -2243x - 13.036 R2 = 0.9894	y = -3085.1x + 10.154 R2 = 0.9973	y = -2101.8x - 3.2939 R2 = 0.9817	y = -3248.8x + 5.6589 R2 = 0.9899	y = -2054.8x - 0.4855 R2 = 0.9923	y = 0.0309x - 2.5944 R2 = 0.9902
Diesel	5	y = -1179.7x + 1.5617 R2 = 0.9887	y = -1349.8x - 11.964 R2 = 0.9908	y = -3576.3x - 9.7321 R2 = 0.9915	y = -4485.2x - 0.9353 R2 = 0.9989	y = -1390.3x + 7.2027 R2 = 0.9832	y = -1737x - 1.1518 R2 = 0.9898	y = -2356.4x + 0.351 R2 = 0.9977	y = -2207.2x + 3.0121 R2 = 0.9853	y = 0.028x - 0.8192 R2 = 0.9989
	10	y = -1418.1x + 2.0753 R2 = 0.994	y = -998.32x - 12.7 R2 = 0.9813	y = -2434.8x - 12.374 R2 = 0.9817	y = -4480.8x - 1.5175 R2 = 0.9987	y = -1481.5x + 7.2716 R2 = 0.9866	y = -1886.1x - 0.9784 R2 = 0.9919	y = -1774.9x - 0.9302 R2 = 0.9915	y = -2112.2x + 2.5029 R2 = 0.9859	y = 0.0256x - 1.2844 R2 = 0.9988
	15	y = -1259.8x + 1.5497 R2 = 0.99	y = -747.5x - 13.487 R2 = 0.9676	y = -2351.2x - 12.749 R2 = 0.9866	y = -4562.7x - 1.5301 R2 = 0.9933	y = -1291.3x + 6.6915 R2 = 0.9849	y = -1703.5x - 1.5195 R2 = 0.9881	y = -2042.7x - 0.5008 R2 = 0.9961	y = -1845.5x + 1.7771 R2 = 0.9971	y = 0.0234x - 1.4366 R2 = 0.9993
Canola Oil	5	y = -3992.27x + 7.0654 R2 = 0.9913	y = -3494.2x - 5.24 R2 = 0.9954	y = -7919.5x + 3.8871 R2 = 0.9928	y = -8073.5x + 4.2999 R2 = 0.9916	y = -6545.2x + 13.973 R2 = 0.9944	y = -4130.1x + 3.2535 R2 = 0.9923	y = -5148.8x + 8.7563 R2 = 0.9964	y = -4129.5x + 6.2251 R2 = 0.9946	y = 0.0493x - 4.4955 R2 = 0.9958
	10	y = -4383.9x + 7.9725 R2 = 0.9921	y = -3007x - 6.5641 R2 = 0.9971	y = -7076.8x + 1.6316 R2 = 0.9954	y = -7490.5x + 2.7722 R2 = 0.9872	y = -6690.7x + 14.015 R2 = 0.992	y = -3835.5x + 2.3985 R2 = 0.9972	y = -3991.5x + 5.8037 R2 = 0.9945	y = -3787.4x + 5.2534 R2 = 0.9977	y = 0.0431x - 4.6108 R2 = 0.9975
	15	y = -3911.94x + 6.6683 R2 = 0.9925	y = -1029.9x - 9.8575 R2 = 0.9846	y = -4177x - 1.985 R2 = 0.9939	y = -5113.3x + 0.7497 R2 = 0.9852	y = -7309.8x + 14.874 R2 = 0.9958	y = -3482.7x + 1.4889 R2 = 0.989	y = -3791.3x + 5.2815 R2 = 0.9906	y = -3518.1x + 4.5289 R2 = 0.9976	y = 0.0396x - 4.6944 R2 = 0.9965

**Table 7.23:** TGA/DTG Activation energies of pyrolysis reactions,  $E_A$ , kJ/mole

	$\beta, ^\circ\text{C}/\text{min}$	Arrhenius	Coast-Redfern P(1)	Coast-Redfern n=1	Coast-Redfern n=2	Ingraham-Marrier	Differential P(1)	Differential n=1	Differential n=2	Horowitz Metzger
B00	10	27.14	19.11	46.60	85.76	28.35	15.68	14.76	17.56	32.90
B05	10	27.36	27.91	82.48	88.74	30.79	15.70	24.45	16.18	37.90
B10	10	30.03	28.58	83.76	88.95	30.76	18.64	24.23	18.28	37.00
B15	10	29.43	34.04	83.60	85.31	30.90	19.85	23.64	16.27	44.46
B20	10	29.93	33.84	94.82	87.46	30.87	20.33	25.54	16.88	42.96
B100	10	59.46	32.87	81.57	46.68	64.56	15.06	27.47	14.60	45.62

06

**Table 7.24:** TGA/DTG Arrhenius constants of the pure samples pyrolysis reactions,  $A^{-1}$ ,  $\text{min}^{-1}$ 

	$\beta, ^\circ\text{C}/\text{min}$	Arrhenius	Coast-Redfern P(1)	Coast-Redfern n=1	Coast-Redfern n=2	Ingraham-Marrier	Differential P(1)	Differential n=1	Differential n=2
B00	10	1.49E+05	3.96E+09	2.48E+07	1.33E+07	1.87E+07	9.52E+00	1.09E+06	3.18E+02
B05	10	4.30E+01	7.08E+09	3.18E+07	9.45E+06	4.09E+07	9.72E+00	9.44E+04	1.18E+02
B10	10	2.37E+02	7.49E+09	2.64E+07	1.28E+07	3.77E+07	1.38E+00	7.04E+04	4.88E+02
B15	10	1.70E+01	1.65E+09	1.26E+08	1.83E+07	1.02E+07	1.69E+00	4.00E+04	9.40E+01
B20	10	2.17E+01	4.36E+09	9.93E+07	1.49E+07	1.86E+07	2.47E+00	1.61E+05	1.51E+02
B100	10	1.19E+02	2.36E+11	3.76E+11	3.72E+11	8.57E+10	5.82E+03	8.52E+00	9.57E+00

In Chapter 7.2.1, biodiesel and diesel blends pyrolysis reaction mechanisms (B05, B10, B15, B20) are analyzed and only one reaction region is obtained. Hence during the analysis of kinetic models of blends only one reaction region of linear slope line is obtained as it can be seen from the figures given in Appendix F. Since the kinetic models derived are used in order for determining an overall process reaction mechanism, the results of pyrolysis are appropriate for the kinetic models contrary to the combustion experiment results stated earlier. As it can be deduced from Table 7.23, as the blending rate of the biodiesel in diesel increases the activation energy required for the pyrolysis reaction to take place increases. Activation energies are in the order of B100>B20>B15>B10>B05>B00. This result implies that biodiesel increases the thermal stability of fuels. Hence adding the biodiesel to diesel with a certain amount makes the fuel more stable against decomposing under heat, i.e. thermal stability of the fuel increases. On the other hand when the Arrhenius constants are compared from the Table 7.24, they are consistent for the same kind of kinetic model but there is not any relation found between the different kinds of blends

## CHAPTER 8

### CONCLUSION

This study has been conducted in order to search whether biodiesel, as renewable energy source, can be replaced by diesel fuel and to observe the effect of biodiesel blending on combustion and pyrolysis at different percentages to diesel. Therefore, biodiesel, diesel canola oil (origin of biodiesel) and blend of biodiesel with diesel at different percentages are exposed to isothermal heating under nitrogen and air atmosphere with constant heating rate of 5°C/min, 10°C/min and 15°C/min by using TGA/DTG and DSC under nitrogen and air atmosphere. Reaction parameters such as reaction interval, peak temperature, weight loss of the samples and heat flow of the reactions are determined by using *Universal Analysis* software. Several kinetic methods have been applied to determine the pyrolysis and combustion kinetic parameters.

Combustion experiments under air atmosphere are carried out through two different sets, at 1<sup>st</sup> set up pure samples are exposed to different heating rates of 5°C/min, 10°C/min and 15°C/min in order to analyze the effect of heating rate on combustion and at 2<sup>nd</sup> set up blends of biodiesel and diesel (B05, B10, B15, B20) are exposed to constant heating rates of 10°C/min for the purpose of observing mixing effect of biodiesel on combustion mechanism. For the 1<sup>st</sup> set up, in combustion with air one reaction step is observed for biodiesel and diesel, on the other hand canola at 5°C/min heating rate exhibits two reaction intervals. It is observed that the combustion temperature of biodiesel is higher than the diesel implying that for the combustion of biodiesel, more time takes place. On the other hand biodiesel has monoglyceride molecules having long chains and oxygen bonds which are more complex than the

simple diesel molecules. Hence biodiesel has a delay time during combustion. On the other hand canola oil, consisting of triglyceride molecules is less ignitable than biodiesel since the combustion reactions take at higher temperatures. Within the scope of this analysis it can be stated that as the molecules getting bigger and as the fuel type gets more complexity, combustion mechanism becomes more complex and occurs at higher temperatures. Additionally, it is observed that as the heating rate of the experiments gets higher the reaction loose its sensitivity which means that, at lower heating rates maximum temperature of the reaction shifts lower and the mass loss recorded increases. For the 2<sup>nd</sup> set up in combustion with air, among the mixtures of biodiesel and diesel samples, B15 and B20 mixtures have exhibited more stable combustion profile than the others. Moreover, B15 recorded mass loss is higher than B20 which implies that B15 takes the combustion reaction more efficiently. Consistently, biodiesel combustion reactions of DSC analysis take place at higher temperature interval implying that cetane number of biodiesel is lower than diesel and this results in delay on diesel engines. When the blending of diesel and biodiesel DSC results are analyzed, it can be stated that B15 grade has the highest exothermic enthalpy flow and the reaction occurs at low temperature levels. Hence it can be stated that B15 grade of diesel and canola oil originated biodiesel has sufficient cetane number and does not lead in delay during combustion on diesel engine when compared to other blending rates.

According to the TGA/DTG curves of pyrolysis reactions, it can be observed that biodiesel exhibits more stable performance when compared to diesel since the pyrolysis reaction of biodiesel takes place at higher temperature levels. Moreover peak temperatures of biodiesel at different heating rate are higher than the diesels'. On the other hand canola oil is more stable than biodiesel since it pyrolysis around 270-494°C which implies that the triglyceride molecules make the samples more stable when compared to monoglyceride molecules of biodiesel. Moreover, as biodiesel mixing rate increases fuel becomes more stable since the pyrolysis temperatures shift to higher temperatures and 2<sup>nd</sup> reaction region becomes clearer. On the other hand, as DSC curves are analyzed, diesel exhibits only one reaction region of endothermic reactions showing

that the hydrocarbon molecules are being cracked by absorbing heat from the surrounding. Biodiesel samples show two reaction regions 1<sup>st</sup> one is endothermic reaction region occurring between 90- 270°C and 2<sup>nd</sup> one is exothermic reaction region at above 270°C. At 1<sup>st</sup> step monoglyceride molecules are cracked into C11-C24 alkyls are formed and remaining molecules form C7-C11 carboxylates by cracking oxygen bonds. At 2<sup>nd</sup> step exothermic reaction, relatively less reaction enthalpy (80-100 J/gr) compared to the 1<sup>st</sup> one occurs (160-200 J/gr). After the oxygen bonds are being cracked and hydrogen molecules are formed, oxygen and hydrogen molecules form water vapour molecules as by product by dissipating energy to surrounding. Hence the pyrolysis mechanism of biodiesel has been completed. Canola oil exhibits different pyrolysis mechanism compared to diesel and biodiesel since it is not refined sample, it is crude and organic as well. So that some volatile components evaporate till to the temperature of 380°C, exhibiting slightly endothermic reaction. At round 400°C, cracking of canola oil start and the pyrolysis reaction requires 1000 J/gr of heat. Also the mixtures of biodiesel and diesel show very similar pyrolysis trend with diesel. In addition to that more heat is required to crack the molecules as the biodiesel content of the mixture increases.

In the course of analyzing thermal properties of fuels, ignition temperatures of the samples are calculated by taking the averages of demarcation points of TGA and DSC curves of combustion and pyrolysis of the samples. Ignition temperatures of the biodiesel, diesel and canola oil are, 141.1, 108.7 and 209.5°C respectively. This result is consistent with the TGA/DTG combustion results, since the biodiesel combustion reaction occurs at higher temperatures compared to diesel. Hence cetane number of biodiesel is lower than diesel; resulting in delay during combustion and canola oil does not have sufficient cetane number to have efficient combustion. In addition to that by using the DSC pyrolysis experimental data of pure samples (biodiesel, diesel and canola oil), DSC sapphire (as the reference material) pyrolysis data and blank heating data, heat capacitances equations of the pure samples are derived according to the equations derived in literature. It is found that for the same temperature the heat capacitances are in the order of; diesel>biodiesel>canola. Therefore, it is clear that diesel has the highest

capacity of absorbing heat when exposed to temperature and canola oil has the lowest capacity.

To sum up, according to the results of biodiesel DSC and TGA analysis, biodiesel originated from canola oil show lower decomposition temperatures and higher volatility under both nitrogen and air atmosphere than canola oil. This indicates that biodiesel approaches to petrochemical fuel diesel by the transesterification reaction mechanisms and fuel characteristics of biodiesel are improved but still needs to be improved.

Several well-known kinetic models based on different approaches are applied to the TGA/DTG experiments data in order to determine the reaction parameters of the samples. According to the kinetic models, first order reaction models fit to the experimental results and give better results. Additionally, for the same kinetic models, similar activation energies are obtained but the activation energies are deviating. It is realized that the activation energies are in the order of canola oil>biodiesel>diesel. On the other hand for different heating rates the activation energies are in the order of 5°C/min>10°C/min>15°C/min. Hence in order for the biodiesel samples to be oxidized more heat is required when compared to diesel and more heat is required for the canola oil than biodiesel samples. In addition to that, as the heating rate of the experiment increases, sample does not response in the same sensitivity i.e. amount of heat absorbed by the sample does not increase at the same magnitude. As the heating rate of the experiment increases, more heat is required for the reaction to take place. Also, according to the kinetic modeling of biodiesel-diesel blends experiments, as the biodiesel blending grade increases, activation energy of the reaction increases. Hence, it can be concluded that as the blending rate of biodiesel increases, fuel becomes less oxidizing.

In addition to that, the experiment results of TGA/DTG pyrolysis of both pure samples and blends are analyzed by using the same kinetic models. It is found that, the activation energies of the reactions are in the order of canola oil> biodiesel>diesel for the pure samples. Hence, it is clear that as the transesterification reaction mechanism takes place

monoglyceride molecules lose their stability. However, biodiesel molecules are still more stable against heat when compared to the diesel molecules. On the other hand, for the different heating rates of reactions the activation energy of the reactions are in the order of  $5^{\circ}\text{C}/\text{min} > 10^{\circ}\text{C}/\text{min} > 15^{\circ}\text{C}/\text{min}$ . Hence, it is proven that as the heating rate of the reactions increase, samples cannot give the same severe response on absorbing the heat supplied, i.e. when the heating rate of the reactions increases the heat required to decompose the molecules gets higher. Arrhenius constants of the reaction are similar for the same kinetic models however they are deviating for different ones. Hence any relation for them cannot be derived.

## REFERENCES

- [1] International Energy Agency, 2009, “Key World Energy Statistics”, Available on web: [www.iea.gov.tr](http://www.iea.gov.tr) (December,2009)
- [2] Dantas, M.B., Conceicao M.M., Fernandes, V.J., Santos, N.A., Rosenhaim,R., Marques, A.L.B., Santos, I.M.G., Souza, A.G., 2007, “ Thermal and kinetic study of corn biodiesel obtained by the methanol and ethanol routes”, *Journal of Thermal Analysis and Calorimetry*, 87:835-839.
- [3] Bozbaş, K., 2003, “Biodiesel as an alternative motor fuel: Production and policies in the European Union”, *Energy Conversion and Management*, 44: 2093-2109.
- [4] Stauffer, E., Byron, D., 2007, “Alternative Fuels in Fire Debris Analysis: Biodiesel Basics”, *J Forensic Science*, 52(2): 371-379.
- [5] Kalligeros, S., Zannikos, Z., Stournas, S., Lois, E., Anastopoulos, G., Teas, Ch., Sakellaropoulos, F., 2003, “An investigation of using biodiesel/marine diesel blends on the performance of a stationary diesel engine”, *Biomass and Bioenergy*, 24: 141-149.
- [6] Demirbas, M.F., Balat, M., 2006, “Recent advances on the production and utilization trends of bio-fuels: A global perspective”, *Energy Conversion and Management*, 47: 2371-2381.
- [7] Wardle, D.A., 2003, “Global sale of green air travel supported using biodiesel”, *Renewable and Sustainable Energy Reviews*, 7: 1-64.
- [8] Monyem, A., Gerpen, J.H.V., 2001, “The effect of biodiesel oxidation on engine performance and emissions”, *Biomass and Bioenergy*, 20: 317-325.
- [9] Agarwal, A.K., 2007, “Biofuels (alcohols and biodiesel) applications as fuels for internal combustion engines”, *Progress in Energy and Combustion Science*, 33: 233-271.
- [10] Santos, J.C.O., Oliveira, A.D., Silva, C.C., Silva, J.D.S., Souza, A.G., Lima, L.N., 2007, “Kinetic and activation thermodynamic parameters on thermal decomposition of synthetic lubricant oils”, *Journal of Thermal Analysis and Calorimetry*, 87:823-829.
- [11] Bae., J.H., 1997, “Characterization of crude oil for fire flooding using thermal analysis methods” SPE AIME, 211-218.

- [12] Vossoughi, S., El-Shoubary, Y.M. 1990, "Kinetics of liquid hydrocarbon combustion using the DSC technique", *Thermochimica Acta*, 157(1):37-44.
- [13] Vossoughi, S. and Bartlett, G.V., 1982, "Development of Kinetic Model For In-Situ Combustion and Prediction Of The Process Variables Using TG/DSC Techniques", *SPE AIME*, 11073: 1-12.
- [14] Verkocy J. and Kamal N.J., 1986, "The Role of Thermal Analysis Techniques in the In-situ Combustion Process", *SPE Reservoir Engineering*, 1107:329-340.
- [15] Kok, M.V., 1993, "Use of thermal equipment to evaluate crude oils" *Thermochimica Acta*, 214(2) :315-324.
- [16] Goncalves M.L.A, Ribeiro D.A., da Mota D.A.P., Teixeira A.M.R.F., Teixeira M.A.G., 2005, "Thermal behaviour of refinery atmospheric residue from some different Oils", *Journal of Thermal Analysis and Calorimetry* , 80:387-391.
- [17] Gonçalves, M.L.A., Teixeira, M.A.G., Pereira, R.C.L., Mercury, R.L.P., and Matos, J.R., 2001, "Contribution of thermal analysis for characterization of asphaltenes from Brazilian crude oil", *Journal of Thermal Analysis and Calorimetry*, 64:697-706.
- [18] Kok, M.V, and Karacan, O., 1998, "Thermogravimetric investigation on prediction of thermal behaviour of petroleum distillation residues." , *Journal of Thermal Analysis and Calorimetry*, 52:781-788.
- [19] Candeia, R.A., Freitas, J.C.O., Souza, M.A.F., Conceicao, Santos, I.M.G., Soledade, L.E.B., Souza, A.G., 2007, "Thermal and rheological behaviour of diesel and methanol biodiesel blends", *Journal of Thermal Analysis and Calorimetry*, 87:653-656.
- [20] Santos, N.A., Tavares, M., L.A., Rosenhaim, R., Silva, F.C., Fernandes Jr., V.J., Santos, I.M.G., Souza, A.G., 2007, "Thermogravimetric and calorimetric evaluation of babassu biodiesel obtained by the methanol route ", *Journal of Thermal Analysis and Calorimetry*, 87:649-652.
- [21] Souza, A.G., Danta, H.J., Silva, M.C.D., Santos, I.M.G., Fernandes Jr., V.J., Sinfronio, F.S.M., Teixeira, L.S.G., Novak, Cs., 2007, "Thermal and kinetic evaluation of cotton oil biodiesel", *Journal of Thermal Analysis and Calorimetry*, 90:945-949.
- [22] Tonbul, Y., "Pyrolysis of pistachio shell as a biomass", *Journal of Thermal Analysis and Calorimetry*, 91:641-647.
- [23] Dweck, J., Sampaio, M.S., "Analysis of the thermal decomposition of commercial vegetable oils in air by simultaneous TG/DTA", *Journal of Thermal Analysis and Calorimetry*, 75:385-391.

- [24] Garcia, C.C., Franco, P.I.B.M., Zuppa, T.O, Filho, N.R.A., Leles, M.I.G., “Thermal stability of some cerrado plant oils”, *Journal of Thermal Analysis and Calorimetry*, 87:645-648.
- [25] Conceicao, M.M., Fernandes, V.J., Bezerra, A.F., Silva, M.C.D., Santos, I.M.G., Silva, F.C., Souza, A.G., 2007, “Dynamic kinetic calculation of castor oil biodiesel”, *Journal of Thermal Analysis and Calorimetry*, 87:865-869.
- [26] Dunn, R.O., 1999, “Thermal Analysis of Alternative Diesel Fuels from Vegetable Oils”, *Journal of the American Oil Chemists' Society*, 76:109-115.
- [27] Hazra, A., Alexander, K., Dollimore, D., Riga, A., 2004, “Characterization of some essential oils and their key components”, *Journal of Thermal Analysis and Calorimetry*, 75:317-330.
- [28] Stenseng, M., Zolin, A., Cenni, R., Frandsen, F., Jensen, A., Dam-Johansen, K., 2001, “Thermal analysis in combustion research”, *Journal of Thermal Analysis and Calorimetry*, 64:1325-1334.
- [29] Han, X.X., Jiang, X.M., Cui, Z.G., 2008, “Study of the combustion mechanism of oil shale semicoke in a thermogravimetric analyzer”, *Journal of Thermal Analysis and Calorimetry*, 92:595-600.
- [30] Guo, A., Zhang, X., Wang, Z., 2007, “Simulated delayed coking characteristics of petroleum residues and fractions by thermogravimetry”, *Fuel Processing Technology*, 89:643-650.
- [31] Santos, J.C.O., Lima, L.N., Santos, I.M.G., Souza, A.G., 2007, “Thermal, spectroscopic and rheological study of mineral base lubricating oils”, *Journal of Thermal Analysis and Calorimetry*, 3:639-643.
- [32] Gonçalves, M. L. A., Pinto da Mota, D.A., Teixeira, A.M.R.F., Teixeira, M.A.G, 2008, “Pyrolysis of petroleum fractions”, *Journal of Thermal Analysis and Calorimetry*, 91(2):341-346.
- [33] Gonçalves, M. L. A., Ribeiro, D.A., Pinto da Mota, D.A., Teixeira, A.M.R.F., Teixeira, M.A.G, 2005, “ Thermal behaviour of refinery atmospheric residue from some different oils ”, *Journal of Thermal Analysis and Calorimetry*, 80:387-391.
- [34] Kok M.V., Iscan A.G., 2001, “Catalytic Effects of Metallic Additives on The Combustion Properties of Crude Oils by Thermal Analysis Techniques”, *Journal of Thermal Analysis and Calorimetry*, 64: 1311-1318
- [35] Kök, M.V., Pamir, M.R., 2000, “Comparative pyrolysis and combustion kinetics of oil shales”, *Journal of Thermal Analysis and Calorimetry*, 55(2):185-194.

- [36] Kök, M.V., Pamir, M.R., 1998, “ASTM kinetics of oil shales”, *Journal of Thermal Analysis and Calorimetry*, 53:567:575.
- [37] Kök, M.V., Pamir, M.R., 2003, “Pyrolysis kinetics of oil shales determined by DSC and TG/DTG”, *Oil Shale*, 20:57-68.
- [38] Aboulkas A., El Harfi K., El Bouadili A., Benchanaa M., Mokhlisse A., Outzourit A., 2007, “Kinetics of Co-pyrolysis of Tarfaya (Morocco) Oil Shale with High-density Polyethylene”, *Oil Shale*, 24(1):15-33.
- [39] Fogler, H.S., 2006, *Elements of Chemical Reaction Engineering*, 4<sup>th</sup> Edition, Pearson Education Inc., USA.
- [40] Dollimore, D., 1992, “The application of thermal analysis in studying the thermal decomposition of solids”, *Thermochimica Acta*, 203:7-23.
- [41] Vyazovkin S., Wight C.A., 1999, “Model-free and model-fitting approaches to kinetic analysis of isothermal and nonisothermal data”, *Thermochimica Acta*, 340:53-58.
- [42] ASTM, 1979, “Standard Test Method for Arrhenius Kinetic Constants for Thermally Unstable Materials”, *ANSI/ASTM*, Philadelphia, 1979: 678 – 79.
- [43] Kissinger, H. E., 1957, “Reaction kinetics in differential thermal analysis”, *Analytical Chemistry*, 29: 1702–1706.
- [44] Horowitz, H.H., Metzger, G., 1963, “A new analysis of thermogravimetric traces”, *Analytical Chemistry* 35:1464-1473.
- [45] Hatakeyama, T., Liu, Z., 1998, *Handbook of Thermal Analysis*, John Willey and Sons Inc., England.
- [46] Mamleev, V., Bourbigot, S., Bras, M.L., Lefebvre, J., 2004, “Three model-free method for calculation of activation energy in TG”, *Journal of Thermal Analysis and Calorimetry*, 78:1009-1027.
- [47] Wampler, T.H., 2006, *Applied Pyrolysis Handbook*, 2<sup>nd</sup> Edition, Taylor and Francis Group, USA.
- [48] Sutcu, H., 2007, “Pyrolysis by thermogravimetric analysis of blends of peat with coals of different characteristics and biomass”, *Journal of Chinese Institute of Chemical Engineers*, 38:245-249.
- [49] Albright, L.F., Crynes, B.L., Corcoran, W.H., 1983, *Pyrolysis: Theory and Industrial Practice*, Academic Press Inc., New York.

- [50] Medeiros, R.I., Leles, M.I.G., Dias, F.C., Kunert, R., Filho, N.R.A., 2007, "Thermogravimetric isolation and chromatographic characterization of volatile fractions of petroleum", *Journal of Thermal Analysis and Chromatography*, 91:225-229.
- [51] Lima, D.G., Soares, V.C.D., Ribeiro, E.B., Carvalho, D.A., Cardoso, E.C.V., Rassi, F.C., Mundim, K.C., Rubim, J.C., Suarez, P.A.Z., 2004, "Diesel-like fuel obtained by pyrolysis of vegetable oils", *Journal of Analytical and Applied Pyrolysis*, 71 (2):987-996.
- [52] Dalai, A.K., Kulkarni, M.G., Bakhshi, N.N., 2007, "Transesterification of canola oil in mixed methanol/ethanol system and use of esters as lubricity additive", *Biosource Technology*, 98:2027-2033.
- [53] Herbinet, O., Pitz, W.J., Westbrook, C.K., 2008, "Detailed chemical kinetic oxidation mechanism for a biodiesel surrogate", *Combustion and Flame*, 154:507-528.
- [54] Daniel, R., Baiardo, M., 2006, *Advanced Materials Characterization by Thermal Analysis, Calorimetry and Rheology*, TGA TA Instruments Guide, New Castle.
- [55] TA Instruments Q Series Getting Started Guide, 2006 (June) *TGA Thermogravimetric Analyzer*, New Castle UK.
- [56] TA Instruments Q Series Getting Started Guide, 2006 (June) *DSC Differential Scanning Calorimeter*, New Castle UK.
- [57] Sharama, Y.C., Singh, B., Upadhyay, S.N., 2008, "Advancements in development and characterization of biodiesel: A review", *Fuel*, 87:2355-2377.
- [58] Demirbaş, A., 2007, "Alternatives to petroleum diesel fuel", *Energy Sources, Part B*, 2:343-351.
- [59] Demirbaş, A., 2003, "Biodiesel from vegetable oils via transesterification in supercritical methanol", *Energy Conversion and Management*, 43: 2349-2356.
- [60] Pischinger, G.M., Falcon, A.M., Siekmann, R.W., Fernandes, F.R., 1982, "Methyl esters of plant oils as diesel fuels, either straight or in blends. Vegetable oils", *ASAE Publication*, 73: 4-82
- [61] Schwab, A.W., Bagby, M.O., Freedman, B., 1987, "Preparation and properties of diesel fuels from vegetable oils", *Fuel*, 66:1372-1378.
- [62] Srivastava, A., Prasad, R., 2000, "Triglycerides-based diesel fuels", *Renewable Sustainable Energy Rev.*, 4:111-133.
- [63] Ali, Y.H.,M.A., Cuppett, S.,L., 1995, "Fuel properties of tallow and soybean oil esters", *JAACS*, 72:1557-1564.

- [64] Sarı, P., 2006, "Preliminary Design and Construction of a Prototype Canola Seed Oil Extraction Machine", A master's Thesis for the degree of Master of Science in Mechanical Engineering, Middle East Technical University, Ankara.
- [65] "World Oilseed Production 2006", *World Statistics*, Available on web: [http://www.soystats.com/2007/page\\_29.htm](http://www.soystats.com/2007/page_29.htm), (December 27<sup>th</sup>, 2009).
- [66] Özdemir, A., 2008, "Experimental Investigation of Use of Canola Oil as a Diesel Fuel", A master's Thesis for the degree of Master of Science in Mechanical Engineering, Middle East Technical University, Ankara.
- [67] Self, F., Ekholm, E., 2000, Bowers, K., Refining Overview - Petroleum, Processes and Products, PennWell Corp, Texas, USA.
- [68] Parkash, S., Refining Processes Handbook, 2003, Gulf Professional Publishing USA.
- [69] Millington A, Price D, Hughes R., 1993, "The use of thermal analysis techniques to obtain information relevant to the in situ combustion process for enhanced oil recovery", *Journal of Thermal Analysis and Calorimetry*, 40: 225–238.
- [70] Kok M.V., Karacan C.O., 2000, "Behaviour and Effect of SARA Fractions of Oil During Combustion", *SPE Reservoir Evaluation & Engineering*, 3(5):380-385.
- [71] Moore, R.G., Bennion D.W., Ursenbach M.G., A, 1998, "Review of In Situ Combustion Mechanisms", *Unitar/Undp*, 5.
- [72] Kok M.V., Pokol G., Keskin C., Madarasz J., 2004, "Light crude oil combustion in the presence of limestone matrix", *Journal of Thermal Analysis and Calorimetry*, 75 (3): 781-786.
- [73] Gündoğar, S.A., 2010, "Thermal Characterization and Kinetics of Crude Oils by TGA and DSC Methods", A master's Thesis for the degree of Master of Science in Petroleum and Natural Gas Engineering, Middle East Technical University, Ankara.
- [74] Ditmars, D.A., 1990, "Calibration standards for differential scanning calorimetric measurement of  $T_{fus}$  and  $\Delta H_{fus}H_m$ ", *The Journal of Chemical Thermodynamics*, 22 (7): 639-651.
- [75] Murugan P., Mahinpey N., Mani T., Freitag N., 2009, "Pyrolysis and combustion kinetics of Fosterton oil using thermogravimetric analysis", *Fuel*, 88 (9):1708-1713.
- [76] Kök, M., V., 2001, "Thermal Analysis Applications in Fossil Fuel Science", *Journal of Thermal Analysis and Calorimetry*, 68:1061-1077.

[77] Hatakeyama, T., Liu, Z., 1998, Handbook of Thermal Analysis, John Willey and Sons Inc., England.

## APPENDIX A

### PETROLEUM FRACTIONS BY GC ANALYSIS

**Table A.1:** Volatile fractions of petroleum sample chemical composition determined by HRGC-MS-EI [50]

Peak	Compound	<i>t</i> /min	Peak	Compound	<i>t</i> /min	Peak	Compound	<i>t</i> /min
01	2,2-dimethyl-butane	12.633	18	1,1,3-trimethyl-cyclohexane	32.050	35	2-methyl-undecane	47.833
02	3-methyl-pentane	13.492	19	2,3,4-trimethyl-hexane	33.775	36	<i>n</i> -dodecane	48.925
03	<i>n</i> -hexane	14.533	20	( <i>o.m.p.</i> ) xylenes	35.108	37	2,6-dimethyl-undecane	49.408
04	methyl-cyclopentane	16.383	21	<i>n</i> -nonane	36.125	38	4,6-dimethyl-undecane	51.083
05	benzene	18.025	22	1-ethyl-2-methyl-cyclohexane	36.875	39	<i>n</i> -tridecane	51.700
06	cyclohexane	18.733	23	1-propenyl-cyclohexane	37.658	40	2,6,10-trimethyl-dodecane	53.708
07	3-methyl-hexane	19.897	24	3-methyl-nonane	38.267	41	<i>n</i> -tetradecane	54.133
08	1,3-cyclopentane	20.842	25	3-ethyl-2-methyl-heptane	38.767	42	<i>n</i> -pentadecane	56.317
09	<i>n</i> -heptane	21.625	26	4-methyl-nonane	39.833	43	<i>n</i> -hexadecane	58.342
10	methyl-cyclohexane	23.350	27	1,1,2,3-tetramethyl-cyclohexane	39.908	44	2,6,10,14-tetramethyl-hexadecane	59.417
11	toluene	25.850	28	trimethyl-benzene	41.008	45	<i>n</i> -heptadecane	60.342
12	2,5-dimethyl-hexane	26.575	29	<i>n</i> -decane	41.533	46	<i>n</i> -octadecane	62.408
13	3-methyl-heptane	27.150	30	trimethyl-benzene	42.375	47	<i>n</i> -nonadecane	64.642
14	1,3-dimethyl-cyclohexane	27.575	31	4-methyl-decane	42.650	48	<i>n</i> -eicosane	67.192
15	<i>n</i> -octane	29.067	32	<i>n</i> -butyl-cyclohexane	43.275	49	<i>n</i> -heneicosane	70.175
16	1,4-dimethyl-cyclohexane	29.567	33	<i>n</i> -undecane	45.633			
17	ethyl-cyclohexane	31.650	34	pentyl-cyclohexane	47.217			

## **APPENDIX B**

### **TA INSTRUMENTS CHARACTERISTICS**

**Table B.1: TGA Instrument Characteristics**

<b>TGA Instrument Properties</b>	
<b>Dimensions</b>	Depth: 55.9 cm (22 in.) Width: 47 cm (18.5 in.) Height: 52.1 cm(20.5 in.)
<b>Weight</b>	30.9 kg(68 lbs) 8.18 kg(18 lbs)
<b>Power</b>	120 Vac, 50/60 Hz, Standard 230 Vac,50/60 Hz, if configured with a step-down transformer
<b>Energy consumption</b>	1.5 kVA
<b>Insulating Rating</b>	All electrical insulation between hazardous components has been designed to meet the requirements of reinforced insulation. Low voltage circuits are grounded.
<b>Room Operating Temperature</b>	15 C to 35 (non-condensing)
<b>Temperature control range</b>	Ambient +5 C to 1000 C
<b>Thermocouple</b>	Platinel II
<b>Heating rate with standart furnace</b>	0.1 to 100 C/min
<b>Sample Pan Properties</b>	
<b>Type</b>	Platinum
<b>Volume Capacity</b>	Platinum 100 mL
<b>Balance Mechanism</b>	
<b>Weighing capacity (sample)</b>	1.0 g
<b>Resolution 0.1 <math>\mu</math>g</b>	< + 0.1%
<b>Ranges 200 mg range: 0.1 <math>\mu</math>g — 200 mg</b>	1000 mg range: 1 $\mu$ g — 1000 mg

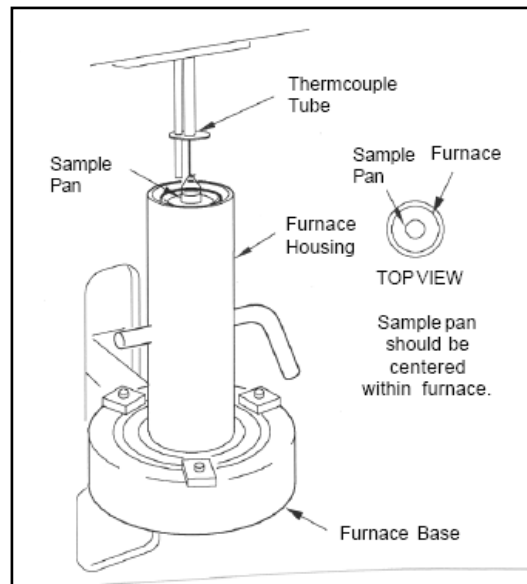
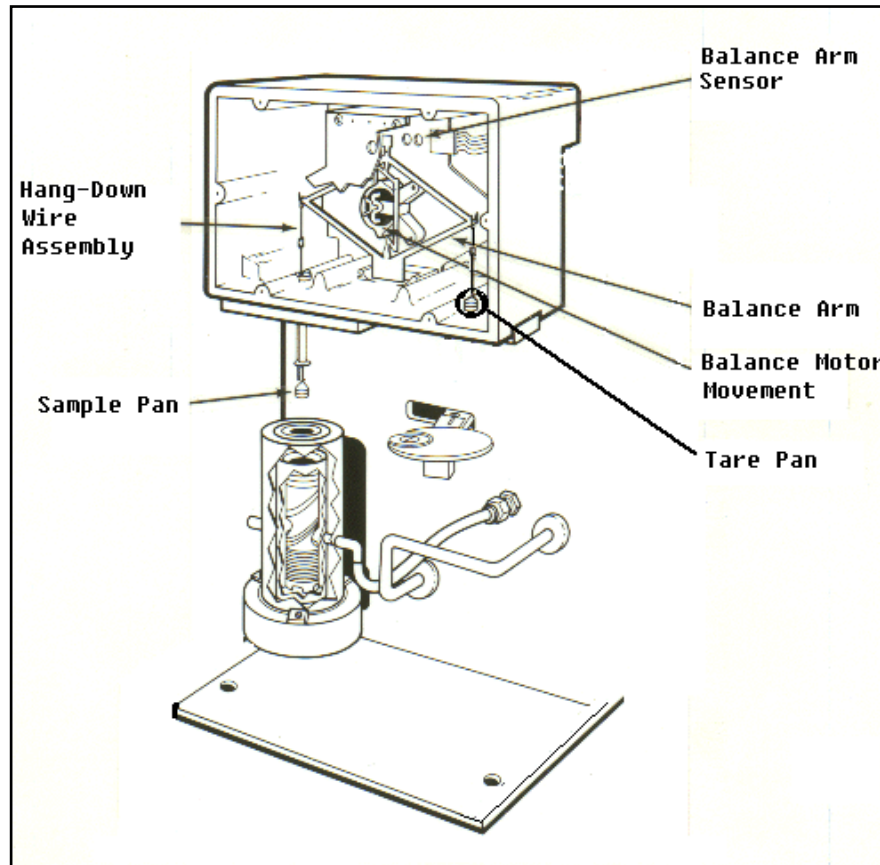


**Figure B.1: a. TGA balance segment, b. TGA furnace segment**

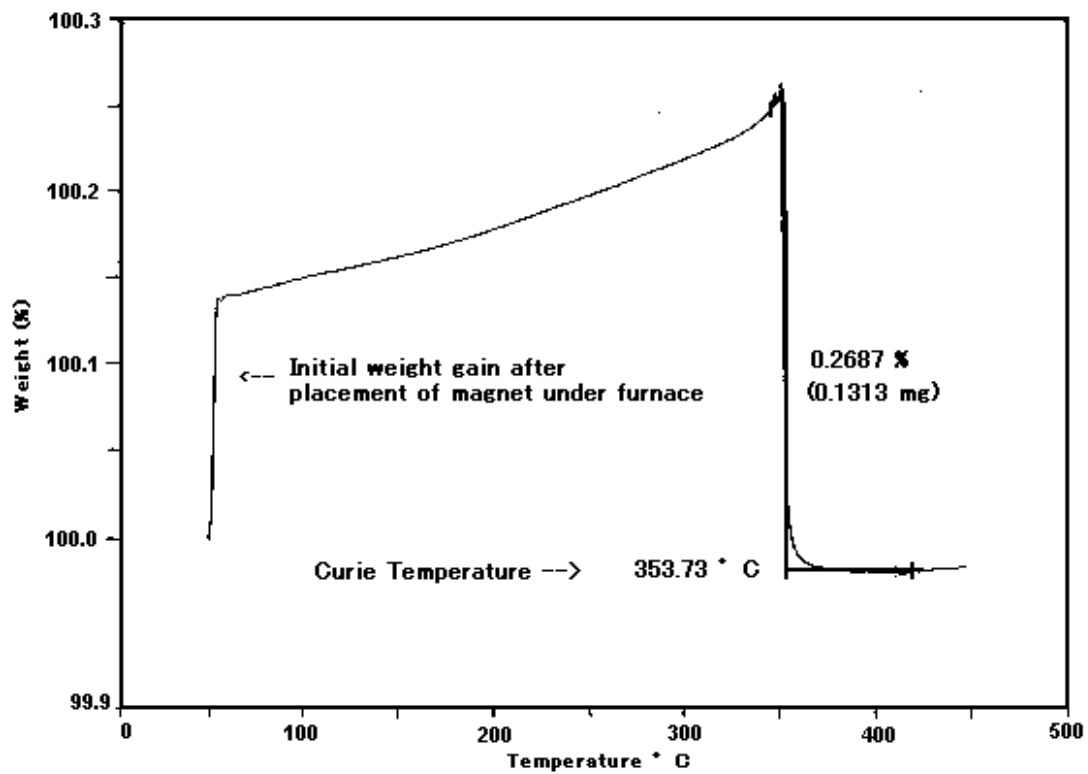
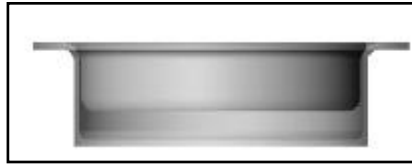


Figure B.2: TGA curie temperature determination by using nickel as sample [55]

**Table B.2:** DSC Instrument Characteristics

<b>DSC Instrument Properties</b>	
<b>Dimensions</b>	Depth 56 cm (22 in.) Width 46 cm (18 in.) Height 48 cm (19 in.)
<b>Weight (without auto sampler)</b>	25 kg (54 lbs) 8.18 kg (18 lbs)
<b>Weight of cell alone</b>	1.6 kg (3.5 lbs)
<b>Weight of transformer</b>	8.6 kg (19 lbs)
<b>Power</b>	120 Vac, 47–63 Hz, 500 W (4.5 amps) standard 230 Vac, 47–63 Hz, 500 W (2.25 amps) if configured with a voltage configuration unit
<b>Operating environment Conditions</b>	Temperature: 15–30 °C Relative Humidity: 5–80 % (non-condensing) Maximum Altitude: 2000 m
<b>with FACS</b>	<b>Temperature Range</b> Room temperature to 725 °C
<b>with Quench Cooler</b>	-180 °C to 550 °C
<b>Sample</b>	
<b>Size</b>	0.5 to 100 mg
<b>Sample volume</b>	10 mm <sup>3</sup> in hermetic pans
<b>Sample pans</b>	various open or hermetically sealed
<b>Purge Gas</b>	
<b>Type</b>	air, argon, helium, nitrogen or oxygen
<b>Typical purge flow rate</b>	50 mL/min
<b>Cell volume</b>	3.4 mL



**Figure B.3:** DSC pan type with sealing equipment of hermetic seal [56]



**Figure B.4:** Squeezing instrument of hermetic seal [56]

## **APPENDIX C**

### **HEAT CAPACITANCE CURVE DERIVATION OF SAPPHIRE**

According to Ditmars et al.s' experimental study, Cp data of sapphire is presented in Table C.1.

**Table C.1:** Cp (J/g°C) data of sapphire with respect to temperature

Temperature °C	Temperature K	Cp, J/g C	Temperature °C	Temperature K	Cp, J/g C	Temperature °C	Temperature K	Cp, J/g C
-183.15	90	0.0949	146.85	420	0.966	546.85	820	1.1837
-173.15	100	0.1261	156.85	430	0.977	566.85	840	1.1888
-163.15	110	0.1603	166.85	440	0.9875	586.85	860	1.1937
-153.15	120	0.1968	176.85	450	0.9975	606.85	880	1.1985
-143.15	130	0.2349	186.85	460	1.007	626.85	900	1.203
-133.15	140	0.2739	196.85	470	1.0161	646.85	920	1.2074
-123.15	150	0.3134	206.85	480	1.0247	666.85	940	1.2117
-113.15	170	0.3526	216.85	490	1.033	686.85	960	1.2159
-103.15	170	0.3913	226.85	500	1.0409	706.85	980	1.2198
-93.15	180	0.4291	236.85	510	1.0484	726.85	1000	1.2237
-83.15	190	0.4659	246.85	520	1.0557	746.85	1020	1.2275
-73.15	200	0.5014	256.85	530	1.0627	766.85	1040	1.2312
-63.15	210	0.5356	266.85	540	1.0692	766.85	1040	1.2312
-53.15	220	0.5684	276.85	550	1.0756	806.85	1080	1.2383
-43.15	230	0.5996	286.85	560	1.0817	826.85	1100	1.2417
-33.15	240	0.6294	296.85	570	1.0876	846.85	1120	1.2451
-23.15	250	0.6579	306.85	580	1.0932	866.85	1140	1.2484
-13.15	260	0.6848	316.85	590	1.0987	886.85	1160	1.2516
-3.15	270	0.7103	326.85	600	1.038	906.85	1180	1.2548
0	273.15	0.718	336.85	610	1.1089	926.85	1200	1.2578
6.85	280	0.7343	346.85	620	1.1137	976.85	1250	1.2653
16.85	290	0.7572	356.85	630	1.1183	1026.85	1300	1.2724
26.85	300	0.7788	366.85	640	1.1228	1076.85	1350	1.2792
36.85	310	0.7994	376.85	650	1.1271	1126.85	1400	1.2856
46.85	320	0.8188	386.85	660	1.1313	1176.85	1450	1.2917
56.85	330	0.8373	396.85	670	1.1353	1226.85	1500	1.2975
66.85	340	0.8548	406.85	680	1.1393	1276.8	1550	1.3028
76.85	350	0.8713	416.85	690	1.1431	1326.8	1600	1.3079
86.85	360	0.8871	426.85	700	1.1467	1376.8	1650	1.3128
96.85	370	0.902	446.85	720	1.1538	1376.8	1700	1.3128
106.85	380	0.9161	466.85	740	1.1604			
116.85	390	0.9296	486.85	760	1.1667			
126.85	400	0.9423	506.85	780	1.1726			
136.85	410	0.9545	526.85	800	1.1783			

By using the data available in C.1 heat capacitance equation of Sapphire on temperature is determined for the temperature interval of -180-1480°C and 0-150°C separately. Since the Cp calculation of samples are performed by using the data of pyrolysis data of DSC between 40-110°C, equation belonging to the interval of 0-150°C is used during the Cp calculation of pure samples.

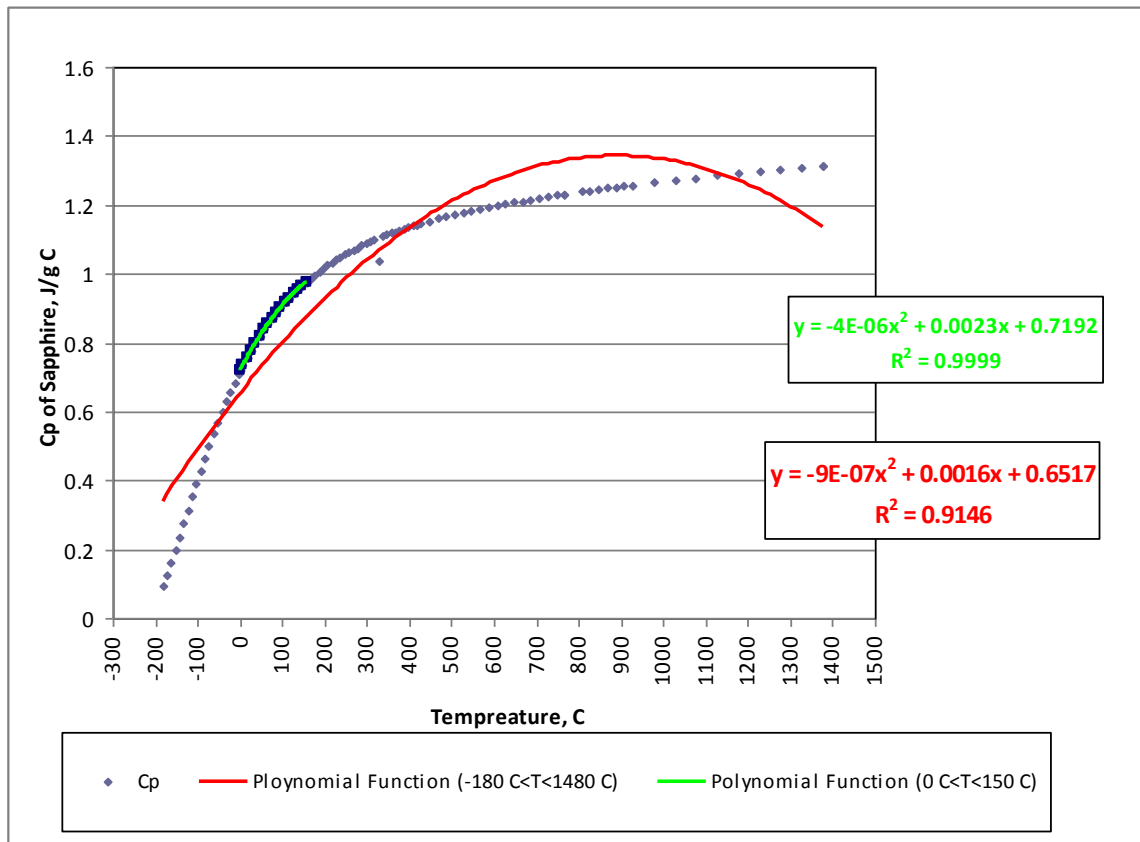


**Figure C.1:** Cp of Sapphire with respect to temperature and equation derivation

## **APPENDIX D**

### **TGA/DTG AND DSC COMBUSTION RESULTS**

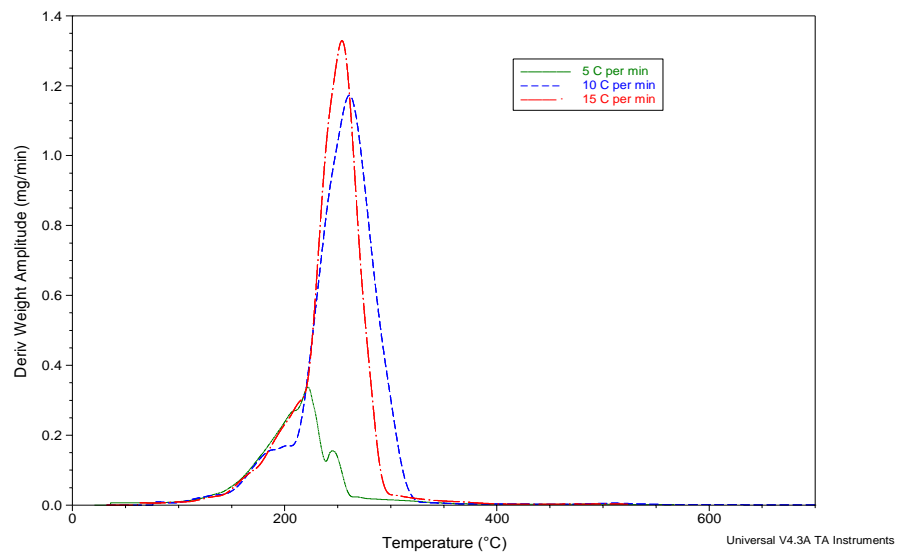
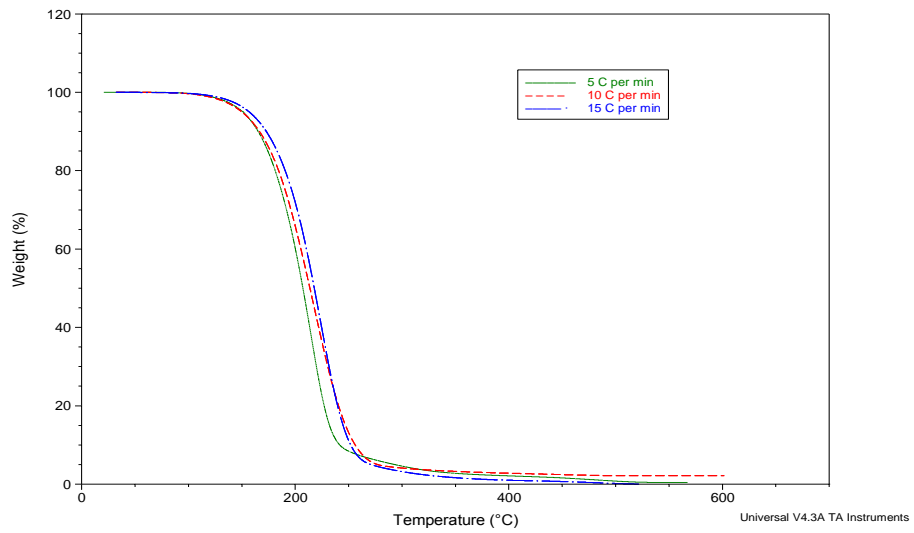


**Figure D.1:** TGA/DTG Thermogram of biodiesel combustion at different heating rates; 5, 10, 15 °C /min

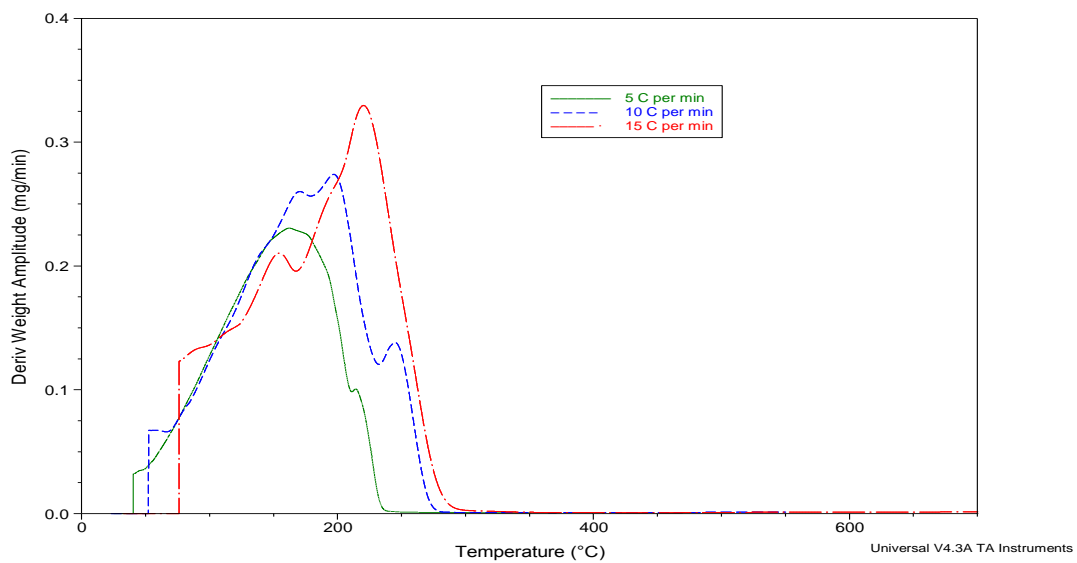
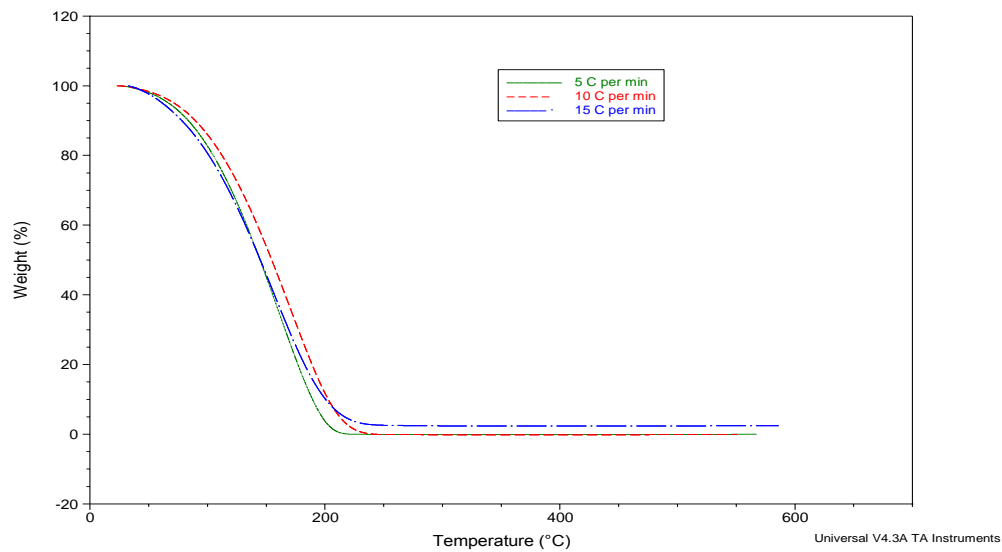


**Figure D.2:** TGA/DTG Thermogram of diesel combustion at different heating rates; 5, 10, 15°C /min

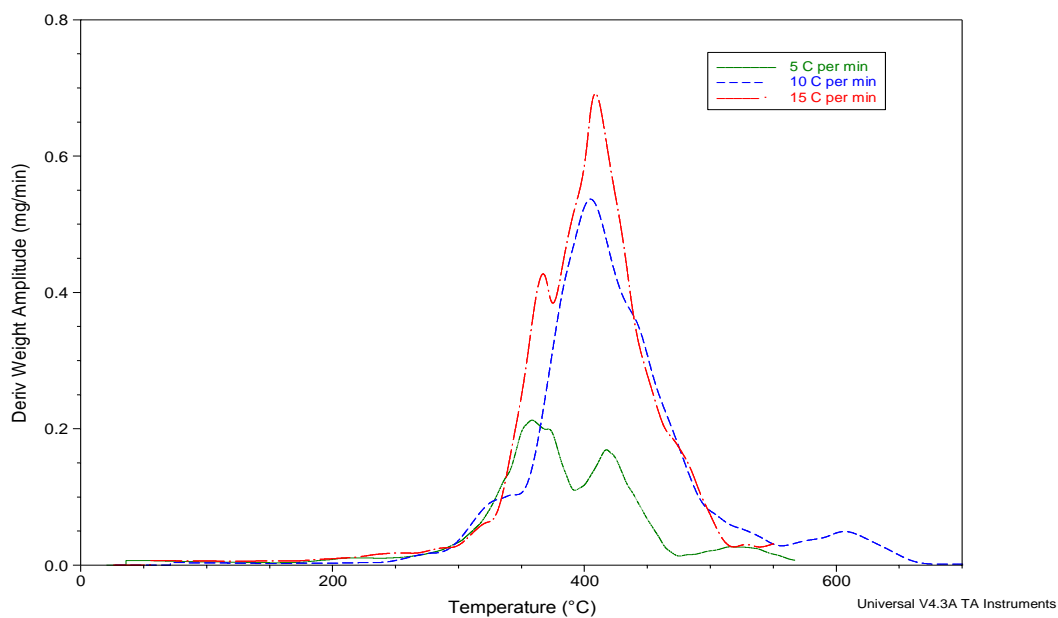
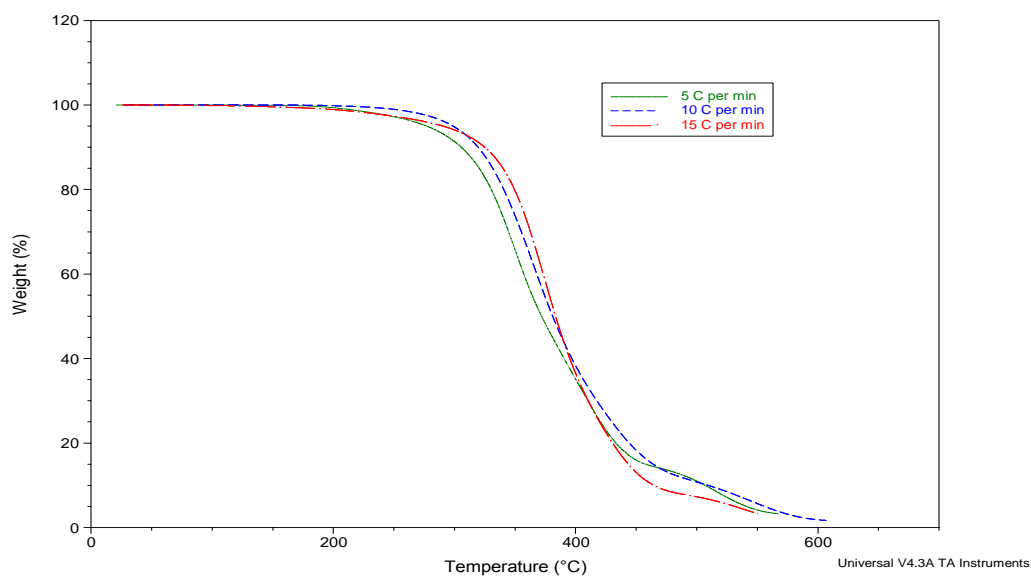


**Figure D.3:** TGA/DTG Thermogram of canola oil combustion at different heating rates; 5, 10, 15 °C /min

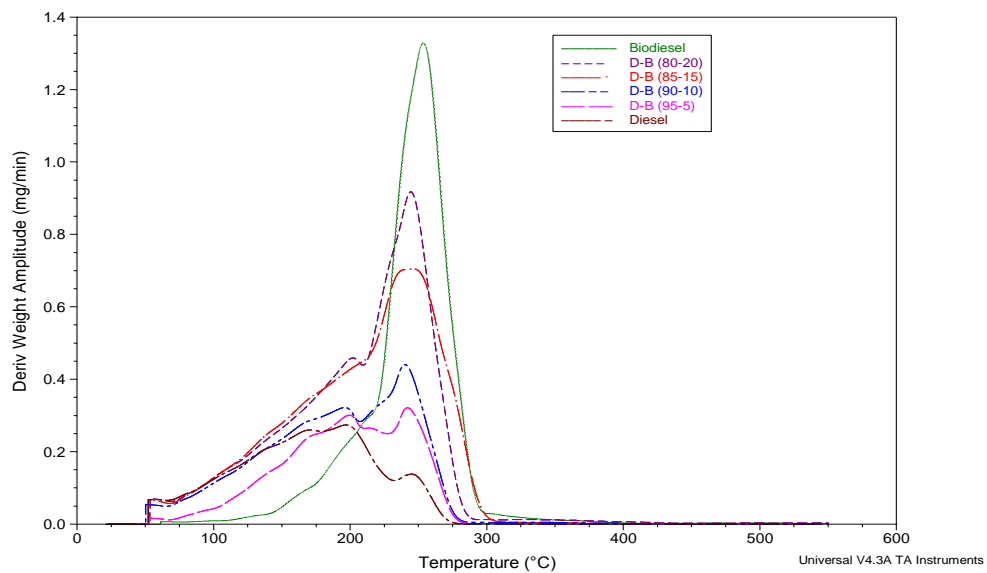
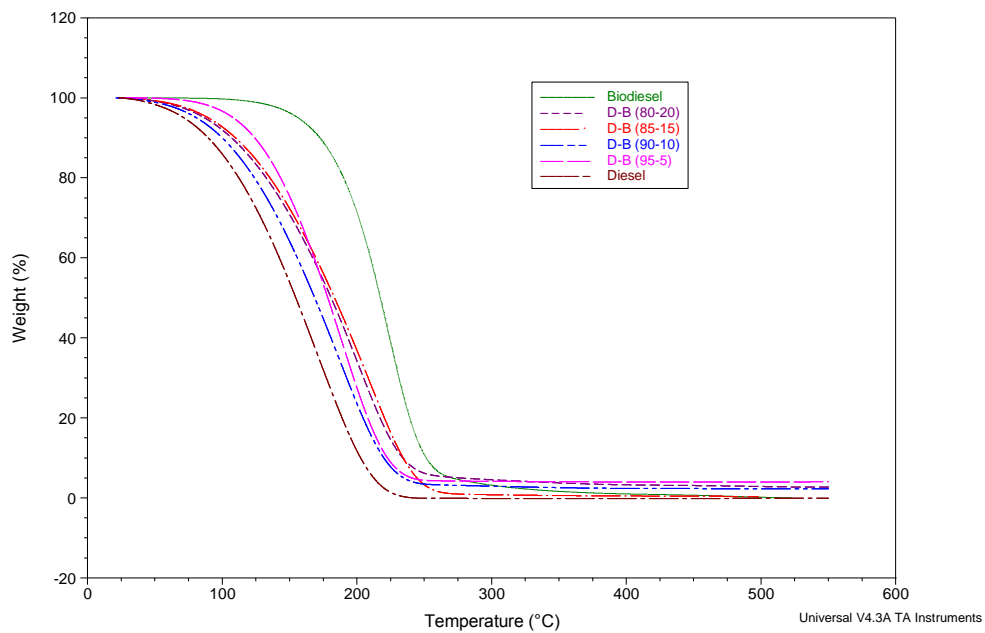


**Figure D.4:** TGA/DTG Thermogram of biodiesel-diesel mixtures combustion at a constant heating rate of  $10^{\circ}\text{C}/\text{min}$

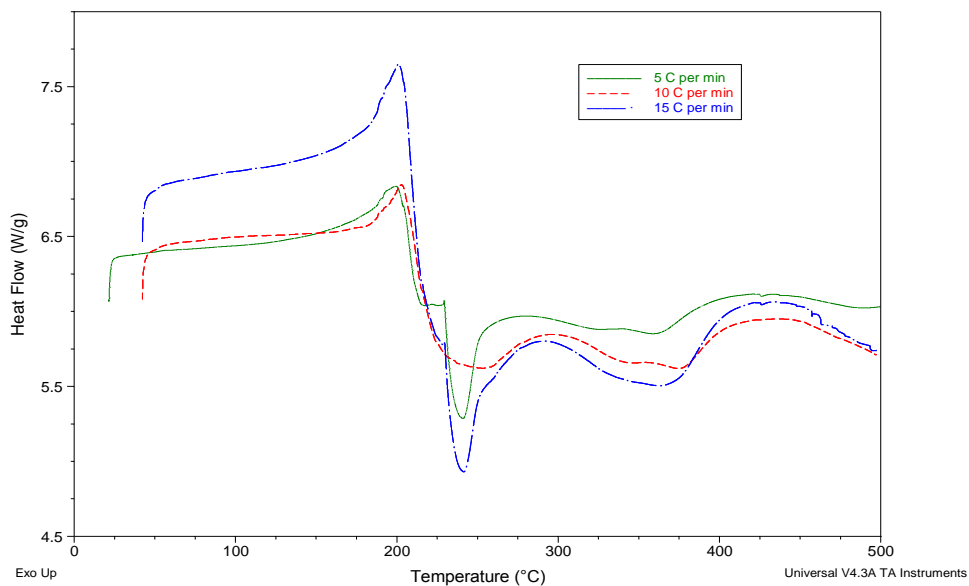


**Figure D.5:** DSC Thermogram of biodiesel combustion at different heating rates; 5, 10, 15°C /min

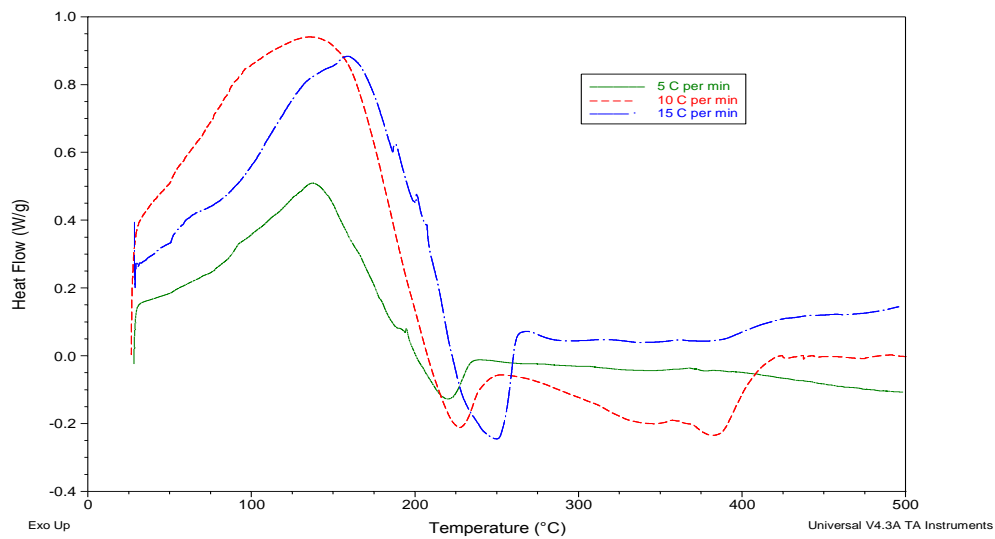


**Figure D.6:** DSC Thermogram of diesel combustion at different heating rates; 5, 10, 15°C /min

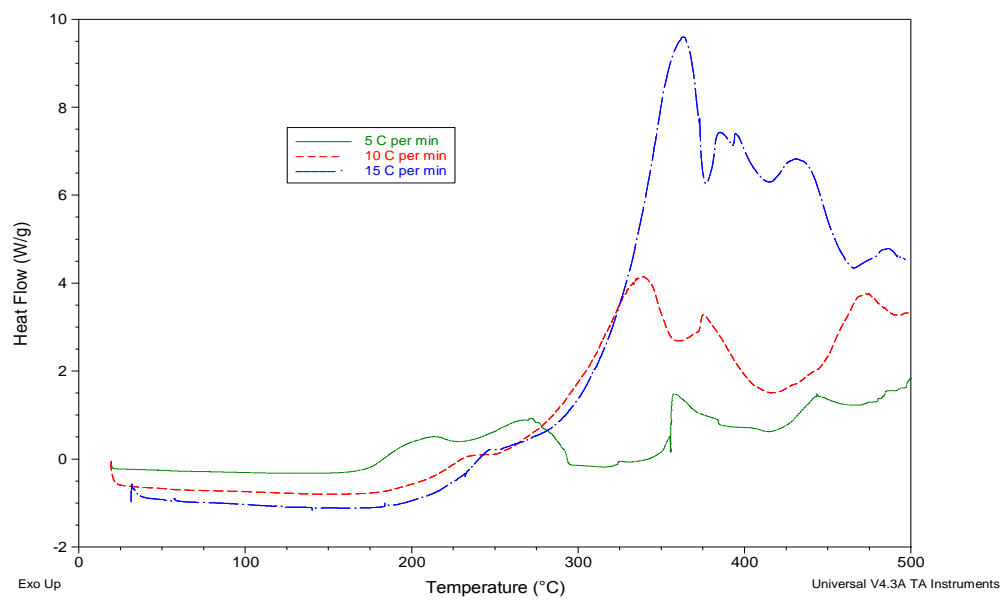


**Figure D.7:** DSC Thermogram of canola combustion at different heating rates; 5, 10, 15 °C /min

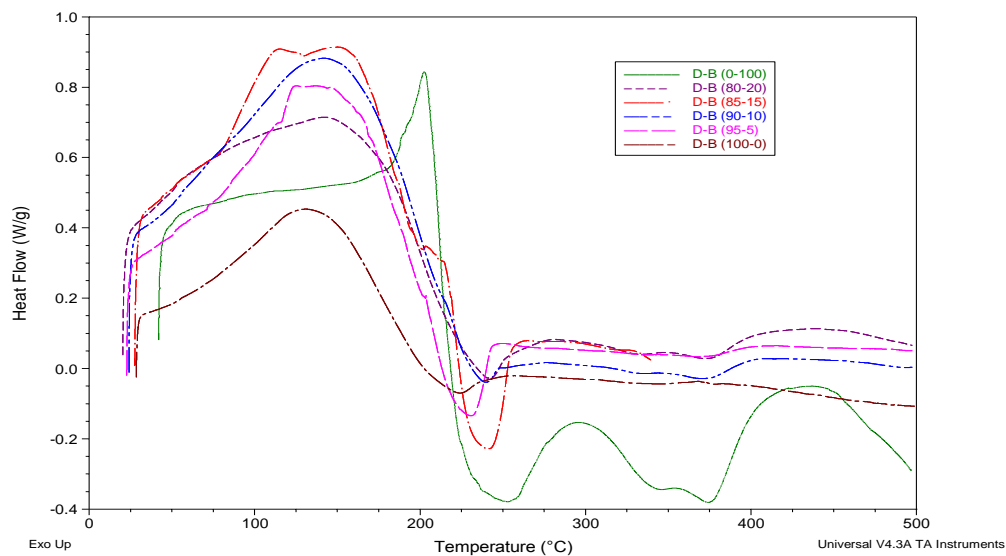


**Figure D.8:** DSC Thermogram of biodiesel-diesel mixtures combustion at a constant heating rate of 10 °C /min

## **APPENDIX E**

### **TGA/DTG AND DSC PYROLYSIS RESULTS**

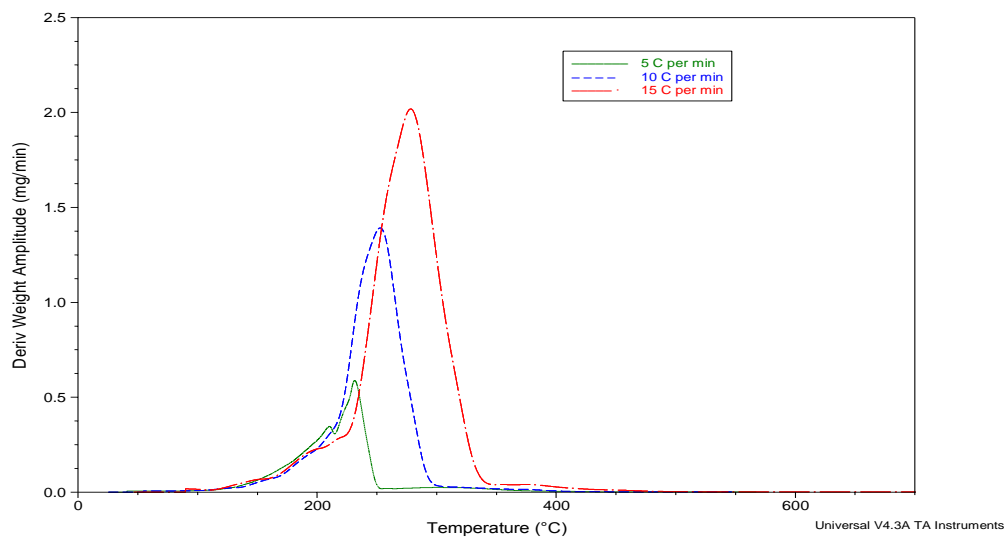
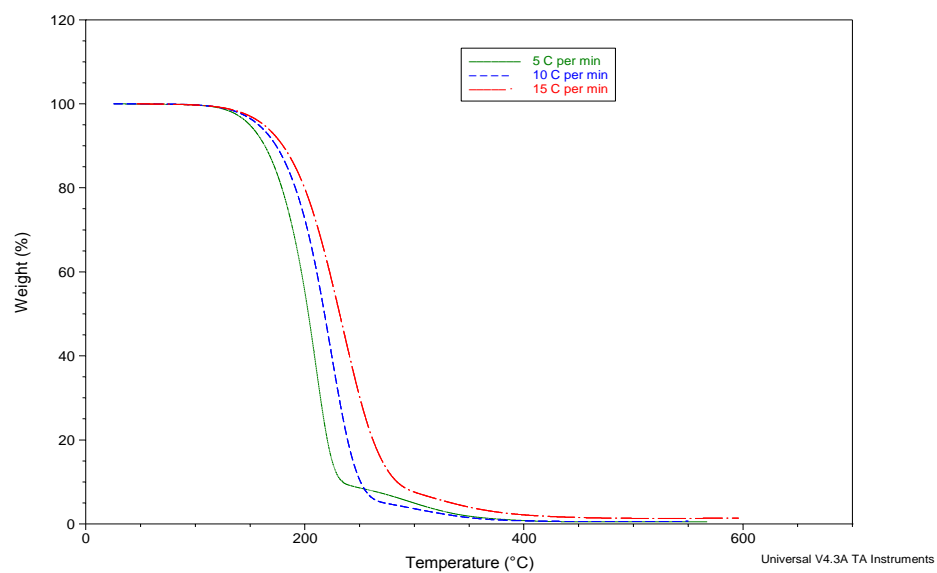


**Figure E.1:** TGA/DTG Thermogram of biodiesel pyrolysis at different heating rates; 5, 10, 15°C /min

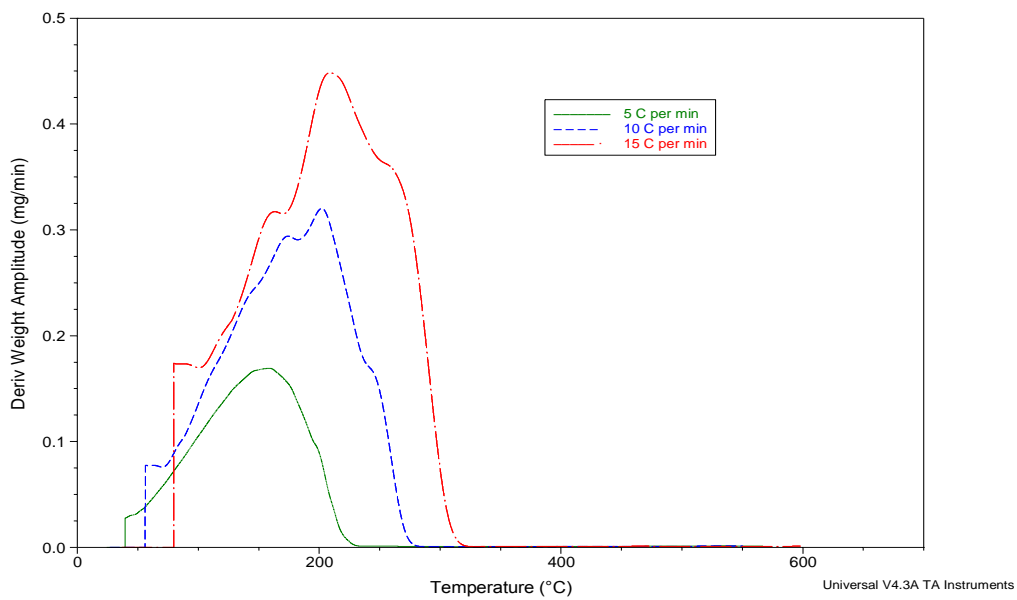
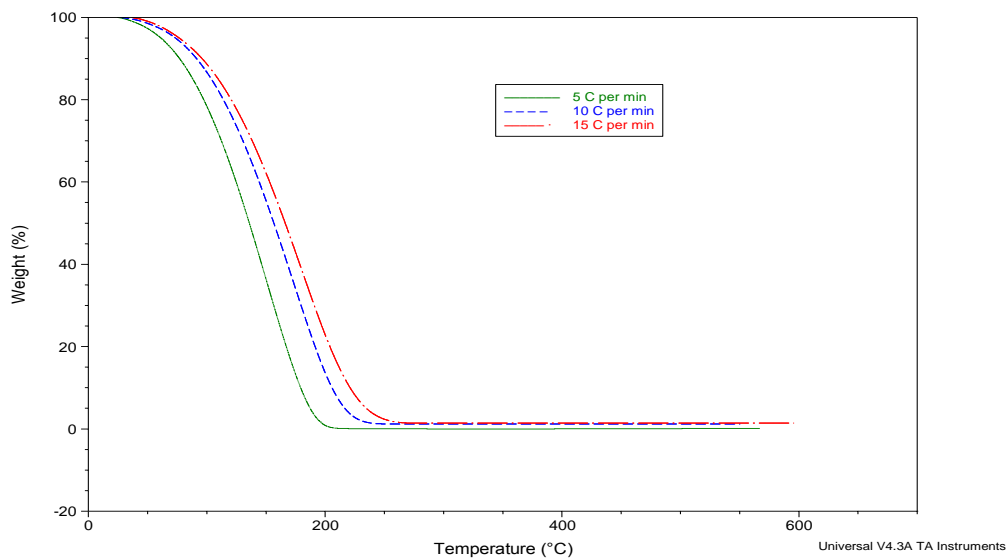


**Figure E.2:** TGA/DTG Thermogram of diesel pyrolysis at different heating rates; 5, 10, 15 °C /min

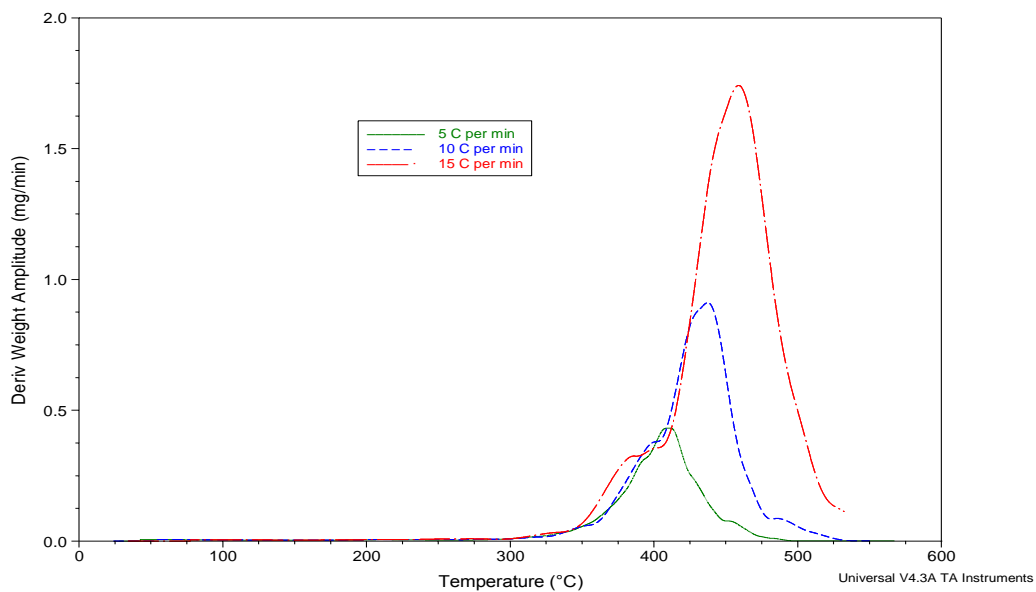
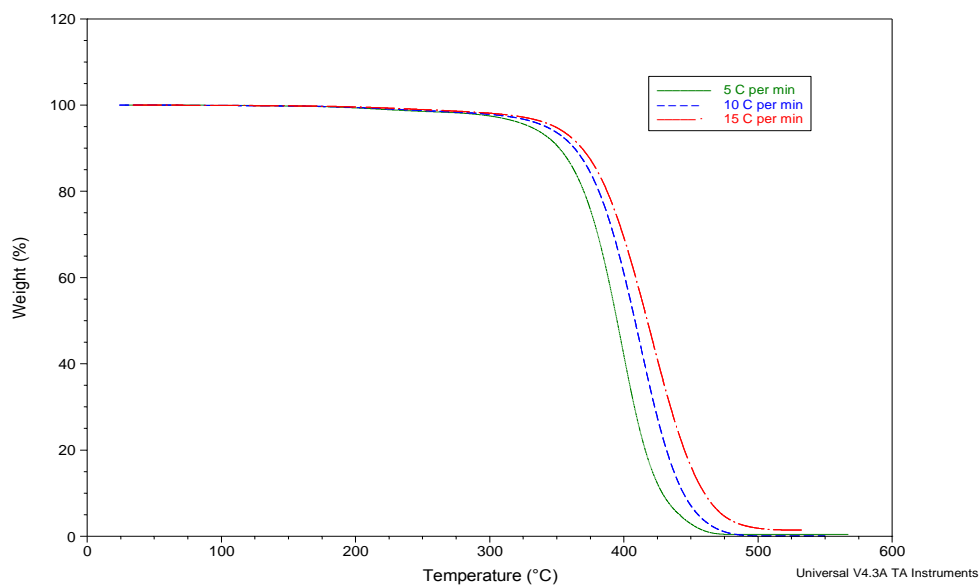


**Figure E.3:** TGA/DTG Thermogram of canola oil pyrolysis at different heating rates; 5, 10, 15°C /min

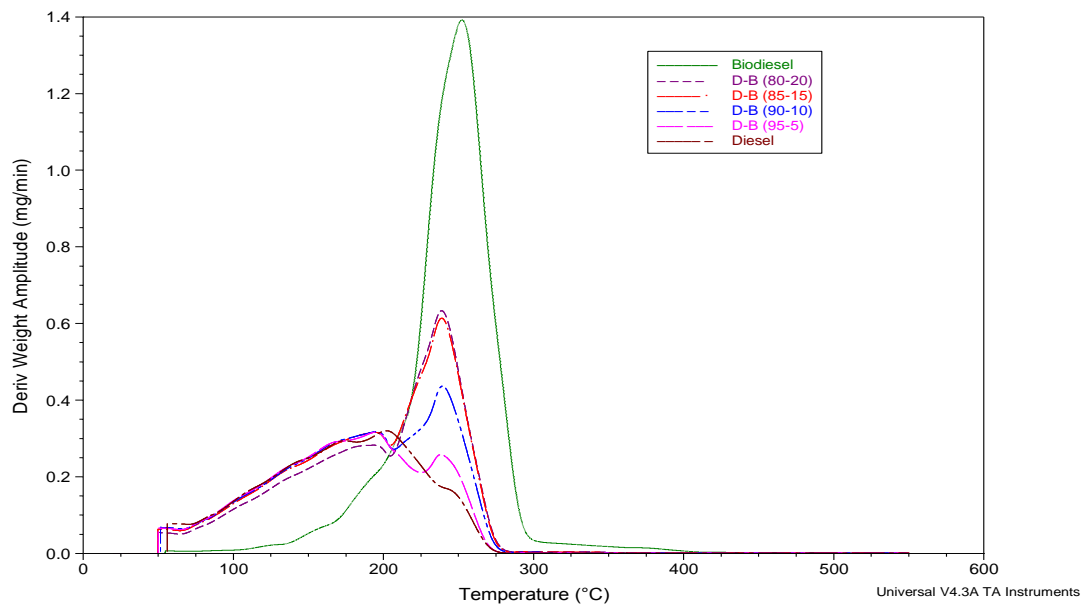
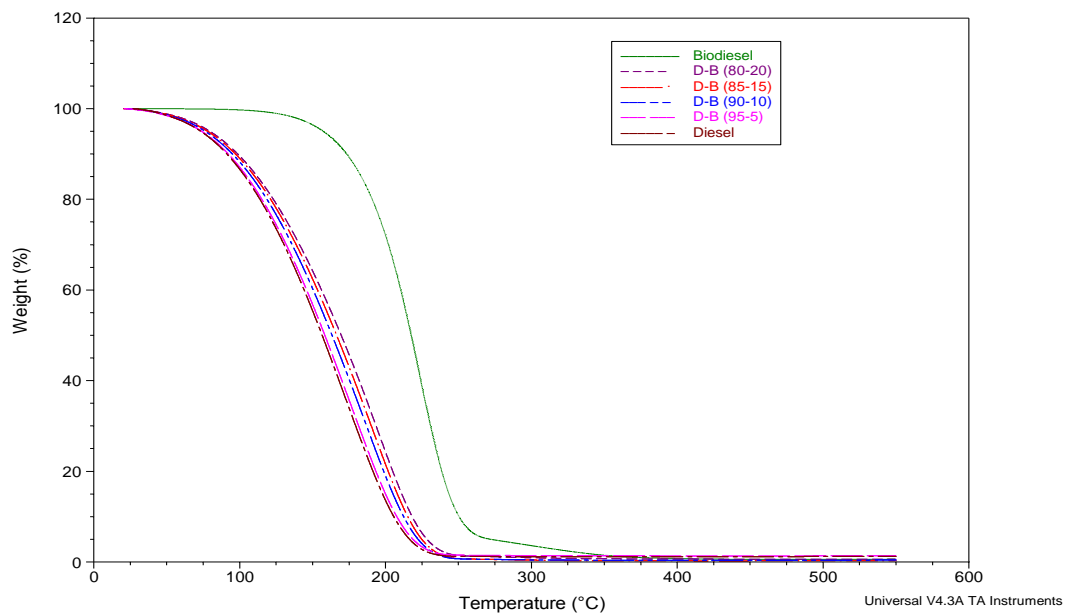


**Figure E.4:** TGA/DTG Thermogram of B100, B20, B15, B10, B05, B00 mixtures pyrolysis at a constant heating rate of 10°C /min

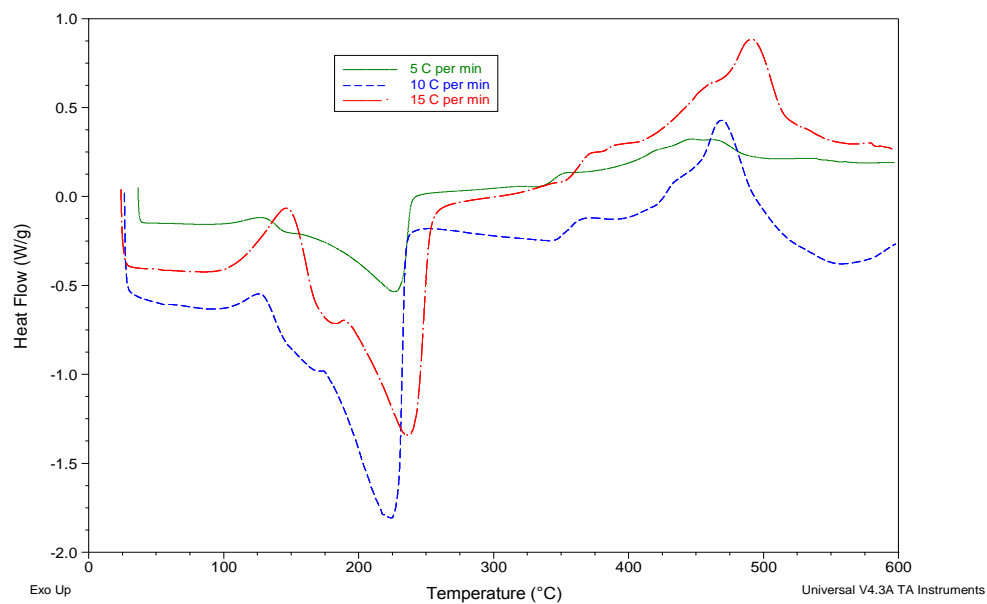


**Figure E.5:** DSC Thermogram of biodiesel pyrolysis at different heating rates; 5, 10, 15°C /min

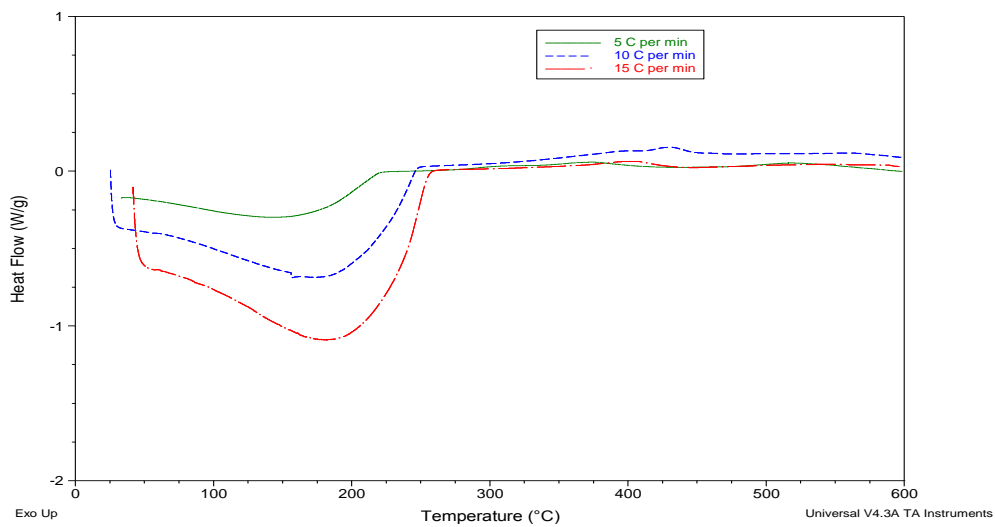


**Figure E.6:** DSC Thermogram of diesel pyrolysis at different heating rates; 5, 10, 15°C /min

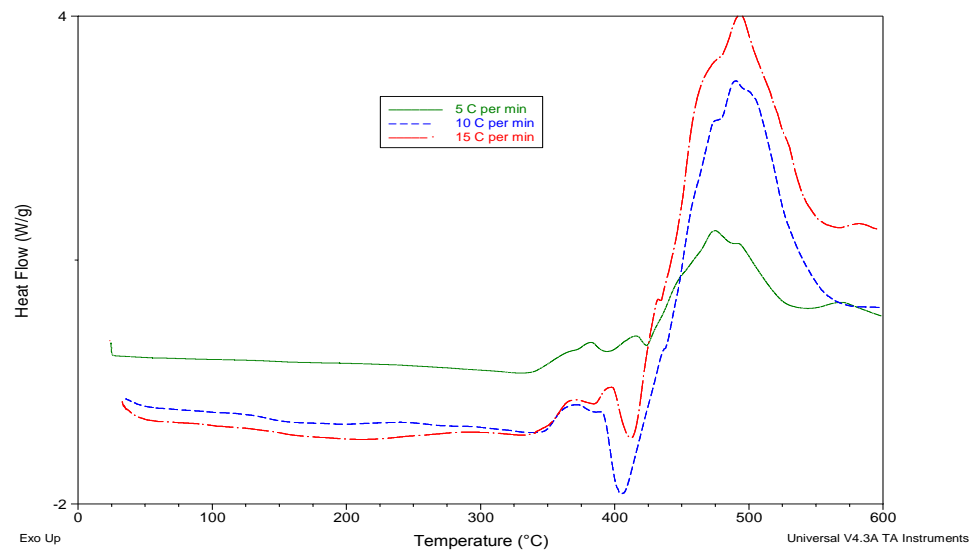


**Figure E.7:** DSC Thermogram of canola oil pyrolysis at different heating rates; 5, 10, 15 °C /min

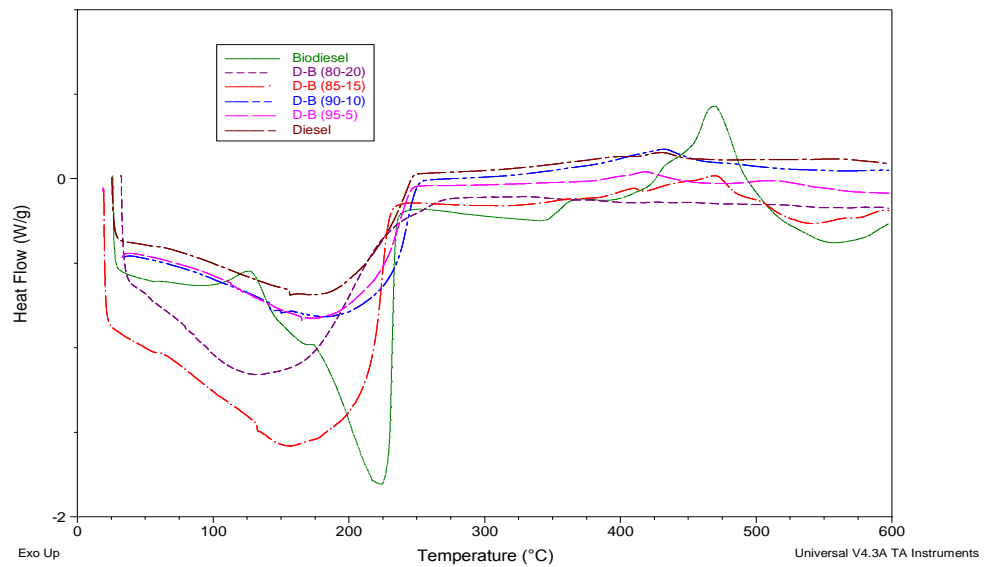


**Figure E.8:** DSC Thermogram of B100, B20, B15, B10, B05, B00 mixtures pyrolysis at a constant heating rate of 10 °C /min

## **APPENDIX F**

### **PLOTS OF TGA/DTG KINETIC METHODS**

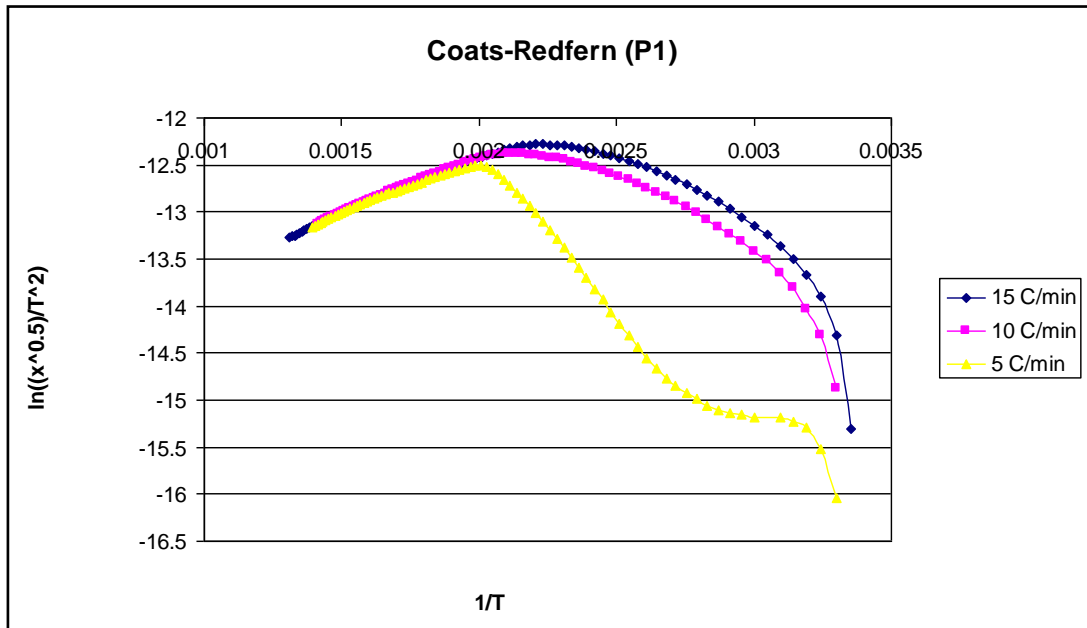


**Figure F.1:** Biodiesel combustion reaction Coats-Redfern (P1) plots of different heating rates of 5°C/min, 10°C/min and 15°C/min

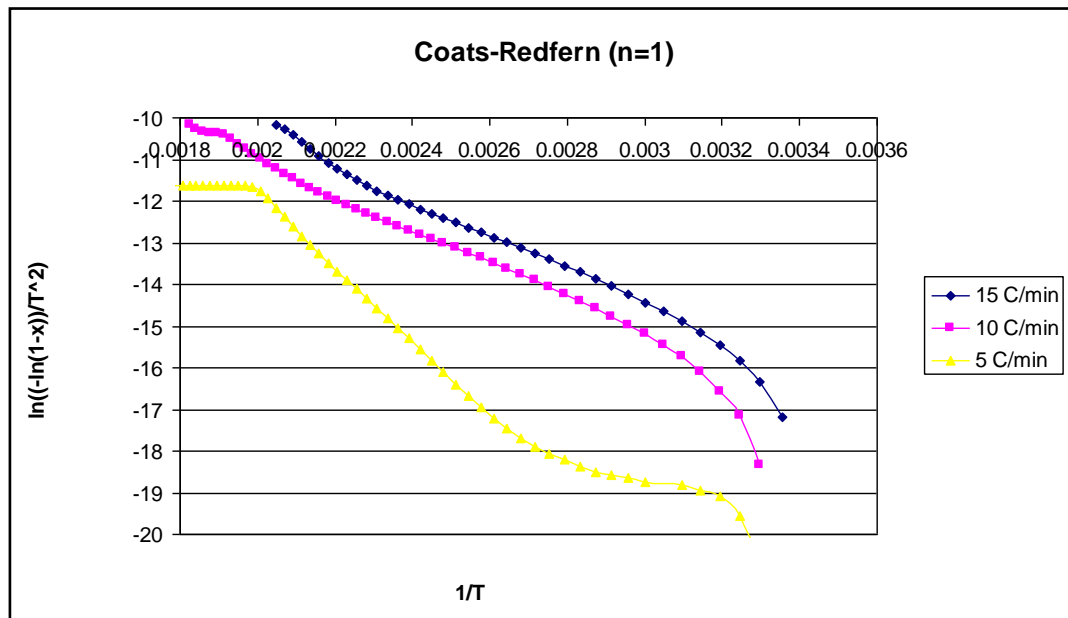


**Figure F.2:** Biodiesel combustion reaction Coats-Redfern (n=1) plots of different heating rates of 5°C/min, 10°C/min and 15°C/min

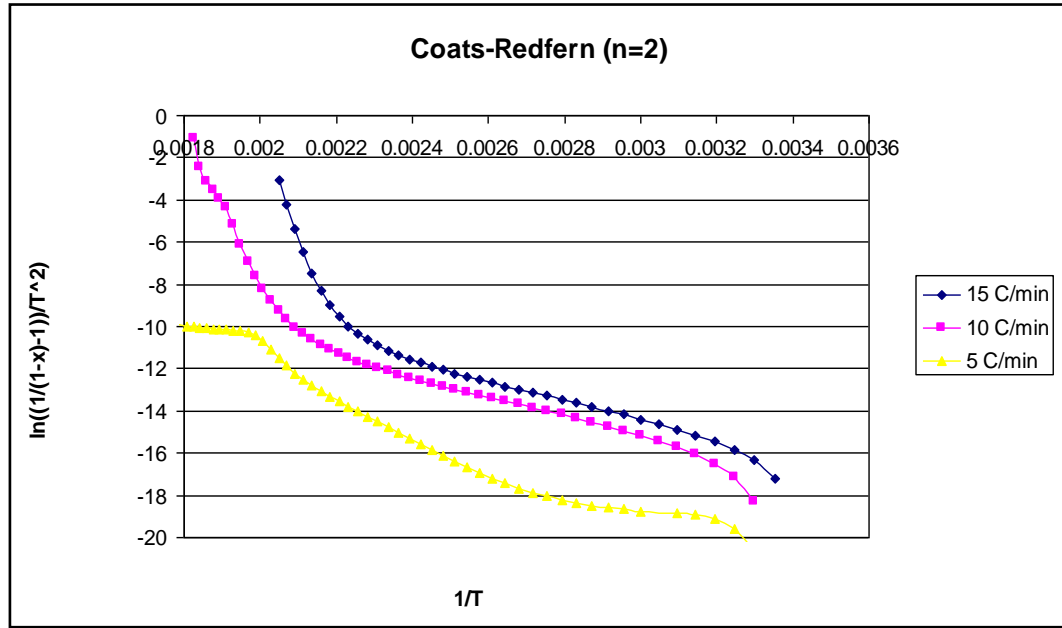


**Figure F.3:** Biodiesel combustion reaction Coats-Redfern (n=2) plots of different heating rates of 5°C/min, 10°C/min and 15°C/min

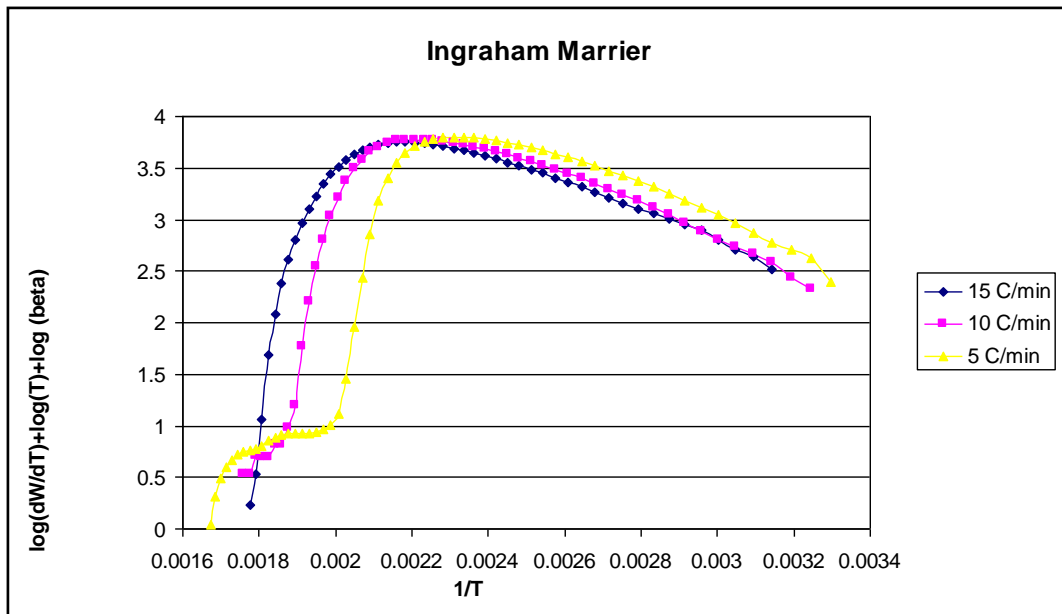


**Figure F.4:** Biodiesel combustion reaction Ingraham Marrier plots of different heating rates of 5°C/min, 10°C/min and 15°C/min

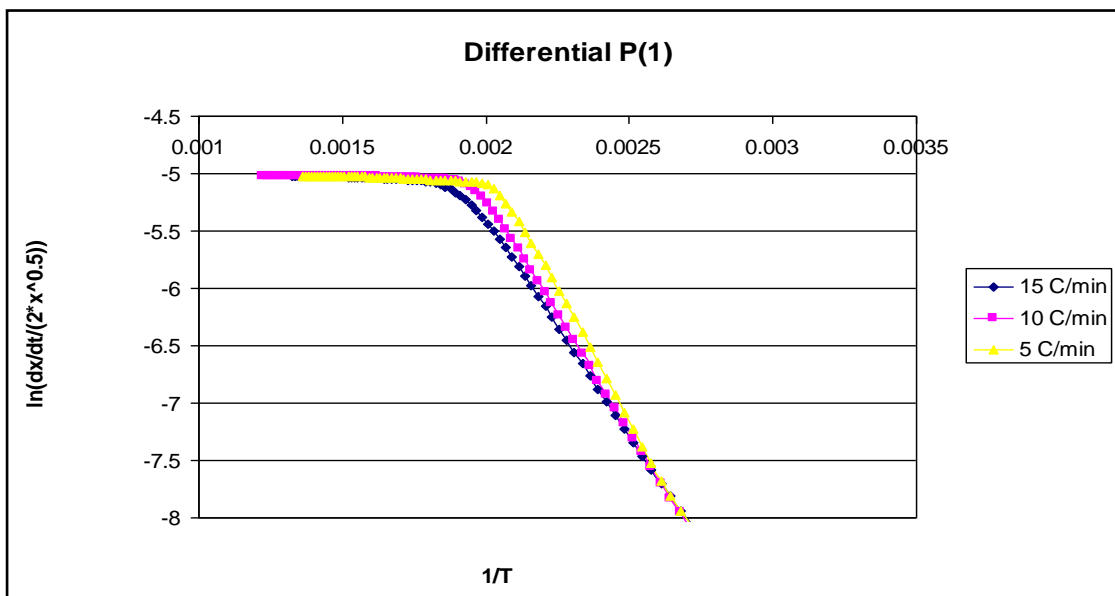


**Figure F.5:** Biodiesel combustion reaction Differential Method P(1) plots of different heating rates of 5°C/min, 10°C/min and 15°C/min

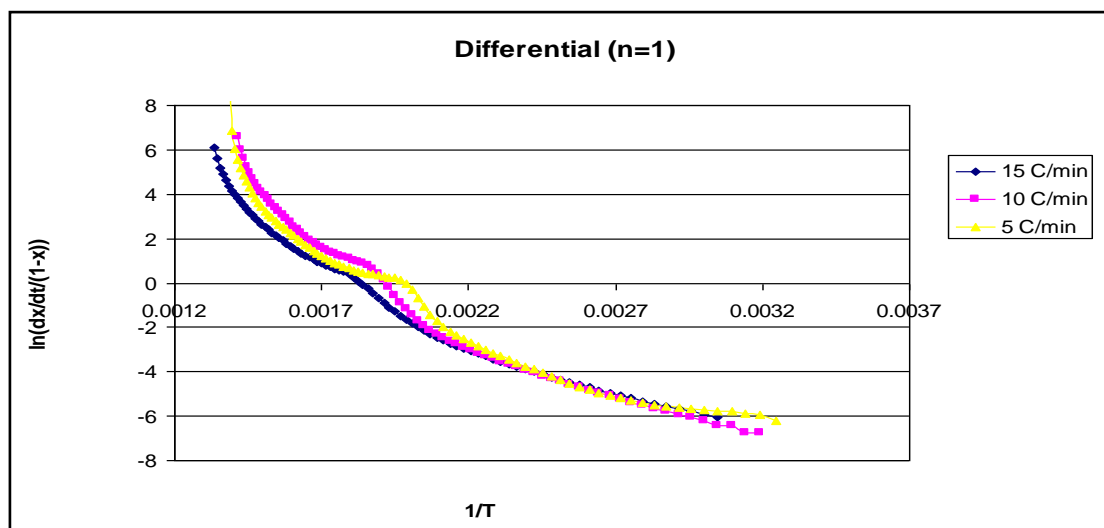


**Figure F.6:** Biodiesel combustion reaction Differential Method (n=1) plots of different heating rates of 5°C/min, 10°C/min and 15°C/min

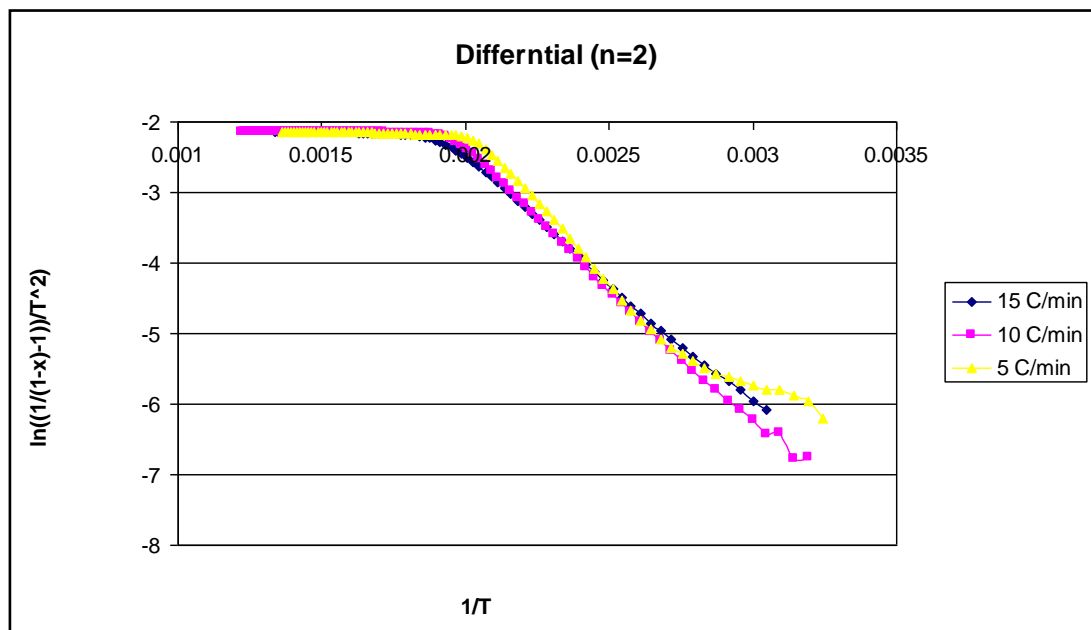


**Figure F.7:** Biodiesel combustion reaction Differential Method (n=2) plots of different heating rates of 5°C/min, 10°C/min and 15°C/min

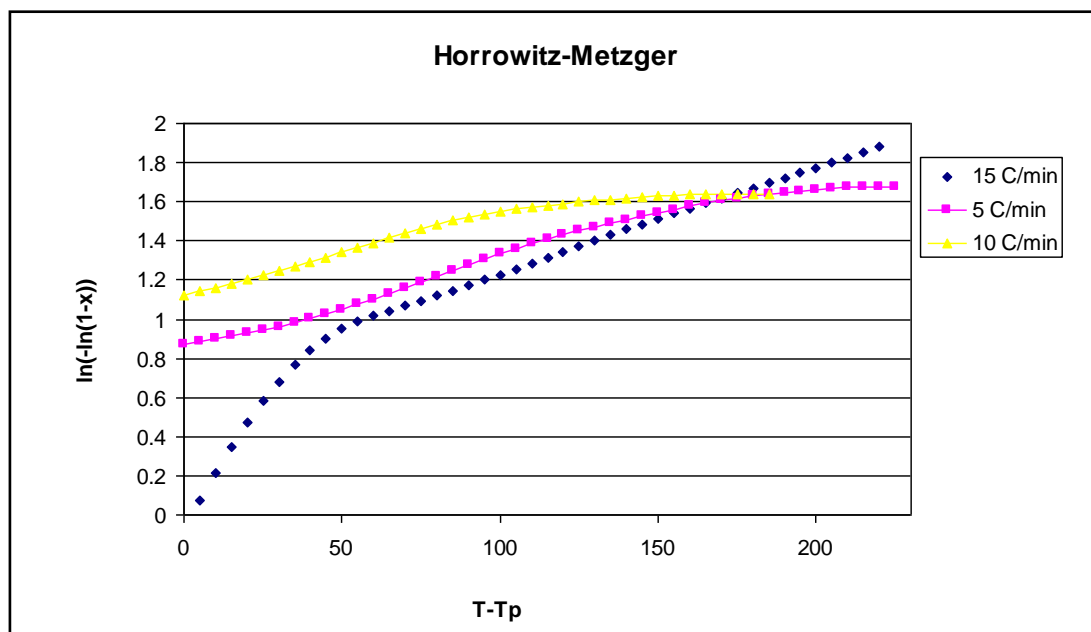


**Figure F.8:** Biodiesel combustion reaction Horowitz-Metzger plots of different heating rates of 5°C/min, 10°C/min and 15°C/min

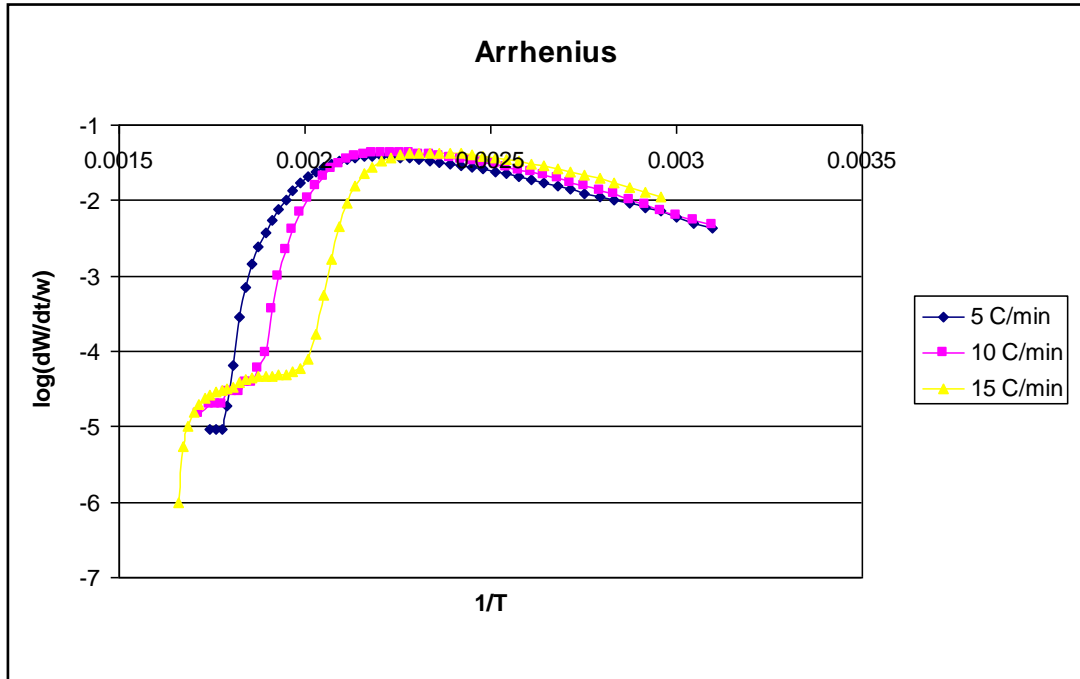


**Figure F.9:** Diesel combustion reaction Arrhenius plots of different heating rates of 5°C/min, 10°C/min and 15°C/min

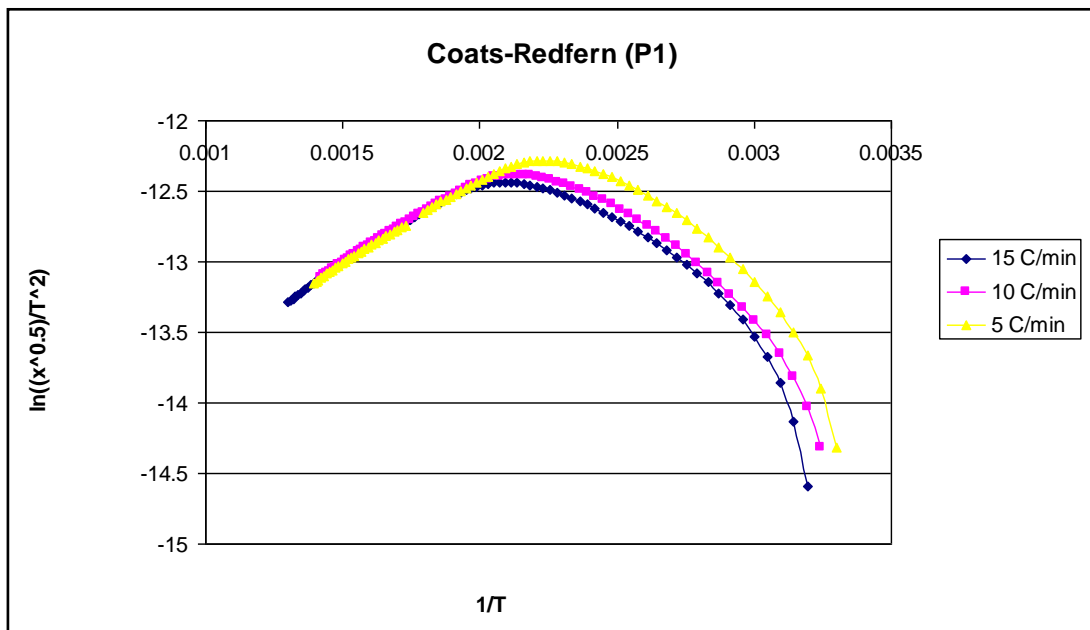


**Figure F.10:** Diesel combustion reaction Coats-Redfern (P1) plots of different heating rates of 5°C/min, 10°C/min and 15°C/min

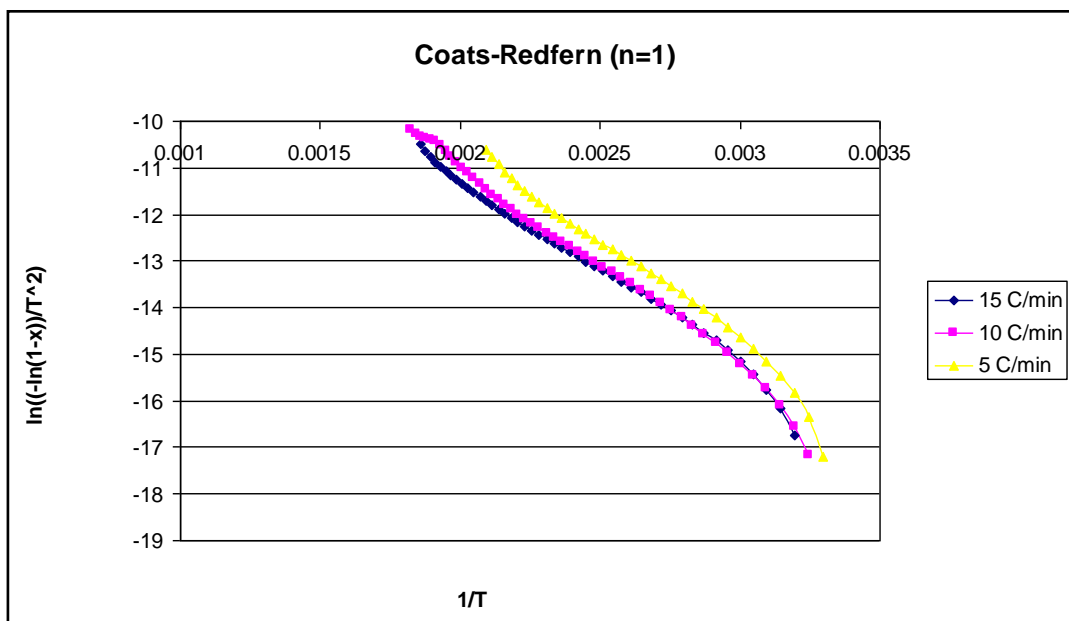


**Figure F.11:** Diesel combustion reaction Coats-Redfern (n=1) plots of different heating rates of 5°C/min, 10°C/min and 15°C/min

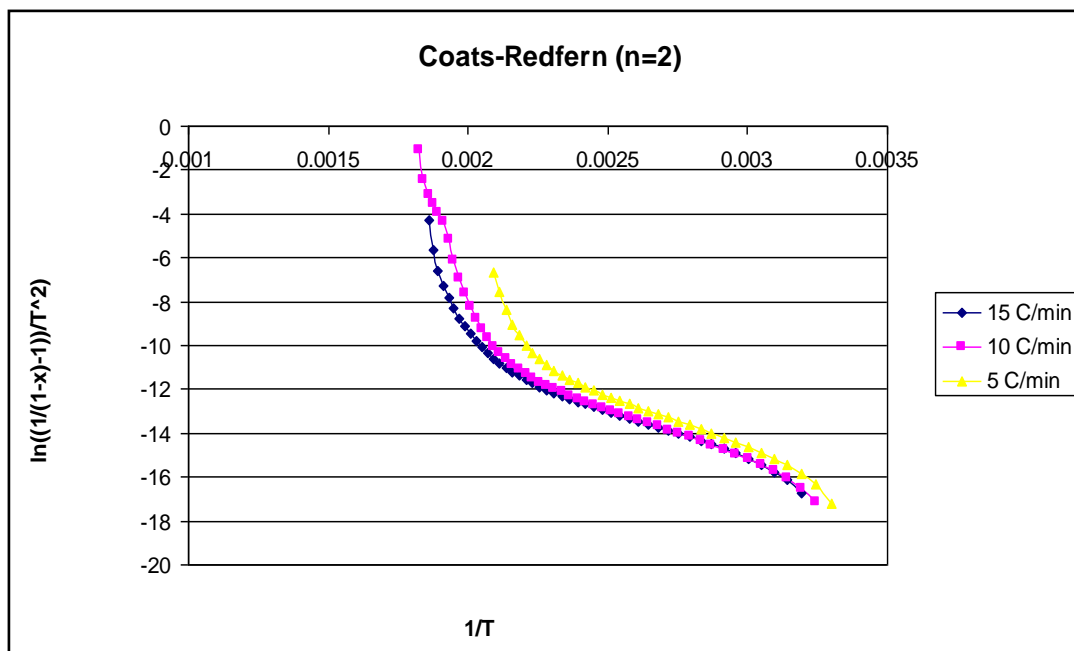


**Figure F.12:** Diesel combustion reaction Coats-Redfern (n=2) plots of different heating rates of 5°C/min, 10°C/min and 15°C/min

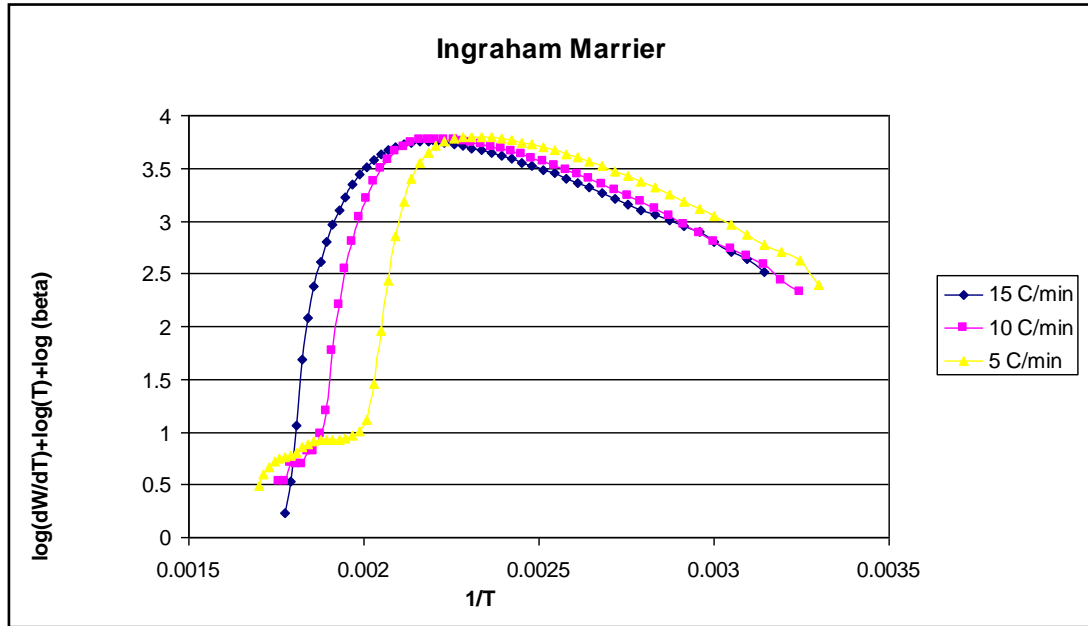


**Figure F.13:** Diesel combustion reaction Ingraham Marrier plots of different heating rates of 5°C/min, 10°C/min and 15°C/min

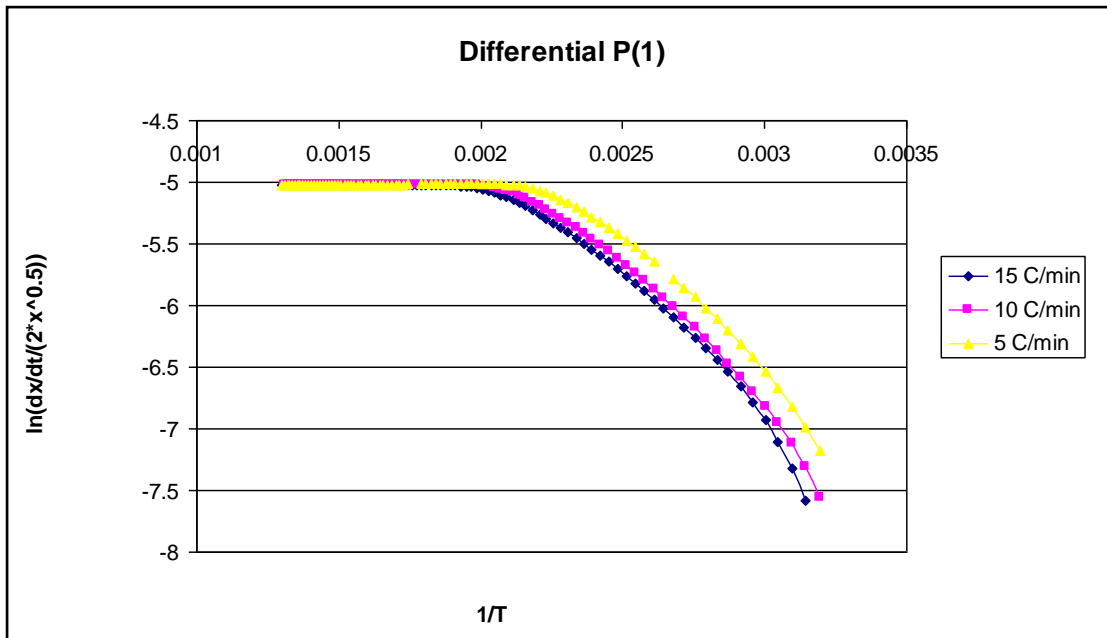


**Figure F.14:** Diesel combustion reaction Differential Method P(1) plots of different heating rates of 5°C/min, 10°C/min and 15°C/min

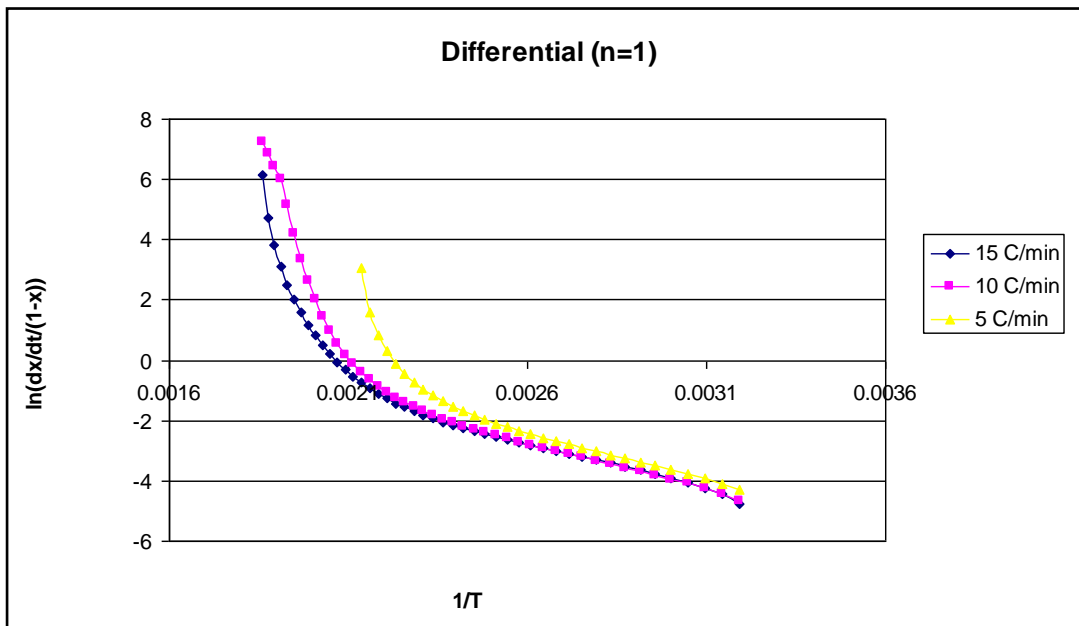


**Figure F.15:** Diesel combustion reaction Differential Method (n=1) plots of different heating rates of 5°C/min, 10°C/min and 15°C/min

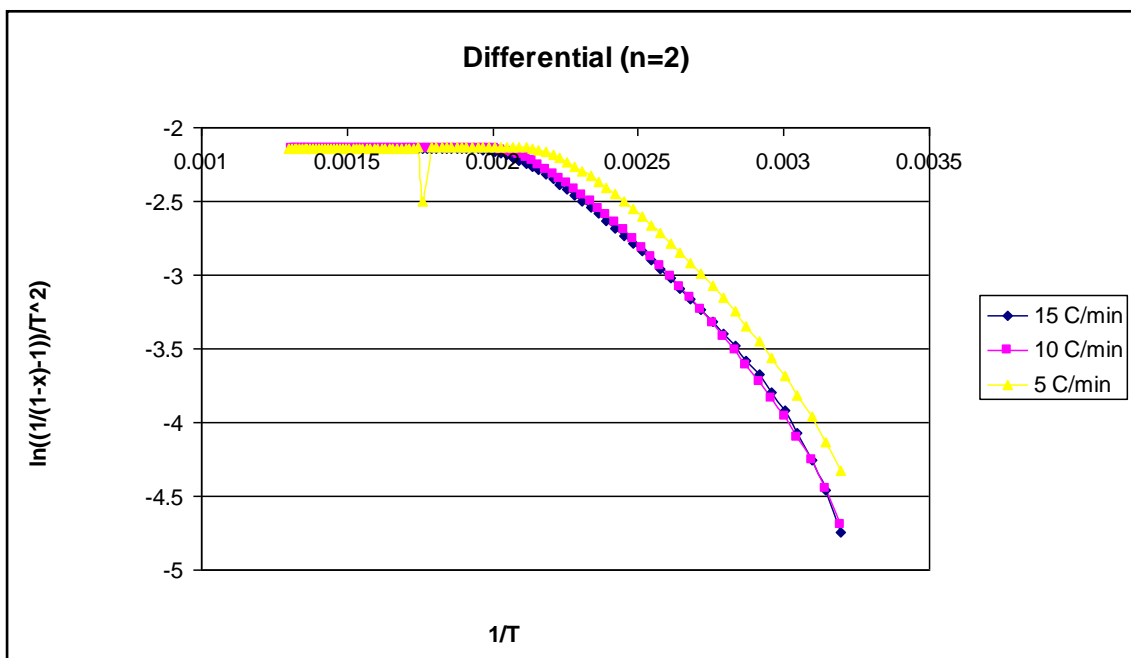


**Figure F.16:** Diesel combustion reaction Differential Method (n=2) plots of different heating rates of 5°C/min, 10°C/min and 15°C/min

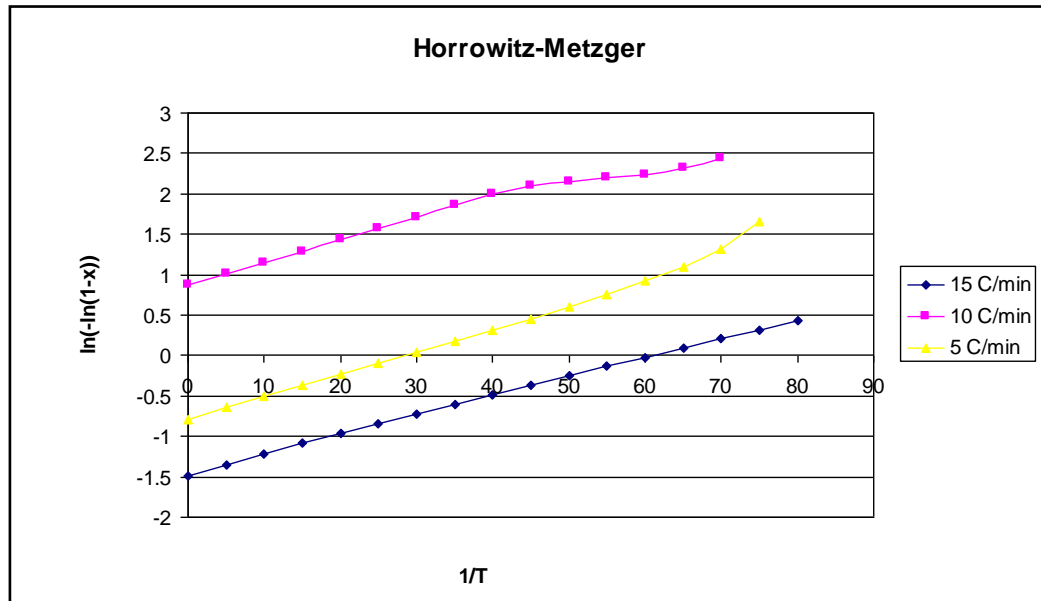


**Figure F.17:** Diesel combustion reaction Horowitz Metzger plots of different heating rates of 5°C/min, 10°C/min and 15°C/min

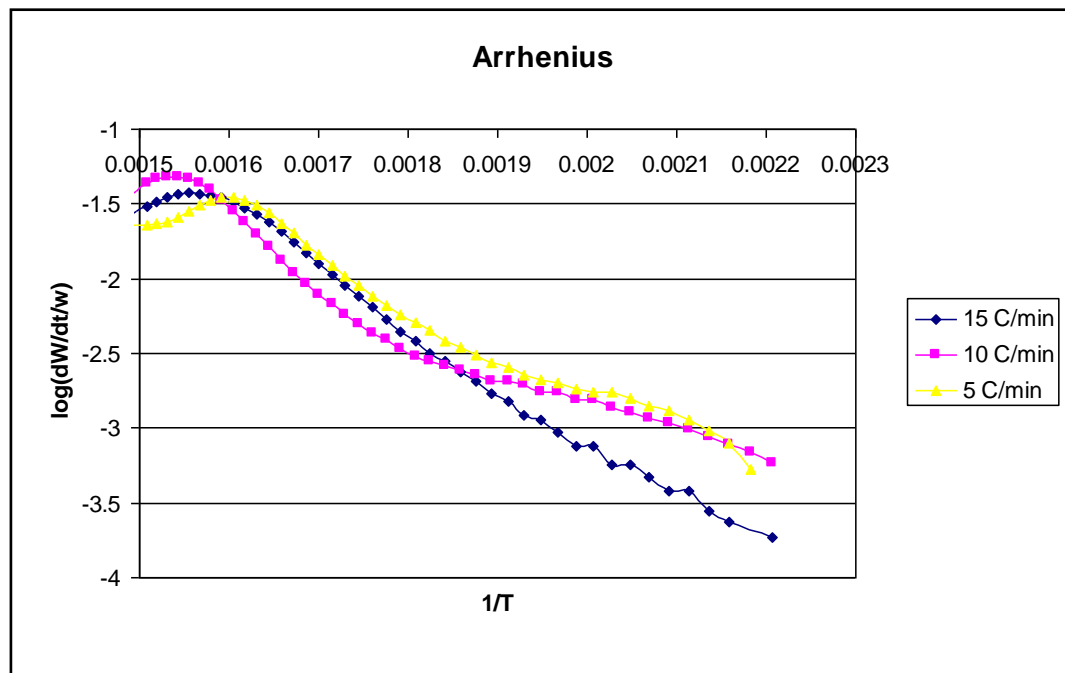


**Figure F.18:** Canola oil combustion reaction Arrhenius plots of different heating rates of 5°C/min, 10°C/min and 15°C/min

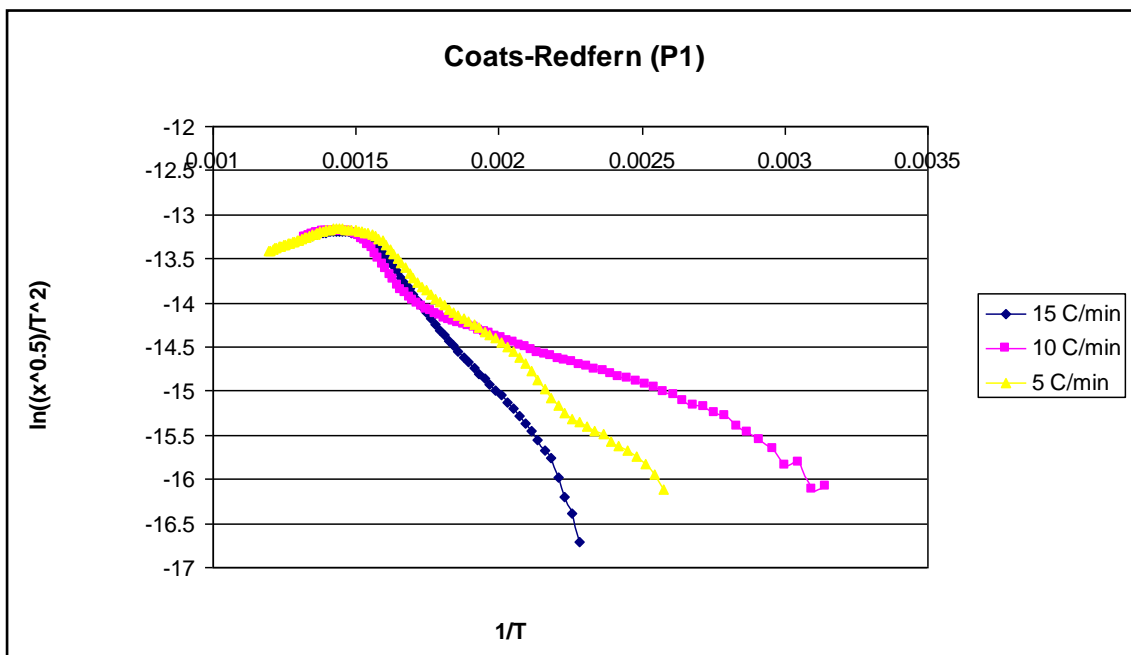


**Figure F.19:** Canola oil combustion reaction Coats-Redfern (P1) plots of different heating rates of 5°C/min, 10°C/min and 15°C/min

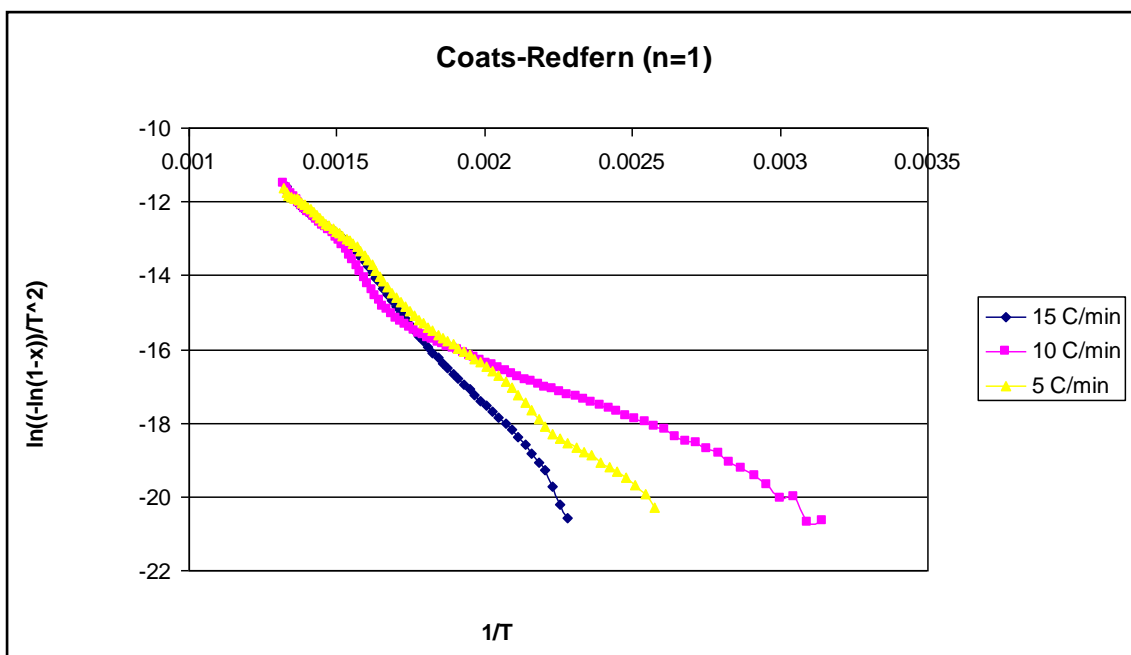


**Figure F.20:** Canola oil combustion reaction Coats-Redfern (n=1) plots of different heating rates of 5°C/min, 10°C/min and 15°C/min

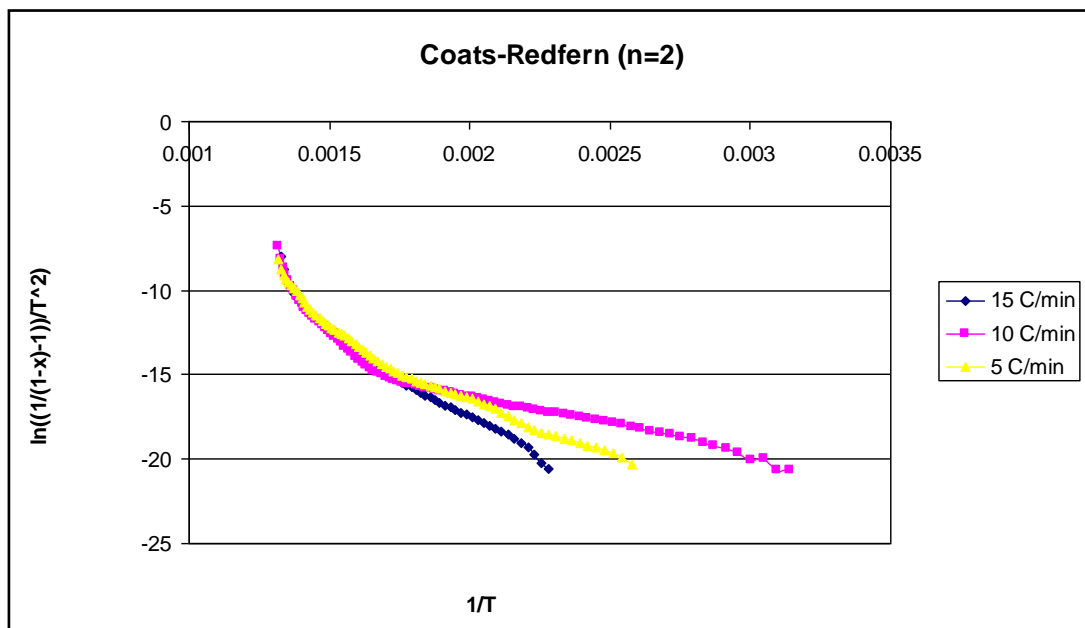


**Figure F.21:** Canola oil combustion reaction Coats-Redfern (n=2) plots of different heating rates of 5°C/min, 10°C/min and 15°C/min

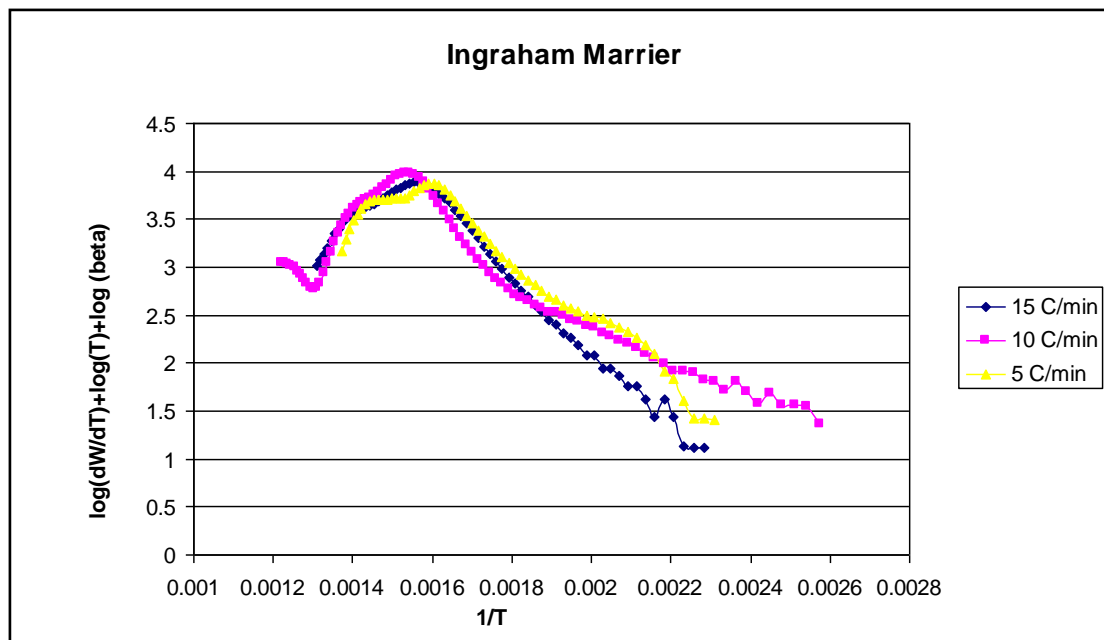


**Figure F.22:** Canola oil combustion reaction Ingraham Marrier plots of different heating rates of 5°C/min, 10°C/min and 15°C/min

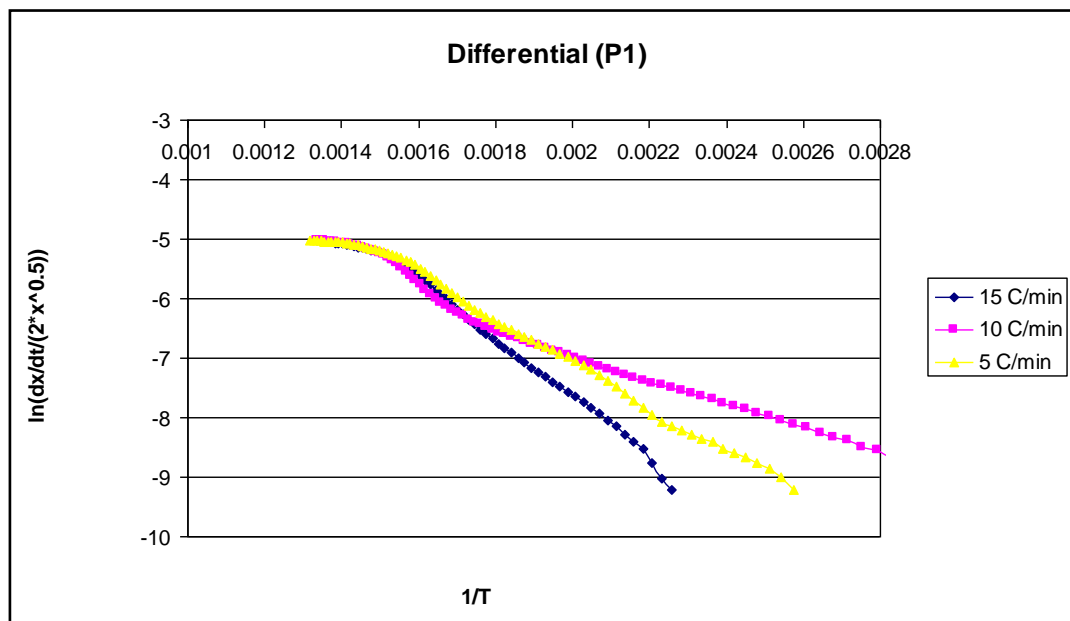


**Figure F.23:** Canola oil combustion reaction Differential (P1) plots of different heating rates of 5°C/min, 10°C/min and 15°C/min

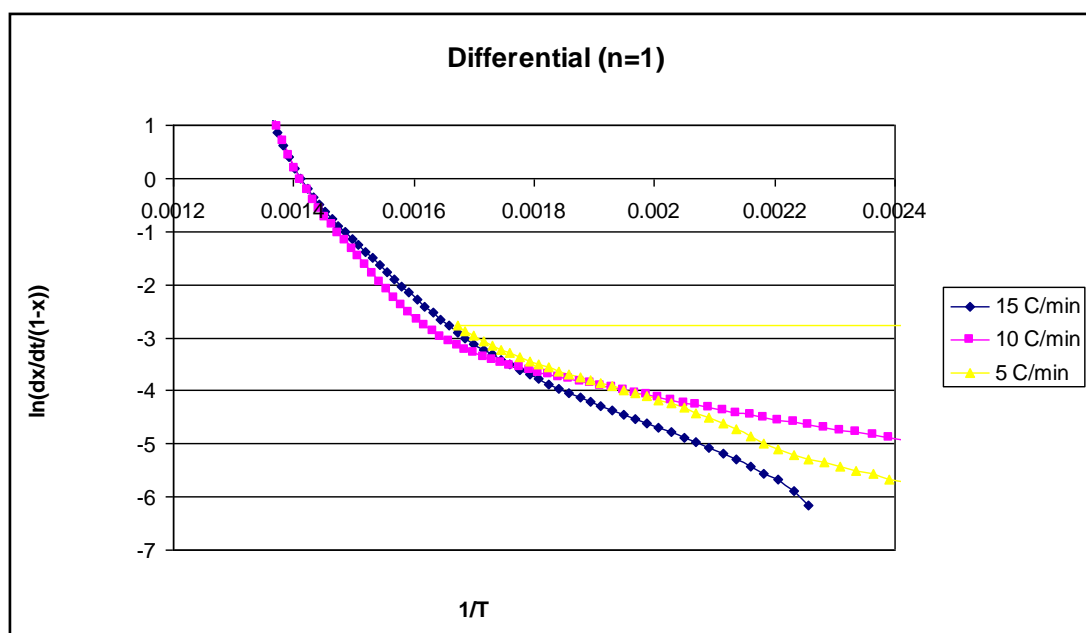


**Figure F.24:** Canola oil combustion reaction Differential (n=1) plots of different heating rates of 5°C/min, 10°C/min and 15°C/min

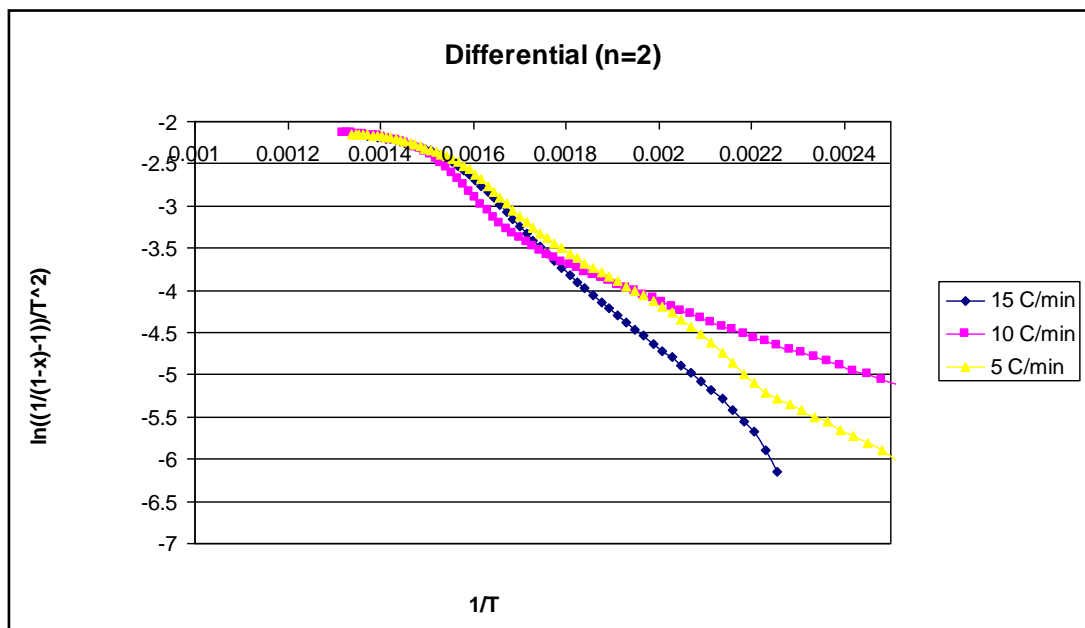


**Figure F.25:** Canola oil combustion reaction Differential (n=2) plots of different heating rates of 5°C/min, 10°C/min and 15°C/min

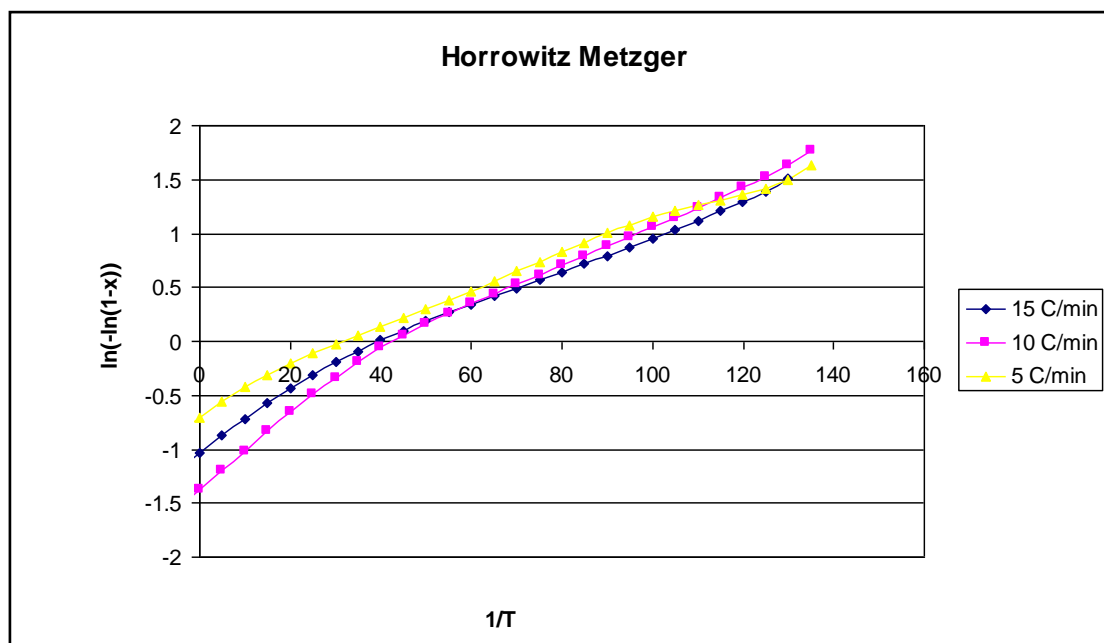


**Figure F.26:** Canola oil combustion reaction Horowitz Metzger plots of different heating rates of 5°C/min, 10°C/min and 15°C/min

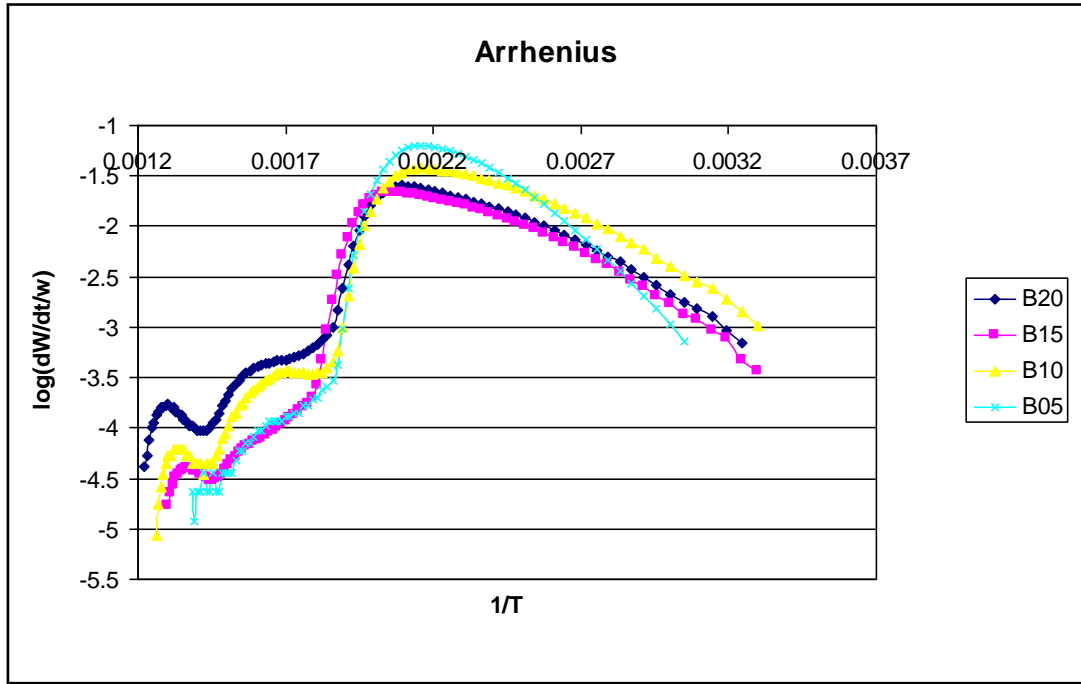


**Figure F.27:** Biodiesel-diesel mixtures combustion reactions Arrhenius plots

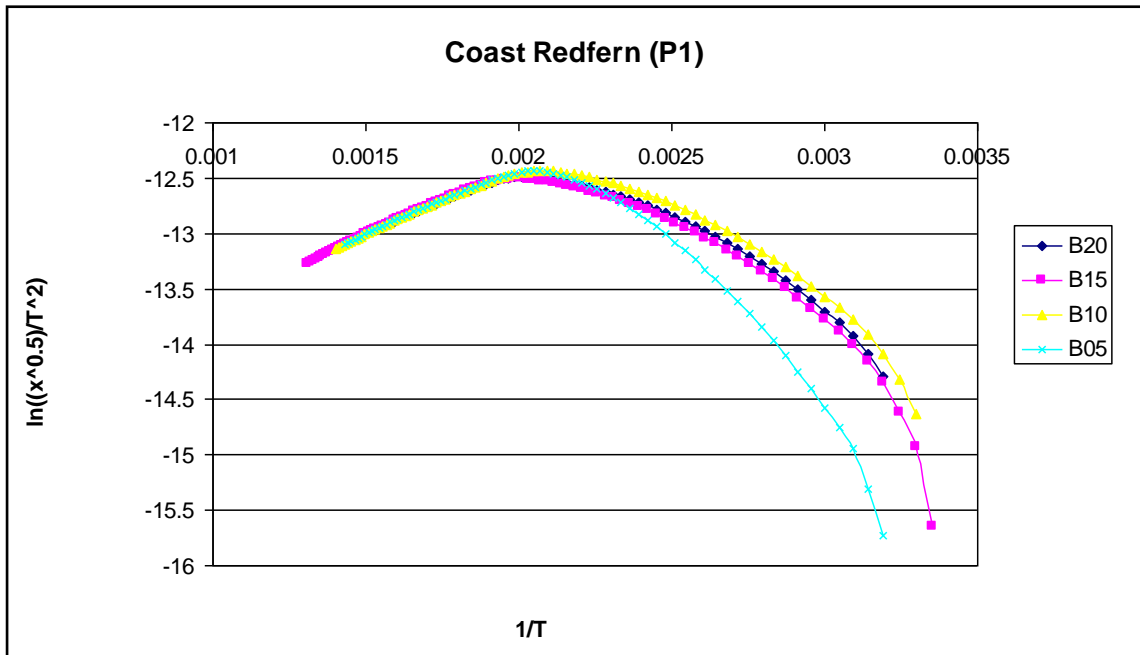


**Figure F.28:** Biodiesel-diesel mixtures combustion reactions Coats Redfern (P1) plots

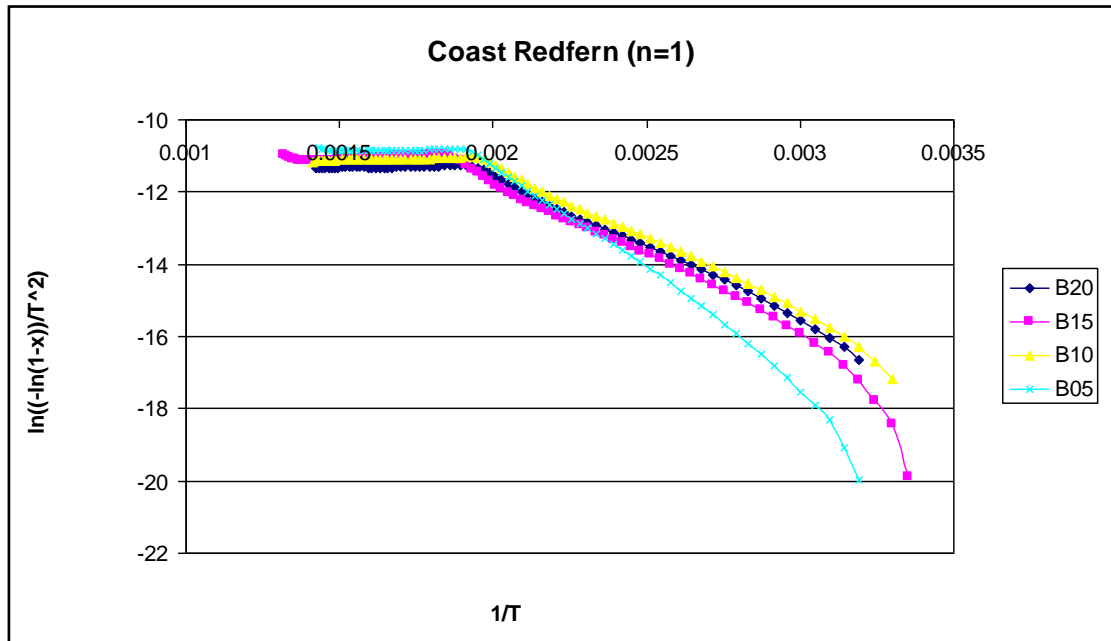


**Figure F.29:** Biodiesel-diesel mixtures combustion reactions Coats Redfern (n=1) plots

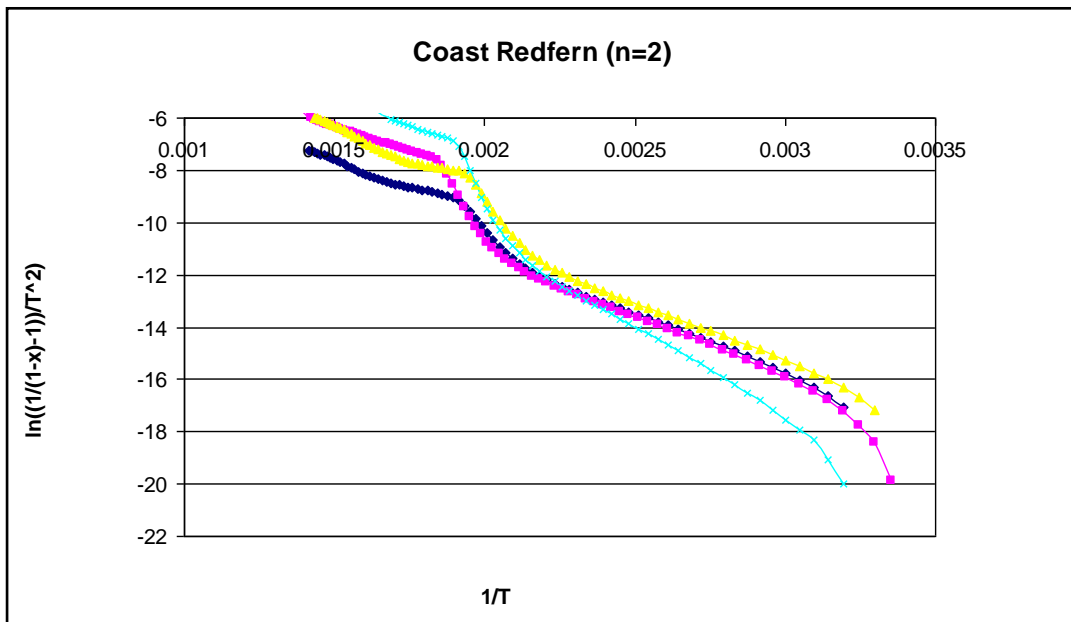


**Figure F.30:** Biodiesel-diesel mixtures combustion reactions Coats Redfern (n=2) plots

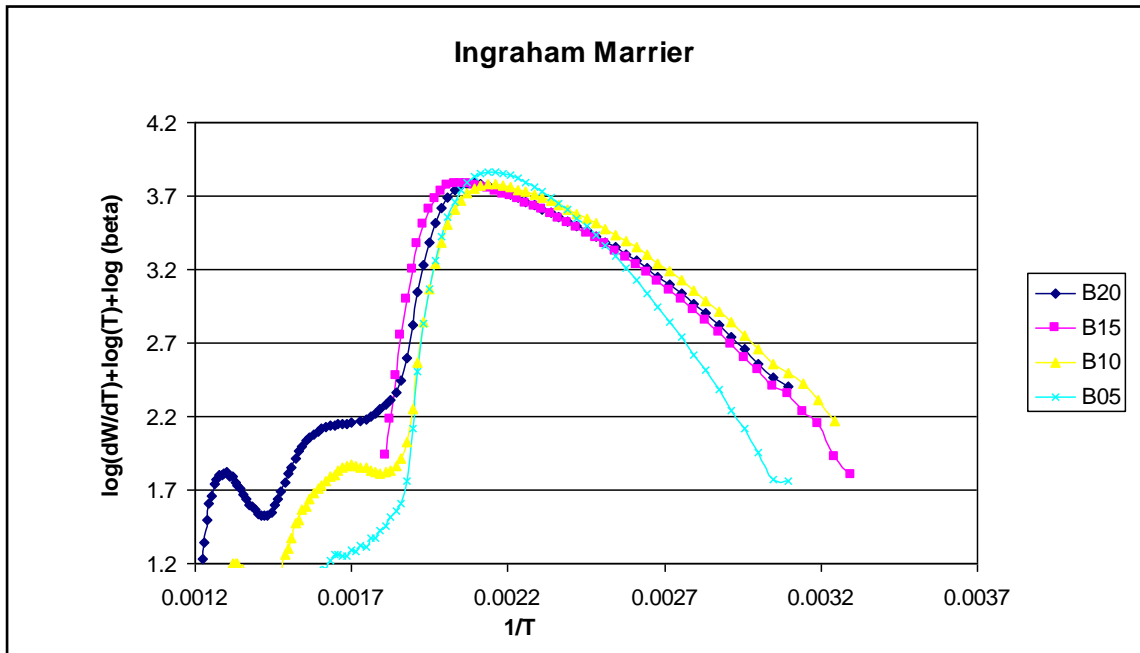


Figure F.31: Biodiesel-diesel mixtures combustion reactions Ingraham Marrier plots

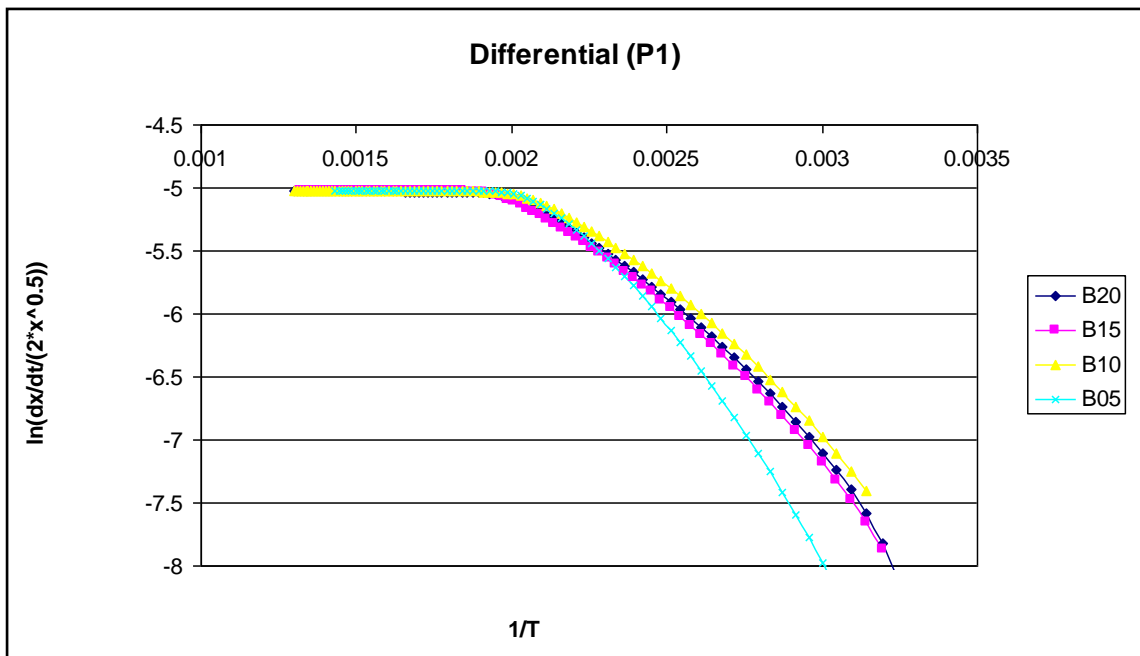
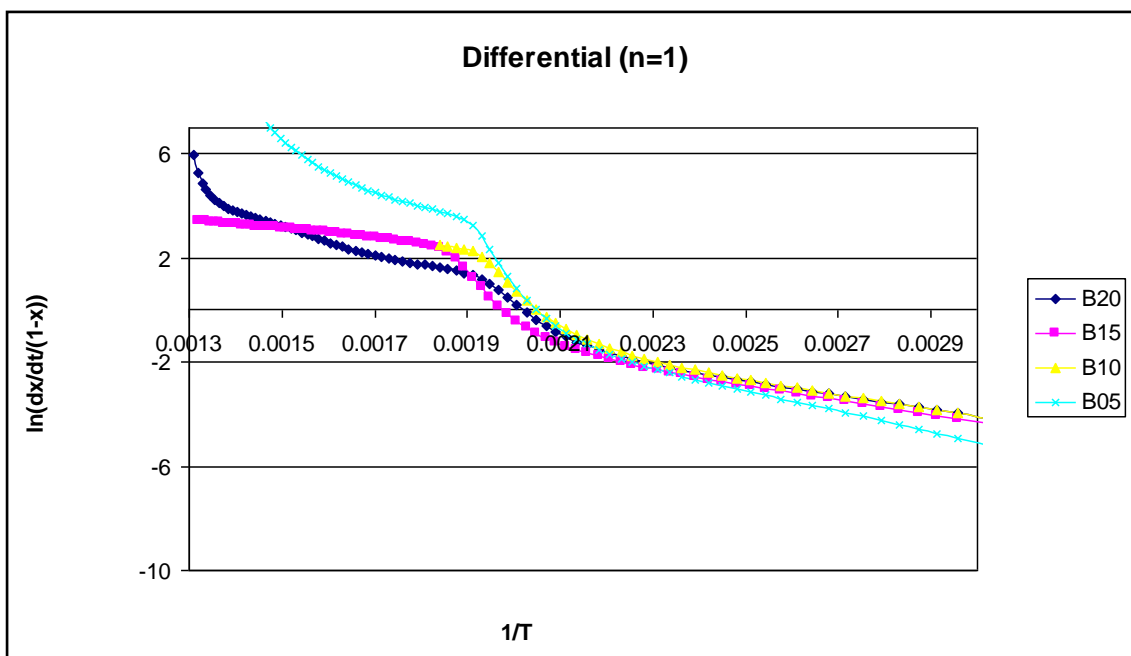
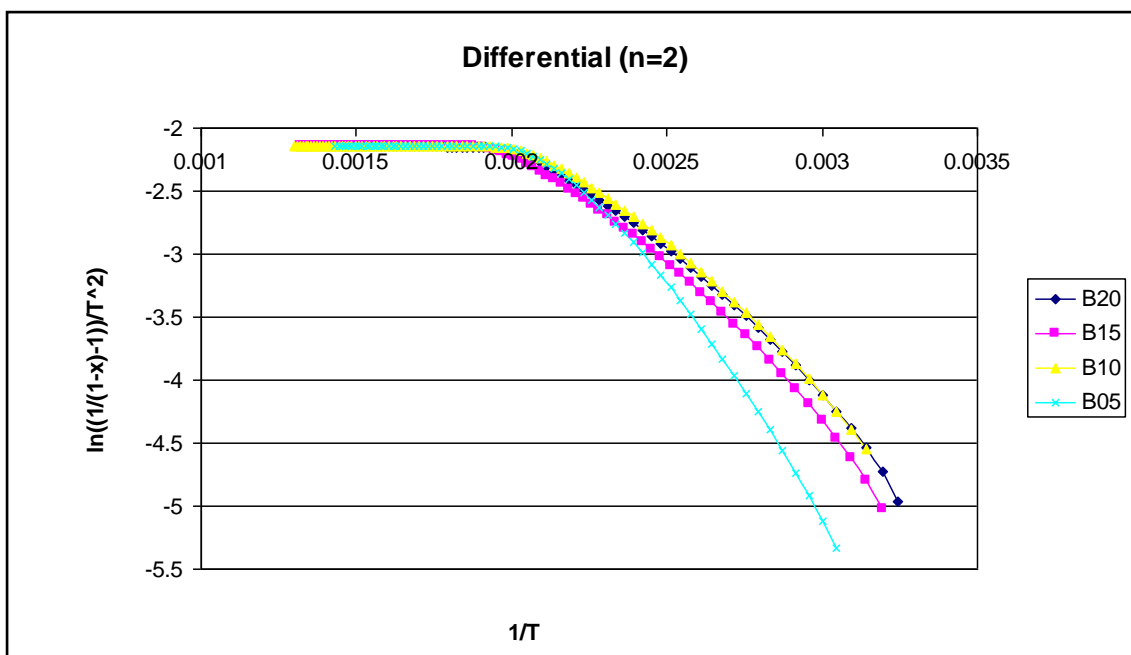


Figure F.32: Biodiesel-diesel mixtures combustion reactions Differential (P1) plots



**Figure F.33:** Biodiesel-diesel mixtures combustion reactions Differential (n=1) plots



**Figure F.34:** Biodiesel-diesel mixtures combustion reactions Differential (n=2) plots

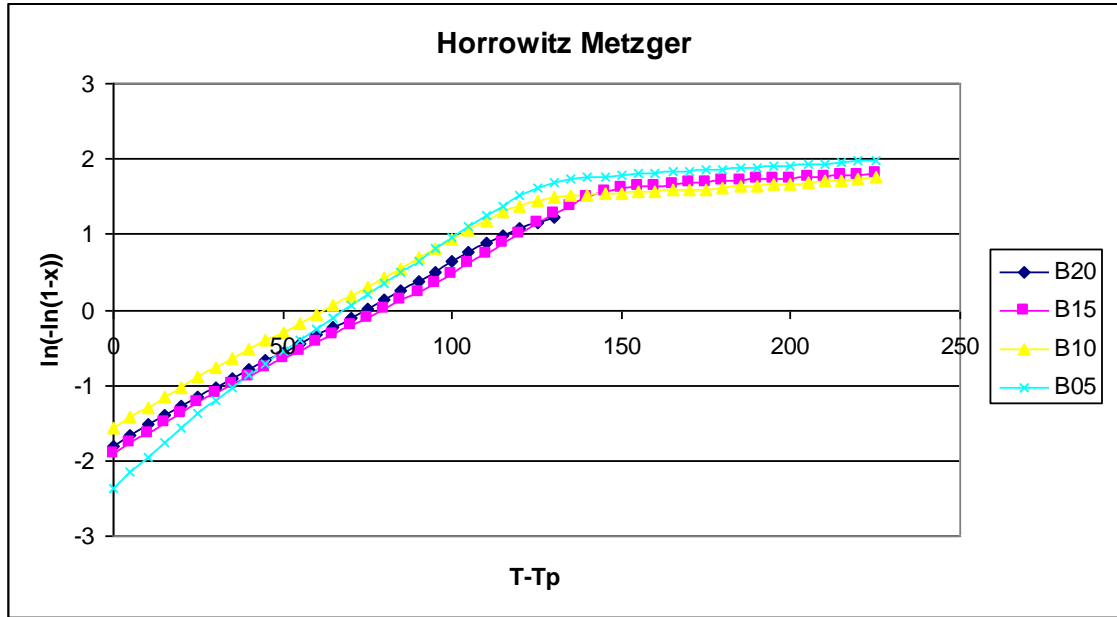


**Figure F.35:** Biodiesel-diesel mixtures combustion reactions Horowitz Metzger plots

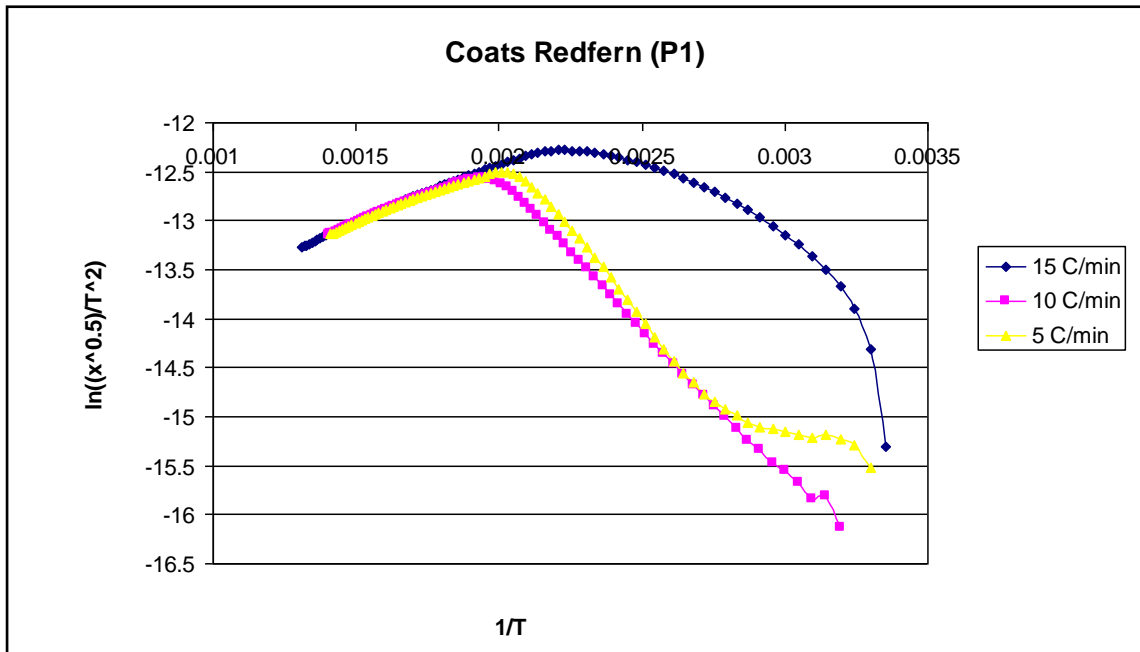


**Figure F.36:** Biodiesel pyrolysis reaction Coats Redfern (P1) plots of different heating rates of 5°C/min, 10°C/min and 15°C/min

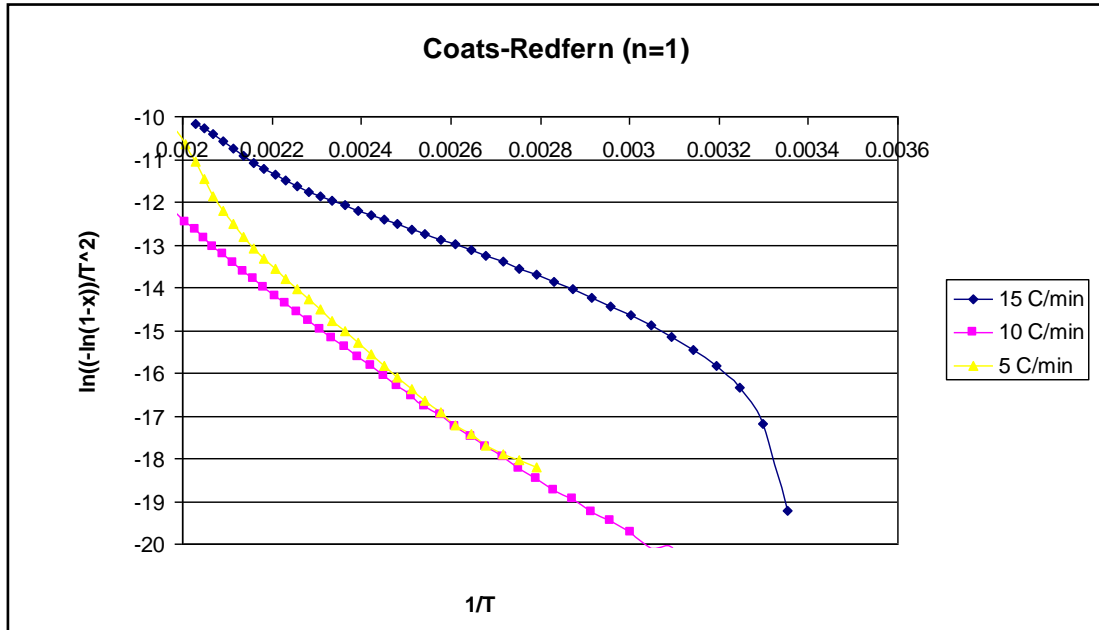


**Figure F.37:** Biodiesel pyrolysis reaction Coats Redfern (n=1) plots of different heating rates of 5°C/min, 10°C/min and 15°C/min

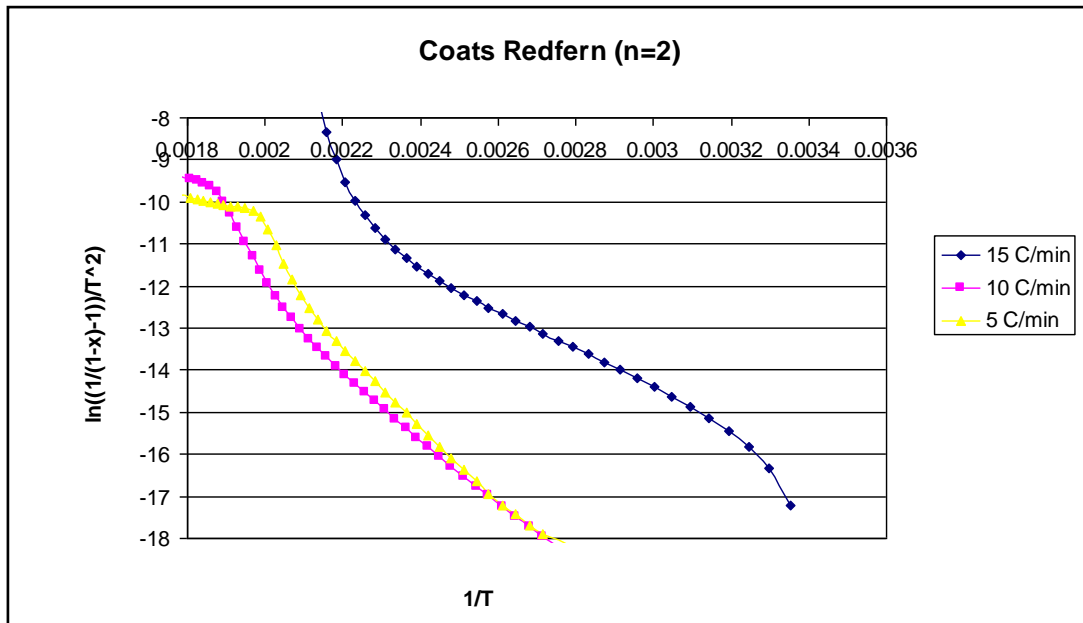


**Figure F.38:** Biodiesel pyrolysis reaction Coats Redfern (n=2) plots of different heating rates of 5°C/min, 10°C/min and 15°C/min

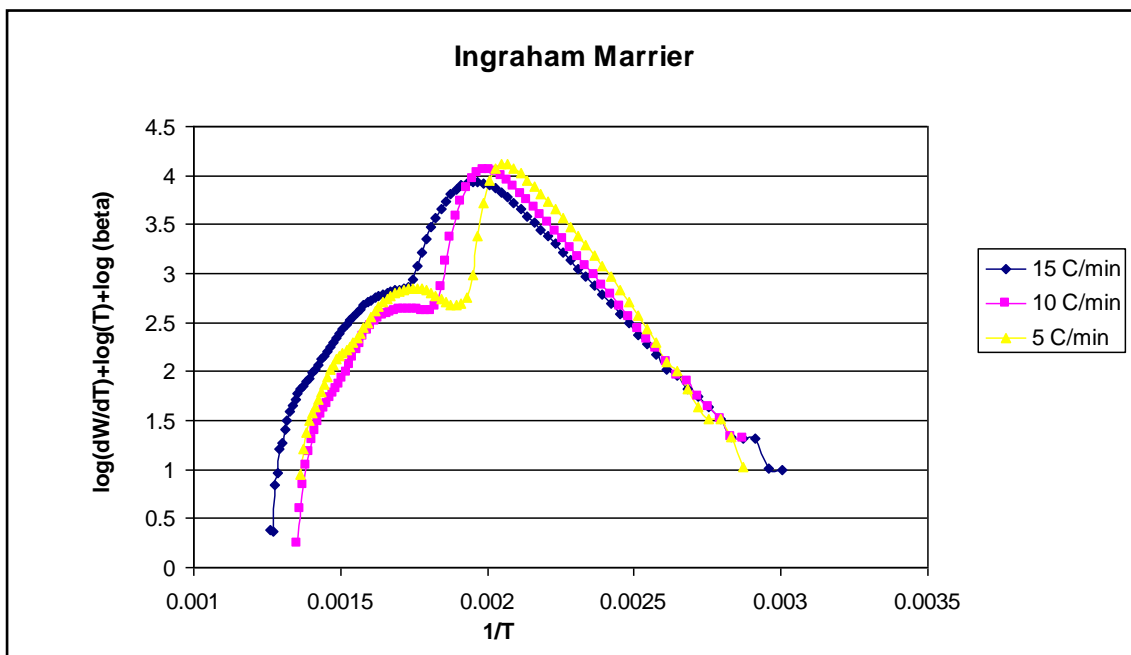


**Figure F.39:** Biodiesel pyrolysis reaction Ingraham Marrier plots of different heating rates of 5°C/min, 10°C/min and 15°C/min

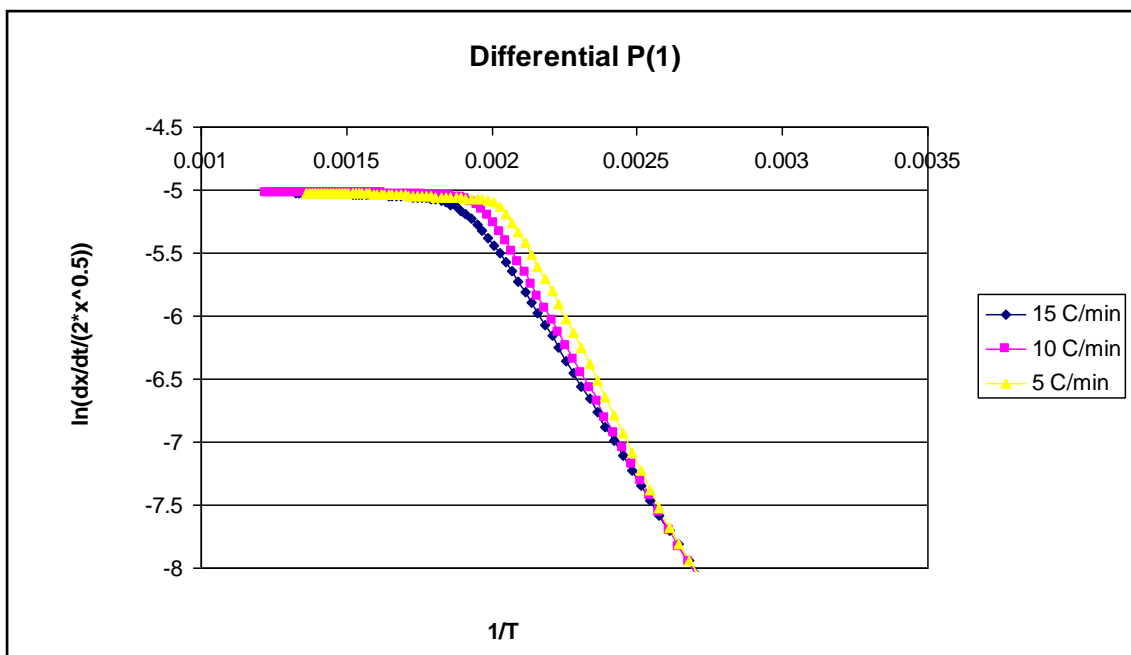


**Figure F.40:** Biodiesel pyrolysis reaction Differential (P1) plots of different heating rates of 5°C/min, 10°C/min and 15°C/min

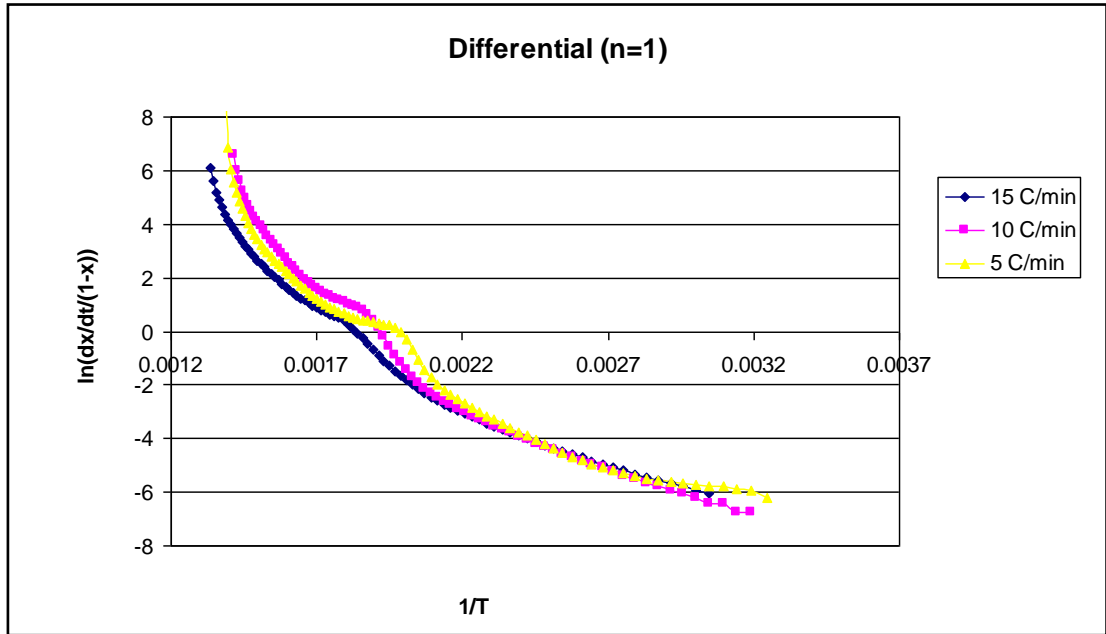


**Figure F.41:** Biodiesel pyrolysis reaction Differential ( $n=1$ ) plots of different heating rates of  $5^{\circ}\text{C}/\text{min}$ ,  $10^{\circ}\text{C}/\text{min}$  and  $15^{\circ}\text{C}/\text{min}$

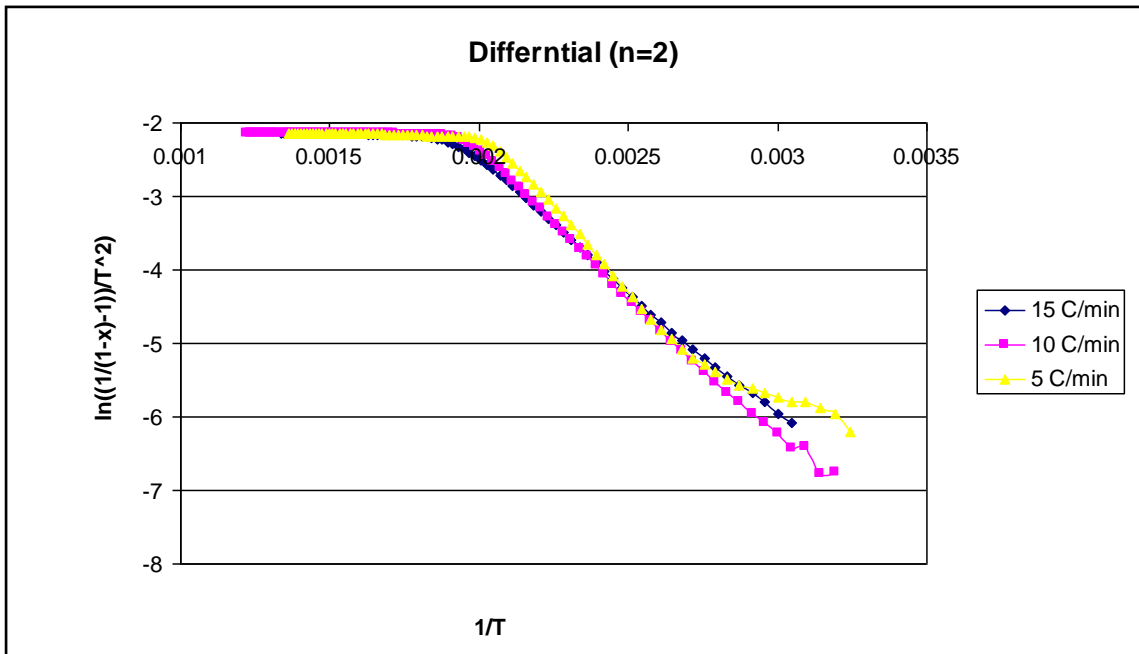


**Figure F.42:** Biodiesel pyrolysis reaction Differential ( $n=2$ ) plots of different heating rates of  $5^{\circ}\text{C}/\text{min}$ ,  $10^{\circ}\text{C}/\text{min}$  and  $15^{\circ}\text{C}/\text{min}$

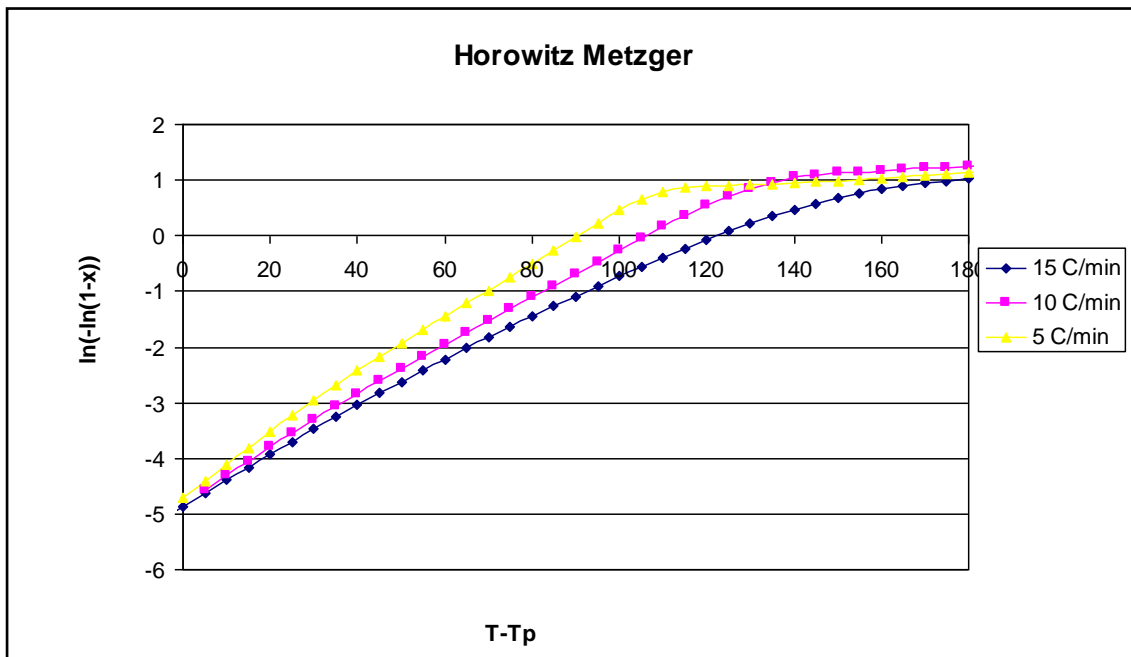


**Figure F.43:** Biodiesel pyrolysis reaction Horowitz Metzger plots of different heating rates of 5°C/min, 10°C/min and 15°C/min

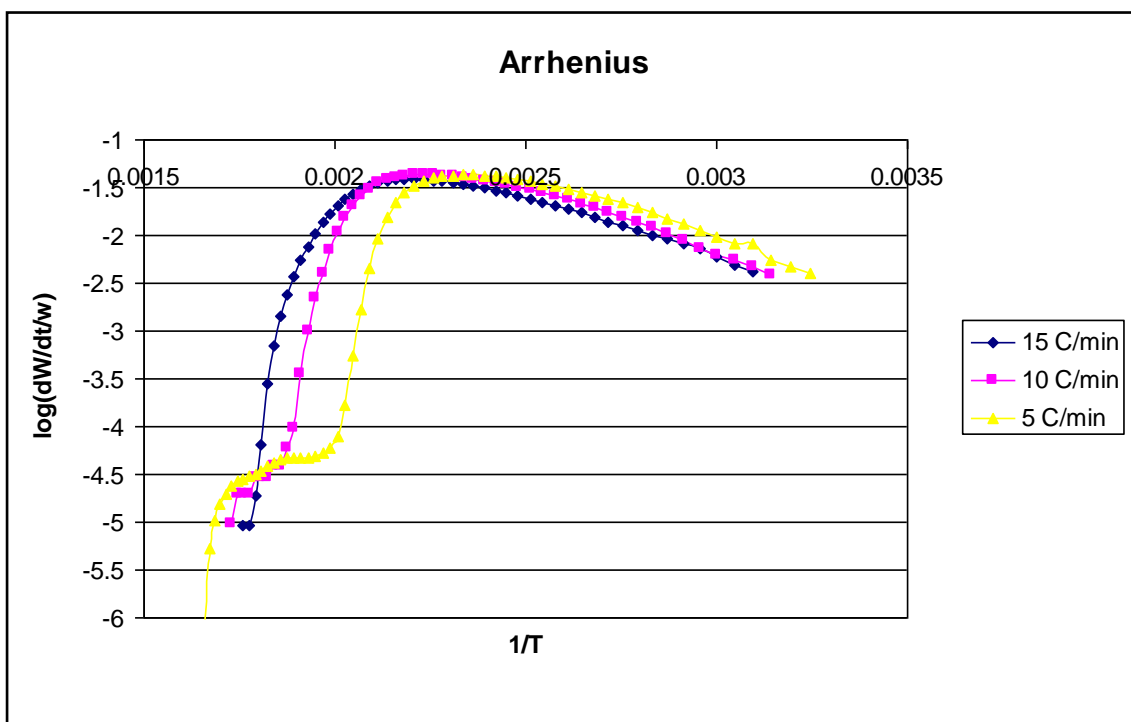


**Figure F.44:** Diesel pyrolysis reaction Arrhenius plots of different heating rates of 5°C/min, 10°C/min and 15°C/min

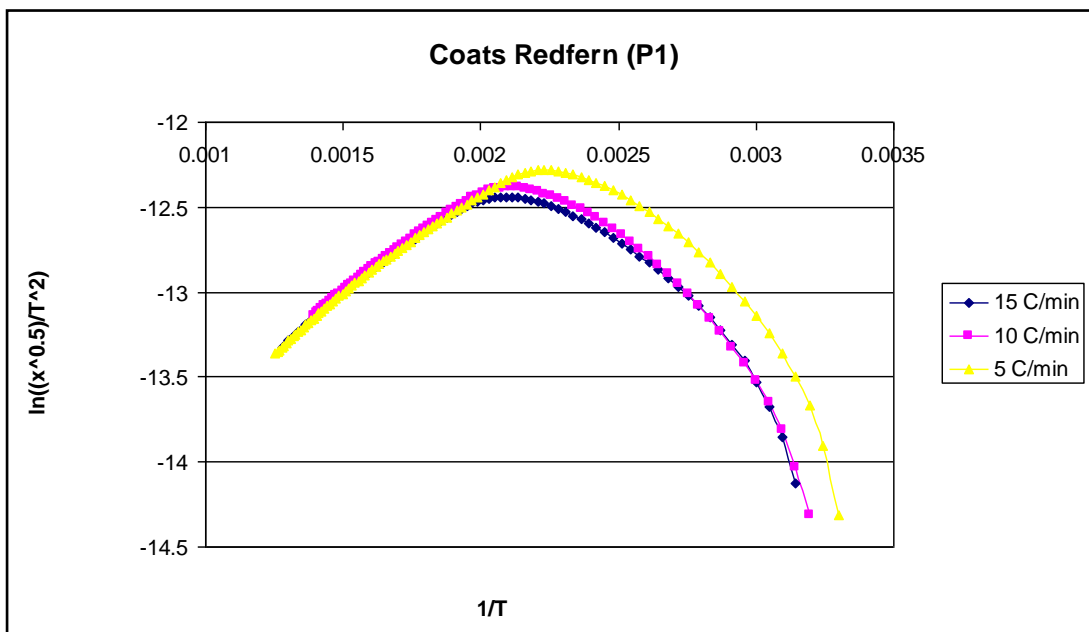


**Figure F.45:** Diesel pyrolysis reaction Coats Redfern (P1) plots of different heating rates of 5°C/min, 10°C/min and 15°C/min

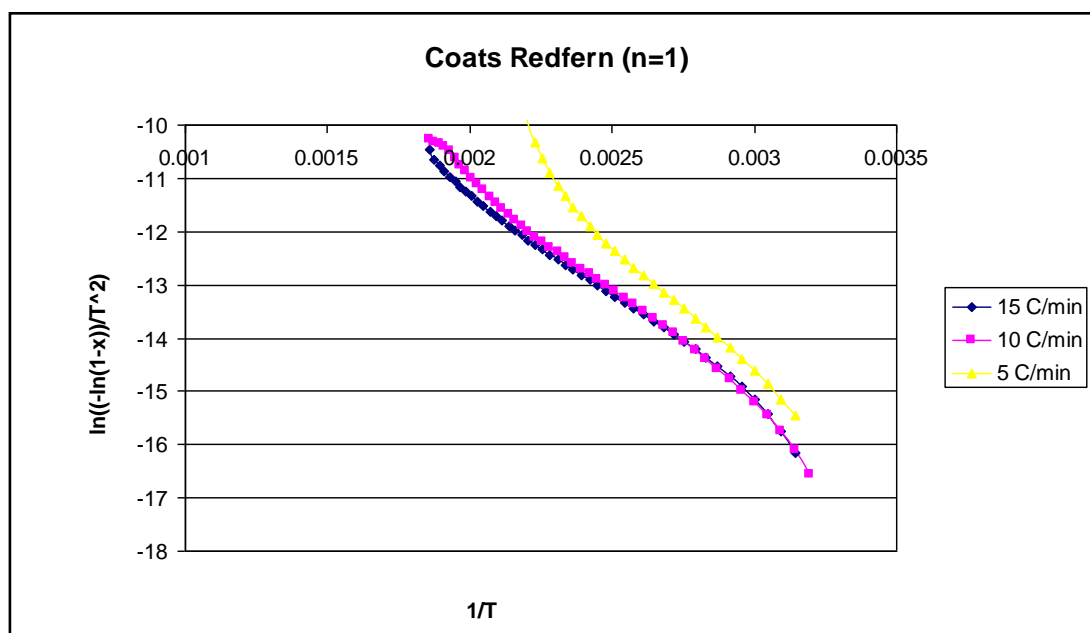


**Figure F.46:** Diesel pyrolysis reaction Coats Redfern (n=1) plots of different heating rates of 5°C/min, 10°C/min and 15°C/min

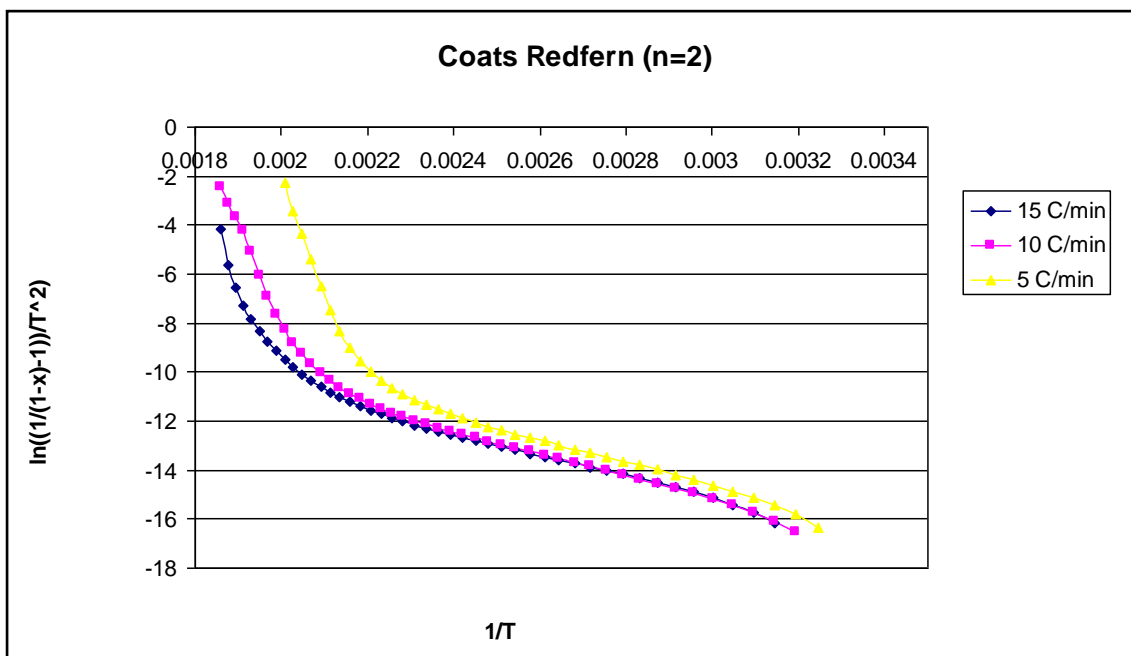


**Figure F.47:** Diesel pyrolysis reaction Coats Redfern (n=2) plots of different heating rates of 5°C/min, 10°C/min and 15°C/min

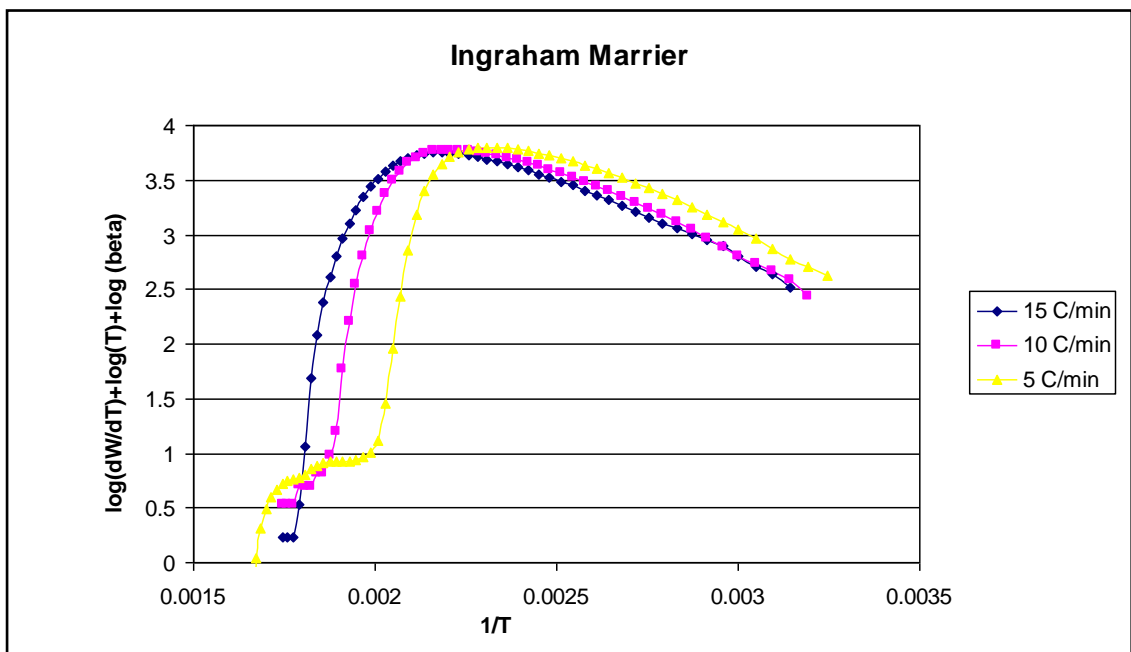


**Figure F.48:** Diesel pyrolysis reaction Ingraham Marrier plots of different heating rates of 5°C/min, 10°C/min and 15°C/min

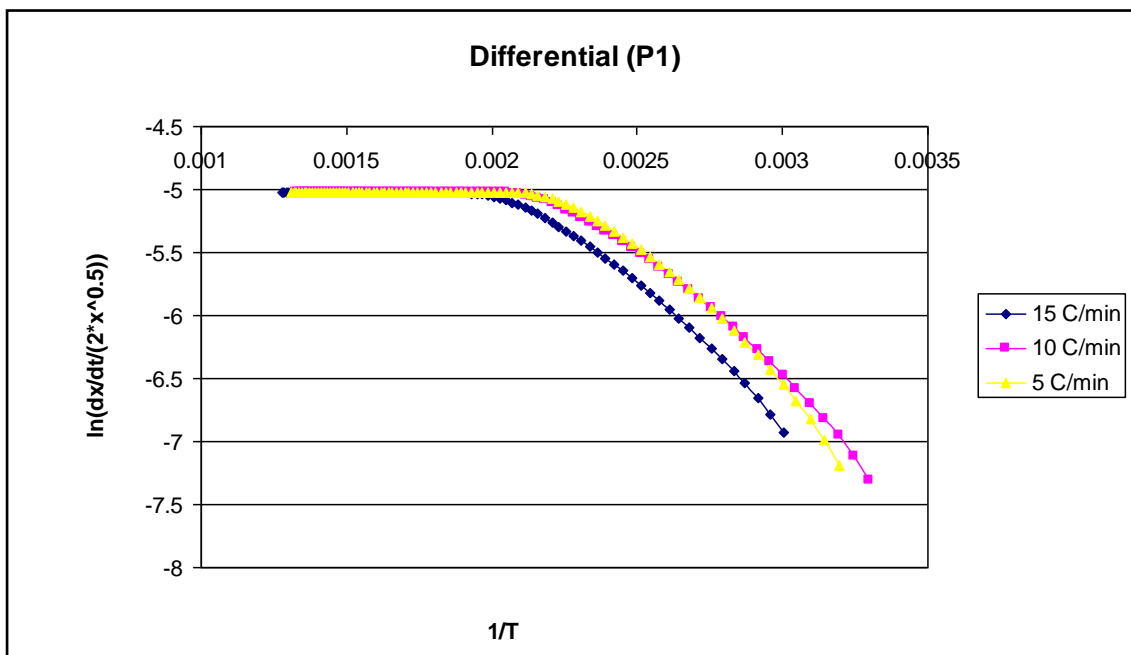


**Figure F.49:** Diesel pyrolysis reaction Differential (P1) plots of different heating rates of 5°C/min, 10°C/min and 15°C/min

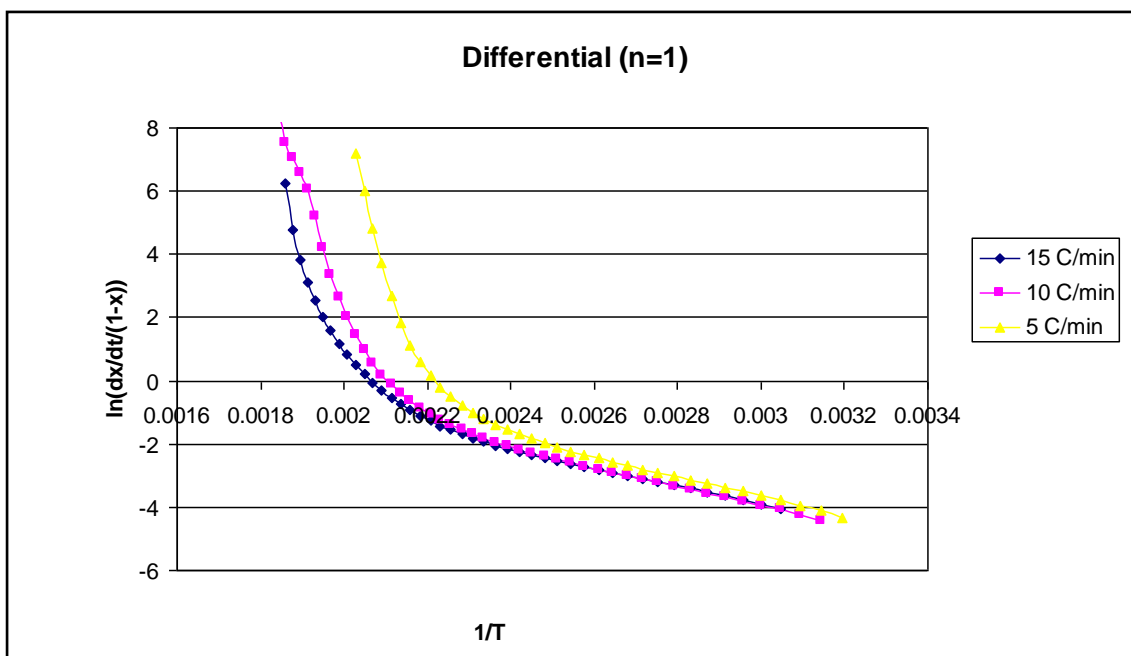


**Figure F.50:** Diesel pyrolysis reaction Differential (n=1) plots of different heating rates of 5°C/min, 10°C/min and 15°C/min

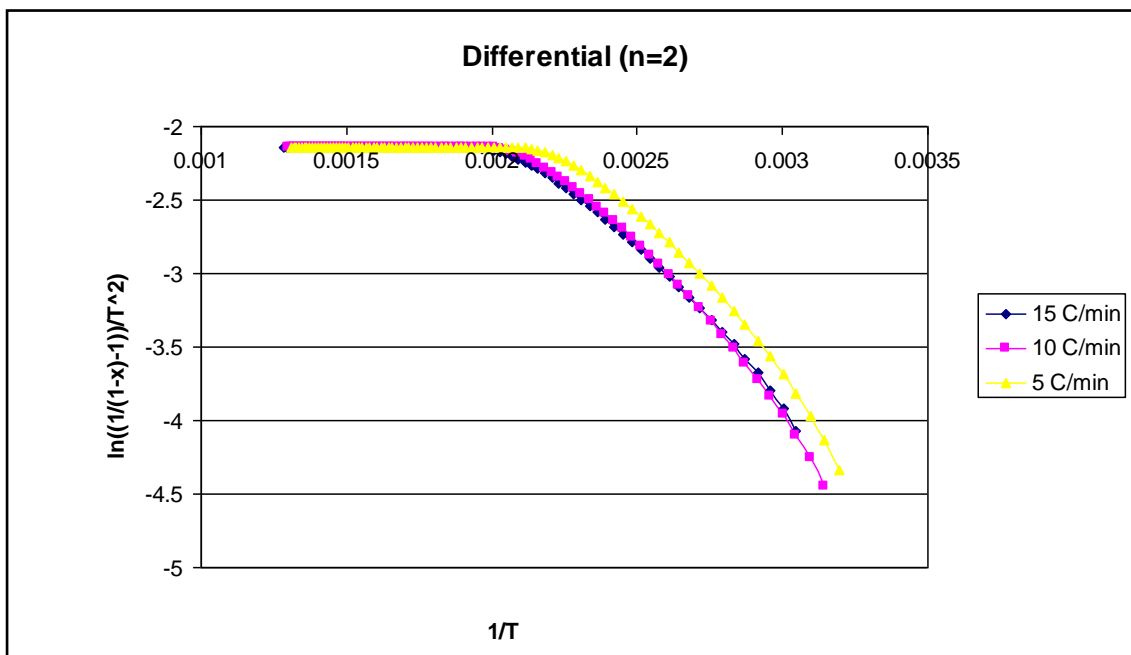


**Figure F.51:** Diesel pyrolysis reaction Differential (n=2) plots of different heating rates of 5°C/min, 10°C/min and 15°C/min

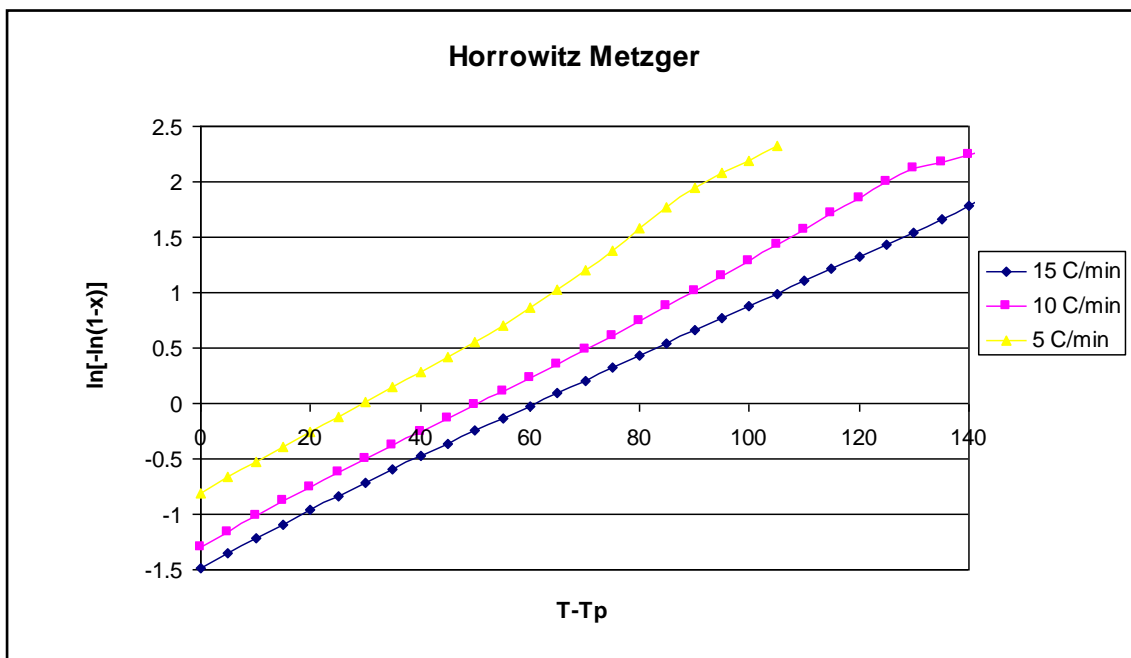


**Figure F.52:** Diesel pyrolysis reaction Horowitz Metzger plots of different heating rates of 5°C/min, 10°C/min and 15°C/min

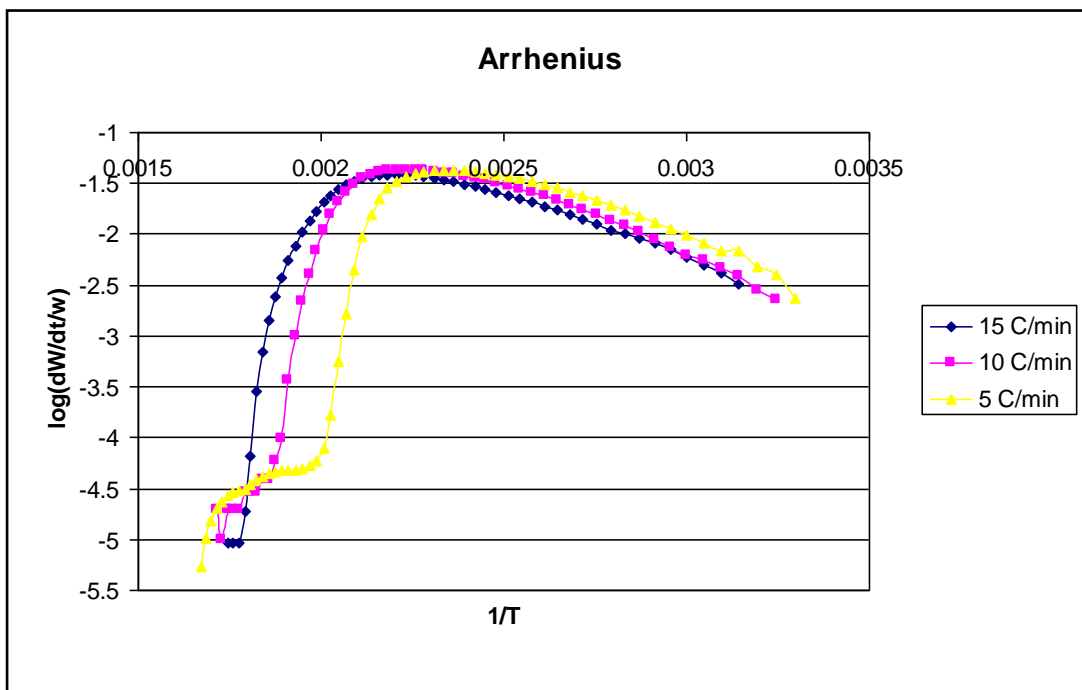


**Figure F.53:** Canola oil pyrolysis reaction Arrhenius plots of different heating rates of 5°C/min, 10°C/min and 15°C/min

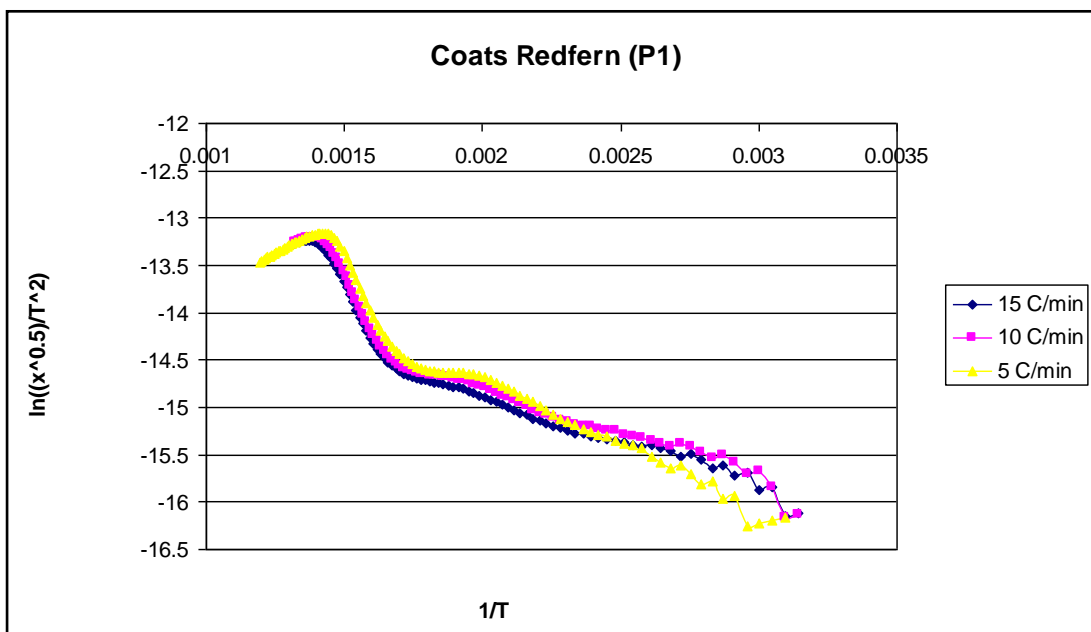


**Figure F.54:** Canola oil pyrolysis reaction Coats Redfern (P1) plots of different heating rates of 5°C/min, 10°C/min and 15°C/min

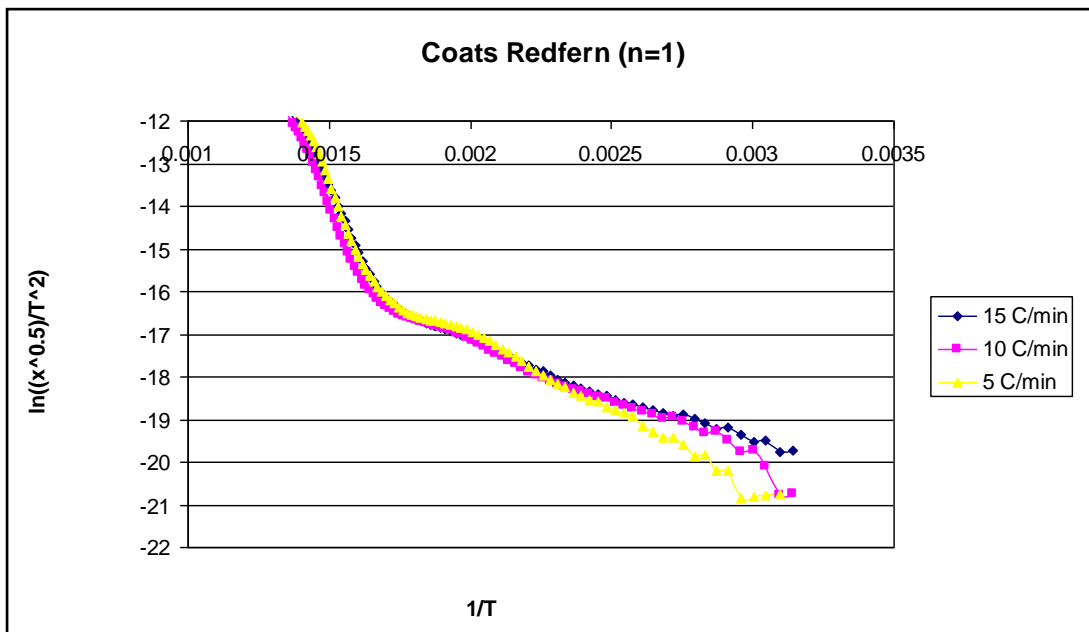


**Figure F.55:** Canola oil pyrolysis reaction Coats Redfern (n=1) plots of different heating rates of 5°C/min, 10°C/min and 15°C/min

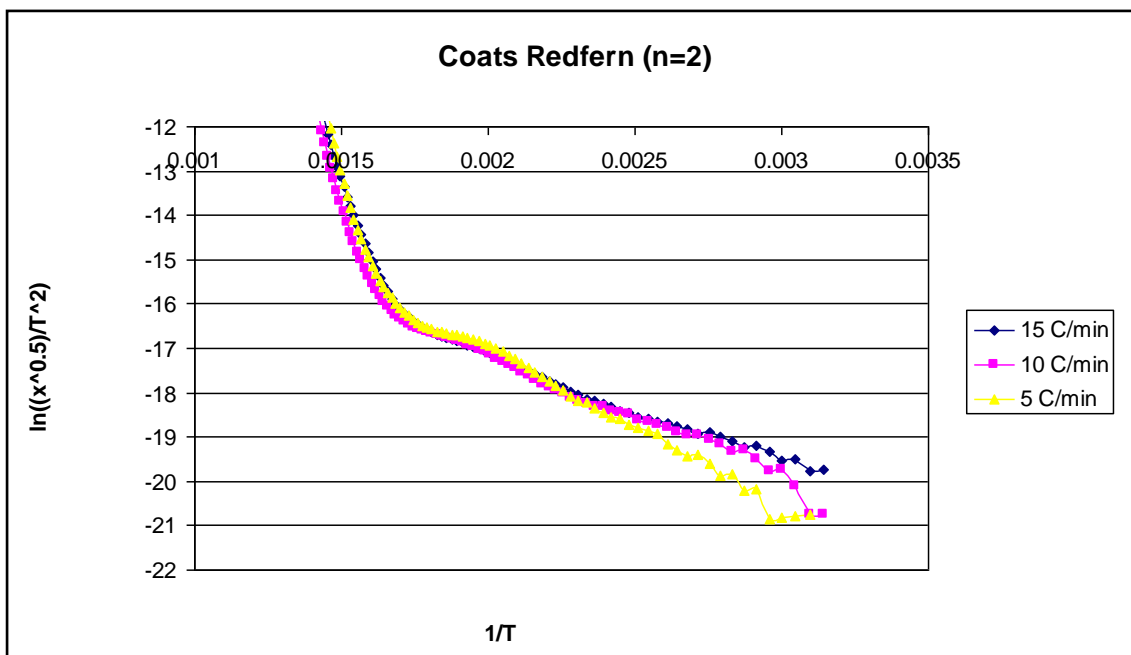


**Figure F.56:** Canola oil pyrolysis reaction Coats Redfern (n=2) plots of different heating rates of 5°C/min, 10°C/min and 15°C/min

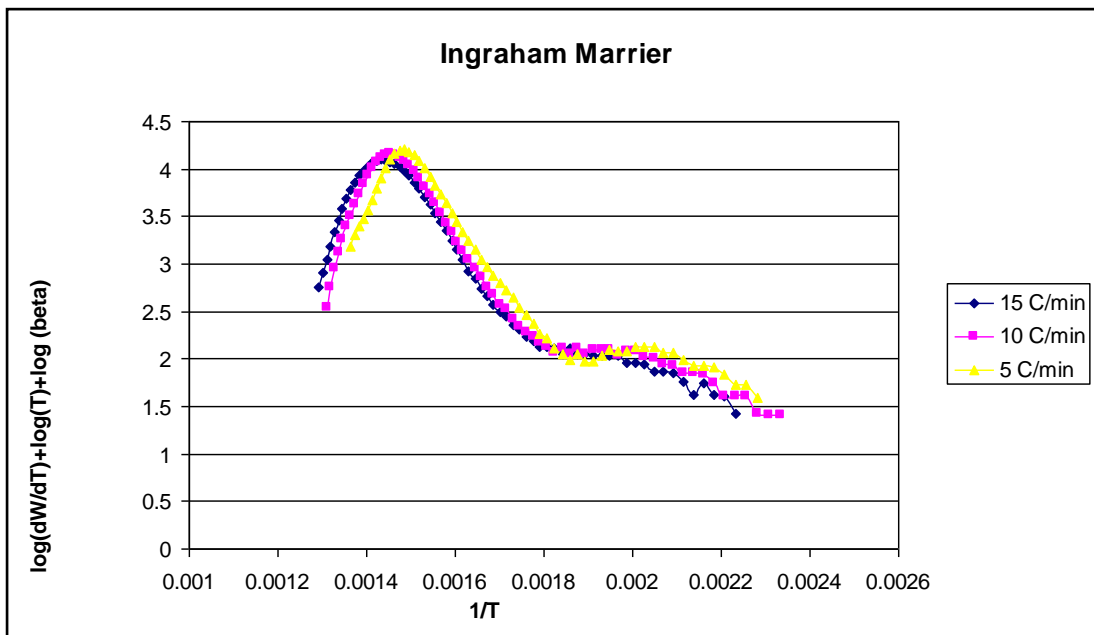


**Figure F.57:** Canola oil pyrolysis reaction Ingraham Marrier plots of different heating rates of 5°C/min, 10°C/min and 15°C/min

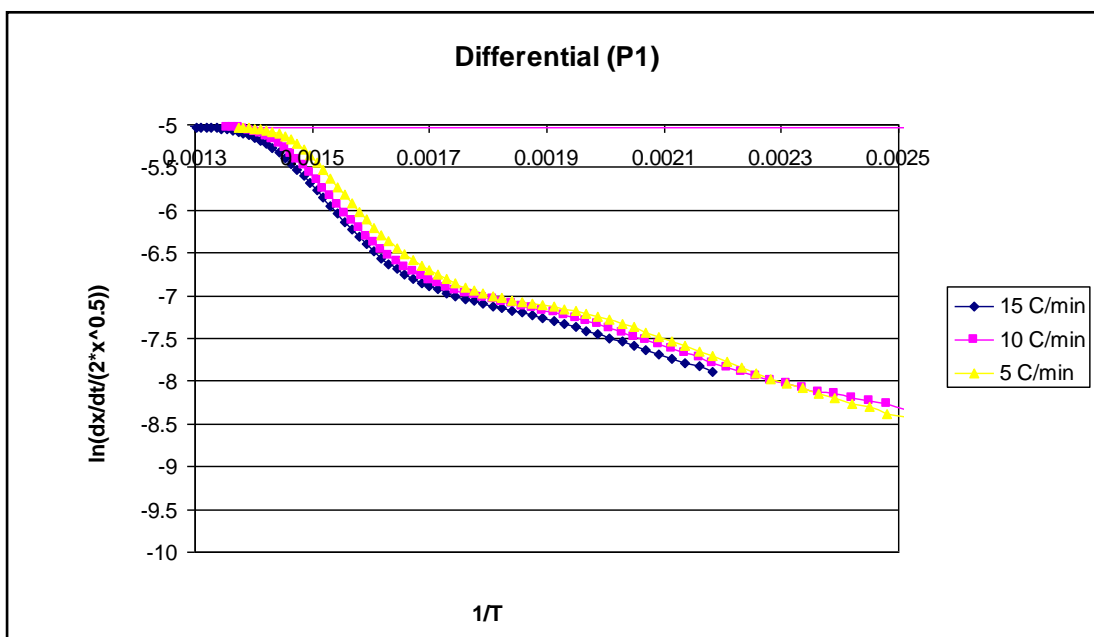


**Figure F.58:** Canola oil pyrolysis reaction Differential (P1) plots of different heating rates of 5°C/min, 10°C/min and 15°C/min

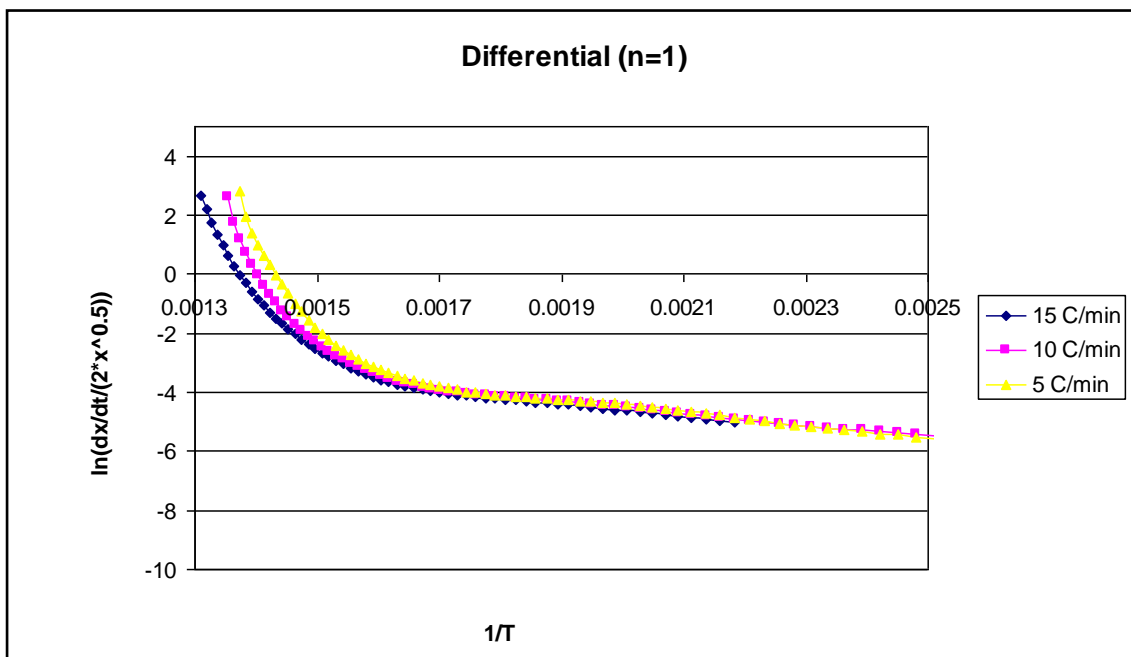


**Figure F.59:** Canola oil pyrolysis reaction Differential (n=1) plots of different heating rates of 5°C/min, 10°C/min and 15°C/min

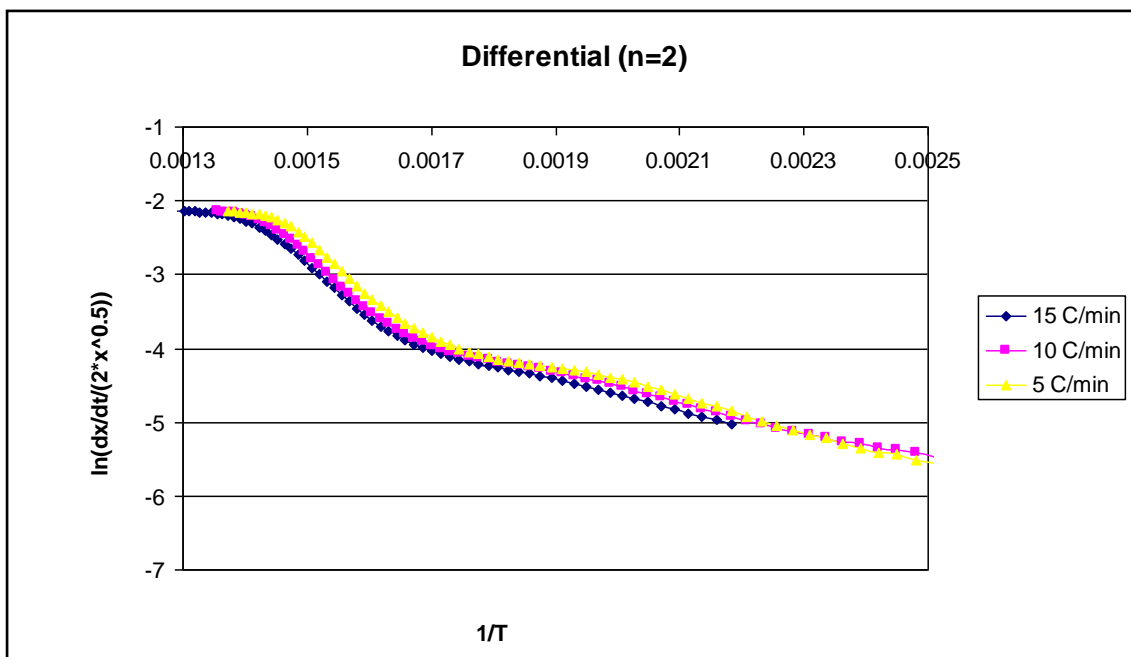


**Figure F.60:** Canola oil pyrolysis reaction Differential (n=2) plots of different heating rates of 5°C/min, 10°C/min and 15°C/min

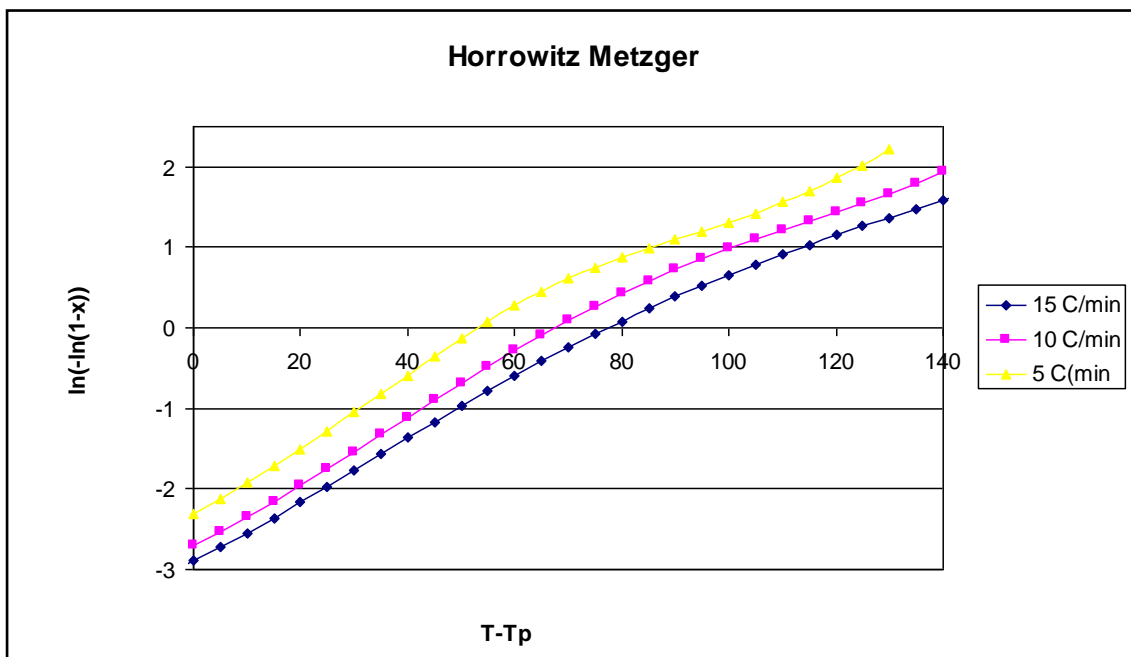


**Figure F.61:** Canola oil pyrolysis reaction Horowitz Metzger plots of different heating rates of 5°C/min, 10°C/min and 15°C/min

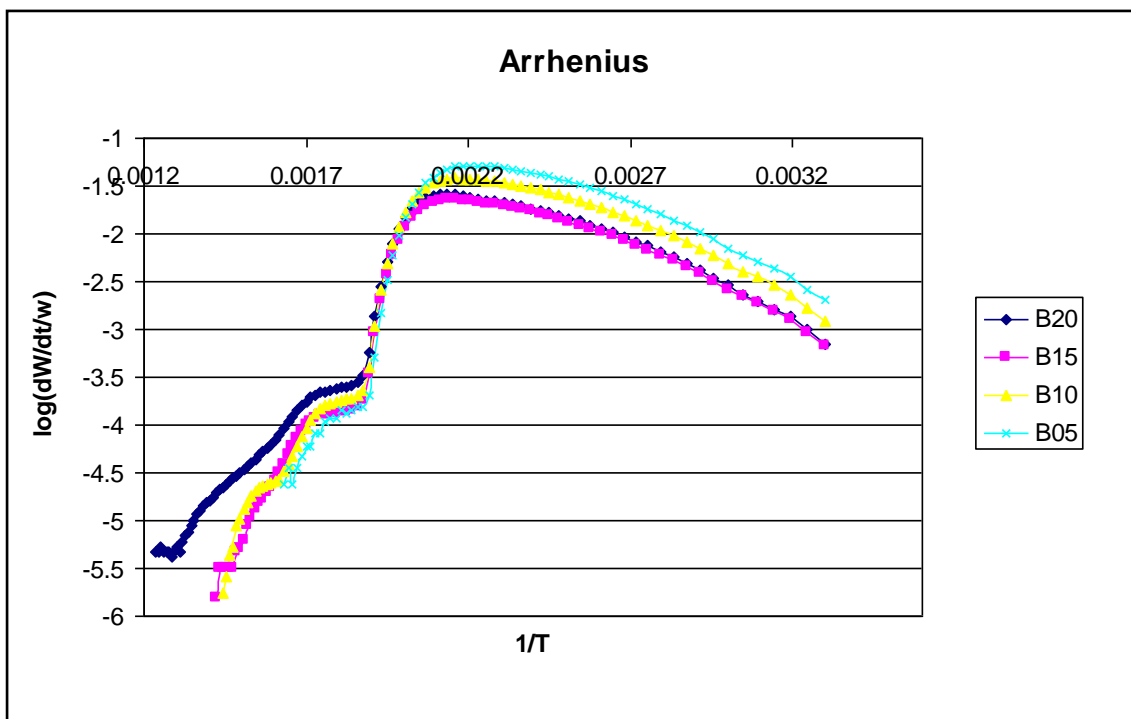


**Figure F.62:** Biodiesel-diesel mixtures pyrolysis reactions Arrhenius plots

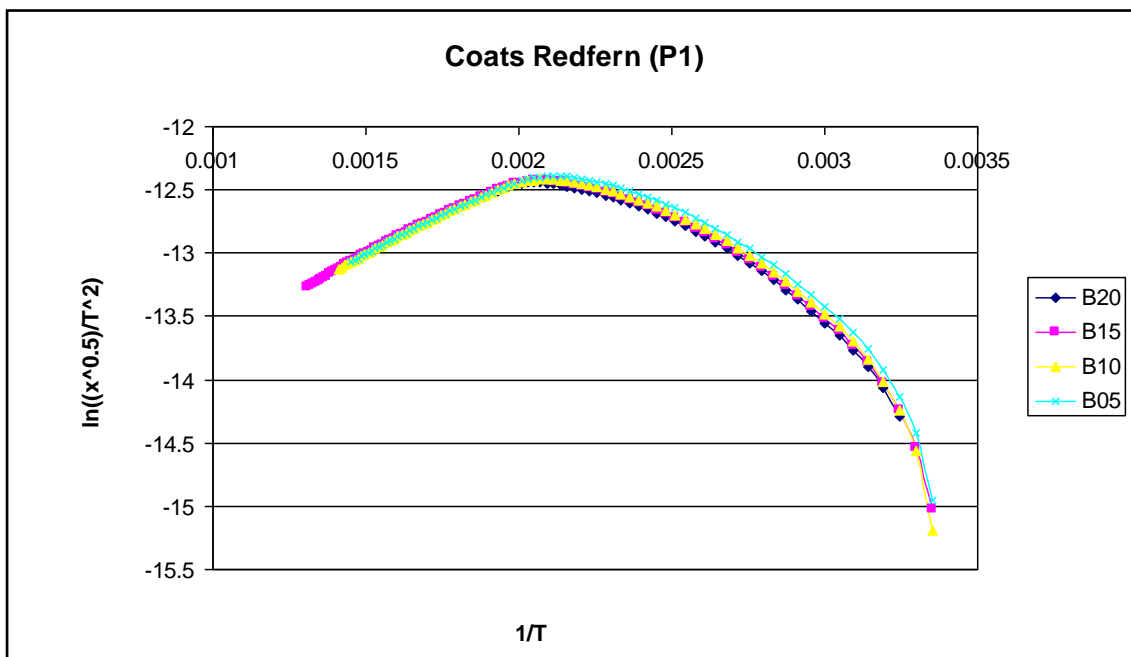


Figure F.63: Biodiesel-diesel mixtures pyrolysis reactions Coats Redfern (P1) plots

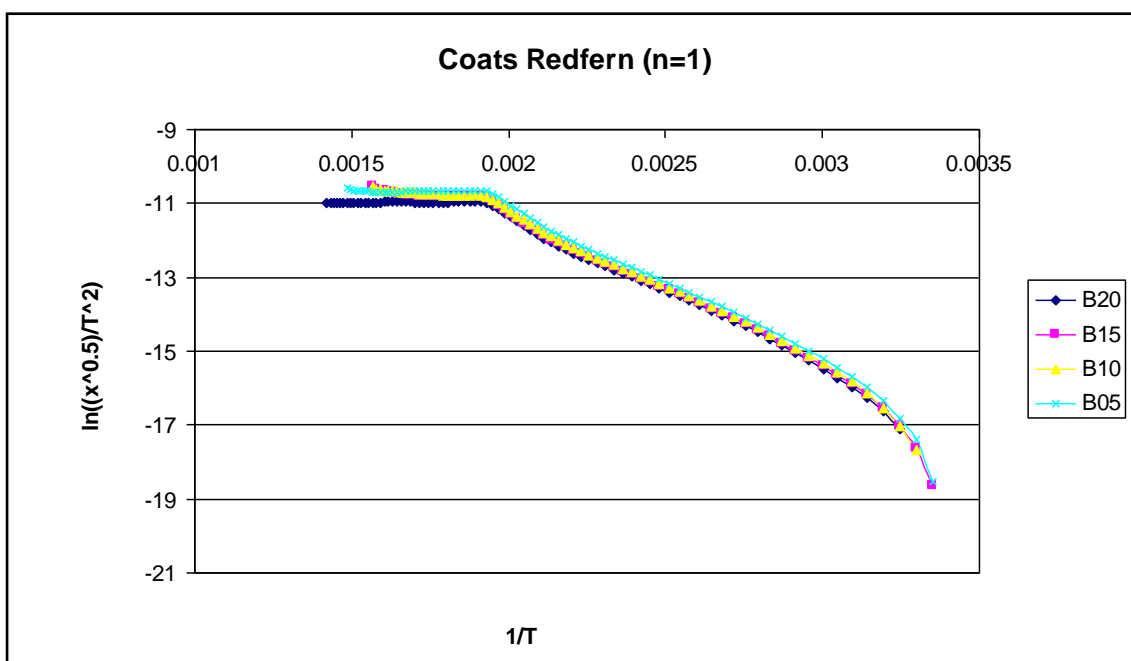


Figure F.64: Biodiesel-diesel mixtures pyrolysis reactions Coats Redfern (n=1) plots

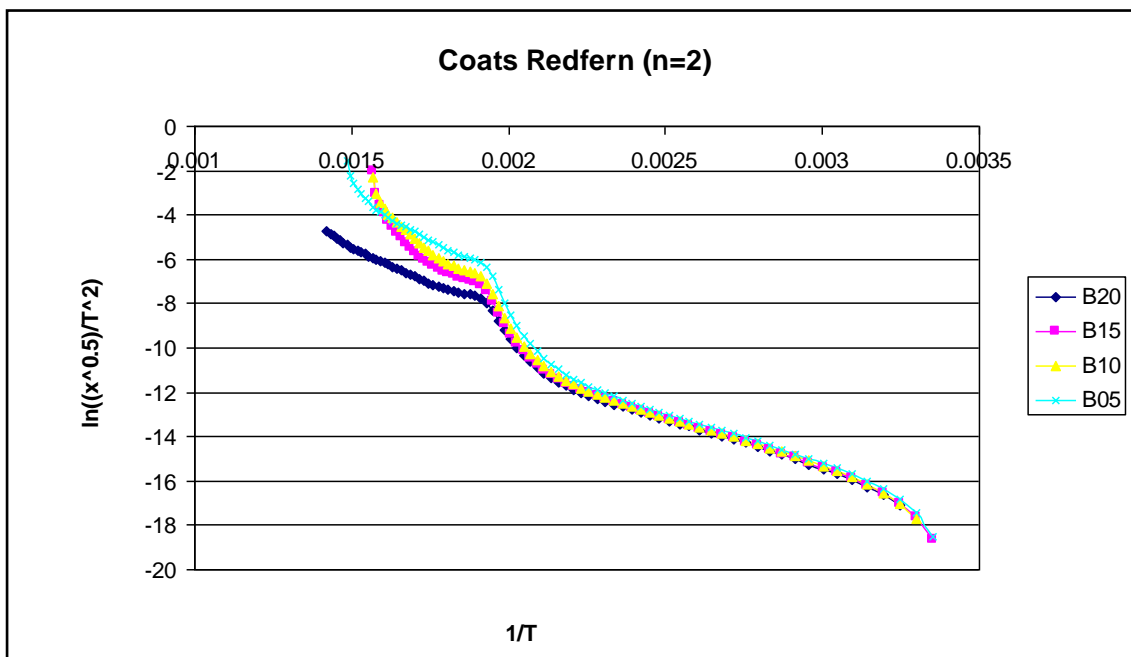


Figure F.65: Biodiesel-diesel mixtures pyrolysis reactions Coats Redfern (n=2) plots

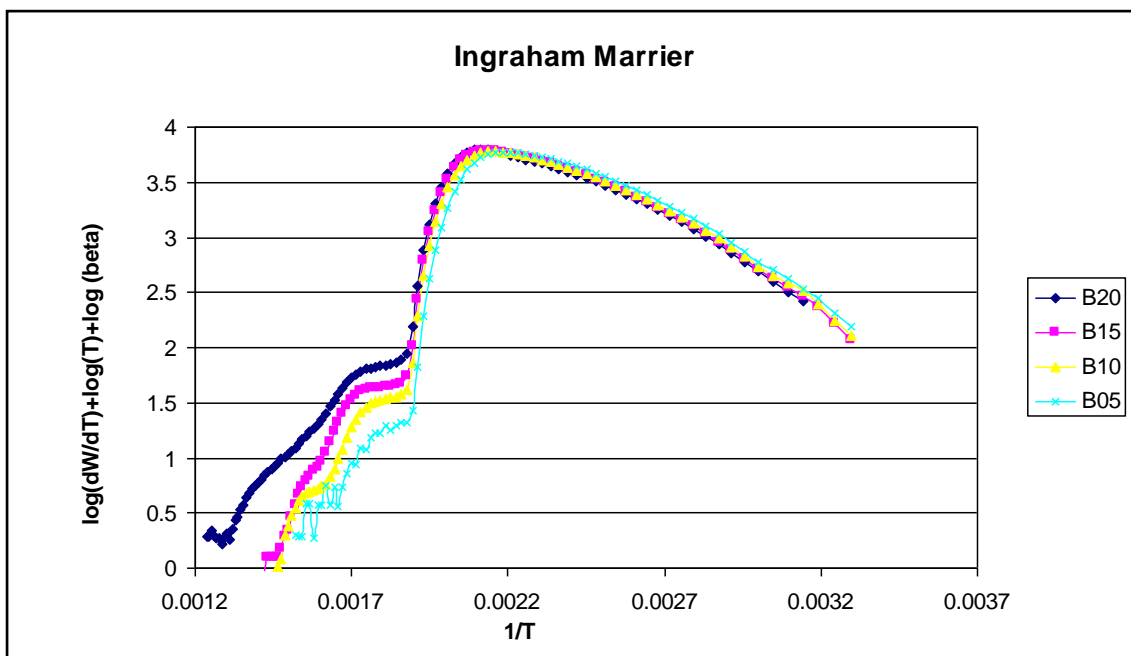
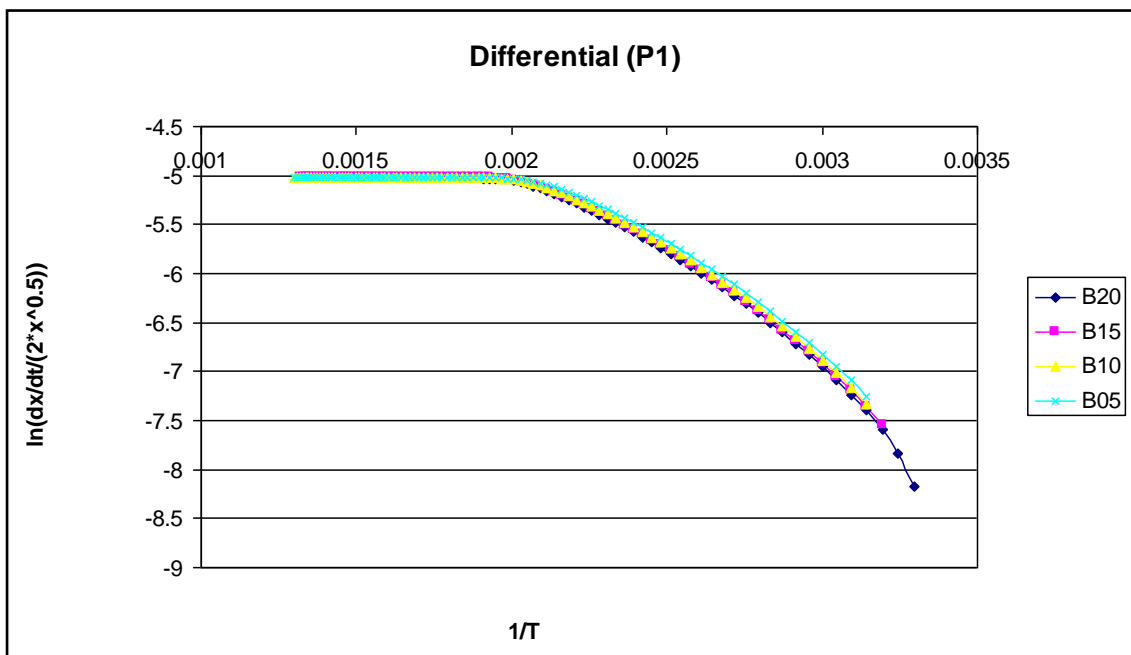
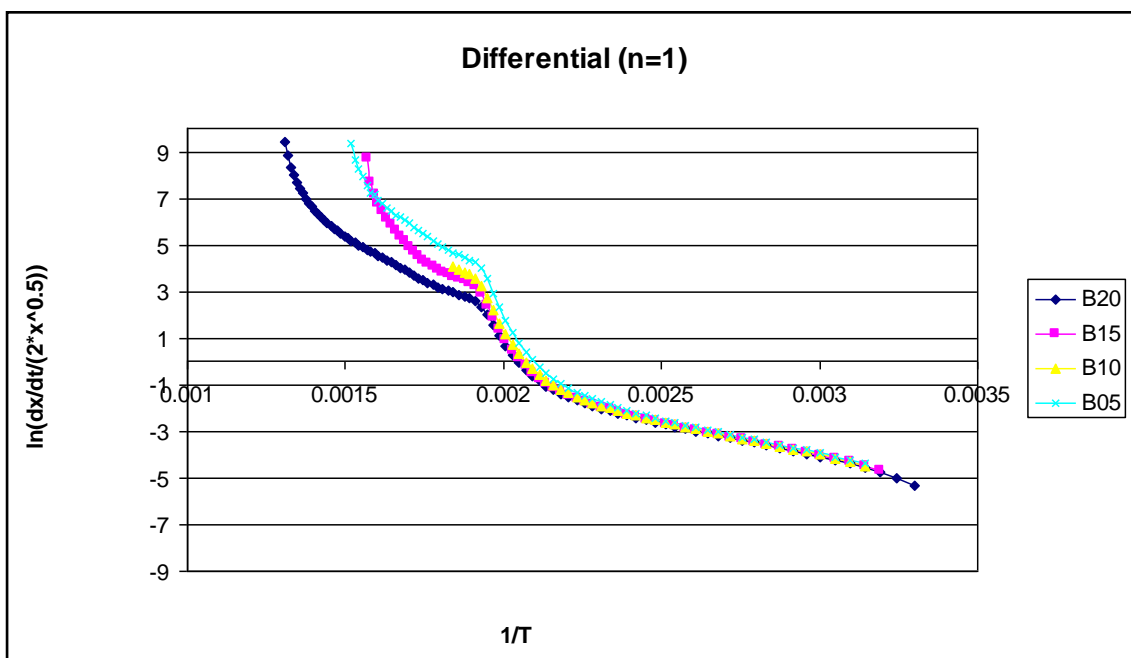


Figure F.66: Biodiesel-diesel mixtures pyrolysis reactions Ingraham Marrier plots



**Figure F.67:** Biodiesel-diesel mixtures pyrolysis reactions Differential (P1) plots



**Figure F.68:** Biodiesel-diesel mixtures pyrolysis reactions Differential (n=1) plots

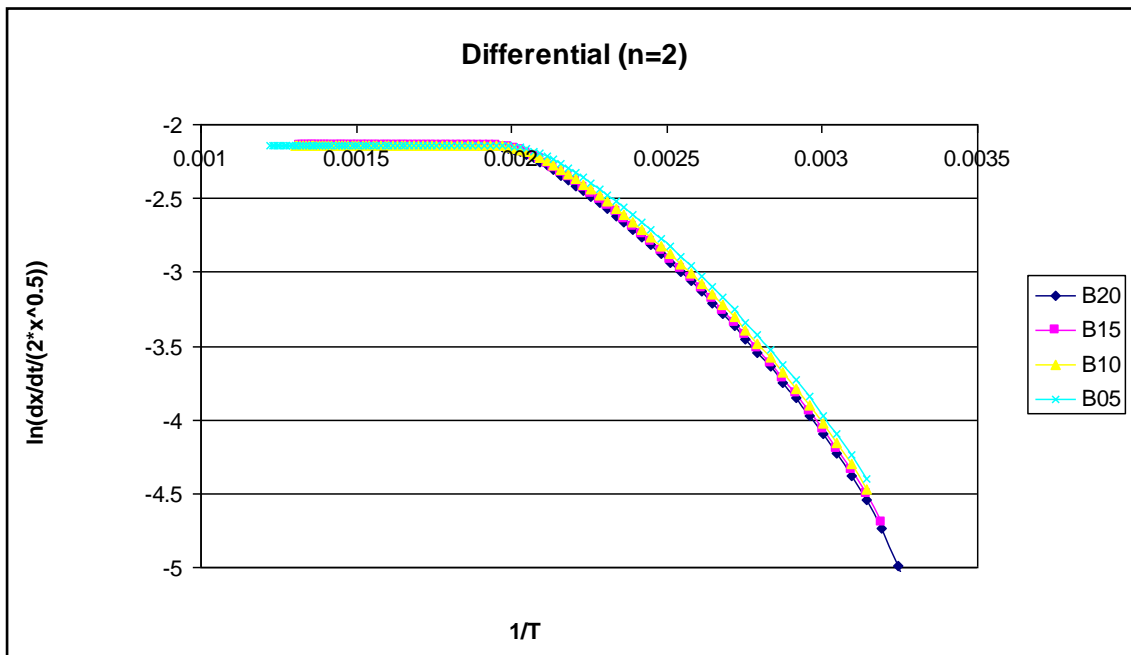


Figure F.69: Biodiesel-diesel mixtures pyrolysis reactions Differential (n=2) plots

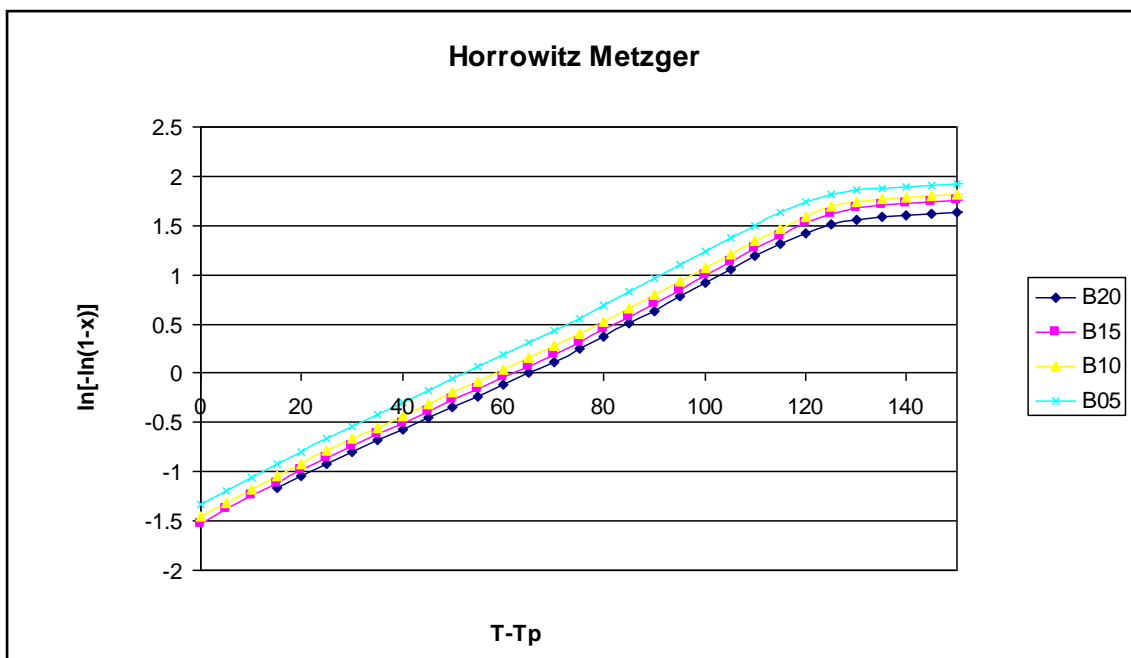


Figure F.70: Biodiesel-diesel mixtures pyrolysis reactions Horowitz Metzger plots